

University of the Western Cape



OPTICAL AND MICROARRAY SILVER-GOLD BASED SENSORS FOR THE DETECTION OF E.COLI 0157:H7 IN SEAWATER

By

SPHAMANDLA NQUNQA

MSc Chemistry-University of the Western Cape

**A Full thesis for Masters Project submitted as fulfilment of the requirements for the
Master's Degree in Chemistry in the Department of Chemistry, University of the
Western Cape, South Africa**

Supervisor: Prof R.F. Ajayi

Co-Supervisor: Dr U. Feleni and Dr T. Mulaudzi

April 2021

TABLE OF CONTENTS

| | |
|--|-----------|
| TABLE OF CONTENTS..... | 2 |
| ABSTRACT..... | 6 |
| DECLARATION | 8 |
| ACKNOWLEDGEMENT | 9 |
| DEDICATION..... | 10 |
| ACADEMIC OUTPUT | 11 |
| KEY WORDS..... | 13 |
| LIST OF ABBREVIATIONS..... | 14 |
| LIST OF TABLES..... | 15 |
| LIST OF FIGURES | 16 |
| CHAPTER ONE | 20 |
| 1 Introduction:..... | 20 |
| 1.1 Problem Statement:..... | 25 |
| 1.2 Research Aim(s), Motivation and Objectives:..... | 28 |
| 1.2.1 Research Aim(s):..... | 28 |
| 1.2.2 Objectives: | 28 |
| 1.2.3 Motivation:..... | 28 |
| 1.3 Research Hypothesis:..... | 29 |
| 1.4 Research Questions:..... | 29 |
| 1.5 Thesis Outline:..... | 29 |
| 1.6 Research Approach:..... | 31 |
| 1.7 References:..... | 32 |
| CHAPTER TWO | 36 |
| 2 Literature Review: | 36 |
| 2.1 Nanoparticles: | 36 |
| 2.2 Green method synthesis:..... | 38 |
| 2.3 Types of Green synthesis methods: | 40 |
| 2.3.1 Ultrasound Synthesis Method:..... | 40 |
| 2.3.2 Photocatalysis Synthesis Method:..... | 41 |

| | | |
|----------------------------|--|----|
| 2.3.3 | Biotransformation Synthesis Method:..... | 42 |
| 2.3.4 | Conventional Heating Synthesis Method:..... | 43 |
| 2.4 | Types of green synthesised nanoparticles:..... | 44 |
| 2.4.1 | Synthesis of Silver and Gold using Banana peels and Grapes:..... | 46 |
| 2.5 | Sensor development based on green synthesised nanoparticles for water detection: | 50 |
| 2.6 | Water Pollution:..... | 52 |
| 2.7 | <i>E. coli</i> Pollution in Freshwater and Seawater: | 54 |
| 2.8 | Chemical Sensors for the detection of <i>E.coli</i> :..... | 55 |
| 2.9 | Optical Sensors: | 57 |
| 2.9.1 | Colorimetric Sensors:..... | 58 |
| 2.9.2 | Photoluminescent Sensors: | 59 |
| 2.9.3 | Surface Plasmon Resonance Sensors:..... | 60 |
| 2.10 | Electrochemical Sensors: | 62 |
| 2.10.1 | Conductometric Sensors: | 63 |
| 2.10.2 | Potentiometric Sensors:..... | 64 |
| 2.10.3 | Amperometric Sensors:..... | 65 |
| 2.11 | References:..... | 68 |
| CHAPTER THREE | | 80 |
| 3 | Characterisation Techniques:..... | 80 |
| 3.1 | Spectroscopy:..... | 80 |
| 3.1.1 | Ultraviolet-visible spectroscopy: | 81 |
| 3.1.2 | Fourier transform infrared spectroscopy:..... | 83 |
| 3.1.3 | X-Ray Powder Diffraction (XRD) analysis: | 84 |
| 3.2 | Microscopic techniques: | 86 |
| 3.2.1 | High-Resolution Transmission Electron Microscopy | 86 |
| 3.3 | Scattering Techniques:..... | 90 |
| 3.3.1 | Small-Angle X-ray scattering (SAX)..... | 90 |
| 3.4 | Electrochemical Techniques: | 91 |
| 3.4.1 | Cyclic Voltammetry:..... | 92 |
| 3.5 | Material and Methods: | 95 |
| 3.5.1 | Chemicals and Reagents: | 95 |
| 3.5.2 | Preparation of Aqueous Grape and Banana peel extracts (GBPE): | 95 |

| | | |
|---|--|-----|
| 3.5.3 | Synthesis of GBPE-Au-NPs: | 96 |
| 3.5.4 | Synthesis of GBPE-AgNPs:..... | 97 |
| 3.5.5 | Synthesis of GBPE capped Ag-Au-NPs | 98 |
| 3.6 | Characterisation of the functionalised nanoparticles: | 98 |
| 3.6.1 | Ultraviolet-visible (UV-Vis) analysis: | 98 |
| 3.6.2 | Fourier Transformation Infrared (FT-IR) analysis:..... | 98 |
| 3.6.3 | X-Ray Diffraction (XRD) analysis: | 99 |
| 3.6.4 | High-Resolution Transmission Electron Microscopy (HR-TEM) analysis: | 100 |
| 3.6.5 | Small-Angle X-ray Scattering (SAX) analysis: | 100 |
| 3.7 | Electrochemical Analysis:..... | 101 |
| 3.7.1 | Cyclic Voltammetry analysis: | 101 |
| 3.8 | References:..... | 103 |
| CHAPTER FOUR | | 106 |
| Results and Discussion: Part 1 | | 106 |
| 4 | Gold Nanoparticles (Au-NPs):..... | 106 |
| 4.1 | Ultraviolet-Visible Spectroscopy (UV-vis) of (Au-NPs):..... | 106 |
| 4.2 | Fourier Transform Infrared Spectroscopy (FT-IR) of GBPE-Au-NPs: | 110 |
| 4.3 | X-ray diffraction analysis (XRD) of Au-NPs: | 113 |
| 4.4 | High-Resolution Transmission Electron Microscopy (HR-TEM) of GBPE Au-NPS:..... | 116 |
| 4.5 | Small-angle x-ray Scattering:..... | 121 |
| 4.6 | Electrochemical characterisation of GBPE capped Au-NPs (CV) of Au-NPs: | 124 |
| 4.7 | References:..... | 131 |
| CHAPTER FIVE | | 137 |
| Results and Discussion: Part 2 | | 137 |
| 5 | Silver Nanoparticles (Ag-NPs): | 137 |
| 5.1 | Ultra-visible Spectroscopy (UV-vis) of Ag-NPs: | 137 |
| 5.2 | Fourier Transformation Infrared (FT-IR) for GBPE-Ag-NPs: | 141 |
| 5.3 | X-ray Diffraction pattern (XRD) of Ag-NPs: | 143 |
| 5.4 | High-Resolution Electron Microscopy (HR-TEM) of Ag-NPs: | 145 |
| 5.5 | Small-angle x-ray Scattering (SAXS) for Ag-NPs: | 150 |
| 5.6 | Electrochemical behaviour of GBPE capped Ag-NPs: | 152 |
| 5.7 | References:..... | 158 |

| | |
|---|-----|
| CHAPTER SIX | 164 |
| Results and Discussion: Part 3 | 164 |
| 6 Silver-Gold Bimetallic Nanoparticles:..... | 164 |
| 6.1 Ultraviolet-Visible Spectroscopy (UV-vis) of (Ag-Au-NPs): | 164 |
| 6.2 Fourier Transform Infrared Spectroscopy (FT-IR) of Ag-Au-NPs:..... | 166 |
| 6.3 X-ray Diffraction for GBPE capped Ag-Au-NPs nanoparticles: | 169 |
| 6.4 High-Resolution Transmission Electron Microscopy (HR-TEM) of Ag-Au-NPs: | 172 |
| 6.5 Small Angle X-ray Scattering for GBPE Ag-Au-NPs: | 177 |
| 6.6 Electrochemical characterisation of GBPE capped Ag-AuNPs:..... | 179 |
| 6.7 References:..... | 186 |
| CHAPTER SEVEN | 190 |
| Detection and Discussion: Part 1 | 190 |
| 7 Detection of Escherichia coli 0157:H7:..... | 190 |
| 7.1 Culture preparation and media plating methods: | 190 |
| 7.2 Bacterial preparation:..... | 190 |
| 7.3 UV-Vis detection of <i>E.coli</i> 0157:H7: | 191 |
| 7.4 References:..... | 201 |
| CHAPTER EIGHT | 204 |
| Detection and Discussion: Part 2 | 204 |
| 8.1 Cyclic Voltammetric detection of <i>E.coli</i> 0157:H7:..... | 205 |
| 8.2 References:..... | 212 |
| CHAPTER NINE | 214 |
| 9.1 Conclusion: | 214 |
| 9.2 Future aims: | 215 |

ABSTRACT

Recently researchers reported that nanoparticles functionalised through chemical methods possess risks to the environment and to the human health since they use hazardous chemicals and produce toxic waste. The increasing demand of nanomaterials for application in the field of science require an alternative method for synthesis of nanomaterials that are environmentally friendly, eco-friendly and non-toxic. The present study describes the green synthesis method for functionalisation of nanomaterials. Green synthesis methods are considered as a novel approach for functionalisation of nanoparticles using biological sources.

Herein, we demonstrate the novel synthesis of cost-effective and environmentally friendly bimetallic silver-gold nanoparticles functionalized with a combination of banana peel and grape fruit extracts (GBPE) to enhance the stability, reactivity and biocompatibility of the nanoparticles. The formation of a bimetallic GBPE capped Ag-Au-NPs was at first visually observed with a change in solution during a reaction mixture of silver and gold ions in a ratio of (Ag-Au = 2:1) and banana peel and grape fruit extracts which revealed a purple-black colour after a reaction time of one hour an indication of the presence of silver-gold nanoparticles which were also confirmed by an absorption band at 457 nm using Ultraviolet visible (UV-vis) spectrophotometer. The polydispersity nature of the nanoparticles was revealed using Small angle x-ray scattering (SAXS) and High-resolution transmission electron microscopy (HR-TEM), techniques which also confirmed the average size of the nanoparticles to be 12-14 nm. X-ray diffraction (XRD) studies confirmed the spherical structure of the nanoparticles while Fourier transform infrared spectroscopy (FT-IR) studies revealed the structure of these nanoparticles which included carbonyl groups, primary amine groups, OH groups and other stabilizing functional groups characteristic of the properties of

combined extracts. Cyclic voltammetry (CV) studies on glassy carbon electrodes further revealed the electrochemical properties of these nanoparticles necessary for the fabrication of sensors. In this study, a simple, quick, less time-consuming surface plasmon resonance (SPR) and electrochemical method in the form of an optical and electrochemical sensors has been developed for the detection of *E.coli* 0157:H7. The limit of detection (LOD) for SPR sensor was 1×10^1 CFU/mL for GBPE Ag-Au-NPs. The electrochemical sensor was fabricated by the deposition of GBPE Ag-Au-NPs composite on composite on glassy carbon electrode and the limit of detection was found to be 3.0×10^1 CFU/mL for GBPE capped Ag-Au-NPs. Therefore, this study successfully demonstrated the use of the combination of grape and banana peel for the synthesis of bimetallic nanoparticles and its application.

DECLARATION

I declare that “*Optical and microarray silver-gold based sensors for the detection of E.coli 0157: H7 in seawater*” is my own work and that all the sources I have used or quoted have been indicated and acknowledged by means of complete references.

ACKNOWLEDGEMENT

Foremost, I would like to give the almighty Lord all the glory and honour for giving me the strength and wisdom to complete this work. My sincere thanks to my supervisor Prof Rachel Fanelwa Ajayi for guidance and supervision and the opportunity to use the facility in Sensor Laboratory. I would also appreciate the support and contribution of my co-supervisors: Dr Usisipho Feleni and Dr Takalani Masuku. The technical contribution and academic assistance of all the staff in the chemistry department is appreciated.

To my parents Mxolisi Nqunqa and Nophumzile Nqunqa, Enkosi!! The love you give to me is so amazing. The fire inside me you've kept it burning. Naxa ndiphela Amandla you keep me going. Nangendlela enindikhuthazaya ngayo, thank you for loving me nihlala nidnixelela uba ndinawo Amandla. You sheltered me until it stopped raining, thank you for loving me, nangamso!!

My sincere gratitude also goes to my siblings Bukelwa Nqunqa, Siyabonga Nqunqa, Andiswa Nqunqa and Sinalo Nqunqa Ooohh! abantwana bakamama I did it again for us. Thank you for sharing my struggles and dreams.

I also thank the Council (CSIR) for funding the research.

My motto that kept me going” **To the stars through difficulties**”

DEDICATION

*To my dearest parents Mxolisi and Nophumzile
Nqunqa
Thank you for loving me!*

ACADEMIC OUTPUT

The following section lists technology transfer activities (posters, conference) derived from the results obtained from this research work.

Conferences:

- **Sphamandla Nqunqa**, Usisipho Feleni, Takalani Mulaudzi-Masuku, Rachel Ajayi. Cost-effective gold nanoparticles functionalised with *Musa paradisiaca* and *Vitis viniferus* extract as sensing platform for the detection of *E.coli* 015:H7. International Society of Electrochemistry 2019, Durban ICC, 05-08 August 2019. Poster Presentation.
- **Sphamandla Nqunqa**, Usisipho Feleni, Takalani Mulaudzi-Masuku, Rachel Ajayi, Cost-effective silver nanoparticles functionalised with *Musa paradisiaca* and *Vitis viniferus* extract as sensing platform for the detection of *E.coli* 015:H7. SACI Symposium, University of the Western Cape (Cape Town), 14 August 2019. Oral Presentation.
- **Sphamandla Nqunqa**, Rachel Ajayi, Takalani Mulaudzi-Masuku, , Usisipho Feleni *Vitis vinifera* and *Musa paradaisica* capped silver nanoparticles for the optical detection of *E.coli* 0157:H7. International Society of Electrochemistry 2020, Belgrade Online, 05-08 August 2020. Poster Presentation.

Publications:

- Rachel Fanelwa Ajayi, **Sphamandla Nqunqa**, Siphokazi Tshoko, Yonela Mgwili, Takalani Mulaudzi, Noluthando Mayedwa and Emmanuel Iwuoha. Green Method

Synthesised Graphene-Silver Electrochemical Nanobiosensors for Ethambutol and Pyrazinamide, Processes 2020, 8(7), 879; <https://doi.org/10.3390/pr8070879>

- Rachel Fanelwa Ajayi, Simone Barry, 2Mulisa Nkuna, Nzumbululo Ndou, Tessia, Rakgotho, **Sphamandla Nqunqa**, Nokwanda Ngema, Velaphi Thipe, Takalani Muluadzi, Nanoparticles in Biosensor Development for the detection of Pathogenic Bacteria in water, Elsevier, (Book Chapter-Accepted).
- Rachel Fanelwa Ajayi, **Sphamandla Nqunqa**, Yonela Mgwili, Siphokazi Tshoko, Nokwanda Ngema, Germana Lyimo, Tessia Rakgotho, Nzumbululo Ndou, Razia Adam, Green Synthesized Nanoparticles as Potential Sensors for Health Hazardous Compounds, Chapter 12, Taylor and Francis, (Book Chapter-Accepted)

KEY WORDS

Green Synthesis

Nanoparticles

Gold Nanoparticle

Silver Nanoparticles

Escherichia Coli 0157:H7

Water Pollution

LIST OF ABBREVIATIONS

Ag - Silver

Au – Gold

AgNO₃ – Silver nitrate

Ag-NPs – Silver nanoparticles

Au-NPs – Gold nanoparticles

Ag-Au-NPs – Silver gold nanoparticles

CH – Conventional Heating

Cu-NPs – Copper nanoparticles

E.coli – Escherichia coli

EPA – Environmental Protection Agency

GBE – Grape Banana Extract

HAuCl₄.3H₂O – Hydrogen tetrachloroaurate (III) hydrate

ICP - Inductively Coupled Plasma mass spectrometer

KBr – Potassium Bromide

LOD - limit of detection

M⁺ - Metal ions

MNP - Mental Nanoparticles

NPs – Nanoparticles

N₂ – Nitrogen gas

ROS – Reactive oxygen species

SANS – South African National Standards

SPR – Surface Plasmon Resonance

WHO – World health organisation

LIST OF TABLES

| | |
|---|-----|
| Table 2.1: Advantages and disadvantages of Bottom-up and Top-down approaches | 38 |
| Table 2.2: Possible biological compounds in banana peel extract responsible for bio-reduction of metal salts. | 49 |
| Table 3.1: Advantages and Disadvantages of H-RTEM. | 89 |
| Table 4.1: Comparison of studies from literature and the present work, for the time taken for complete reduction of gold chloride using natural products as reducing agents. | 110 |
| Table 4.2: Comparison of Braggs diffraction peaks at 2Θ value and the size of crystalline green synthesised nanoparticles (from literature) and the present work..... | 115 |
| Table 4.3: Comparison of size (calculated based on HR-TEM measurements) of green synthesised nanoparticles..... | 120 |
| Table 5.1: Comparison of studies from literature and the present work, for the time taken for complete reduction of silver nitrate using natural products as reducing agents. | 141 |
| Table 5.2: Comparison of Braggs diffraction peaks at 2Θ value and the size of crystalline green synthesised nanoparticles (from literature) and the present work..... | 145 |
| Table 5.3: Comparison of size (calculated based on HR-TEM measurements) of green synthesised silver-gold bimetallic alloy nanoparticles. | 149 |
| Table 6.1: Comparison of SPR band and Reaction times for silver-gold nanoparticles synthesis via green methods from literature and this study. | 166 |
| Table 6.2: Comparison of Braggs diffraction peaks at 2Θ value and the size of crystalline green synthesised nanoparticles (from literature) and the present work..... | 172 |
| Table 6.3: Comparison of size (calculated based on HR-TEM measurements) of green synthesised silver-gold bimetallic alloy nanoparticles. | 176 |
| Table 6.4: Summary of the average particle size of GBPE capped nanoparticles determined by XRD, HR-TEM and SAX in this study. | 179 |
| Table 6.5: Summary of electrochemical data obtained in this study. | 184 |
| Table 7.1: Comparison of SPR sensor for detection <i>E.coli</i> 0157:H7 using different material. | 200 |
| Table 8.1: Limit of Detection of more relevant studies reported in the literature for detection of <i>E.coli</i> 0157:H7 compared to this study. | 211 |

LIST OF FIGURES

| | |
|--|----|
| Figure 1.1: Research framework..... | 31 |
| Figure 2.1: A diagram illustrating the types of Synthesis for nanomaterials [9]. | 37 |
| Figure 2.2: Examples of natural products that can be used to synthesise nanoparticles using green chemistry. | 40 |
| Figure 2.3: Schematic representation of Ultrasound method [18] | 41 |
| Figure 2.4: Schematic representation of Photocatalysis method [19]..... | 42 |
| Figure 2.5: A typical presentation of Biotransformation method [21]. | 43 |
| Figure 2.6: Figure Schematic representation of conventional heating method for synthesis of nanoparticles [24]..... | 44 |
| Figure 2.7: Picture of Banana peel sample. | 47 |
| Figure 2.8: An image of a Grape sample. | 48 |
| Figure 2.9: Typical representation of nanoparticles attacking and kill bacteria cells [79]. | 52 |
| Figure 2.10: Escherichia coli structure [93]..... | 55 |
| Figure 2.11: A typical representation diagram of a chemical sensor..... | 56 |
| Figure 2.12: Schematic diagram of optical sensor [104] | 58 |
| Figure 2.13: An example of Colorimetric sensor [107]. | 59 |
| Figure 2.14: Schematic diagram of Photoluminescent band [109]..... | 60 |
| Figure 2.15: Presentation of SPR sensor principle [114]..... | 61 |
| Figure 2.16: Principle of electrochemical sensor [115]. | 62 |
| Figure 2.17: A typical representation of a connected conductometric sensor [117]..... | 63 |
| Figure 2.18: Typical diagram of ion selective electrode [119]. | 65 |
| Figure 2.19: A typical representation of amperometric sensor | 67 |
| Figure 3.1: Various energy levels and types of electronic transitions [3]..... | 82 |
| Figure 3.2: Typical diagram of FT-IR spectrometer primary component [5]..... | 83 |
| Figure 3.3: Schematic set-up of X-ray Power Diffraction [12]. | 86 |
| Figure 3.4: Typical presentation of a transmission electron microscope (HR-TEM) [14]. ... | 88 |
| Figure 3.5: An example of an HR-TEM image. | 89 |
| Figure 3.6: Typical representation of Small-Angle X-ray Scattering (SAXS) [20]. | 91 |

| | |
|---|-----|
| Figure 3.7: A typical cyclic voltammogram [25]..... | 92 |
| Figure 3.8: A typical representation of a connected cell-set up [27]. | 94 |
| Figure 3.9: Reaction condition of GBPE-Au-NPs. | 96 |
| Figure 3.10: Presentation of GBPE capped nanoparticles and their application. | 97 |
| Figure 3.11: A sample mixture of KBr and GBPE capped Au-NPs. | 99 |
| Figure 3.12: A typical example of a simple way of polishing an electrode on a cloth polishing pad [28,29]. | 101 |
| Figure 3.13: A typical representation of a three-electrode set-up in an electrochemical cell [30]..... | 102 |
| Figure 4.1: Photograph showing colour of solutions, (a) GBPE extract, (b) gold chloride, (c) GBPE Au-NPs. | 107 |
| Figure 4.2: Visual inspection of the colour change after the synthesis of Au-NPs achieved at different time interval; (a) 10 min, (b) 20 min, (c) 30 min, (d) 40 min, (e) 50 min and (f) 60 min. | 107 |
| Figure 4.3: UV-Vis spectra of GBPE-AuNPs..... | 108 |
| Figure 4.4: UV-Vis spectra of GBPE-AuNPs at different time intervals. | 109 |
| Figure 4.5: FT-IR spectra of the green synthesised Au-NPs and GBPE. | 113 |
| Figure 4.6: X-ray diffraction pattern of green synthesised Au-NPs. | 114 |
| Figure 4.7: (a) HR-TEM images; (b) Lattice fringes; (c) SAED pattern; (d) Particle size distribution of the GBPE-AuNPs..... | 119 |
| Figure 4.8: Energy Dispersive Spectroscopy patterns of GBPE capped Au-NPs. | 121 |
| Figure 4.9: SAXS pair-distance distribution function (PDDF) of GBPE-AuNPs..... | 122 |
| Figure 4.10: Size distribution functions weighted by number (black line) and intensity (red line). | 124 |
| Figure 4.11: Cyclic voltammogram of bare GCE (Black line), Au-NPs/ GCE (Red line) in 0.2 M PBS, pH 7.4 at 50 mV/s. | 125 |
| Figure 4.12: Represent Multi-scan voltammograms of Au-NPs in 0.2M PBS, pH 7.4 at (10- 100 mV/s)..... | 126 |
| Figure 4.13: Plots of log current versus log scan rate of GBPE capped AuNPs. | 129 |
| Figure 4.14: Randel-Sevcik Plot for GBPE capped Au-NPs..... | 130 |
| Figure 5.1: Photograph showing colour of solutions, (a) GBPE extract, (b) AgNO ₃ , (c) Ag- NPs..... | 138 |
| Figure 5.2: Visual inspection of the colour change of reaction solution in the process of Ag- NPs synthesis at different time intervals, (a) 3 min, (b) 6 min, (c) 9 min, (d) 12 min, (e) 15 min, (f) 18 min. | 138 |

| | |
|--|-----|
| Figure 5.3: UV-Vis spectra of GBPE capped AgNPs..... | 139 |
| Figure 5.4: UV-Vis spectra of GBPE capped Ag-NPs at different time intervals..... | 140 |
| Figure 5.5: FT-IR spectra of the green synthesised Ag-NPs and GBPE. | 143 |
| Figure 5.6: X-ray diffraction pattern of GBPE capped Ag-NPs. | 144 |
| Figure 5.7: (a) HR-TEM image of Ag-NPs at 200 nm range, (b) lattice fringes, (c) Selected area electron diffraction (SAED) patterns, (d) histogram..... | 148 |
| Figure 5.8: Energy Dispersive Spectroscopy patterns of GBPE capped Ag-NPs. | 150 |
| Figure 5.9: SAXS pair distance distribution function (PDDF) of GBPE AgNPs. | 151 |
| Figure 5.10: Size distribution functions weighted by number (black line) and intensity (red line). | 152 |
| Figure 5.11: Cyclic voltammogram of bare GCE (Black line), Ag-NPs/ GCE (Red line) recorded in 0.2 PBS, pH 7.4 at 50 mV/s..... | 153 |
| Figure 5.12: Multi-Scan Voltammograms of Ag-NPs in 0.2 PBS, pH 7.4 at (10-100 mV/s). | 154 |
| Figure 5.13: Plots of log current versus log scan rate of GBPE capped Ag-NPs. | 155 |
| Figure 5.14: Randel-Sevcik Plot for GBPE capped Ag-NPs. | 157 |
| Figure 6.1: Photograph showing colour of solutions, (a) GBPE extract, (b) H ₂ AuCl ₄ , (c) AgNO ₃ , and Ag-AuNPs..... | 165 |
| Figure 6.2: UV -visible absorption spectra of Au-NPs (Black), Ag-NPs (Red), and Ag-AuNPs (Green)..... | 166 |
| Figure 6.3: FT-IR Spectra of the Green Synthesised Ag-AuNPs (Red curve) and GBPE (Black curve)..... | 167 |
| Figure 6.4: FT-IR Spectra of Au-NPs (Black), Ag-NPs (Red) and Ag-AuNPs (Green)..... | 168 |
| Figure 6.5: XRD pattern of the synthesised GBPE Ag-AuNPs..... | 169 |
| Figure 6.6: XRD pattern of GBPE capped Au, Ag and Ag-AuNPs. | 171 |
| Figure 6.7: HR-TEM image of Ag-AuNPs at 50 nm range (a); lattice fringes (b); selected area electron diffraction (SAED) patterns (c); histogram (d). | 174 |
| Figure 6.8: HR-TEM images of GBPE capped (a) Au-NPs (b) Ag-NPs (c) Ag-AuNPs (2:1) bimetallic alloy nanoparticles. | 176 |
| Figure 6.9: Energy Dispersive Spectroscopy patterns of GBPE Ag-AuNPs..... | 177 |
| Figure 6.10: SAXS pair-distance distribution function (PDDF) of GBPE capped Ag-AuNPs. | 178 |
| Figure 6.11: Size distribution functions weighted by number and intensity. | 179 |

| | |
|--|-----|
| Figure 6.12: Cyclic voltammogram of a Bare GCE (Black Curve) and Ag-AuNPs/GCE (Red Curve) in 0.2 M PBS (pH 7.4) Scan rate 50 mV/s..... | 180 |
| Figure 6.13: Cyclic voltammograms of Ag-AuNPs/ GCE in 0.2M PBS at different scan rates (10-100 mV/s)..... | 182 |
| Figure 6.14: Plots of log current versus log scan rate of GBPE capped Ag-AuNPs. | 183 |
| Figure 6.15: Randel-Sevcik plot for GBPE capped Ag-AuNPs. | 184 |
| Figure 7.1: Schematic diagram of preparing <i>E.coli</i> 0157:H7. | 191 |
| Figure 7.2: Detection of <i>E.coli</i> 0157:H7 in water, Au-NPs before the interaction (Black line) with the interaction of <i>E.coli</i> at different concentration $10^1 - 10^6$ (red, green, navy, blue, purple, yellow). | 192 |
| Figure 7.3: Detection of <i>E.coli</i> 0157:H7 in seawater, Ag-NPs before the interaction (Black line) with the interaction of <i>E.coli</i> at different concentration (other). | 194 |
| Figure 7.4: Schematic procedure for attaching GBPE Ag-AuNPs to <i>E.coli</i> 0157:H7 and its assay detection concept..... | 195 |
| Figure 7.5: Detection of <i>E.coli</i> 0157:H7 in water, AuNPs before the interaction (Black line) with the interaction of <i>E.coli</i> (other) at different concentration. | 197 |
| Figure 7.6: The linear relationship between the $A_{527\text{ nm}} / A_{457\text{ nm}}$ values and the volume of <i>E.coli</i> 0157:H7..... | 198 |
| Figure 8.1: Schematic procedure for detection <i>E.coli</i> 0157:H7 using GBPE Ag/AuNPs/ GCE to <i>E.coli</i> 0157:H7..... | 204 |
| Figure 8.2: GBPE Ag-NPs/ GCE modified electrode with different concentration of <i>E.coli</i> 0157:H7 in PBS solution (0.2M pH 7.4). | 207 |
| Figure 8.3: GBPE Au-NPs/GCE modified electrode with different concentration of <i>E.coli</i> 0157:H7 in PBS solution (0.2M pH 7.4) and the insert represent GBPE Ag-AuNPs before interaction with <i>E.coli</i> 0157:H7..... | 208 |
| Figure 8.4: Calibration curve for electrochemical response corresponding to different concentration of <i>E.coli</i> 0157:H7 bacteria in a range of 10^1 to 10^6 CFU/ mL. | 210 |

CHAPTER ONE

This chapter presents the introduction of the study, and it also contains information about the problem statement, study motivations, aims and objectives. The research approach, and the research hypothesis, are also presented in the chapter.

1 Introduction:

In South Africa, the pathogenic pollution of seawaters is analysed according to local and international guidelines by examining the levels of concentrations of indicator microorganisms such as *Escherichia coli* (*E.coli*) [1]. According to South African guidelines, the average water quality of south African seawaters and recreational waters is generally acceptable however the assessments indicates low water quality for recreational waters during some seasons (mainly in summertime) based on international guidelines [2]. This variation is caused by the absence of *E.coli* and enterococci standards in South African procedures, which were found to be very important when the levels of pollution are low. Therefore, that indicates that *E.coli* and enterococci are more sensitive, making them better indicators for pathogenic pollution in seawaters [3].

Currently, nanoparticles are essential components in the development of nanomaterials; they are more extensive when compared to molecules or atoms that fall under quantum mechanics. Metal nanoparticles (MNP) gained much interest in research due to their properties, availability and specific targeting. Metal nanoparticles can either be monometallic or bimetallic. As the name proposes, monometallic nanoparticles have a single metal, whereas bimetallic nanoparticles consist of two different metals [4–6]. There are different types of

monometallic nanoparticles based on the nature of the existing metal atom such as transition, metallic and magnetic metal nanoparticles Etc. The constituted metal atom determines the properties of these nanoparticles. Monometallic nanoparticles can be functionalised by different methods, and other functional groups can be employed to stabilise their structure. Years ago, monometallic nanoparticles made tremendous interest due to their enhanced chemical and physical properties. Hence, they are engaged in several applications such as catalysis, optical and electronic [7]. Moreover, they have been used as antimicrobial agents against many bacteria such as *Bacillus subtilis* [8], *Streptococcus pyogenes* and *Escherichia coli* [9].

As mentioned before bimetallic nanoparticles are made up of two different metals. Usually, bimetallic nanoparticles are formed by concurrent reduction of two metal ions in the presence of suitable stabilisation strategies such as static-electronic repulsive force and steric hindrance. They have exciting size depended properties such as optical, chemical and electrical properties [10]. Several studies in the field of bimetallic synthesis started about ten years ago, and from both a technological and scientific point of view, bimetallic nanoparticles have gained more interest compared to monometallic nanoparticles due to their properties. The properties of bimetallic nanoparticles are determined by their nanometric sizes and constituting metals. These properties could be different from those of pure elements, and they have unique size-dependent optical, catalytic, thermal and electronic effects. Bimetallic nanoparticles are more critical in the field of catalysis since they have better catalytic properties compared to monometallic nanoparticles. Higher catalytic properties of bimetallic nanoparticles result from their increased surface area [11]. The main advantage of bimetallic nanoparticles is that the catalytic properties of the functionalised nanoparticles can be enhanced to a greater extent, and that is not possible through monometallic catalysis.

Moreover, there is a possibility that the bimetallic nanoparticles could not only show combined properties associated to the individual metals that are present in bimetallic nanoparticles, but also new properties because of a synergy between the two metals [12]. There are two kinds of bimetallic nanoparticles known as core-shell nanoparticles and alloy nanoparticles. The difference between the two types of nanoparticles is the method of synthesis, whereby core-shell nanoparticles are formed from a continuous reduction of the more noble metal salt followed by the decrease in the less noble metal salt. In contrast, bimetallic alloy nanoparticles are created by the simultaneous reduction of the metal salts. Core-shell nanoparticles have the inner part known as a core of the structure and the outer part known as the external shell. Bimetallic alloy nanoparticles are homogeneously scattered at an atomic scale over the whole volume [13]. The reaction conditions under which these bimetallic nanoparticles are prepared to determine the miscibility as well as the structure of the two metals in bimetallic nanoparticles. However, by controlling the reduction rates of the two metals, the morphology and size of the nanoparticles can be controlled. The size and morphology of monometallic nanoparticles and bimetallic nanoparticles are strongly dependent on the conditions and the preparation methods, and they also affect the physicochemical properties of the final product [14]. Literature reports different methods and correlations for the synthesis of other bimetallic nanoparticles, and the findings also show that the catalytic activities of these nanoparticles are also various [15].

Thus, in this study, silver-gold bimetallic alloy nanoparticles were synthesised. Silver-gold bimetallic alloys have gained considerable interest since silver (Ag), and gold (Au) consist of identical lattice constants which are 0.408 and 0.409 respectively. They ultimately form homogenous mixtures over the entire composition, thus resulting in a strong tendency towards the formation of bimetallic alloy nanoparticles. Literature reports different methods for the synthesis of silver-gold bimetallic nanoparticles such as physical and chemical

methods. Using chemical and physical methods for the synthesis of nanoparticles is time-consuming, expensive, and these methods involve hazardous chemicals. Hence in this research, biosynthesis methods were used for the synthesis of silver-gold bimetallic nanoparticles. These biological methods are also termed as green synthesis methods since they employ natural resources such as microbes and plants for synthesis of nanoparticles [16,17]. Advantages of green synthesis methods over physical and chemical methods include the use of non-toxic chemicals, use less time, are cheap, are safe, are environmentally friendly and involve almost negligible industrial waste. Green synthesis methods hold several applications compared to chemical and physical processes, and some are not possible through these methodologies [18].

Literature reports that green synthesised bimetallic nanoparticles have been used before in nanomedicine and they possess promising results. A study by Mitta and co-workers reported silver-selenium bimetallic nanoparticles synthesised using flavonoids, quercetin and gallic acid against cancer cells [19]. Since Bimetallic nanoparticles have a high surface area to volume ratio, they can also be effectively applied in drug delivery because they can cross epithelial cell junction and the blood-brain barrier to reach the target site due to their optical and electrical properties [20].

Thus, in this study, optical and electrochemical sensors were fabricated using silver-gold bimetallic alloy nanoparticles. Grapes and banana peel extract were combined and used as reducing and stabilising agent for the synthesis of silver-gold bimetallic nanoparticles in this study. During the synthesis of nanoparticles, a stabilising agent is essential to prevent agglomeration of nanoparticles which reduces their catalytic properties. Masato and co-workers reported that the electrocatalytic and electrochemical properties of silver-gold bimetallic alloy nanoparticles with varied compositions of silver and gold depending on the composition of silver in the bimetallic alloys. Thus, in bimetallic alloy nanoparticles, a much

higher amount of silver content will not show any improved electrocatalytic reactions. Therefore, when the silver content in bimetallic nanoparticles is above 70 %, it will show low electrocatalytic properties [21]. Silver-gold bimetallic nanoparticles with atomic ratios of 50:25, commonly known as 2:1 ratio, showed improved electrocatalytic and electrochemical properties compare to the atomic ratio of 75:25 [22]. Thus, in this study, the silver-gold bimetallic alloy nanoparticles were synthesised using an atomic ratio of (silver: gold 2:1). Bimetallic alloys of gold with silver, palladium, platinum have portrayed significant results in optical and electrochemical systems. We have chosen silver-gold bimetallic alloy because it has decreased inertness, which causes a high performance as an electrode [23]. Additionally, gold is mostly known to have good biocompatibility, whereas silver is known as the best conductor among metals [24]. Furthermore, silver-gold bimetallic nanoparticles are electroactive and show high catalytic activities.

In recent years, the resistance of pathogens to antibiotics and bactericides because of the development of resistant strains has been a significant concern. Researchers have noticed that some of the antimicrobial agents are toxic and irritant; therefore, there is a need to discover new ways to formulate new safe and cost-effective biocidal materials. It has been reported that nanoparticles could be used in antimicrobial formulations since they possess useful bactericidal materials [25,26]. Silver-gold based compounds are well known as being highly toxic to micro-organisms. The silver-gold ions have previously shown significant biological effects in more than 16 species of micro-organisms, including *E.coli*. They have also been used in the construction of dental resin as antimicrobial components [27–29]. Silver-gold bimetallic alloy nanoparticles have been recorded as effective antimicrobials since they can complement the role of antibiotics in fighting with bacteria [30]. Thus, in this study, an optical and electrochemical sensor for the detection of *E.coli* 0157:H7 was fabricated using green synthesised silver-gold bimetallic alloy nanoparticles.

1.1 Problem Statement:

The bacteriological control of water quality requires the quantification and detection of faecal contamination indicators to signal the presence of potentially harmful pathogens of faecal origin. In particular, the monitoring of recreational beach waters for faecal indicator bacteria is performed using culture-based technologies which require more than a day for laboratory analysis. During this time, swimmers are at risk. Among the indicators of faecal contamination, *Escherichia coli* (*E.coli*) is now recognised in South Africa as the most fatal by the Department of Environmental Affairs; however, most of the standard methods used for the quantification of *E.coli* require at least 8 hours. Therefore, rapid methods for detecting and counting *E.coli* in recreational waters (seawater and freshwater) must be designed and implemented to predict any contamination better and to allow for improved water quality management. Most notably is the fact that the result would be fewer fatality cases associated with *E.coli* infections, particularly in children [31,32]. This need is reinforced by some well-known limitations of currently available methods such as culture-based methods. In this technique, the low specificity of solid media used for the detection of *E.coli* requires (i) biochemical confirmation steps and is unfortunately associated with a delay in the results output by 2 or 3 days (ii) the presence of stressed and starved slow-growing cells or viable but non-culturable (VBNC) micro-organisms in aquatic environments. It is still unclear how the significance of VBNC cells functions in causing diseases.

Nevertheless, these cells should be detected in addition to culturable cells because VBNC cells can potentially become pathogenic when favourable conditions are present. Alternative methods should allow the detection of all viable cells and provide results within a few hours or minutes [33]. A more modern technique is the target capture method, in which the microbial group of interest (or some chemical/molecular/ or biochemical signature of the

group of interest) is removed, tagged or amplified to differentiate it from the remaining material in the sample. The disadvantage of this method is lack of sensitivity since it is recommended that seawater standards are less than one cell per ml and most detection technologies measure sample volumes less than 1 ml. of the three available target capture methods; enzyme/substrate methods may be the first rapid methods adopted since they are based on the same capture technology as currently-approved methods, and their relationship to health risk can be established by demonstrating equivalency to existing procedures [34].

To combat these challenges, while improving the quality of life in humans and surrounding ecosystems through the detection and monitoring of *E.coli* in seawater, a portable and affordable monitoring system should be used. Herein an electrochemical and optical biosensor systems were developed for the detection of *E.coli* in seawater. The importance of developing these devices is derived from the importance of having clean and relatively healthy seawater not only in the Cape Peninsula but along all the shores of South Africa. Contaminated seawater is a health hazard which, in some cases, leads to fatality. Swimmers and surfers swallow significant amounts of water where adult swimmers are prone to ingest between 10 and 100 ml seawater, while children probably consume more massive quantities of water. The highest risk lies primarily with young children, grown-ups and people infected with HIV and (Tuberculosis) TB who are at risk to suffer health hazards by ingesting sewage polluted seawater. Therefore, they need to be informed about the risk and health hazards of diseases such as skin infection, diarrhoea, respiratory tract infection, and hepatitis which they can easily contract by swimming in contaminated seawater. Sewage stakeholders should, therefore, be held accountable for their actions because, in South Africa, it is a fundamental right for all to be exposed to healthy and clean water [35].

It should also be noted that contaminated beaches also negatively affect the economy of South Africa, which rely a great deal on tourism and foreign investments. The likelihood of a

tourist returning to South Africa after falling ill as a result of exposure to contaminated seawater is very slim. For example, tourist and holidaymakers may decide to change their bookings and book holidays in other regions or countries in which case tour operators, hotels and potentially their suppliers may suffer financial losses. This may also affect national parks, transport companies, and other local, tourism-dependent businesses. It should also be remembered that the fisheries sector will feel the economic impacts following *E.coli* contamination. The environmental and physical characteristics of the coast and marine environment also play a role in determining the range and extent of the economic effects [36].

Similarly, the extent to which market confidence in the quality of seafood from the affected area is also a significant factor. With optical and electrochemical sensors available, officials will be able to test seawater promptly and on a more regular basis where results will be available within a matter of seconds or minutes. A positive test will enable officials to alert swimmers immediately of their findings, and if available, a suitable treatment method will be introduced. To any tourist visiting South African shores, this knowledge would be desirable, allowing a sense of security and comfort from the government. The availability of these devices would grow the economy because more tourists would opt to come to a country where there is regular seawater testing indicating transparency from officials. This advantage would also translate to a healthier nation because there would be fewer other infections to swimmers resulting from a lack of exposure to contaminated seawater. On the other hand, ocean ecosystems would be less at risk of deterioration and extinction resulting from exposure to *E.coli* [37].

1.2 Research Aim(s), Motivation and Objectives:

1.2.1 Research Aim(s):

This study aimed at development of nanosensor systems based on silver-gold bimetallic nanoparticles modified optical and electrochemical designs for point-of-site analyses of *E.coli* O157:H7 in seawater.

1.2.2 Objectives:

The investigations of this study had the following objectives:

- Preparation and characterization of silver-gold bimetallic nanoparticles using Ultraviolet-visible spectroscopy (Uv-Vis) and Cyclic Voltammetry (CV).
- To characterise the structure and morphology of the silver-gold bimetallic nanoparticles and silver, gold nanoparticle using Fourier-Transform Infrared Spectroscopy (FT-IR), X-ray diffraction spectroscopy (XRD), Small-angle X-ray scattering (SAXS), High-resolution electron microscopy (HR-TEM).
- To fabricate an optical sensor using UV-vis spectroscopy based on silver-gold nanoparticles.
- To fabricate an electrochemical -sensor using a glassy carbon electrode modified with silver-gold nanoparticles.
- To detect *E.coli* O157:H7 in water using the two fabricated nanosensor systems based on silver-gold nanoparticles as a sensing platform.

1.2.3 Motivation:

Failure of conventional detection methods to detect faecal pollution of recreational waters on time which poses a threat to public health.

1.3 Research Hypothesis:

- The antioxidants, flavanols and polyphenols present in aqueous extract of grapes and banana peel extract may be involved in the bio-reduction of silver nitrate and gold chloride to form nanoparticles.
- The fabricated bimetallic silver-gold nanoparticles would be able to detect *E.coli* 0157:H7 without the support of antibody or aptamers.

1.4 Research Questions:

- Does aqueous grape banana peel extract ultimately reduce silver and gold ions to Ag^0 and Au^0 ?
- Will the functionalised green synthesised nanoparticles be able to detect the targeted bacteria effectively?

1.5 Thesis Outline:

The thesis consists of one chapter responsible for introducing the study, one chapter outlining the literature review followed by seven research-based chapters. Additionally, the final chapter also presents the conclusions and recommendations for future work.

Chapter 1: Introduction; this chapter presents the introduction of the study where the problem statement, motivations, aims and objectives, research approach are outlined

Chapter 2: Literature review; this chapter reviews current literature relevant to the study such as green synthesis methods, including water pollution and the use of nanoparticles for sensors development for detection of pathogens in water.

Chapter 3: Characterisation techniques and methodology. This chapter provides a brief description of the methods used for characterising the nanoparticles. These techniques include UV-visible spectrophotometry, High-resolution electron microscopy, Fourier transform infrared spectroscopy, X-ray diffraction Spectroscopy, Small-angle X-ray scattering spectroscopy. Moreover, in this chapter, the scientific experimental procedures used to obtain data to achieve the aim of the study are explained

Chapter 4: Data on green synthesised gold nanoparticles are presented here.

Chapter 5: Data on green synthesised silver nanoparticles are presented here.

Chapter 6: Data on green synthesised silver-gold nanoparticles are presented.

Chapter 7: Data on the detection of *E.coli* 0157:H7 using the developed optical sensor are presented here.

Chapter 8: Data on the detection of *E.coli* 0157:H7 using the fabricated electrochemical sensor are presented here.

Chapter 9: This chapter presents conclusions based on the overall findings drawn from this research project and based on these conclusions, provides recommendations for future research.

1.6 Research Approach:

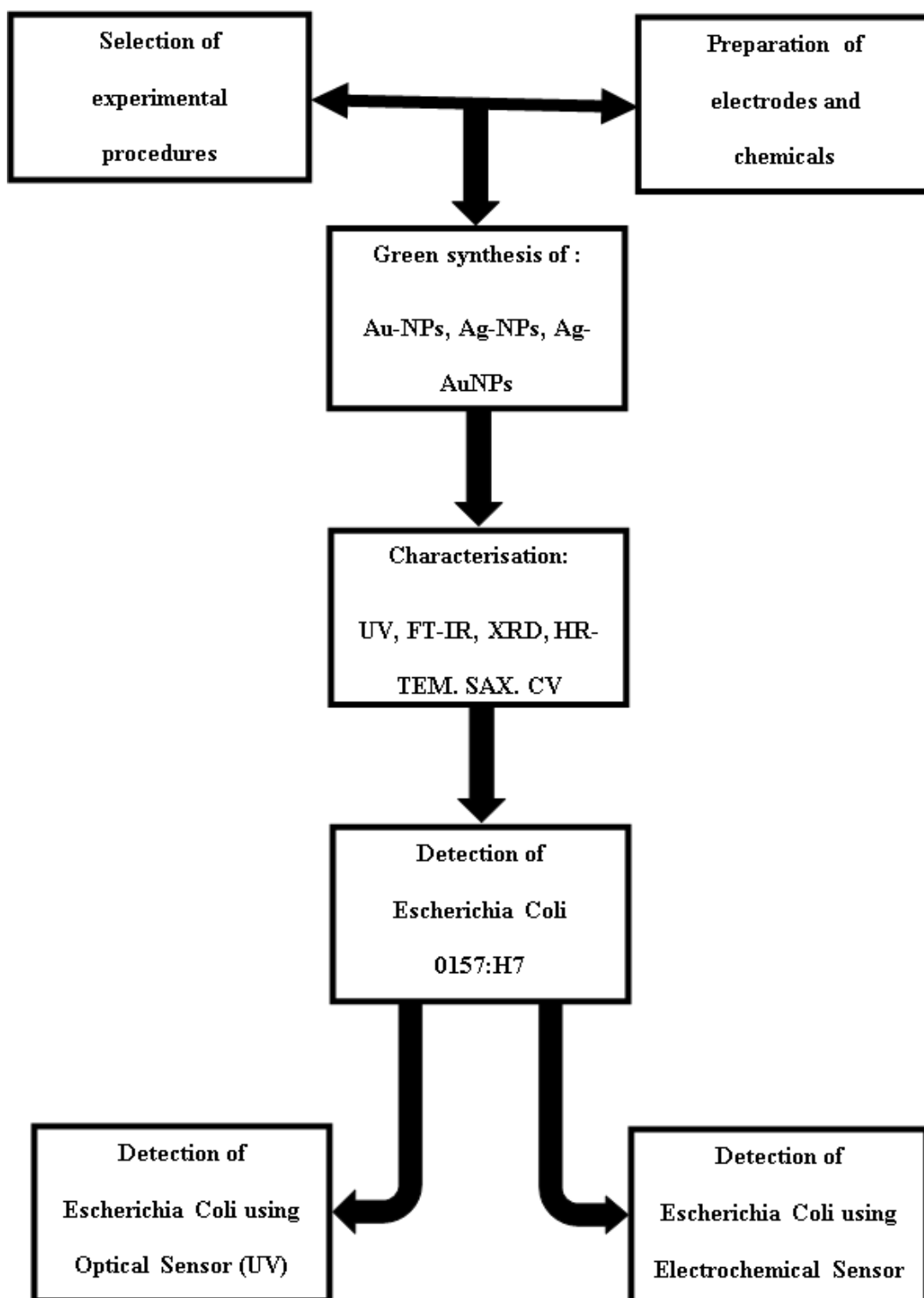


Figure 1.1: Research framework.

References:

- [1] H. Kaur, M. Shorie, P. Sabherwal, Electrochemical aptasensor using boron-carbon nanorods decorated by nickel nanoparticles for detection of *E. coli* O157:H7, *Microchim. Acta.* 187 (2020). <https://doi.org/10.1007/s00604-020-04444-y>.
- [2] M. Kaushik, A. V Nandi, V.B. Mungurwadi, ScienceDirect Portable Sensors for Water Pathogens Detection, *Mater. Today Proc.* 5 (2018) 10821–10826. <https://doi.org/10.1016/j.matpr.2017.12.368>.
- [3] A. Manuscript, *rsc.li/njc*, (2020). <https://doi.org/10.1039/D0NJ01335H>.
- [4] M. Arruebo, R. Fernández-Pacheco, M.R. Ibarra, J. Santamaría, Magnetic nanoparticles for drug delivery The potential of magnetic NPs stems from the intrinsic properties of their magnetic cores combined with their drug loading capability and the biochemical properties that can be bestowed on them by means of a suitab, 2 (2007) 2232. <https://pdfs.semanticscholar.org/1844/8eb43dc235f82cb591983bc8df5ed799984c.pdf>.
- [5] J. Jeevanandam, A. Barhoum, Y.S. Chan, A. Dufresne, M.K. Danquah, Review on nanoparticles and nanostructured materials: History, sources, toxicity and regulations, *Beilstein J. Nanotechnol.* 9 (2018) 1050–1074. <https://doi.org/10.3762/bjnano.9.98>.
- [6] V. Mody, R. Siwale, A. Singh, H. Mody, Introduction to metallic nanoparticles, *J. Pharm. Bioallied Sci.* 2 (2010) 282. <https://doi.org/10.4103/0975-7406.72127>.
- [7] I. Sondi, B. Salopek-sondi, Silver nanoparticles as antimicrobial agent : a case study on *E. coli* as a model for Gram-negative bacteria, 275 (2004) 177–182. <https://doi.org/10.1016/j.jcis.2004.02.012>.
- [8] M. Rai, A. Yadav, A. Gade, Silver nanoparticles as a new generation of antimicrobials, *Biotechnol. Adv.* 27 (2009) 76–83. <https://doi.org/10.1016/j.biotechadv.2008.09.002>.
- [9] A. Nanda, M. Saravanan, Biosynthesis of silver nanoparticles from *Staphylococcus aureus* and its antimicrobial activity against MRSA and MRSE, *Nanomedicine Nanotechnology, Biol. Med.* 5 (2009) 452–456. <https://doi.org/10.1016/j.nano.2009.01.012>.
- [10] S. Devarajan, B. Vimalan, S. Sampath, Phase transfer of Au – Ag alloy nanoparticles from aqueous medium to an organic solvent : effect of aging of surfactant on the formation of Ag-rich alloy compositions, 278 (2004) 126–132. <https://doi.org/10.1016/j.jcis.2004.05.038>.
- [11] A.I.N. Press, *AC AC*, 33 (2006) 28–34. <https://doi.org/10.1016/j.physe.2005.10.012>.
- [12] J. Stejskal, Interaction of conducting polymers, polyaniline and polypyrrole, with organic dyes: polymer morphology control, dye adsorption and photocatalytic decomposition, Springer International Publishing, 2020. <https://doi.org/10.1007/s11696-019-00982-9>.
- [13] A.I. Journal, H.T. Nasrabadi, E. Abbasi, S. Davaran, A. Akbarzadeh, H.T. Nasrabadi,

- E. Abbasi, S. Davaran, M. Kouhi, A. Akbarzadeh, Bimetallic nanoparticles : Preparation , properties , and biomedical applications Bimetallic nanoparticles : Preparation , properties , and biomedical applications, 1401 (2016).
<https://doi.org/10.3109/21691401.2014.953632>.
- [14] J.R. Kitchin, J.K. Nørskov, M.A. Barteau, J.G. Chen, Role of Strain and Ligand Effects in the Modification of the Electronic and Chemical Properties of Bimetallic Surfaces Role of Strain and Ligand Effects in the Modification of the Electronic and Chemical Properties of Bimetallic Surfaces, (2014).
<https://doi.org/10.1103/PhysRevLett.93.156801>.
- [15] K. Wong, C. Chen, K. Wei, V.A.L. Roy, S.M. Chathoth, Diffusion of gold nanoparticles in toluene and water as seen by dynamic light scattering, (2015).
<https://doi.org/10.1007/s11051-015-2965-x>.
- [16] M. Science, D.R. Majumder, Waste to health : Bioleaching of nanoparticles from e-waste and their medical applications Devipriya R Majumder, (2015) 277–286.
- [17] S.M. Roopan, T.V. Surendra, Biosynthetic trends and future aspects of bimetallic nanoparticles and its medicinal applications, (2014). <https://doi.org/10.1007/s00253-014-5736-1>.
- [18] C. Singh, J. Kumar, P. Kumar, B. Singh, K.N. Tiwari, S.K. Mishra, S. Srikrishna, G. Nath, J. Singh, Green synthesis of silver nanoparticles using aqueous leaf extract of *Premna integrifolia* (L .) rich in polyphenols and evaluation of their antioxidant , antibacterial and cytotoxic activity, *Biotechnol. Equip.* 33 (2019) 359–371.
<https://doi.org/10.1080/13102818.2019.1577699>.
- [19] A.K. Mittal, J. Bhaumik, S. Kumar, U.C. Banerjee, *Nanotek & Expo*, 4 (2013) 7439.
- [20] R. Vaidyanathan, K. Kalishwaralal, S. Gopalram, S. Gurunathan, *RE*, 27 (2009) 924–937. <https://doi.org/10.1016/j.biotechadv.2009.08.001>.
- [21] M. Tominaga, T. Shimazoe, M. Nagashima, I. Taniguchi, Composition – activity relationships of carbon electrode-supported bimetallic gold – silver nanoparticles in electrocatalytic oxidation of glucose, 615 (2008) 51–61.
<https://doi.org/10.1016/j.jelechem.2007.11.030>.
- [22] X. Ren, X. Meng, F. Tang, Preparation of Ag – Au nanoparticle and its application to glucose biosensor, 110 (2005) 358–363. <https://doi.org/10.1016/j.snb.2005.02.016>.
- [23] E.I. Iwuoha, A. Wilson, M. Howel, N.G.R. Mathebe, K. Montane-Jaime, D. Narinesingh, A. Guiseppi-Elie, Cytochrome P4502D6 (CYP2D6) Bioelectrode for Fluoxetine, *Anal. Lett.* 37 (2004) 929–941. <https://doi.org/10.1081/AL-120030288>.
- [24] T. Shanmugasundaram, M. Radhakrishnan, V. Gopikrishnan, K. Kadirvelu, R. Balagurunathan, Biocompatible silver, gold and silver/gold alloy nanoparticles for enhanced cancer therapy: In vitro and in vivo perspectives, *Nanoscale*. 9 (2017) 16773–16790. <https://doi.org/10.1039/c7nr04979j>.

- [25] S. Pal, Y.K. Tak, J.M. Song, Does the antibacterial activity of silver nanoparticles depend on the shape of the nanoparticle? A study of the gram-negative bacterium *Escherichia coli*, *Appl. Environ. Microbiol.* 73 (2007) 1712–1720. <https://doi.org/10.1128/AEM.02218-06>.
- [26] M. Fresta, G. Puglisi, G. Giammona, G. Cavallaro, N. Micali, P.M. Furneri, Pefloxacin mesilate- and ofloxacin-loaded polyethylcyanoacrylate nanoparticles: Characterization of the colloidal drug carrier formulation, *J. Pharm. Sci.* 84 (1995) 895–902. <https://doi.org/10.1002/jps.2600840721>.
- [27] R.M. Slawson, M.I.V.A.N. Dyke, H. Lee, J.T. Trevors, Germanium and Silver Resistance, Accumulation, and Toxicity in Microorganisms, 79 (1992) 72–79.
- [28] G. Zhao, S.E. Stevens, Multiple parameters for the comprehensive evaluation of the susceptibility of *Escherichia coli* to the silver ion, 11 (1998) 27–32.
- [29] J.A. Spadaro, T.J. Berger, S.D. Barranco, S.E. Chapin, R.O. Becker, Antibacterial effects of silver electrodes with weak direct current., *Antimicrob. Agents Chemother.* 6 (1974) 637–642. <https://doi.org/10.1128/AAC.6.5.637>.
- [30] R.M. Walczak, J.R. Reynolds, Poly(3,4-alkylenedioxyppyroles): The PxDOPs as versatile yet underutilized electroactive and conducting polymers, *Adv. Mater.* 18 (2006) 1121–1131. <https://doi.org/10.1002/adma.200502312>.
- [31] C. Ruan, F. Yang, C. Lei, J. Deng, Thionine covalently tethered to multilayer horseradish peroxidase in a self-assembled monolayer as an electron-transfer mediator, *Anal. Chem.* 70 (1998) 1721–1725. <https://doi.org/10.1021/ac970605m>.
- [32] J.B.Y.H. Behrendorff, E.M.J. Gillam, Prospects for applying synthetic biology to toxicology: Future opportunities and current limitations for the repurposing of cytochrome P450 systems, *Chem. Res. Toxicol.* 30 (2016) 453–468. <https://doi.org/10.1021/acs.chemrestox.6b00396>.
- [33] T. Ramamurthy, A. Ghosh, G.P. Pazhani, S. Shinoda, Current perspectives on viable but non-culturable (VBNC) pathogenic bacteria, *Front. Public Heal.* 2 (2014) 1–9. <https://doi.org/10.3389/fpubh.2014.00103>.
- [34] P. Munyao, Amperometric biosensor systems prepared on poly(aniline-ferrocenium hexafluorophosphate) composites doped with poly(vinyl sulfonic acid sodium salt)., (2008).
- [35] S.N. Mailu, T.T. Waryo, P.M. Ndagili, F.R. Ngece, A.A. Baleg, P.G. Baker, E.I. Iwuoha, Determination of anthracene on Ag-Au alloy nanoparticles/overoxidized-polypyrrole composite modified glassy carbon electrodes, *Sensors (Switzerland)*. 10 (2010) 9449–9465. <https://doi.org/10.3390/s101009449>.
- [36] P.M. Ndagili, R.A. Olowu, S.N. Mailu, R.F. Ngece, A. Jijana, A. Williams, F. Iftikhar, P.G.L. Baker, E.I. Iwuoha, Impedimetric response of a label-free genosensor prepared on a 3-mercaptopropionic acid capped gallium selenide nanocrystal modified

gold electrode, *Int. J. Electrochem. Sci.* 6 (2011) 1438–1453.

- [37] R. F. Ngece, Nanoparticulate of silver-modified poly (8-anilino-1-naphthalene sulphonic acid) nanobiosensor systems for the determination of Tuberculosis treatment drugs, (2011).

CHAPTER TWO

This chapter provides and discusses literature content relevant to this study with emphasis on green synthesis processes, the bacteria Escherichia Coli and information with regards to sensor construction, in particular, the for the detection of Escherichia Coli.

2 Literature Review:

2.1 Nanoparticles:

In the past ten years, nanoparticles have been the topic of concern, and recent advances have made nanoparticles far more attractive [1]. Nanoparticles are tiny particles; Aragay defines nanoparticles as objects that range from 1 to 100 nanometres in size [2]. Nanoparticles are building blocks of nanotechnology which is the combination of principles involving chemical, physical and biological material [3]. They are used in many fields such as electronic engineering, pharmacology, agriculture and medicine [4–6] and literature indicates that nanoparticles have better properties based on specific characteristics such morphology, distribution and size and are chemically active compared to the bulk materials due to their high surface energy [7]. There are two approaches for the synthesis of nanomaterials; Top-down and Bottom-up approach, as shown in **Figure 2.1**. The top-down approach refers to cutting or breaking of bulk material to obtain nano-sized particles. Size reduction is obtained by different chemical and physical techniques.

In contrast, the bottom-up approach refers to the build-up of materials from the bottom, molecule by molecule or atom by atom. In this approach, nanoparticles can be synthesised

using chemical and biological methods. Both approaches play an important role in modern industry and most likely in nanotechnology, and each approach has its advantages and disadvantages as shown in **Table 2.1**[8].

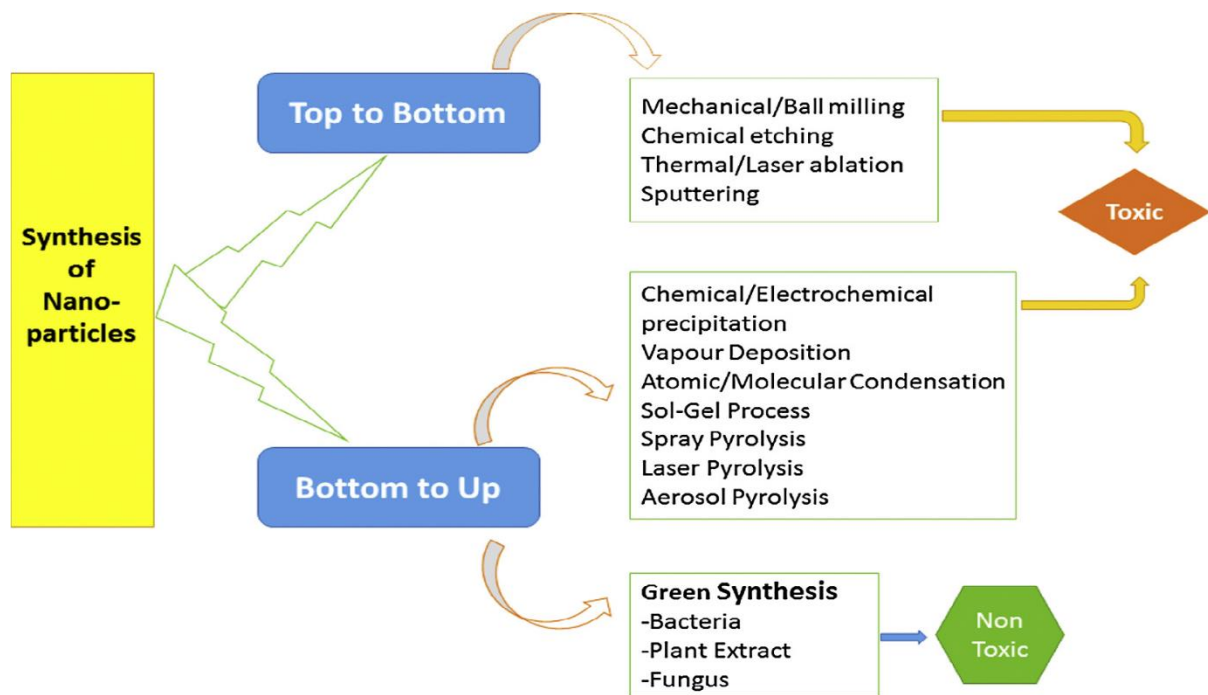


Figure 2.1: A diagram illustrating the types of Synthesis for nanomaterials [9].

Table 2.1: Advantages and disadvantages of Bottom-up and Top-down approaches

| Approaches | Advantages | Disadvantages |
|-------------------|---|--|
| Bottom-up | <ul style="list-style-type: none">• Provide Self-assembly methods with low-cost and rapid for production of nanostructured materials• More homogenous features with minimum defects• Allow smaller geometries | <ul style="list-style-type: none">• Chemical purification of nanomaterials is needed• Difficult to achieve large scale production |
| Top-down | <ul style="list-style-type: none">• Old and well understood approach• Well-developed methods and popular in micro fabricating• Reproducible methods | <ul style="list-style-type: none">• Expensive approach compared to self-assembly approach• Surface imperfection• As elements become smaller, they become more sensitive to defects• Limited for nanofabrication |

2.2 Green method synthesis:

The term "green chemistry" can be defined as the technique that develops a chemical process aimed to eliminate or reduce the generation and use of hazardous substances. Green chemistry is under the umbrella of a sustainable environment, and the concept of green chemistry methods was established in the United States by the Environmental Protection Agency (EPA) in 1990 as a Pollution Prevention Act [10,11]. Then in 1998, Paul Anastas and

John Warner constructed a set of principles of green chemistry to guide scientist and researchers to practise green chemistry. The primary purpose of these principles was to reduce the environmental and health effects of chemical production and to highlight priorities for the development of green chemistry [12]. Currently, in the research field, green synthesis methods for synthesis of nanoparticles are adopted as an alternative to the physical and chemical methods which are considered as toxic, non-compatible, and costly. In contrast, green synthesis methods are considered as eco-friendly, compatible, and cheaper approach.

These environmentally friendly methods of biological production of nanoparticles provide rates of synthesis that are faster compared to those of physical and chemical methods. In green chemistry, the preparation of nanoparticles has two main steps (i) choice of non-toxic and environmentally friendly reducing and stabilising agent. (ii) Choice of solvent used for synthesis. In literature, most of the synthetic approaches reported, use organic solvent such as water because of the hydrophobic nature of the capping materials. Although preparation of nanoparticles requires two steps, the synthesis is a one-step procedure [8]. **Figure 2.2** show examples of natural products that can be used as capping and reducing agents in green synthesis of nanoparticles. In the present study, grapes and banana peel were used as reducing and stabilising materials and water as an organic solvent for the synthesis of metal alloy nanoparticles. Preparation of metal nanoparticles involves the reduction of metal ions in solutions [13,14].

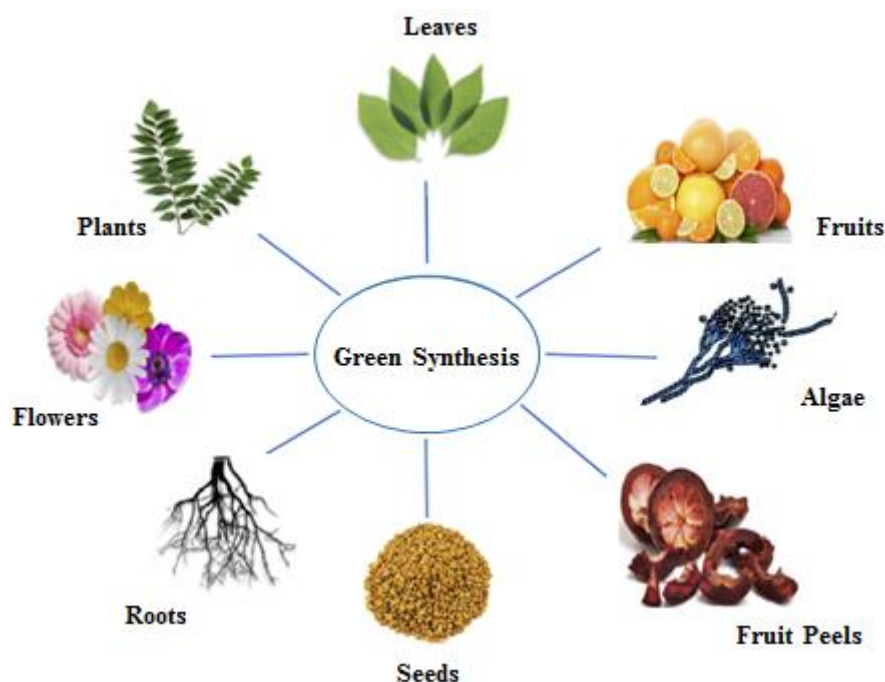


Figure 2.2: Examples of natural products that can be used to synthesise nanoparticles using green chemistry.

2.3 Types of Green synthesis methods:

2.3.1 Ultrasound Synthesis Method:

The method known as ultrasound method is considered as one of the safe methods for the environment hence is taken as a green synthesis approach. The ultrasound method is used for synthesising metal nanoparticles and is reported as one of the quickest methods. The main advantage of this method is that it produces simple, environmentally friendly non-toxic nanoparticles, and it can improve the yield of nanoparticles. **Figure 2.3** shows an example of ultrasound method. In ultrasound methods, the process of synthesis can control size distribution and morphology of the nanoparticles. In a narrower range by thermal convection, this method is effective in size distribution due to penetration property of ultrasonic irradiation which results in uniform activation energy for the reaction solution. In

environmental chemistry, ultrasound is used frequently since it allows activation energy, reduces reaction times and avoids the addition of phase transfer agents [15–17]

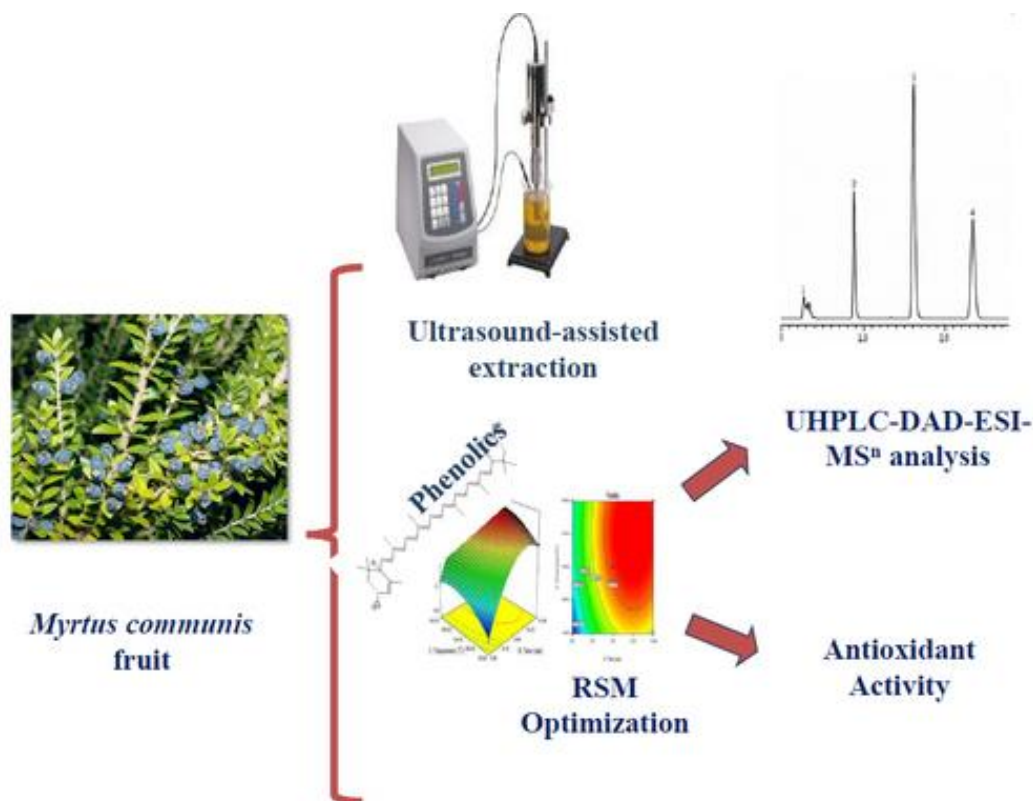


Figure 2.3: Schematic representation of Ultrasound method [18].

2.3.2 Photocatalysis Synthesis Method:

Another method that plays a crucial role in green synthesis methods is photocatalysis method which provides an alternative to classical chemistry. Photocatalysis methods use cells and enzymes in mild conditions to provide suitable tools for industrial reactions, and also with significant control over the stereo-, regio- and chemoselectivity using a specific enzyme and with the use of heavy metals. Moreover, the activation through photocatalysis under visible light could be considered as another method in chemistry. Photocatalysis methods are gaining interest since they avoid the use of heavy metals. **Figure 2.4** shows an example of

Photocatalysis method. Light is abundant, non-toxic and does not generate waste which makes it environmentally friendly and more suitable for green synthesis methods and in this technique, it is considered as an ideal reagent, and the reaction process of this technique is usually driven by photo redox catalysts, as well as organometallic complexes containing ruthenium and iridium [15].

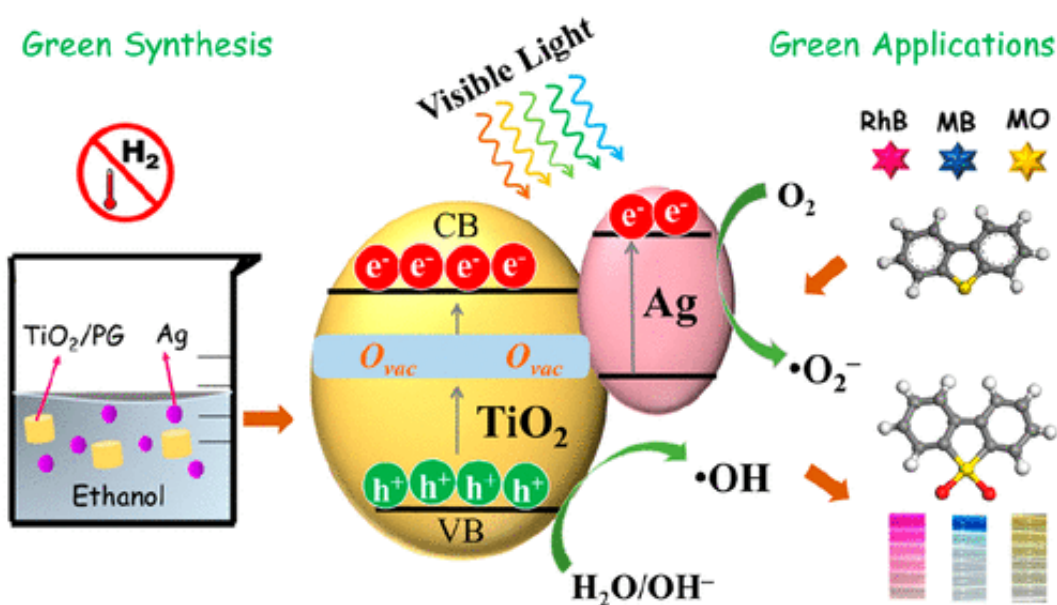


Figure 2.4: Schematic representation of Photocatalysis method [19].

2.3.3 Biotransformation Synthesis Method:

Biotransformation is considered as a green chemistry method, and it plays a significant role in the development of chiral chemistry in aqueous media. In biotransformation methods, a biocatalyst is used for the synthesis of organic chemicals and the mediation of a chemical reaction as shown in **Figure 2.5**. Currently, this technique is widely employed in many industries such as chiral drug formation, vitamin production and animal feed-stock.

Nowadays, the public regulations force industries to employ green methods in their manufacturing process since they use clean chemicals, safe and fewer toxicity effluents [20].

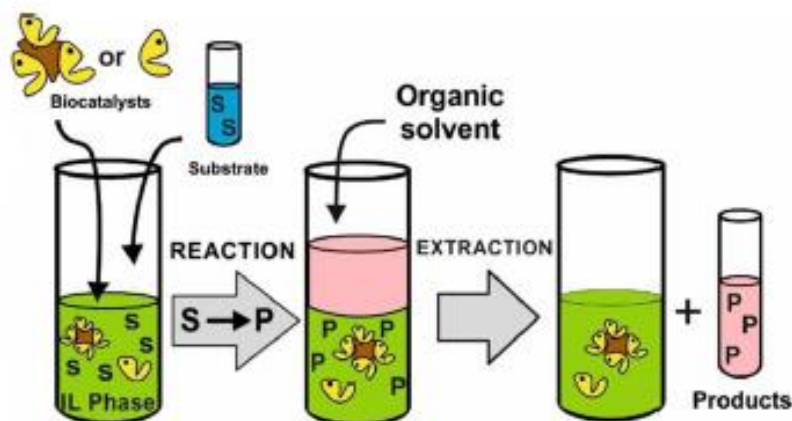


Figure 2.5: A typical presentation of Biotransformation method [21].

2.3.4 Conventional Heating Synthesis Method:

Conventional heating is the most widely used method in green synthesis. In this method, oil baths are used to heat the walls of the reactors through convection or conduction. In the conventional heating method, the process usually starts to generate heat from the source, and then it is transferred from the external to the internal part of the used material via radiation, conduction and convection [22]. This particular method can functionalise nanoparticles in enormous quantities in a short period producing nanoparticles with well-defined shape and size. However, this method is considered as one of the complicated methods, outdated and inefficient. **Figure 2.6** shows an example of conventional heating method for synthesis of nanoparticles. Recently there is an increasing demand for green synthesised nanoparticles, that produce non-toxic waste products during the manufacturing process, which are cheap

and environmentally friendly. Current studies have already reported successful results through biological processes using biotechnological techniques that are considered safe for the fabrication of nanoparticles, which are now replacing conventional chemical and physical techniques [23].

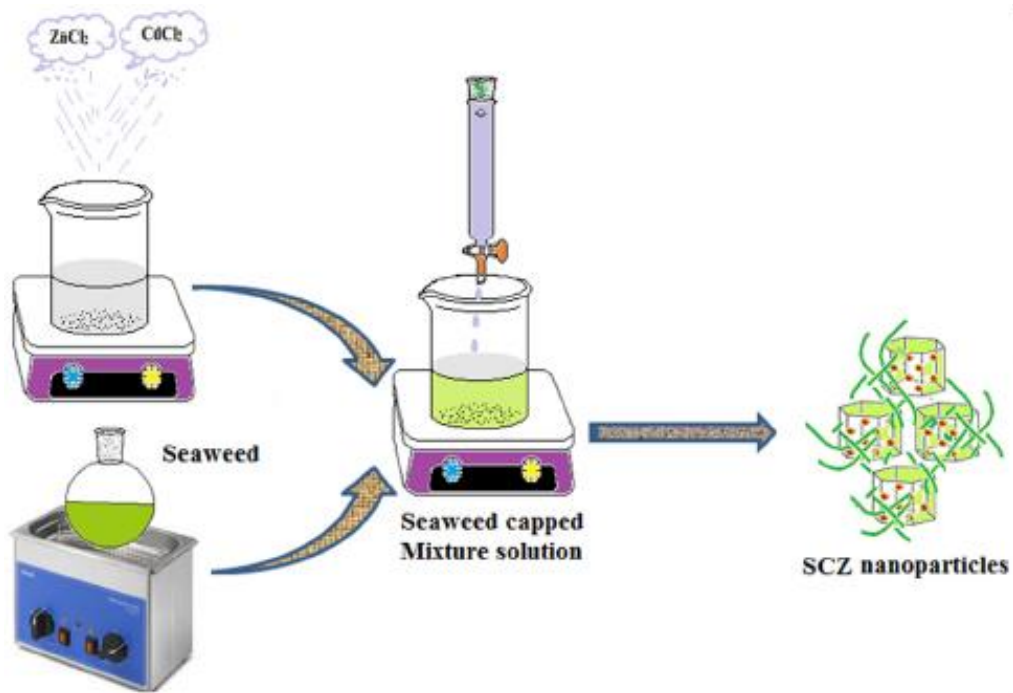


Figure 2.6: A schematic representation of conventional heating method for synthesis of nanoparticles [24].

2.4 Types of green synthesised nanoparticles:

For a long time, nanoparticles have been produced chemically and physically. Green biochemical methods introduced the natural routes that helped researchers to functionalise and control the size and morphology of nanoparticles [25]. Present researchers focus on the production of metallic nanoparticles of noble metals such as platinum, silver, palladium and gold since they exhibit advanced properties based on the morphology and dimension of the particles. Metal nanoparticles (MNPs) have broad applications in the field of electrochemical

analysis, photonics, electronics, optical devices and biomedical materials. The synthesis of MNPs via biological resources are available in nature, including fruit, plants and micro-organisms is flourishing as an important area of research [26]. Different methods have been reported for synthesising different nanoparticles as discussed below.

Copper nanoparticles (Cu-NPs): Recently Niharika Nagar and Vijay Devra, reported the synthesis of copper nanoparticles using *Azadirachta indica* (*A. indica*) leaf well known as neem. This Indian medicinal plant is from the family Meliaceae and is mostly found in India and nearby sub-Saharan African countries. During the synthesis of Cu-NPs *A.indica* leaf extract was used as the reducing and capping agent and the biomolecules that are present in the leaf were able to reduce and stabilise the synthesised Cu-NPs [27]. Literature also reports the synthesis of copper nanoparticles through green synthesis method using *Plantago Asiatica* leaf extract [28], *Ocimum sanctum* leaf broth [29] and many other plant extracts, were also used as reducing and capping agents.

Silver nanoparticles (Ag-NPs): Silver is famous for its bacteriological control against almost all micro-organisms. Literature reports several studies that have used green synthesis methods for the synthesis of silver nanoparticles. For example, Li Yumei and co-workers, synthesised Ag-NPs using *Arthrobacter Sp.B4*. The obtained nanoparticles displayed a face-centred cubic structure with size ranging from 9 - 72 nm in less 20 min [30]. Thus this study proves that the use of green synthesis methods to synthesise nanoparticles is faster compared to intracellular methods which take one day or more to complete the reaction [31,32].

Moreover, Alsalhi and co-workers, conducted a study where Ag-NPs were synthesised using *Pimpinella anisum* seed [33], while Masum and co-workers reported on the synthesis of silver nanoparticles using *P.emblica* fruit extract [34]. Other biosynthesis studies conducted on silver nanoparticles include those of Samari and co-workers who used mango leaf extract

[35], Carica papaya peel extract [36] and Aloe vera plant extracts [34, 35]. Thus far silver nanoparticles are the most commonly used nanoparticles.

Gold nanoparticles (Au-NPs): Existing literature reports successfully functionalised gold nanoparticles through green synthetic methods. These reports include but are not limited to the work of Abootorabi and co-workers who employed Berberis and Crocus sativus plants for the synthesis of gold nanoparticles [39]; and Karuppiah who used Justicia glauca leaves [40] and Gopinath and co-workers who synthesised gold nanoparticles from fruit extract of Terminalia arjuna [41]. Moreover, gold nanoparticles were also successfully synthesised from the extract of onion peels [42].

However, although the literature reveals many studies for biological synthesis of silver and gold nanoparticles using plants leaves and fruit, not much has been reported on the synthesis of these nanoparticles using a combination of extracts. The focus of this study was on the use of combined extracts for the synthesis of bimetallic nanoparticles.

2.4.1 Synthesis of Silver and Gold using Banana peels and Grapes:

Banana is classified as a family of Musaceae species [43], and its scientific name is known as Musa Paradaisica [44]. Peels from consumed bananas are regarded as waste, and at times they add to real environmental problems; thus, it is crucial to find a use of these banana peels. **Figure 2.7** shows a picture of a banana peel sample. Studies report that banana peels have been used to heal wounds and also used in the reduction of swelling and pain in burnt areas. Recent studies indicate that banana peels have large amounts of phenols which play a vital role in the formation of metallic nanoparticles.

Additionally, it has also been reported that banana peels are the best antioxidants and are rich in phytochemical compounds [45] catecholamines, β -carotene, gallic acid, D-Limonene,

carotenoid and cellulose [44,46] as indicated in **Table 2.2** column 1. Fatemeh and co-workers reported that gallic acid and phenolic are more abundant in peels than in pulp, thus making the banana peels better antioxidants than its pulp [47]. As such, banana peels have been reported in successful synthesis of silver, palladium and other nanoparticles (NPs) resultant from the massive amounts of phenols and pectin present in them.



Figure 2.7: Picture of Banana peel sample.

Similarly, grapes have such properties as well, and traditionally they have been used as wound healers and as anti-inflammatory agents. Grapes are classified as a family of Vitaceae species and are known to have polyphenolic compounds which are present in all parts of the grape such as the pulp, the skin and the seeds. **Figure 2.8** shows an image of a grape sample. Phenolic compounds found in grapes are kaempferol, ellagic acid, myricetin, gallic acid, and quercetin, as shown in **Table 2.2**, column 2. These compounds are believed to have antioxidants and antimicrobial activities and have since found particular interest in different fields, mainly in medicine. Myricetin is one of the most abundant antioxidants in grapes and has been reported to play a significant role in the preparation of gold nanoparticles [46] as

confirmed by Reddy and co-workers who described the reaction sequence for green synthesis of gold nanoparticles as follows:

Reduction process: Gold salt ($\text{HAuCl}_4 \cdot 3\text{H}_2\text{O}$) + $\text{H}_2\text{O} \rightarrow \text{Au}^+$ ions

Au^+ ions + extract ($-\text{OH}$ groups + carboxyl groups) $\rightarrow \text{Au}^0$ (AuNPs) + extract (carboxyl groups)

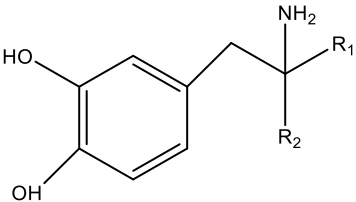
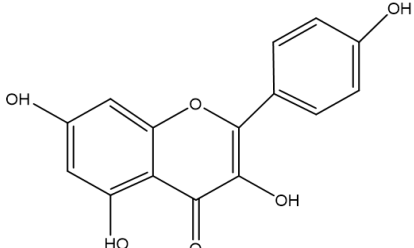
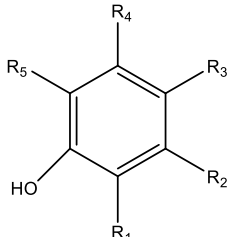
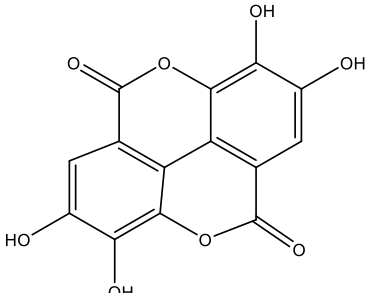
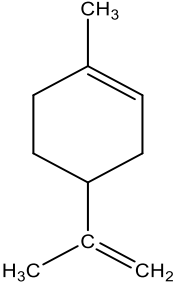
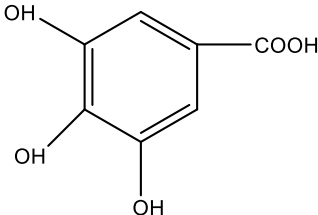
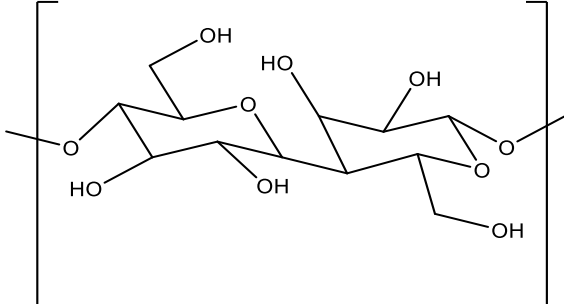
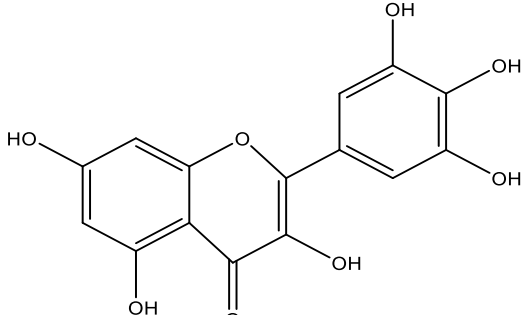
Stabilizing process: Au^0 (AuNPs) + extract (carboxyl groups) \rightarrow Stabilized AuNPs [48].

This study reports for the first time a method that uses a combination of grape and banana peel extracts for the synthesis of gold nanoparticles without using any form of external chemical stabilising or reducing agents.



Figure 2.8: An image of a Grape sample.

Table 2.2: Possible biological compounds in banana peel extract responsible for bio-reduction of metal salts.

| Column 1: Banana Peel | Column 2: Grapes |
|---|--|
| <p style="text-align: center;">Catecholamine</p>  | <p style="text-align: center;">Kaempferol</p>  |
| <p style="text-align: center;">Phenolic Compounds</p>  | <p style="text-align: center;">Ellagic Acid</p>  |
| <p style="text-align: center;">D-Limonene</p>  | <p style="text-align: center;">Gallic Acid</p>  |
| <p style="text-align: center;">Cellulose</p>  | <p style="text-align: center;">Myricetin</p>  |

2.5 Sensor development based on green synthesised nanoparticles for water detection:

The use of nanoparticles (NPs) for the development of sensors is relatively a new approach in research. However, researchers have already reported different studies incorporating NPs into biodevices. Metal nanoparticles (MNPs) are widely used due to their unique properties [49], and several studies report the effect of metal ions (M^+) in water as disinfectants [50,51]. Studies report MNPs such as zinc, copper, silver, gold, titanium and magnesium for development of sensors to detect various micro-organism in water [52]. Gold and silver NPs are the most used MNPs and reported in studies both on the development of biosensors and chemical sensors due to their well-known antimicrobial properties, high surface area and easy bio-functionalisation [53]. Metal nanoparticles such as silver and gold have metal ions that can destroy bacteria, fungi and other pathogens [54–57]. Literature review reports various proposed mechanisms that prove the effectiveness of silver and gold nanoparticles on micro-organisms as antimicrobial. Ag-NPs and Au-NPs are positively charged; therefore, they can easily interact with the cell membrane, which is negatively charged [58]. **Figure 2.9** is an example of Ag-NPs of different sizes and shapes attacking bacterial cells. As seen from the figure, when the nanoparticles attach to the surface of a microbial cell-wall, they bind to the enzyme because of their surface charge through sulfhydryl (-SH) groups, and they disrupt and damage the cell membrane and the enter inside of the bacteria and release metal ions. After that, the reactive oxygen species (ROS) will be released due to the physicochemical surface modification between NPs and bacteria. Then the M^+ will react with proteins and disable it [59]. This will cause protein denaturation, mitochondrial dysfunction, DNA destruction, and leads to cell death [60]. Literature also reports that the binding of metal ions may also occur through electrostatic interactions. The work of Jongjinakool and co-workers, indicates the development a colorimetric sensor based on gold NPs for the detection of cysteine and their

findings support literature, where they observe binding of Au-NPs and cysteine through sulphhydryl (-SH) and amino (-NH₂) groups via non-covalent interactions. The size of MNPs has a significant impact on antimicrobial activity, the smaller they are, the better antimicrobial properties they have, as a result of the increased surface to volume ratio [61]. Some studies report that MNPs have been used in medical equipment as coatings for filters and other parts of antimicrobial properties.

Several studies in literature reviews report that MNPs have been used in the development of sensors for water treatment. To mention a few, the work of Ruth Chrisnasari and co-workers established a DNA biosensor based on Ag-NPs for the detection of *E.coli* [62]. Jin and co-workers reported lanthanide-doped Au-NPs for the detection of *E.coli* in water samples based on fluorescence resonance energy [63]. Raj and co-workers studied the interaction between cysteine and Au-NPs in order to detect *E.coli* using cysteine modified Au-NPs [64]. However, the studies mentioned above are part of the current conventional methods used to synthesise NPs, which have their inherent disadvantages.

Green NPs-based sensors are a new alternative method for fabricating low-cost, simple, fast and easy disposable analytical sensors for many application areas including water treatment. NPs of noble metals such as silver and gold have simple synthesis methods, are easily modified, are biocompatibility and have low cytotoxicity [65–67]. Hence due to these advantages, MNPs obtained through green synthesis methods have an excellent potential for application in different fields [68–70] such as drug delivery, environmental monitoring and biological analysis [71–75]. Green synthesised MNPs have slower kinetics which makes them have better manipulation, stabilisation and control over crystal growth. Recently Gayda and co-workers reported green synthesised NPs as a platform for biosensor development [76]. Chandrakant and co-workers reported polysaccharide stabilised gold nanoparticles synthesised via green methods for vapour sensing [77]. Silva-De Hoyos and his co-workers

fabricated a calorimetric and plasmon sensor based on Au-NPs as a sensing platform for detecting Zn^{2+} , Cu^{2+} , Sr^{2+} and Ca^{2+} in water. In this project, they synthesised the Au-NPs through green synthesis using green tea extract as a reducing and stabilising agent [78].

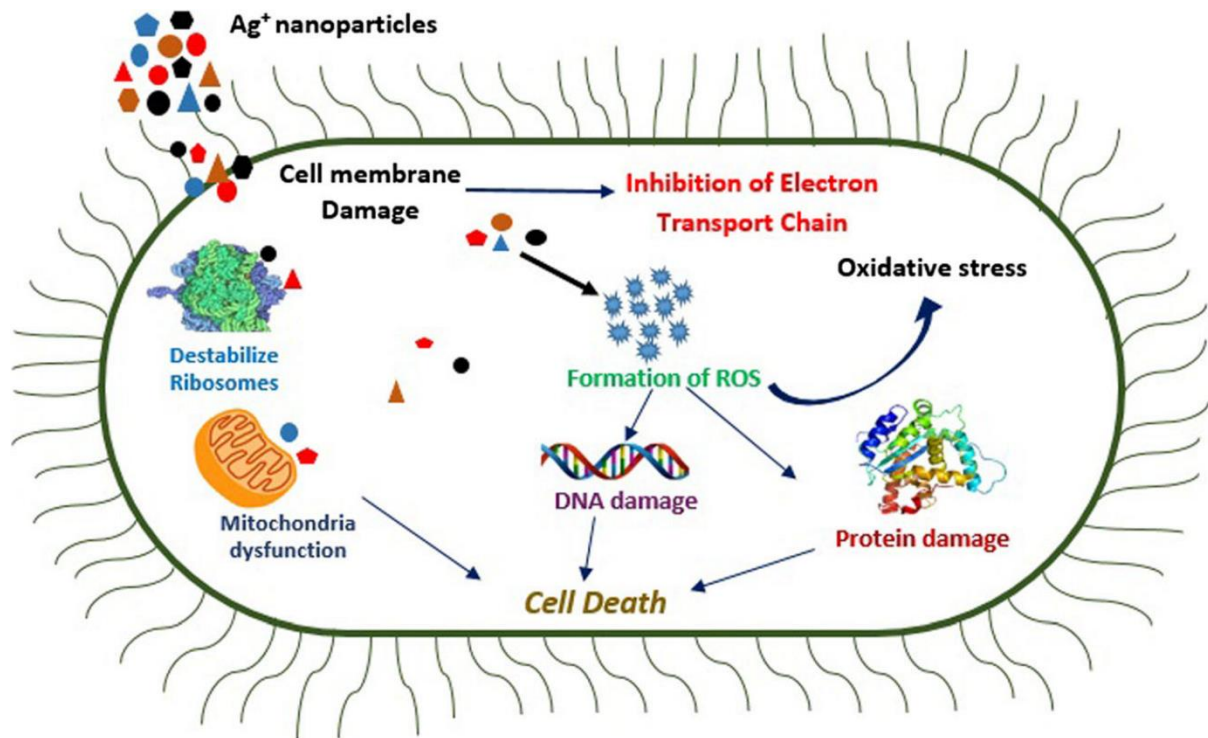


Figure 2.9: Typical representation of nanoparticles attacking and kill bacteria cells [79].

2.6 Water Pollution:

Water safety is the primary concern for public health and conservation of the natural environment. In several countries like South Africa and India, the accessibility of clean water has remained a challenge till today. Water pollution can be defined as contamination of water bodies such as seas, water supply, rivers and lakes by human activities. Studies report that seawater and recreational water is polluted by sewage contamination, and factors such as

climate change and the increasing growth of the human population contribute to water pollution. As mentioned earlier swimming and consumption of poor-quality water has adverse effects against human health. Detection and quantification of pathogens are essential to predict the infection risk associated with surface waters and recreational water facilities [80–82].

Human waterborne diseases result from exposure to water that is contaminated or untreated. According to WHO pathogen contamination is a significant issue throughout the world, and the health protection programs in South Africa reveal studies that show a high level of contamination in seawater by micro-organisms such as *E.coli* and other pathogens. Thousands of deaths each year are caused by polluted water, especially amongst children under the age of 5 years [83,84]. Several pathogenic waterborne outbreaks have been recorded worldwide. In Sweden, they reported that more than 27 000 people were infected by cryptosporidium, which is caused by drinking contaminated water in November 2010. The water sources in South Africa has been under growing threat of pollution [85,86]. South Africa is known as one of the dry places, so the demand for water between humans and animals is high which cause humans to end-up using the same water as animals such as cattle which exposes the water to microbial contamination. Another issue in South Africa is the growing number of informal settlements that do not have proper water supply and appropriate sanitary infrastructure, which may lead to many waterborne diseases. Olaniran and co-workers examined the microbiological quality for domestic use in two rivers, namely "Palmiet and Umngeni river" in Durban, South Africa; and observed that the microbiological quality for both rivers was low. They were above the South African recommended limits, indicating that the water was not safe for human consumption before treatment [87]. In 2017 a study conducted by Leslie and co-workers shows that the Cape Town seawater and recreational beaches were contaminated by common household chemicals, pharmaceuticals

and microbial pollution [88]. The access of safe drinking water in South Africa is known as a fundamental human right; therefore, the current technologies used for the treatment of water in South Africa needs to be improved.

2.7 *E. coli* Pollution in Freshwater and Seawater:

Escherichia coli is a gram-negative, rod-shaped bacterium, as shown in **Figure 2.10** and it is well known as *E.coli*. This bacterium is usually in the lowest guts of warm-blooded animal or the intestines; it may also be found in the guts of human beings. This type of bacterium may or may not be mobile since some of them have flagellated rods, and some are not. Some strains of *E.coli* are harmless, but there is one dangerous strain called *E.coli* 0157:H7. *E.coli* 0157:H7 strain is well known as the most aggressive strain among hundreds of bacteria, due to its ability to produce a dominant toxin known as Shiga toxin that can cause diarrhoea, kidney failure, haemolytic uremic syndrome or death. *E.coli* 0157:H7 bacteria was recognised in 1982 for the first time as a cause of illness during an outbreak which caused bloody diarrhoea in people who drank contaminated water. According to the report made by Tam and co-workers, 600 million cases of human diarrhoea and 800 000 worldwide deaths mainly in children under the age of 5 years were due to *E.coli* 0157:H7 [89]. *E.coli* in water indicates that the water source or water supply is contaminated with human or animal waste. According to WHO and national standards when viable cell numbers of *E.coli* in water ranges between 10 – 100 CFU / mL, the water is considered to be at intermediate risk and high risk is declared when the *E.coli* cells range between 100 - 1000 CFU / mL [90,91]. However, the South African National Standards (SANS) declares drinking water to be safe only when there are no cells of *E.coli* detected [92]. The presence of micro-organisms such as *E.coli*, Mycobacterium avium, Listeria monocytogenes, salmonella and viruses like Noro-

virus, Hepatitis A and others in freshwater or seawater indicate a sign of pollution [93] and possess a significant risk to human health. Previous reports of microbiological quality of South African rivers showed that the water source was unsafe for human consumption in some areas. Furthermore, they report that *E.coli* was one of the primary potential pathogens found [94]. Thus, the objective of this study is to functionalise a sensor based on nanoparticles as a sensing platform for seawater monitoring of *E.coli* O157:H7.

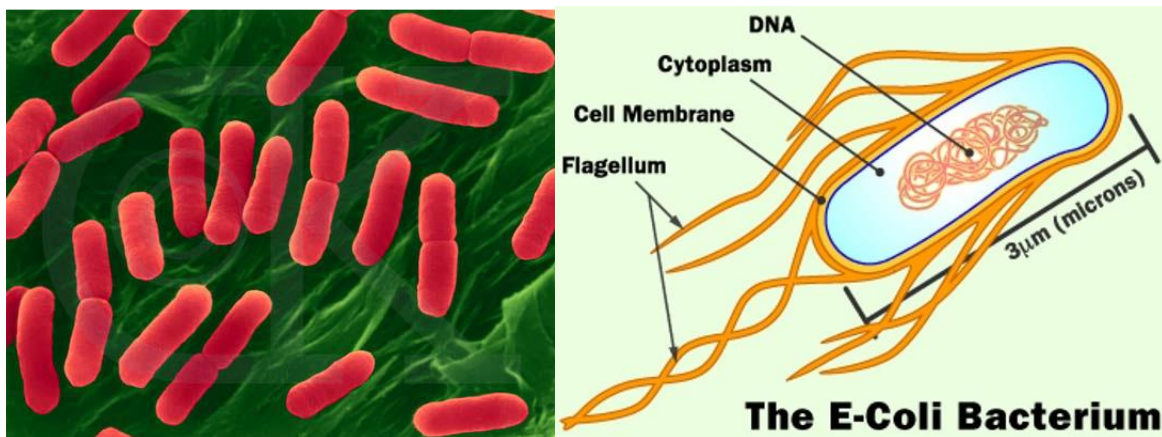


Figure 2.10: Escherichia coli structure [93].

2.8 Chemical Sensors for the detection of *E.coli*:

A sensor is characterised as a device that detects or measures a physical property then responds, shows or records it. In general, there are three types of sensors which are chemical, physical and biosensors. A chemical sensor is an apparatus that responds to a specific analyte in a particular manner into a measurable signal, through a synthetic reaction that can be quantitative or selective. On the other hand, a physical sensor is an apparatus that measures

the physical amount, for example, temperature and pressure. In comparison, a biosensor is an apparatus that uses a biological sensing component for detection [95].

In this study, chemical sensors were fabricated to detect *E.coli* 0157:H7. A chemical sensor is termed as a device that can detect and determine chemical qualities or interactions between the sensor and the analyte. Then the sensor converts the biochemical or chemical data of a quantitative type into an electronic signal. This type of sensor has a transducer that is capable of converting the response into a detectable signal into a computer, and the selective layer separates the response of the analyte from its immediate surroundings as shown in **Figure 2.11**. Chemical sensors are categorised based on the material that is detected, such as thermal and mass, optical or electrical properties. These sensors are fabricated in order to detect and respond to a specific analyte in a solid, liquid or gaseous state. Recently optical and electrochemical sensors have gained more interest compared to thermal and mass sensors due to their outstanding detection, low cost, experimental simplicity and capability. They are the best among the currently available sensors for commercialisation and are employed at different sectors such as agricultural, environmental, as well as in clinical analyses [96].

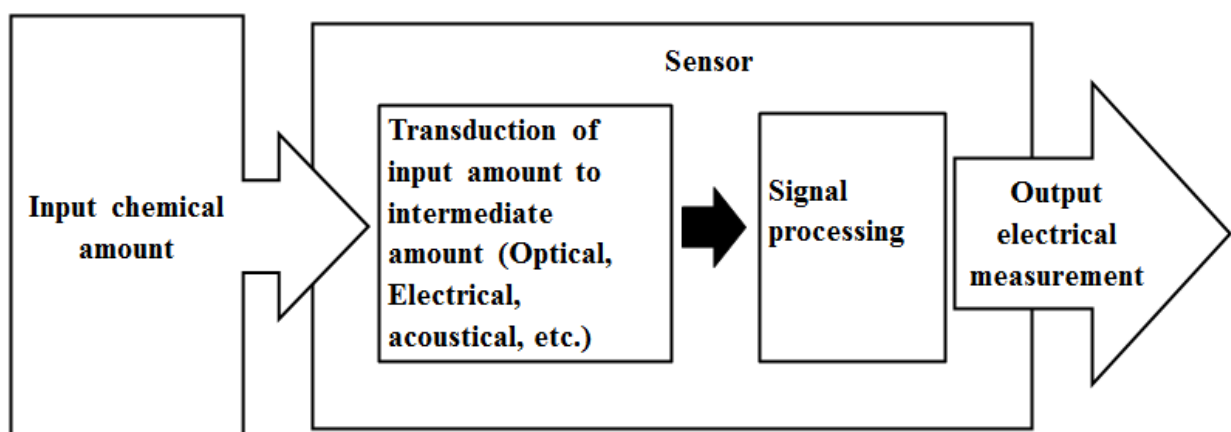


Figure 2.11: A typical representation diagram of a chemical sensor.

Literature reviews report several studies that use the current conventional methods for the detection of *E.coli* 0157:H7 in water and food using Plate Count Enumeration Method and Membrane Filter (MF) technique [97], Multiple Tube Fermentation (MTF) [98]. Colony counting and culture-based methods [99] enzyme-linked immunosorbent assay [100] and polymerase chain reaction (PCR) [101] are also widely used. This is due to their effectiveness and high reliability; however, these methods have their drawbacks such as the use of toxic substances, are time-consuming assays and are high cost, resulting to limited applications of these methods. Optical and electrochemical methods as quick microbial detection methods are developed and are promising methods due to their simplicity of operation, high surface area, selectivity and highly sensitive instrumentation for microbial detection [102].

In this present study, a type of sensor that was used for detection of *E.coli* 0157:H7 was an Optical sensor and an Electrochemical sensor. These types of sensors are discussed below.

2.9 Optical Sensors:

An optical sensor is a device that converts light rays into detectable electrical signals. It determines the physical quantity (e.g. amount) of light rays depending on the nature of the optical sensor and converts it into a readable form on the instrument. These types of sensors demonstrated themselves as vital due to their characteristics. In order to get a signal during the implantation of the probe, light rays are transported through the fibre optics to the instrument as shown in **Figure 2.12** thus there is no need for electrical wires and electrodes which make the sensing process easier. Optical sensors are easy to use, fast and their sensitivity is high. A few types of optical sensing methods are described below [103].

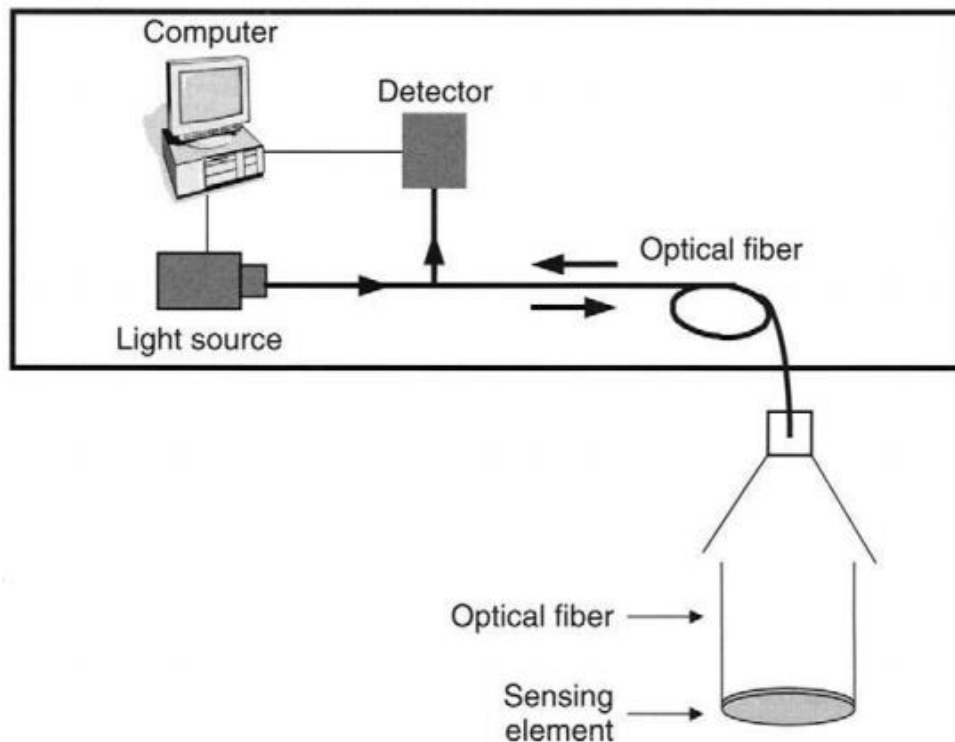


Figure 2.12: Schematic diagram of optical sensor [104].

2.9.1 Colorimetric Sensors:

Colorimetric sensors are sensors that work with colour change when influenced by external stimuli. In a chemical reaction between the analyte and the sensing material, this type of sensor will determine the associated colour change. Usually, this colour change can be observed with the naked eyes or can be detected using unique instrumentation within visible range of 400-800 nm. Chemical or physical change in the property of the tested environment can be considered as the cause of the stimulus, and it distinguishes the design of a particular colorimetric sensor **Figure 2.13** shows an example of colorimetric sensor in which the results (colour change) can be observed by the naked eyes depending on the concentration of the analyte [105,106].

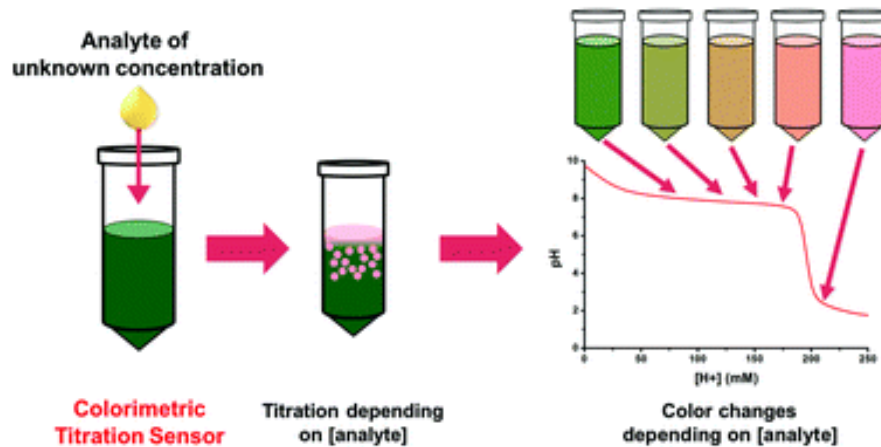


Figure 2.13: An example of Colorimetric sensor [107].

2.9.2 Photoluminescent Sensors:

These are a subdivision of optical sensors that are similar to fluorescent sensors. Photoluminescent sensors are abbreviated or are well known as PL. They are light-based sensors that brighten up molecules when the materials they are combined with gets under heavy mechanical stress. In these types of sensors, a matter (any form of matter) absorbs electromagnetic radiation known as photons and emits light of longer wavelength. Usually, it involves a much stronger force in order to break the exact chemical bond between atoms. In this phenomenon material absorbs at light at lower range of wavelength and re-emits the light that was absorbed at higher wavelength. **Figure 2.13** shows photoluminescent diagram three different energy level. A low energy level is represented by E1, and a higher energy level is represented by E3. Generally, E1 contains more electron than E3. Electrons are pumped by ultraviolet stimulus from E1 to E3 then after to E2 where they decay non-radioactively this state (E2) is known as metastable state and it is a long-lived state and electrons accumulate here up to a point where E2 has more electrons than E1 [108].

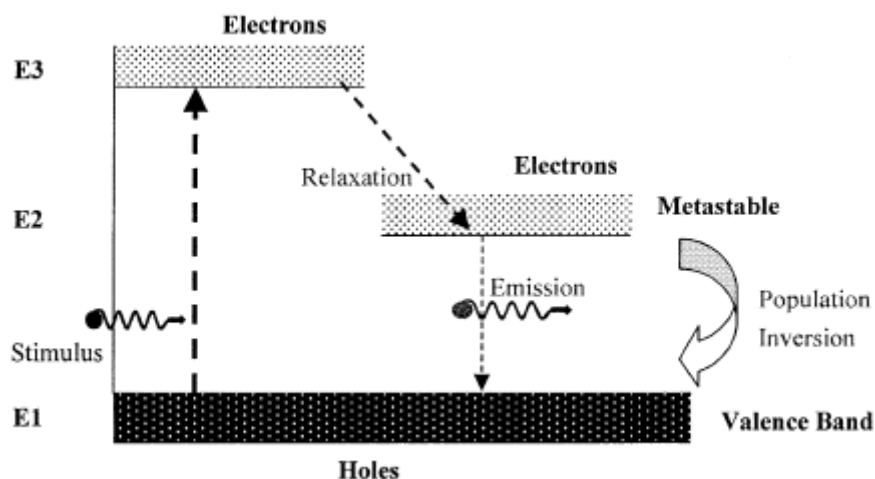


Figure 2.14: Schematic diagram of Photoluminescent band [109].

2.9.3 Surface Plasmon Resonance Sensors:

Surface Plasmon resonance (SPR) sensors are also known as optical sensors. They are based on collective oscillations of free electrons in confined metal systems that require excitations by external ultraviolet radiation waves on a metal surface and these ultraviolet rays reflect back to the detector through a glass prism as shown in **Figure 2.15**. The frequency of SPR depends on factors such as composition, shape, size and inter-particle distance of the NPs. SPR sensing is obtained through the aggregation of NPs. Aggregation of NPs occurs when NPs that are close to each other combine to form a cluster due to their interaction and show an additional resonance. When the NPs combine, the surface plasmon resonance (SPR) will shift to higher wavelength (redshift) or lower wavelength (blue shift), and this shift will depend on the concentration of the metal ions that are in nanoparticles in tested solution [110]

In this study, SPR sensor was used since it has few drawbacks compared to colorimetric and photoluminescent sensors. Colorimetric sensors can only be used once and are not appropriate for applications that require consistent and continuous quantitative sensing. In

comparison, photoluminescent is not a quantitative technique and literature reports that the need for sample labelling with fluorescent reagents as its main drawback when it is used for the detection of bacteria since the process is time-consuming and expensive. The detection of bacteria using SPR sensors is a label-free method it has been used since the launched of the first commercially device.

Literature reports several studies that used optical methods for the detection of *E.coli* and other bacteria. Recently Kaushik and co-workers developed a molybdenum disulfide nanosheets based SPR immunosensor for detection of *E.coli* in food and water [111]. In another study, Zheng and co-workers developed a microfluidic calorimetric biosensor based on gold nanoparticles for detection of *E.coli* 0157:H7 in chicken samples [112]. In a study by Wand and co-workers, they made use of gold nanorods modified with amine for simultaneous detection of *S. Typhimurium* and *E.coli* bacterium [113]. Besides optical sensors, Electrochemical detection methods appeared as effective methods for sensing bacteria as well.

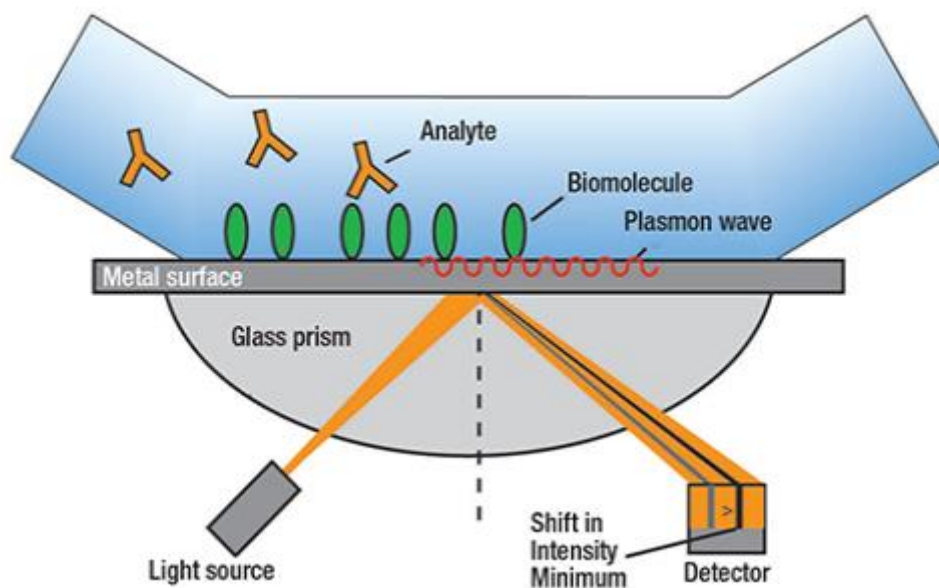


Figure 2.15: Presentation of SPR sensor principle [114].

2.10 Electrochemical Sensors:

An electrochemical Sensor is a form of a chemical sensor. It is a device that converts electrochemical data into a useful analytical signal as shown in **Figure 2.16**. Electrochemical sensors have two major parts, a molecular (chemical) recognition part which is considered as the most crucial part of the sensor and a physicochemical transducer which is known as an apparatus that transforms chemical responses into a signal that can be recorded by modern electrical equipment. Therefore, these two components construct a sensing electrode known as a working electrode. A counter electrode together with a reference electrode is used in electrochemical studies. Electrochemical sensors function by reacting with the target analytes and producing electric signals that are relative to the concentration of the analyte. There are different types of electrochemical sensors known as conductometric, potentiometric and amperometric sensors.

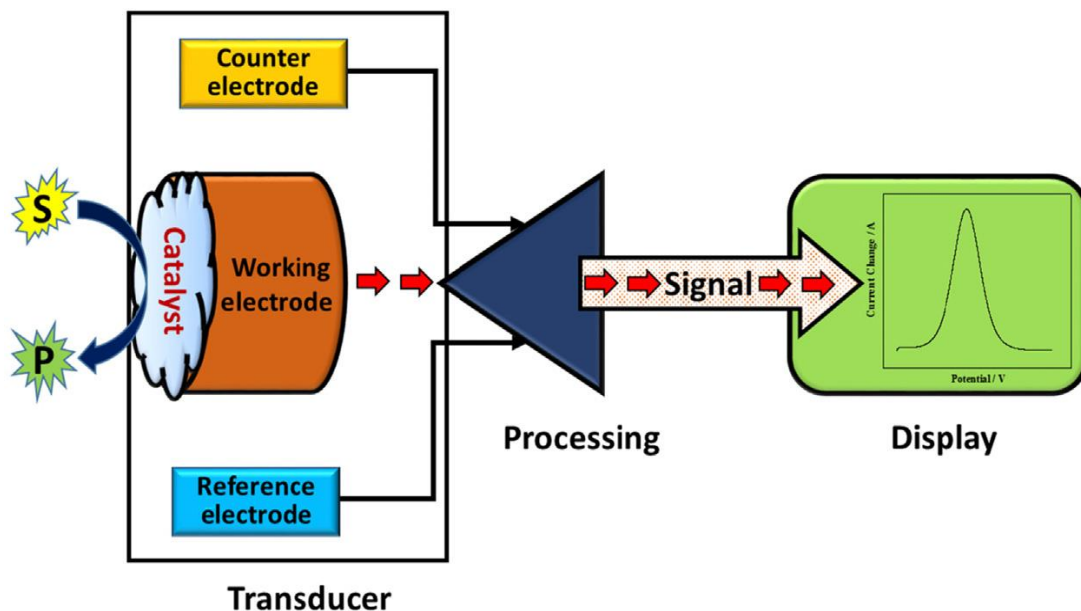


Figure 2.16: Principles of electrochemical sensors [115].

2.10.1 Conductometric Sensors:

Conductometric sensors are determined by the changes of electric conductivity of bulk material or a film of which the conductivity is affected by the analyte present. This type of sensor is easy to use, cheap, and it does not require a reference electrode. The analyte determines the measurements of the conductivity. **Figure 2.17** shows a connected system for conductometric sensing. From the figure label 1 is the sensor with different conductometric transducer, label 2 conductometry holder and label 3 conductometry support lastly label 4 is the working cell together with testing solution placed on top of the conductometry support, label 5 magnetic stir is the magnetic stir with the whole sensing set [116].

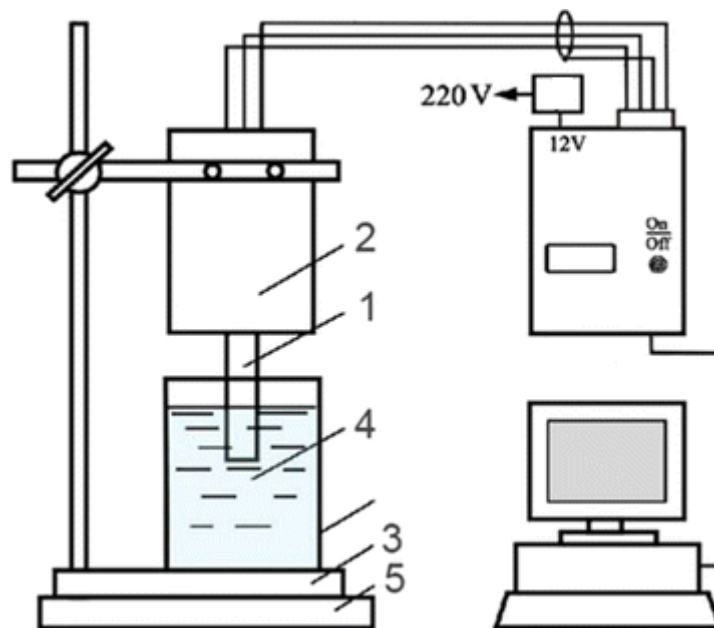


Figure 2.17: A typical representation of a connected conductometric sensor [117].

2.10.2 Potentiometric Sensors:

Potentiometric sensing is an electrochemical method that determines the electrical potential of an electrode under zero current flow. It involves potential measurement at the sensor surface under local equilibrium conditions. In this technique, there are only two electrodes that are involved, namely an indicator electrode and a reference electrode. Mostly in potentiometric sensors, the difference between the indicator electrode and the reference electrode is determined without polarising the potentiometric cell with zero current allowed. A fixed half-cell potential is expected from the reference electrode, whereas a variable potential will be developed from the indicator electrode depending on the concentration or the activity of an analyte in solution. The analyte concentration is responsible for the change in potential in a logarithmic manner. This type of sensor is divided into three types; Ion-Selective Electrode (ISE), Coated Wire Electrode (CWE) and Field Effect (FET).

Ion-selective electrode (ISE) is an indicator electrode, and it is more sensitive than the ion of interest, and it can respond to changes in the concentration or the activity of the analyte. Thus, the reference electrode is relative to the measured voltage or potential as shown in **Figure 2.17**. Whereas in Coated Wire Electrode (CWE) an ion-selective polymer such as poly(acrylic acid), poly(vinyl benzyl chloride) or poly(vinyl chloride) is used to coat the conductor directly, to develop an electrode that is more sensitive to the electrolyte concentration. Moreover, field-effect transistor (FET) is a device that uses an electric field to regulate the current. It shows low output impedance and high input impedance; therefore, it can control the charge formed on the ion sensing membrane. In potentiometric sensors, the electrode modifiers (polymer matrix) can be different by the immobilisation of biomedical/biological materials resulting in the formation of potentiometric biosensors [118].

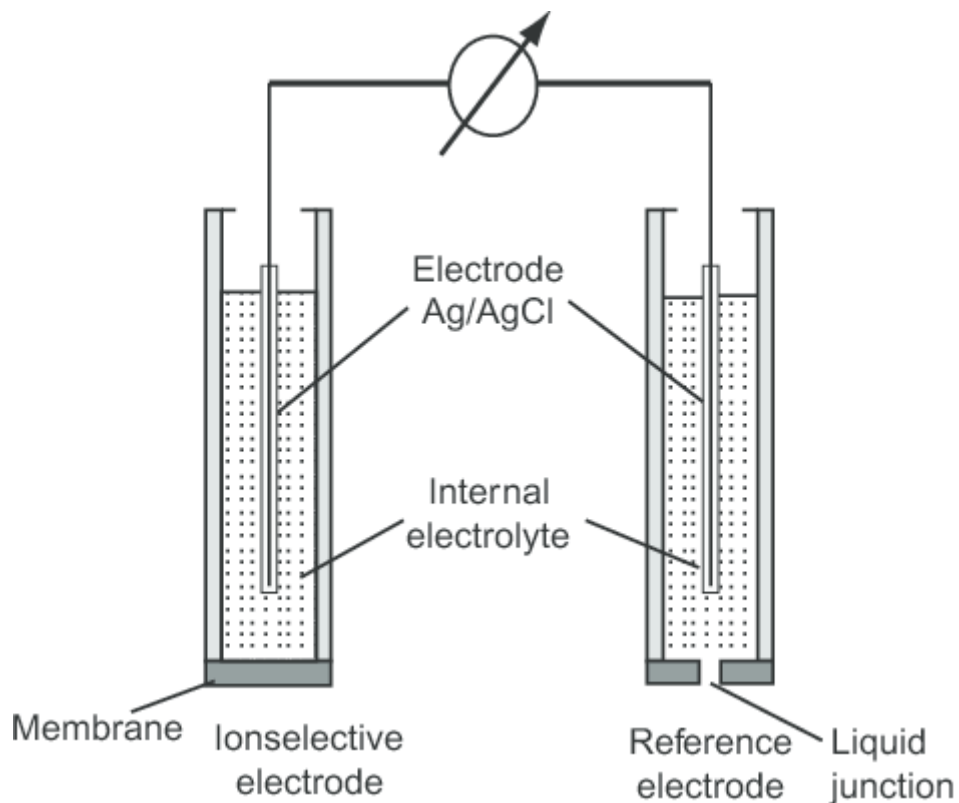


Figure 2.18: Typical diagram of ion selective electrode [119].

2.10.3 Amperometric Sensors:

These are sensors that determine the flow of the current response, which depends on the concentration of the analyte at a constant potential. Usually, they use a potentiometric cell which consists of an auxiliary, reference and working electrodes and this potentiometric cell function at the working electrode under a fixed potential. In a solution of electro-active species, an electrochemical redox reaction occurs at inert metal electrodes. Where the electrons flow from the analyte to the working electrode, the direction of the flow is determined by the properties of the analyte. These types of sensors require a supporting electrolyte in order to keep a constant potential that will help to maintain the ionic strength regularly, decrease the resistance of the solution and eliminate electromigration. **Figure 2.19** show a typical representation of an amperometric sensor and is described as follows. The

interface of the immobilised layer that is capped with (e.g. enzymes, nanoparticles, polymers etc.) will interact with the molecules on the analyte in a lock and key mechanism resulting in an electric signal through a specific transducer. The electrical signal is modified and monitored with a processor such as a computer, and it will create a measurable analytical signal.

Moreover, the properties of this type of sensor can be changed or controlled by changing the parameters (e.g. temperature or sensing material) during operation or fabrication of the sensor to enhance sensitivity and selectivity. When current is a form of an analytical signal, it is possible to measure its potential difference or a constant potential across the potentiometric cell, and it is scanned from one pre-set value to another while the cell current is measured as a function of the potential applied. The concentration of the analyte is proportional to the rate of flow of electrons. Different materials such as (nanoparticles, polymers, composite of nanoparticles and polymers etc.) are used to modify the working electrode to reduce electrode fouling of oxidised or reduced species and to increase its sensitivity [120].

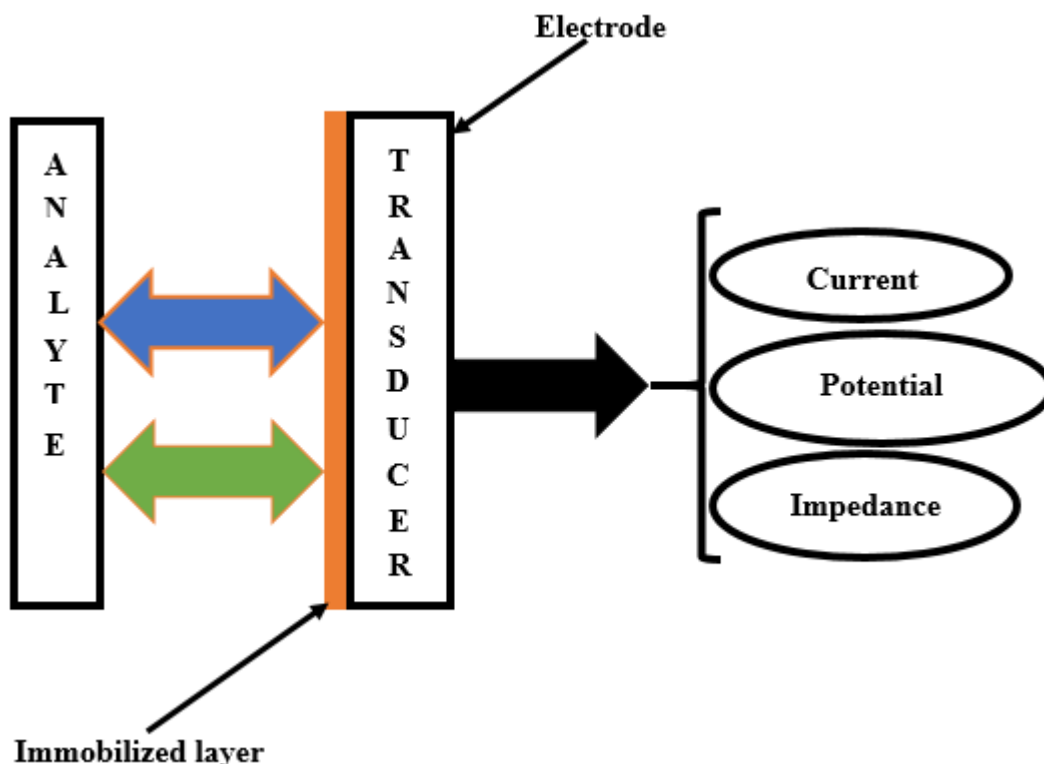


Figure 2.19: A typical representation of an amperometric sensor.

Literature studies report a study by Xu and co-workers who developed an electrochemical sensing technique using a modified electrode with multi-walled carbon nanotube for detection of *E.coli* 0157:H7 in water [121]. In another study, Chowdhury and co-workers reported an impedimetric sensor based on Au/PANI/Glu linked with antibody-antigen for the detection of *E.coli* 0157:H7 in water [122]. Recently Pangajam and co-workers made use of carbon dot capped with ZnO nanorod/ PANI composite to fabricate an electrochemical sensor for the detection of *E.coli* 0157:H7 in water. Electrochemical sensors are well known due to their affordability, reliability and reasonable limit of detection (LOD). Moreover, they have an extra advantage of specificity and high selectivity. Therefore, in the present research, we fabricated a GBPE capped Ag-AuNPs modified glassy carbon electrode-based electrochemical sensor for rapid, specific and sensitive detection of pathogenic *E.coli* 0157:H7 bacteria [123–125].

2.11 References:

- [1] N. Kumar, R.K. Salar, R. Kumar, M. Prasad, B. Brar, V. Nain, Green Synthesis of Silver Nanoparticles and its Applications - A Review, *A J. Nanotechnol. Its Appl.* 19 (2017) 1–22.
- [2] G. Aragay, A. Merkok, Recent Trends in Macro-, Micro-, and Nanomaterial-Based Tools and Strategies for Heavy-Metal Detection, (2011) 3433–3458. <https://doi.org/10.1021/cr100383r>.
- [3] S. Menon, R. S., V.K. S., A review on biogenic synthesis of gold nanoparticles, characterization, and its applications, *Resour. Technol.* 3 (2017) 516–527. <https://doi.org/10.1016/j.refit.2017.08.002>.
- [4] R. Hoshyar, G. Reza, M. Poorgholami, M. Kaykhaii, *Journal of Photochemistry & Photobiology, B: Biology* A novel green one-step synthesis of gold nanoparticles using crocin and their anti-cancer activities, *JPB.* 159 (2016) 237–242. <https://doi.org/10.1016/j.jphotobiol.2016.03.056>.
- [5] S.K. Boruah, P.K. Boruah, P. Sarma, C. Medhi, Green synthesis of gold nanoparticles using camellia sinensis and kinetics of the reaction, (2012). <https://doi.org/10.5185/amlett.2012.icnano.103>.
- [6] V. Gopinath, D. MubarakAli, S. Priyadarshini, N.M. Priyadharsshini, N. Thajuddin, P. Velusamy, Biosynthesis of silver nanoparticles from *Tribulus terrestris* and its antimicrobial activity: A novel biological approach, *Colloids Surfaces B Biointerfaces.* 96 (2012) 69–74. <https://doi.org/10.1016/j.colsurfb.2012.03.023>.
- [7] S.N. Mailu, Symmetrical Pt (100) Nanoalloy Electrocatalysts for Ammonia Oxidation, 13 (2020) 43–48. <https://doi.org/10.9790/5736-1310014348>.
- [8] J. Mittal, A. Batra, A. Singh, M.M. Sharma, Phytofabrication of nanoparticles through plant as nanofactories, *Adv. Nat. Sci. Nanosci. Nanotechnol.* 5 (2014). <https://doi.org/10.1088/2043-6262/5/4/043002>.
- [9] S. Ahmed, M. Ahmad, B.L. Swami, S. Ikram, REVIEW A review on plants extract mediated synthesis of silver nanoparticles for antimicrobial applications : A green expertise, *J. Adv. Res.* 7 (2016) 17–28. <https://doi.org/10.1016/j.jare.2015.02.007>.
- [10] S. Singh Gujral, M.A. Sheela, S. Khatri, R.K. Singla, A Focus & Review on the Advancement of Green Chemistry, *Indo Glob. J. Pharm. Sci.* 2 (2012) 397–408. https://www.researchgate.net/profile/Rajeev_K_Singla/publication/235731092_A_Focus_Review_on_the_Advancement_of_Green_Chemistry/links/02bfe512f04b5844f0000000/A-Focus-Review-on-the-Advancement-of-Green-Chemistry.pdf.
- [11] J.A. Linthorst, An overview: Origins and development of green chemistry, *Found.*

- Chem. 12 (2010) 55–68. <https://doi.org/10.1007/s10698-009-9079-4>.
- [12] J.H. Clark, R. Luque, A.S. Matharu, Green Chemistry, Biofuels, and Biorefinery, *Annu. Rev. Chem. Biomol. Eng.* 3 (2012) 183–207. <https://doi.org/10.1146/annurev-chembioeng-062011-081014>.
- [13] P. Raveendran, J. Fu, S.L. Wallen, Completely “Green” Synthesis and Stabilization of Metal Nanoparticles, *J. Am. Chem. Soc.* 125 (2003) 13940–13941. <https://doi.org/10.1021/ja029267j>.
- [14] M. Mishra, K. Dashora, A. Srivastava, V.D. Fasake, R.H. Nag, Prospects, challenges and need for regulation of nanotechnology with special reference to India, *Ecotoxicol. Environ. Saf.* 171 (2019) 677–682. <https://doi.org/10.1016/j.ecoenv.2018.12.085>.
- [15] M.J. Hernáiz, A.R. Alcántara, J.I. García, J. V. Sinisterra, Applied biotransformations in green solvents, *Chem. - A Eur. J.* 16 (2010) 9422–9437. <https://doi.org/10.1002/chem.201000798>.
- [16] V. Popov, I. Hinkov, S. Diankov, M. Karsheva, Y. Handzhiyski, Ultrasound-assisted green synthesis of silver nanoparticles and their incorporation in antibacterial cellulose packaging, *Green Process. Synth.* 4 (2015) 125–131. <https://doi.org/10.1515/gps-2014-0085>.
- [17] M. Faried, K. Shamel, M. Miyake, A. Hajalilou, A. Zamanian, Z. Zakaria, E. Abouzari-Lotf, H. Hara, N.B.B. Ahmad Khairudin, M.F. Binti Mad Nordin, A Green Approach for the Synthesis of Silver Nanoparticles Using Ultrasonic Radiation’s Times in Sodium Alginate Media: Characterization and Antibacterial Evaluation, *J. Nanomater.* 2016 (2016). <https://doi.org/10.1155/2016/4941231>.
- [18] N. Bouaoudia-Madi, L. Boulekbache-Makhlouf, K. Madani, A.M.S. Silva, S. Dairi, S. Oukhmanou-Bensidhoum, S.M. Cardoso, Optimization of ultrasound-assisted extraction of polyphenols from myrtus communis L. Pericarp, *Antioxidants.* 8 (2019) 1–17. <https://doi.org/10.3390/antiox8070205>.
- [19] Y. Chen, C. Shen, J. Wang, G. Xiao, G. Luo, Green Synthesis of Ag-TiO₂ Supported on Porous Glass with Enhanced Photocatalytic Performance for Oxidative Desulfurization and Removal of Dyes under Visible Light, *ACS Sustain. Chem. Eng.* 6 (2018) 13276–13286. <https://doi.org/10.1021/acssuschemeng.8b02860>.
- [20] L.M. Pera, M.D. Baigori, A. Pandey, G.R. Castro, *Biocatalysis*, Elsevier B.V., 2015. <https://doi.org/10.1016/B978-0-444-63453-5.00012-4>.
- [21] P. Lozano, J.M. Bernal, S. Nieto, C. Gomez, E. Garcia-Verdugo, S. V. Luis, Active biopolymers in green non-conventional media: A sustainable tool for developing clean chemical processes, *Chem. Commun.* 51 (2015) 17361–17374. <https://doi.org/10.1039/c5cc07600e>.

- [22] S. Jin, C. Guo, Y. Lu, R. Zhang, Z. Wang, M. Jin, Comparison of microwave and conventional heating methods in carbonization of polyacrylonitrile-based stabilized fibers at different temperature measured by an in-situ process temperature control ring, *Polym. Degrad. Stab.* 140 (2017) 32–41. <https://doi.org/10.1016/j.polymdegradstab.2017.04.002>.
- [23] J.K. Patra, K.H. Baek, Green Nanobiotechnology: Factors Affecting Synthesis and Characterization Techniques, *J. Nanomater.* 2014 (2014). <https://doi.org/10.1155/2014/417305>.
- [24] S. Rajaboopathi, S. Thambidurai, Green synthesis of seaweed surfactant based CdO-ZnO nanoparticles for better thermal and photocatalytic activity, *Curr. Appl. Phys.* 17 (2017) 1622–1638. <https://doi.org/10.1016/j.cap.2017.09.006>.
- [25] S. Iravani, Green synthesis of metal nanoparticles using plants, *Green Chem.* 13 (2011) 2638–2650. <https://doi.org/10.1039/c1gc15386b>.
- [26] N.S. Al-radadi, A.N. Al-youbi, One-Step Synthesis of Au Nano-Assemblies and Study of Their Anticancer One-Step Synthesis of Au Nano-Assemblies and Study of Their Anticancer Activities, (2018). <https://doi.org/10.1166/jctn.2018.7323>.
- [27] N. Nagar, V. Devra, Green synthesis and characterization of copper nanoparticles using *Azadirachta indica* leaves, *Mater. Chem. Phys.* 213 (2018) 44–51. <https://doi.org/10.1016/j.matchemphys.2018.04.007>.
- [28] M. Nasrollahzadeh, S.S. Momeni, S.M. Sajadi, Green synthesis of copper nanoparticles using *Plantago asiatica* leaf extract and their application for the cyanation of aldehydes using $K_4Fe(CN)_6$, *J. Colloid Interface Sci.* 506 (2017) 471–477. <https://doi.org/10.1016/j.jcis.2017.07.072>.
- [29] C. Soundarrajan, A. Sankari, P. Dhandapani, S. Maruthamuthu, S. Ravichandran, G. Sozhan, N. Palaniswamy, Rapid biological synthesis of platinum nanoparticles using *Ocimum sanctum* for water electrolysis applications, (2012) 827–833. <https://doi.org/10.1007/s00449-011-0666-0>.
- [30] L. Yumei, L. Yamei, L. Qiang, B. Jie, Rapid biosynthesis of silver nanoparticles based on flocculation and reduction of an exopolysaccharide from *arthrobacter* sp. B4: Its antimicrobial activity and phytotoxicity, *J. Nanomater.* 2017 (2017). <https://doi.org/10.1155/2017/9703614>.
- [31] M.S. Akhtar, J. Panwar, Y.S. Yun, Biogenic synthesis of metallic nanoparticles by plant extracts, *ACS Sustain. Chem. Eng.* 1 (2013) 591–602. <https://doi.org/10.1021/sc300118u>.
- [32] S.S. Shankar, A. Ahmad, M. Sastry, Geranium Leaf Assisted Biosynthesis of Silver Nanoparticles, *Biotechnol. Prog.* 19 (2003) 1627–1631.

<https://doi.org/10.1021/bp034070w>.

- [33] M.S. Alsalhi, S. Devanesan, A.A. Alfuraydi, R. Vishnubalaji, M.A. Munusamy, K. Murugan, M. Nicoletti, G. Benelli, Green synthesis of silver nanoparticles using *Pimpinella anisum* seeds: Antimicrobial activity and cytotoxicity on human neonatal skin stromal cells and colon cancer cells, *Int. J. Nanomedicine*. 11 (2016) 4439–4449. <https://doi.org/10.2147/IJN.S113193>.
- [34] M.M.I. Masum, M.M. Siddiqa, K.A. Ali, Y. Zhang, Y. Abdallah, E. Ibrahim, W. Qiu, C. Yan, B. Li, Biogenic Synthesis of Silver Nanoparticles Using *Phyllanthus emblica* Fruit Extract and Its Inhibitory Action Against the Pathogen *Acidovorax oryzae* Strain RS-2 of Rice Bacterial Brown Stripe, *Front. Microbiol.* 10 (2019) 1–18. <https://doi.org/10.3389/fmicb.2019.00820>.
- [35] F. Samari, H. Salehipoor, E. Eftekhari, S. Yousefinejad, Low-temperature biosynthesis of silver nanoparticles using mango leaf extract: catalytic effect, antioxidant properties, anticancer activity and application for colorimetric sensing, *New J. Chem.* 42 (2018) 15905–15916. <https://doi.org/10.1039/C8NJ03156H>.
- [36] J. Balavijayalakshmi, V. Ramalakshmi, Carica papaya peel mediated synthesis of silver nanoparticles and its antibacterial activity against human pathogens, *J. Appl. Res. Technol.* 15 (2017) 413–422. <https://doi.org/10.1016/j.jart.2017.03.010>.
- [37] K. Logaranjan, A.J. Raiza, S.C.B. Gopinath, Y. Chen, K. Pandian, Shape- and Size-Controlled Synthesis of Silver Nanoparticles Using Aloe vera Plant Extract and Their Antimicrobial Activity, *Nanoscale Res. Lett.* 11 (2016). <https://doi.org/10.1186/s11671-016-1725-x>.
- [38] F. Moradi, S. Sedaghat, O. Moradi, S.A. Salmanabadi, Review on green nanobiosynthesis of silver nanoparticles and their biological activities : with an emphasis on medicinal plants, *Inorg. Nano-Metal Chem.* 0 (2020) 1–10. <https://doi.org/10.1080/24701556.2020.1769662>.
- [39] Z. Abootorabi, M. Poorgholami, M.Y. Hanafi-Bojd, R. Hoshyar, Green Synthesis of Gold Nanoparticles Using Barberry and Saffron Extracts, *Mod. Care J.* 13 (2017) 4–6. <https://doi.org/10.5812/modernc.13000>.
- [40] C. Karuppiyah, S. Palanisamy, S. Chen, R. Emmanuel, K. Muthupandi, P. Prakash, RSC Advances application for the trace level determination of, *RSC Adv.* 5 (2015) 16284–16291. <https://doi.org/10.1039/C4RA14988B>.
- [41] K. Gopinath, S. Gowri, V. Karthika, A. Arumugam, Green synthesis of gold nanoparticles from fruit extract of *Terminalia arjuna*, for the enhanced seed germination activity of *Gloriosa superba*, *J. Nanostructure Chem.* 4 (2014). <https://doi.org/10.1007/s40097-014-0115-0>.

- [42] J. Kumar, Y. Kwon, K. Baek, Green biosynthesis of gold nanoparticles by onion peel extract : Synthesis , characterization and biological activities, *Adv. Powder Technol.* 27 (2016) 2204–2213. <https://doi.org/10.1016/j.apt.2016.08.005>.
- [43] B. Singh, J.P. Singh, A. Kaur, N. Singh, Bioactive compounds in banana and their associated health benefits - A review., *Food Chem.* 206 (2016) 1–11. <https://doi.org/10.1016/j.foodchem.2016.03.033>.
- [44] A. Pereira, M. Maraschin, Banana (*Musa spp*) from peel to pulp: Ethnopharmacology, source of bioactive compounds and its relevance for human health, *J. Ethnopharmacol.* 160 (2015) 149–163. <https://doi.org/10.1016/j.jep.2014.11.008>.
- [45] A. Bankar, B. Joshi, A.R. Kumar, S. Zinjarde, Banana peel extract mediated novel route for the synthesis of silver nanoparticles, *Colloids Surfaces A Physicochem. Eng. Asp.* 368 (2010) 58–63. <https://doi.org/10.1016/j.colsurfa.2010.07.024>.
- [46] E.H. Ismail, A.M.A. Saqer, E. Assirey, A. Naqvi, R.M. Okasha, Successful Green Synthesis of Gold Nanoparticles using a *Corchorus olitorius* Extract and Their Antiproliferative Effect in Cancer Cells, (2018) 1–14. <https://doi.org/10.3390/ijms19092612>.
- [47] S.F.S. Reihani, A.F.M. Alkarkhi, S. Ramli, A.M. Easa, Total phenolics , flavonoids and antioxidant activity of banana pulp and peel flours : influence of variety and stage of ripeness, *Int. Food Res. J.* 19 (2012) 1041–1046.
- [48] N.K.R. Bogireddy, L. Martinez Gomez, I. Osorio-Roman, V. Agarwal, Synthesis of gold nanoparticles using *Coffea Arabica* fruit extract, *Adv. Nano Res.* 5 (2017) 253–260. <https://doi.org/10.1007/s00217-008-0973-0>.
- [49] T. Zarda, D. La Torre, M. Stro, C. Russell, P. Svedlindh, M. Strømme, M. Nilsson, Letters to Analytical Chemistry Sensitive Detection of Bacterial DNA by Magnetic, 82 (2010) 9138–9140. <https://doi.org/10.1021/ac102133e>.
- [50] M. Fan, L. Gong, Y. Huang, D. Wang, Z. Gong, Science of the Total Environment Facile preparation of silver nanoparticle decorated chitosan cryogels for point-of-use water disinfection, *Sci. Total Environ.* 613–614 (2018) 1317–1323. <https://doi.org/10.1016/j.scitotenv.2017.09.256>.
- [51] P. Jain, T. Pradeep, Potential of Silver Nanoparticle-Coated Polyurethane Foam As an Antibacterial Water Filter, (2005) 3–7. <https://doi.org/10.1002/bit.20368>.
- [52] M.A. Bhat, B.K. Nayak, A. Nanda, Evaluation of Bactericidal Activity of Biologically Synthesised Silver Nanoparticles from *Candida albicans* in Combination with Ciprofloxacin, *Mater. Today Proc.* 2 (2015) 4395–4401. <https://doi.org/10.1016/j.matpr.2015.10.036>.

- [53] R. Singh, R. Verma, A. Kaushik, G. Sumana, S. Sood, Biosensors and Bioelectronics Chitosan – iron oxide nano-composite platform for mismatch-discriminating DNA hybridization for *Neisseria gonorrhoeae* detection causing sexually transmitted disease, *Biosens. Bioelectron.* 26 (2011) 2967–2974. <https://doi.org/10.1016/j.bios.2010.11.047>.
- [54] N. Abdel-raouf, Green biosynthesis of gold nanoparticles using *Galaxaura elongata* and characterization of their antibacterial activity, *Arab. J. Chem.* 10 (2017) S3029–S3039. <https://doi.org/10.1016/j.arabjc.2013.11.044>.
- [55] K.S.U. Suganya, K. Govindaraju, V.G. Kumar, T.S. Dhas, V. Karthick, G. Singaravelu, M. Elanchezhiyan, Blue green alga mediated synthesis of gold nanoparticles and its antibacterial efficacy against Gram positive organisms, *Mater. Sci. Eng. C.* 47 (2015) 351–356. <https://doi.org/10.1016/j.msec.2014.11.043>.
- [56] K.M. Kumar, B.K. Mandal, M. Sinha, V. Krishnakumar, *Spectrochimica Acta Part A : Molecular and Biomolecular Spectroscopy Terminalia chebula mediated green and rapid synthesis of gold nanoparticles*, *Spectrochim. Acta Part A Mol. Biomol. Spectrosc.* 86 (2012) 490–494. <https://doi.org/10.1016/j.saa.2011.11.001>.
- [57] M. Dhayalan, M. Immanuel, J. Denison, L. Jegadeeshwari, K. Krishnan, N.G. N, potential of gold and silver nanoparticles prepared using *Embelia ribes*, *Nat. Prod. Res.* 6419 (2017) 1–4. <https://doi.org/10.1080/14786419.2016.1166499>.
- [58] L.C. Yun'an Qing, R. Li, G. Liu, Y. Zhang, X. Tang, J. Wang, H. Liu, Y. Qin, Potential antibacterial mechanism of silver nanoparticles and the optimization of orthopedic implants by advanced modification technologies, *Int. J. Nanomedicine.* 13 (2018) 3311–3327.
- [59] K. Yoon, J.H. Byeon, J. Park, J. Hwang, Susceptibility constants of *Escherichia coli* and *Bacillus subtilis* to silver and copper nanoparticles, 373 (2007) 572–575. <https://doi.org/10.1016/j.scitotenv.2006.11.007>.
- [60] S. Vanaraj, J. Jabastin, Production and Characterization of Bio-AuNPs to Induce Synergistic Effect Against Multidrug Resistant Bacterial Biofilm, *J. Clust. Sci.* 28 (2017) 227–244. <https://doi.org/10.1007/s10876-016-1081-0>.
- [61] X. Zhang, P. Geng, H. Liu, Y. Teng, Y. Liu, Q. Wang, Biosensors and Bioelectronics Development of an electrochemical immunoassay for rapid detection of *E. coli* using anodic stripping voltammetry based on Cu @ Au nanoparticles as antibody labels, 24 (2009) 2155–2159. <https://doi.org/10.1016/j.bios.2008.11.019>.
- [62] U. Surabaya, J.R. Kalirungkut, UV-Vis ABSORPTION SPECTRA FOR *Escherichia coli* DETECTION, 2 (2015) 382–389.
- [63] B. Jin, S. Wang, M. Lin, Y. Jin, S. Zhang, X. Cui, Y. Gong, A. Li, F. Xu, T.J. Lu,

- Upconversion nanoparticles based FRET aptasensor for rapid and ultrasensitive bacteria detection, *Biosens. Bioelectron.* 90 (2017) 525–533.
<https://doi.org/10.1016/j.bios.2016.10.029>.
- [64] D.R. Raj, C. Sudarsanakumar, Colorimetric and Fiber Optic Sensing of Cysteine Using Green Synthesized Gold Nanoparticles, (2018) 327–334.
<https://doi.org/10.1007/s11468-017-0517-1>.
- [65] P. Mukherjee, A. Ahmad, D. Mandal, S. Senapati, S.R. Sainkar, M.I. Khan, R. Ramani, R. Parischa, P. V Ajayakumar, M. Alam, M. Sastry, R. Kumar, Verticillium sp . and Surface Trapping of the Gold Nanoparticles Formed **, (2001) 3585–3588.
- [66] S. Anbazhagan, S. Azeez, G. Morukattu, Synthesis , characterization and biological applications of mycosynthesized silver nanoparticles, *3 Biotech.* 7 (2017) 1–9.
<https://doi.org/10.1007/s13205-017-0961-9>.
- [67] M. Khatami, H.Q. Alijani, I. Sharifi, Biosynthesis of bimetallic and core – shell nanoparticles : their biomedical applications – a review, (2018) 1–9.
<https://doi.org/10.1049/iet-nbt.2017.0308>.
- [68] I. Adelere, A. Lateef, A novel approach to the green synthesis of metallic nanoparticles : the use of agro-wastes , enzymes , and pigments, (2016).
<https://doi.org/10.1515/ntrev-2016-0024>.
- [69] M. Schlüter, T. Hentzel, C. Suarez, M. Koch, W.G. Lorenz, L. Böhm, R. Düring, K.A. Koinig, M. Bunge, Chemosphere Synthesis of novel palladium (0) nanocatalysts by microorganisms from heavy-metal-influenced high-alpine sites for dehalogenation of polychlorinated dioxins, *117* (2014) 462–470.
<https://doi.org/10.1016/j.chemosphere.2014.07.030>.
- [70] S. Sunkari, B.R. Gangapuram, R. Dadigala, R. Bandi, M. Alle, V. Guttena, Microwave-irradiated green synthesis of gold nanoparticles for catalytic and anti-bacterial activity, (2017) 1–9. <https://doi.org/10.1186/s40543-017-0121-1>.
- [71] C. Ramesh, K.M. Kumar, N. Latha, V. Rangunathan, Green Synthesis of Cr 2 O 3 Nanoparticles Using Tridax procumbens Leaf Extract and its Antibacterial Activity on Escherichia coli, (2012) 603–607.
- [72] M.N. Owaid, T.A. Zaidan, R.F. Muslim, Biosynthesis , Characterization and Cytotoxicity of Zinc Nanoparticles Using Panax ginseng Roots , *Araliaceae*, *57* (2019).
<https://doi.org/10.23893/1307-2080.APS.05702>.
- [73] A.S. Sonker, J. Pathak, K. Vinod, R.P. Sinha, Characterization and in vitro antitumor , antibacterial and antifungal activities of green synthesized silver nanoparticles using cell extract of Nostoc sp . strain, *01* (2017) 26–37. <https://doi.org/10.24870/cjb.2017-000103>.

- [74] S.G. Ali, M.A. Ansari, H.M. Khan, M. Jalal, A.A. Mahdi, Antibacterial and Antibiofilm Potential of Green Synthesized Silver Nanoparticles against Imipenem Resistant Clinical Isolates of *P. aeruginosa*, (2018) 544–553.
- [75] S. Muayad, A. Majeed, M.N. Owaid, Phyto-fabrication , characteristics and anti-candidal effects of silver nanoparticles from leaves of *Ziziphus mauritiana* Lam, (2018). <https://doi.org/10.23893/1307-2080.APS.05620>.
- [76] G.Z. Gayda, O.M. Demkiv, N.Y. Stasyuk, R.Y. Serkiz, M.D. Lootsik, A. Errachid, M. V Gonchar, applied sciences Metallic Nanoparticles Obtained via “ Green ” Synthesis as a Platform for Biosensor Construction, (n.d.). <https://doi.org/10.3390/app9040720>.
- [77] C.K. Tagad, K.S. Rajdeo, A. Kulkarni, P. More, R.C. Aiyer, S. Sabharwal, Green synthesis of polysaccharide stabilized gold nanoparticles: Chemo catalytic and room temperature operable vapor sensing application, *RSC Adv.* 4 (2014) 24014–24019. <https://doi.org/10.1039/c4ra02972k>.
- [78] L.E.S. Hoyos, V. Sánchez-mendieta, A.R. Vilchis-nessor, M.A. Camacho-lópez, J. Trujillo-reyes, M. Avalos-borja, Plasmonic Sensing of Aqueous-Divalent Metal Ions by Biogenic Gold Nanoparticles, 2019 (2019) 1–12.
- [79] S. Rahman, L. Rahman, A.T. Khalil, N. Ali, D. Zia, M. Ali, Z.K. Shinwari, Endophyte-mediated synthesis of silver nanoparticles and their biological applications, *Appl. Microbiol. Biotechnol.* 103 (2019) 2551–2569. <https://doi.org/10.1007/s00253-019-09661-x>.
- [80] A. Taha, M. Shamsuddin, Biosynthesis of gold nanoparticles using psidium guajava leaf extract, *Malaysian J. Fundam. Appl. Sci.* 9 (2014) 119–122. <https://doi.org/10.11113/mjfas.v9n3.95>.
- [81] S. Purnell, A. Halliday, F. Newman, C. Sinclair, J. Ebdon, Science of the Total Environment Pathogen infection risk to recreational water users , associated with surface waters impacted by de facto and indirect potable reuse activities, *Sci. Total Environ.* 722 (2020) 137799. <https://doi.org/10.1016/j.scitotenv.2020.137799>.
- [82] 2008. National Environmental Management Amendment Act, Government Gazette, Prevention. 469 (2008) 4–6. http://www.nsw.gov.au/sites/default/files/Government_Gazette_2_December.pdf#page=15.
- [83] S. Bush, B. Dorn, Shaping the future, *Resour. Recycl.* 35 (2016) 23–26.
- [84] T.H.E. Urban, R. Challenge, O.F. The, Drinking water and sanitation, SpringerReference. (2011). https://doi.org/10.1007/springerreference_30327.
- [85] E.O. Igbinsosa, A.I. Okoh, Impact of discharge wastewater effluents on the physico-

- chemical qualities of a receiving watershed in a typical rural community, *Int. J. Environ. Sci. Technol.* 6 (2009) 175–182. <https://doi.org/10.1007/BF03327619>.
- [86] O.S. Fatoki, N.Y.O. Muyima, N. Lujiza, Situation analysis of water quality in the Umtata River catchment, *Water SA.* 27 (2001) 467–473. <https://doi.org/10.4314/wsa.v27i4.4959>.
- [87] W. Journal, C. Diseases, Antibiotic Resistance Profiles of Escherichia coli Isolates from River Sources in Durban , South Africa Antibiotic resistance profiles of Escherichia coli isolates, (2009). <https://doi.org/10.1007/s11274-009-0071-x>.
- [88] L. Green, Desalination and seawater quality at Green Point , Cape Town : A study on the effects of marine sewage outfalls Desalination and seawater quality at Green Point , Cape Town : A study on the effects of marine sewage outfalls, (2017). <https://doi.org/10.17159/sajs.2017/a0244>.
- [89] C. Tam, A. Erebara, A. Einarson, Food-borne illnesses during pregnancy: Prevention and treatment, *Can. Fam. Physician.* 56 (2010) 341–343.
- [90] R. Baum, J. Bartram, A systematic literature review of the enabling environment elements to improve implementation of water safety plans in high-income countries, *J. Water Health.* 16 (2018) 14–24. <https://doi.org/10.2166/wh.2017.175>.
- [91] Y. Sayato, WHO Guidelines for Drinking-Water Quality, *Eisei Kagaku.* 35 (1989) 307–312. <https://doi.org/10.1248/jhs1956.35.307>.
- [92] W. This, SANS 241-1 : 2015 SOUTH AFRICAN NATIONAL STANDARD Drinking water Part 1 : Microbiological , physical , aesthetic, (2015).
- [93] M. Kaushik, A. V. Nandi, V.B. Mungurwadi, Portable sensors for water pathogens detection, *Mater. Today Proc.* 5 (2018) 10821–10826. <https://doi.org/10.1016/j.matpr.2017.12.368>.
- [94] C.D. Luyt, R. Tandlich, W.J. Muller, B.S. Wilhelmi, Microbial Monitoring of Surface Water in South Africa: An Overview, *Int. J. Environ. Res. Public Health.* 9 (2012) 2669–2693. <https://doi.org/10.3390/ijerph9082669>.
- [95] H. So, K. Won, Y.H. Kim, B. Kim, B.H. Ryu, P.S. Na, H. Kim, J. Lee, Single-Walled Carbon Nanotube Biosensors Using Aptamers as Molecular Recognition Elements, (2005) 11906–11907. <https://doi.org/10.1021/ja053094r>.
- [96] J.R. Stetter, W.R. Penrose, S. Yao, Sensors, Chemical Sensors, Electrochemical Sensors, and ECS, *J. Electrochem. Soc.* 150 (2003) S11. <https://doi.org/10.1149/1.1539051>.
- [97] A.P. Dufour, E.R. Strickland, V.J. Cabelli, Membrane filter method for enumerating Escherichia coli, *Appl. Environ. Microbiol.* 41 (1981) 1152–1158.

<https://doi.org/10.1128/aem.41.5.1152-1158.1981>.

- [98] S.C. Edberg, M.J. Allen, D.B. Smith, M. LeChevallier, N. Kriz, D. Callan, R. Ward, D. Calvert, L. Hmurciak, T. Trok, M. Burns, V. Shinn, B. Kraus, C. Dery, V. Coluccio, J. Iwan, National field evaluation of a defined substrate method for the simultaneous detection of total coliforms and *Escherichia coli* from drinking water: comparison with presence-absence techniques, *Appl. Environ. Microbiol.* 55 (1989) 1003–1008. <https://doi.org/10.1128/aem.55.4.1003-1008.1989>.
- [99] E. Leoni, G. De Luca, P.P. Legnani, R. Sacchetti, S. Stampi, F. Zanetti, Legionella waterline colonization : detection of Legionella species in domestic , hotel and hospital hot water systems, (2005) 373–379. <https://doi.org/10.1111/j.1365-2672.2004.02458.x>.
- [100] B.W. Brooks, J. Devenish, D. Milnes, R.H. Robertson, Evaluation of a monoclonal antibody-based enzyme-linked immunosorbent assay for detection of *Campylobacter fetus* in bovine preputial washing and vaginal mucus samples, 103 (2004) 77–84. <https://doi.org/10.1016/j.vetmic.2004.07.008>.
- [101] A.K. Bej, M.H. Mahbubani, J.L. Dicesare, R.M. Atlas, Polymerase Chain Reaction-Gene Probe Detection of Microorganisms by Using Filter-Concentrated Samples, 57 (1991) 3529–3534.
- [102] Y. Wang, Z. Ye, Y. Ying, New Trends in Impedimetric Biosensors for the Detection of Foodborne Pathogenic Bacteria, (2012) 3449–3471. <https://doi.org/10.3390/s120303449>.
- [103] A. Lobnik, Wearable optical chemical sensors, *NATO Sci. Peace Secur. Ser. B Phys. Biophys.* (2012) 29–52. https://doi.org/10.1007/978-94-007-0576-0_2.
- [104] I. Biran, X. Yu, D.R. Walt, *Optrode-based fiber optic biosensors (bio-optrode)*, Second Edi, Elsevier B.V., 2008. <https://doi.org/10.1016/B978-044453125-4.50003-6>.
- [105] C. Lin, Y. Zhu, J. Yu, X. Qin, X. Xian, F. Tsow, S. Forzani, D. Wang, N. Tao, U. States, *HHS Public Access*, 90 (2018) 5375–5380. <https://doi.org/10.1021/acs.analchem.8b00506>.Lin.
- [106] I.I. Ebralidze, N.O. Laschuk, J. Poisson, O. V Zenkina, *Colorimetric Sensors and Sensor Arrays*, Elsevier Inc., 2019. <https://doi.org/10.1016/B978-0-12-814505-0.00001-1>.
- [107] H.H. Cho, S.H. Kim, J.H. Heo, Y.E. Moon, Y.H. Choi, D.C. Lim, K.H. Han, J.H. Lee, A one-step colorimetric acid-base titration sensor using a complementary color changing coordination system, *Analyst.* 141 (2016) 3890–3897. <https://doi.org/10.1039/c6an00744a>.
- [108] M. Chern, J.C. Kays, S. Bhuckory, A.M. Dennis, Sensing with photoluminescent

- semiconductor quantum dots, *Methods Appl. Fluoresc.* 7 (2019).
<https://doi.org/10.1088/2050-6120/aaf6f8>.
- [109] M. McSherry, C. Fitzpatrick, E. Lewis, An optical fiber sensor for the detection of germicidal UV irradiation using narrowband luminescent coatings, *IEEE Sens. J.* 4 (2004) 619–626. <https://doi.org/10.1109/JSEN.2004.833504>.
- [110] Y.T. Chen, Y.S. Huang, C.S. Liu, An optical sensor for measuring the position and slanting direction of flat surfaces, *Sensors (Switzerland)*. 16 (2016).
<https://doi.org/10.3390/s16071061>.
- [111] S. Kaushik, U.K. Tiwari, S.S. Pal, R.K. Sinha, Biosensors and Bioelectronics Rapid detection of Escherichia coli using fiber optic surface plasmon resonance immunosensor based on biofunctionalized Molybdenum disulfide, *Biosens. Bioelectron.* 126 (2019) 501–509. <https://doi.org/10.1016/j.bios.2018.11.006>.
- [112] L. Zheng, G. Cai, S. Wang, M. Liao, Y. Li, J. Lin, Biosensors and Bioelectronics A microfluidic colorimetric biosensor for rapid detection of Escherichia coli O157 : H7 using gold nanoparticle aggregation and smart phone imaging, *Biosens. Bioelectron.* 124–125 (2019) 143–149. <https://doi.org/10.1016/j.bios.2018.10.006>.
- [113] Gold Nanorod Probes for the Detection of Multiple Pathogens**, (2008) 2204–2208.
<https://doi.org/10.1002/sml.200800309>.
- [114] S. Mariani, M. Minunni, Surface plasmon resonance applications in clinical analysis, *Anal. Bioanal. Chem.* 406 (2014) 2303–2323. <https://doi.org/10.1007/s00216-014-7647-5>.
- [115] K.Y. Goud, M. Satyanarayana, A. Hayat, K.V. Gobi, J.L. Marty, Nanomaterial-based electrochemical sensors in pharmaceutical applications, Elsevier Inc., 2019.
<https://doi.org/10.1016/B978-0-12-816504-1.00015-6>.
- [116] J. Janata, Chapter 8. Conductometric sensors., *Princ. Chem. Sensors.* (2009) 241–266.
<https://doi.org/10.1007/978-0-387-69931-8>.
- [117] T.P. Velychko, Soldatkin, V.G. Melnyk, S. V. Marchenko, S.K. Kirdeciler, B. Akata, A.P. Soldatkin, A. V. El'skaya, S. V. Dzyadevych, A Novel Conductometric Urea Biosensor with Improved Analytical Characteristic Based on Recombinant Urease Adsorbed on Nanoparticle of Silicalite, *Nanoscale Res. Lett.* 11 (2016) 1–6.
<https://doi.org/10.1186/s11671-016-1310-3>.
- [118] N.R. Stradiotto, H. Yamanaka, M.V.B. Zanoni, Electrochemical sensors: A powerful tool in analytical chemistry, *J. Braz. Chem. Soc.* 14 (2003) 159–173.
<https://doi.org/10.1590/S0103-50532003000200003>.
- [119] B. Kuang, H.S. Mahmood, M.Z. Quraishi, W.B. Hoogmoed, A.M. Mouazen, E.J. van

Henten, Sensing soil properties in the laboratory, in situ, and on-line. A review, 1st ed., Elsevier Inc., 2012. <https://doi.org/10.1016/B978-0-12-394275-3.00003-1>.

- [120] J. Janata, Principles of Chemical Sensors, 2009. <https://doi.org/10.1007/b136378>.
- [121] L. Xu, J. Du, Y. Deng, N. He, Electrochemical Detection of *E. coli* O157 : H7 Using Porous Pseudo-Carbon Paste Electrode Modified with Carboxylic Multi-Walled Carbon Nanotubes , Glutaraldehyde and 3-Aminopropyltriethoxysilane, (2012) 1006–1011. <https://doi.org/10.1166/jbn.2012.1456>.
- [122] H. Abdullah, N.M. Naim, N. Azwen, N. Azmy, A.A. Hamid, PANI-Ag-Cu Nanocomposite Thin Films Based Impedimetric Microbial Sensor for Detection of *E. coli* Bacteria, 2014 (2014).
- [123] S. Mura, G. Greppi, M.L. Marongiu, P.P. Roggero, S.P. Ravindranath, L.J. Mauer, N. Schibeci, F. Perria, M. Piccinini, P. Innocenzi, J. Irudayaraj, FTIR nanobiosensors for *Escherichia coli* detection, (2012) 485–492. <https://doi.org/10.3762/bjnano.3.55>.
- [124] S. Ohk, A.K. Bhunia, Multiplex fiber optic biosensor for detection of *Listeria monocytogenes* , *Escherichia coli* O157 : H7 and *Salmonella enterica* from ready-to-eat meat samples, *Food Microbiol.* 33 (2013) 166–171. <https://doi.org/10.1016/j.fm.2012.09.013>.
- [125] H. Zhu, S. Mavandadi, A.F. Coskun, O. Yaglidere, A. Ozcan, Optofluidic fluorescent imaging cytometry on a cell phone, *Anal. Chem.* 83 (2011) 6641–6647. <https://doi.org/10.1021/ac201587a>.

CHAPTER THREE

Characterisation of the green synthesised nanoparticles was mainly aimed to determine the morphology, the dispersity, as well as their specific size and shape. This chapter describes the techniques used for characterising the nanoparticles. These techniques include Ultraviolet-visible spectrometry, Transmission electron microscopy, Fourier transform infrared spectroscopy, Small-angle X-ray scattering spectroscopy and X-ray diffraction. Furthermore, Cyclic Voltammetry was used for the electrochemical characterisation of the nanoparticles. This chapter also provides descriptions about the materials, methods, chemicals and characterisation techniques used in obtaining the outlined aims and objectives of the present study. The preparation of solutions such as stock solutions, buffer solutions and working solutions are also outlined in this chapter. Lastly, this chapter will also describe the techniques used for the characterisation of green synthesised Gold, Silver and Silver-gold nanoparticles.

3 Characterisation Techniques:

3.1 Spectroscopy:

Spectroscopy techniques are techniques that analyse properties or characteristics of the material using radiated energy. Spectroscopy methods are used to determine the intensity as a function of wavelength, and they subsequently produce a spectrum for comparison purposes, and in general, these techniques employ qualitative and quantitative analysis for material [1].

The advantages of spectroscopic methods include easy availability, accuracy and simplicity of the instrument [2].

3.1.1 Ultraviolet-visible spectroscopy:

Ultraviolet-visible (UV-Vis) spectroscopy is a technique that makes use of electromagnetic radiation in both the ultraviolet and visible regions. It is used to study the sample reactions towards the electromagnetic radiation. A well-known basic principle of spectroscopy is that, when the electromagnetic radiation of a specific wavelength passes through the sample, some of the electromagnetic radiation may be absorbed by the molecules. Some of the radiation passes through, and it is referred to as being transmitted. According to the Bouguer's law which mostly known as (Lambert law), the absorbance is directly proportional to the path length (thickness). The ratio of the intensity of the electromagnetic radiation entering the sample (I_0) to that of exiting the sample (I) at a particular wavelength is defined as the transmittance (T) given by:

$$T = \frac{I}{I_0} \quad (3.1)$$

While Lambert-Beer's law states that the absorbance is directly proportional to the concentration of the absorbing species and the path length of the absorbing medium, the previous formula can be transformed into a linear expression by taking the logarithm, given by:

$$A = -\log T = \epsilon \times l \times c \quad (3.2)$$

Where: A is absorbance, ϵ is the molar extinction coefficient (ϵ , $\text{L}\cdot\text{mol}^{-1}\cdot\text{cm}^{-1}$), l is the path length of light through the cell in (cm), C is the concentration of the sample in (mol /L). Therefore, according to Lambert-Beer's law at a fixed concentration, a linear relationship between absorbance and path length is observed. Nevertheless, factors such as instrumental and chemical factors limit the linear relationship.

In order for a molecule to absorb radiation in ultra-violet regions, it has to contain valence bonds or non-bonding orbitals. When the radiation is absorbed, electrons are transmitted from a lower energy state to a higher energy state in a molecular orbital. Various properties of a substance such as colour, structure as well as energy associated, can be obtained from electron movement, as shown in **Figure 3.1**.

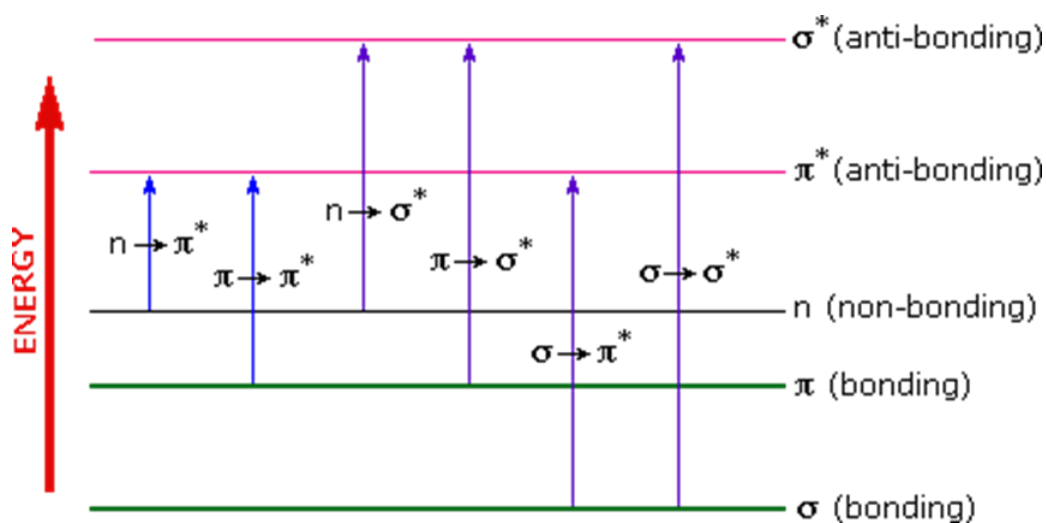


Figure 3.1: Various energy levels and types of electronic transitions [3].

Wiley and co-workers proved that this technique could be used to examine the size and shape of nanoparticles in aqueous solutions [4]. Several research studies where gold nanoparticles were synthesised have reported using UV-Vis as one of their characterisation techniques. In the present study, UV-Vis was performed using the instrument described in chapter 3. UV-

Vis was used to study the spectro-electro properties of green synthesised GBPE capped gold-nanoparticles (GBPE Au-NPs), GBPE capped silver-nanoparticles (GBPE Ag-NPs) and bimetallic GBPE capped Silver-Gold-nanoparticles (GBPE Ag-Au-NPs). The synthesised nanoparticles were dissolved in water and placed in 1 cm³ quartz cuvettes. The UV-VIS absorption spectra of these NPs were recorded in the region of 200-800 nm.

3.1.2 Fourier Transform infrared Spectroscopy:

Fourier transform infrared (FT-IR) spectroscopy is one of the essential spectroscopic technique used to acquire infrared (IR) spectrum of emission or absorption of matter. It can also be used to obtain chemical structures in organic or inorganic samples for qualitative identification of compounds. FT-IR has a more extended wavelength range (4500–500 cm⁻¹) compared to that of visible light. Shown in **Figure 3.2** are the essential components of FT-IR spectrometer namely; source, Michelson interferometer that consists of fixed and moving mirrors and a beam splitter (BS), then a sample compartment and a detector.

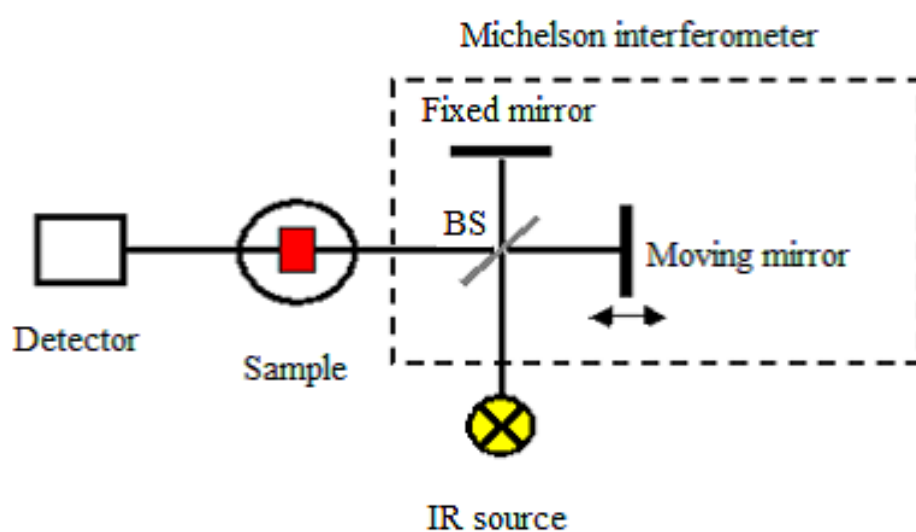


Figure 3.2: Typical diagram of FT-IR spectrometer primary component [5].

The source emits light that enters Michelson interferometer then after when the light reaches the beam splitter denoted as BS in the diagram is split into two creating two different paths. The primary function of the interferometer is to determine the interference between two paths waves. Then each mirror reflects the beam to the beam splitter (BS), and the two beams recombine and form a single beam at the BS region and moves to the detector. The combination of the two beams could be destructive or constructive depending on the optical path difference when the moving mirror is moved. When the combined beam is transferred through the sample, it is now called an interferogram. A signal produced due to the changes on the path length has all the information found on the sample. The interferogram is modified and converted to a digital signal [6]

In this technique, frequency is a characteristic of a specific functional group of molecules. Molecules contain a dipole moment, and its oscillating frequency matches that of infrared light. The infrared light transfers the energy to the molecules, and that causes stretching, twisting or bending of covalent bonds. However, molecules such as N₂ and O₂ lack dipole moment; as a result, they do not absorb IR radiation [7].

In the present study, the FT-IR analysis was employed to validate the significant functional groups on the extract and their involvement in the synthesis and stabilisation of gold nanoparticles (Au-NPs), silver nanoparticles (Ag-NPs) and silver-gold nanoparticles (Ag-Au-NPs) and the band intensities in different regions of the spectra.

3.1.3 X-Ray Powder Diffraction (XRD):

X-ray powder diffraction analysis is the most useful X-ray based characterisation technique. Its name reveals that it is a characterisation technique that is used to examine fine grain or powder material and the obtained information reveals crystal structure, (crystalline size and

shape) and chemical composition of the synthesised material [8]. It is well-known as a non-destructive technique and widely used to determine the orientation of single-crystal structures of synthesised or natural material. In this technique, the diffraction occurs when the distance between the planes is similar to the wavelength of an X-ray such that it can be reflected. The angle of reflection is equivalent to the angle of incidence, and the average distance between layers or planes can be used to determine the average particle size. Therefore, the formation of crystals by the diffraction of X-rays can be described by the Braggs law **Equation 3.3**. This representation on XRD is regarded as intensity versus 2Θ (theta), it can be used to determine the crystallinity of the material and the obtained information is used to confirm whether the target compound has been successfully produced or not. From XRD, the size of synthesised nanoparticles can be determined using the Debye-Scherrer **Equation 3.4** [9]. A Journal Committee Powder Diffraction Standards (JCPDS) folder which consists of XRD database reference for different material can also be used to confirm if the target product is achieved. As shown in **Figure 3.3** during the analysis, X-rays are scattered from the beam to the sample; then, they interact with the sample. This interaction causes rearrangement of atoms within the crystal sample, then the X-ray is reflected in the detector, and the final output will be displayed on the computer as reflecting planes [10].

$$n \lambda = 2d \sin \Theta \quad (3.3)$$

Where: n is an integer denoting the order of the reflection, λ is the wavelength of x-ray, d is the inter-planar spacing and θ is one-half the angle between the incident and scattered x-ray beams.

$$d = \frac{K \lambda}{\beta \cos \theta} \quad (3.4)$$

Where: d = particle/crystal size, K is a constant and can be defined as the dimensionless shape factor and is equal to $0.94 K$ usually range from $0.5 - 1$, and λ is the X-ray wavelength (0.154 nm), β is the full-width half-maximum (FWHM in radians), θ is the angle of reflection [11].

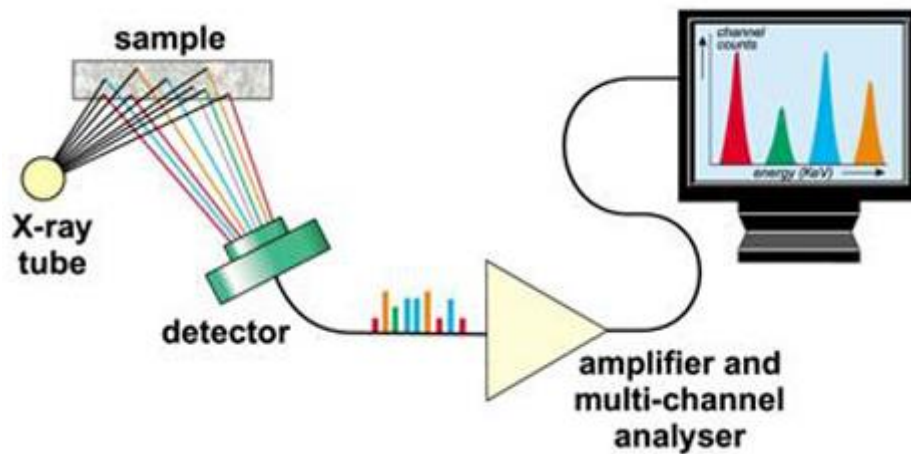


Figure 3.3: Schematic set-up of X-ray Power Diffraction [12].

3.2 Microscopic techniques:

Microscopic techniques play an essential role in the characterisation of particles since they are used to determine the morphology of particles as well as size. Currently, microscopic techniques are the most relevant techniques for size analysis of particles within solid products.

3.2.1 High-Resolution Transmission Electron Microscopy

High-Resolution Transmission Electron Microscopy (HR-TEM) is an imperative microscopic technique in the field of nanotechnology. Since the existence of TEM shown in **Figure 3.4**,

particles can be observed at the molecular level in solids and surfaces in different fields such as material science, biology and medicine. The technique can be used to obtain morphological, topographical and crystalline information of the sample through high magnification and high-resolution imaging. In HR-TEM a beam of electrons from the cathode in the electron gun is transferred through a specimen. An ultrathin specimen (<100 nm) is preferred in order to allow an adequate number of electrons to pass through and form an image with a minimum loss of energy. An image will be formed during the interaction of electrons and the specimen. Thus the image formed is then magnified and focused by the objective lens up until it is recorded by a sensitive detector like a charge-coupled device (CCD). It is directed to an imaging device such as a fluorescent screen, a film or a charge-coupled device camera, then a direct identification from the information obtained can be performed for a specific sample [13]. As shown in **Figure 3.5**, the dark regions on the image obtained from HR-TEM are due to the inadequate number of electrons transmitted through. The bright or clear regions are due to the adequate number of electrons that are transmitted through.

The TEM instrument consists of several equipped detectors such as bright-field and dark-field STEM, and backscattered detectors which are involved in imaging. These detectors can also tell the chemical composition of the sample. Energy dispersive X-ray (EDX) is another example of equipped detectors which is mostly used for the identification of elements in MNP and surface angles (SAED). SAED shows the crystalline nature of the sample. Although TEM is a crucial characterisation technique it has its advantages and disadvantages, as illustrated in **Table 3.1**

In the present study, HR-TEM was done using the instrument described in chapter 3. HR-TEM was used to determine the size, structure and shape of the synthesised gold, silver,

silver-gold nanoparticles. It was also used to determine the elemental composition of the nanoparticles. A copper grid was used as a platform for sample preparation and was allowed to dry by leaving it for 10 minutes under an infra-red lamp before performing HR-TEM analysis.

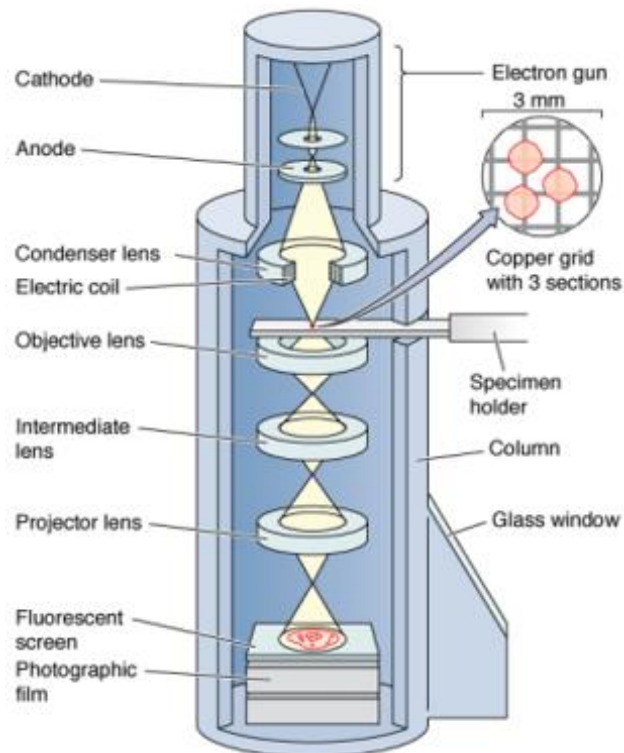


Figure .3.4: Typical presentation of a transmission electron microscope (HR-TEM) [14].

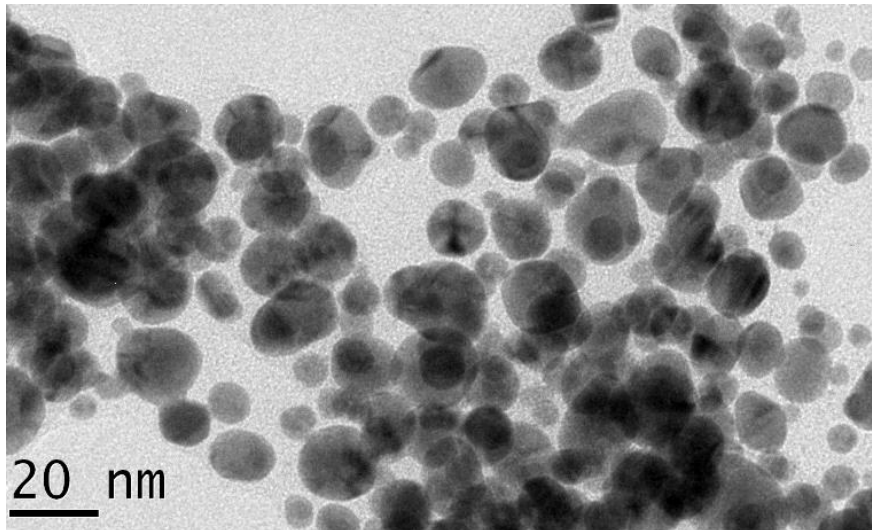


Figure 3.5: An example of an HR-TEM image.

Table 3.1: Advantages and Disadvantages of H-RTEM.

| Advantages | Disadvantages |
|--|---|
| HR-TEM gives information about surface features, structure, size and shape | Allow a small sample in order to fit into the chamber, and the sample must be transparent to allow electrons to pass through and tolerate the vacuum chamber. |
| HR-TEM consist of high magnifications of over 1 million times or more | The instrument is expensive and large. |
| Wide range of application in various scientific fields | Sample preparation is time-consuming. |
| Easy to operate when fully trained | Requires professional personnel. |
| | Produce a colourless image (Black & White). |

3.3 Scattering Techniques:

Scattering techniques provide quantitative measurements of colloidal particles on size, shape and structure of the material. These techniques are based on the interaction between the colloidal particle and incident radiation, for example, light, X-ray or neutrons [15].

3.3.1 Small-Angle X-ray scattering (SAX):

Small-angle X-ray scattering (SAXS) characterisation technique is used to study particle size and size dispersion of colloidal particles. Generally, in this technique, the elastic collision between the sample and the X-ray results in elastic scattering of X-rays [16]. This elastic scattering of (0.1 – 0,2 nm wavelength) by a sample which has inhomogeneities in the nanometer range, is recorded at shallow angles ranging from 0.1 to 10 °C [17]. This angular range holds information about the:

- shape and magnitude of macromolecules.
- The characteristic distance of partially ordered materials.
- Structure and pore size

In SAXS a beam of X-rays is emitted from the source, subsequently monochromated and directed to X-ray optics. Then the size of this beam is adjusted by the slit; then, it hits the sample and goes through the flight path [18]. The flight path is located underneath the vacuum so that the beam can be scattered by the air. This is to provide an extensive distance between the sample and the detector in order to record the elastic scattering of the beam at small angles. Moreover, a centrosymmetric pattern is due to unoriented samples on the 2D detector. **Figure 3.6** shows a typical SAXS instrument with a 2D detector [19].

In this present study, SAX was done using the instrument described in later in chapter 3 in order to determine size dispersion and particle size of green synthesised GBPE capped gold-nanoparticles (GBPE-Au-NPs), GBPE capped silver-nanoparticles (GBPE-Ag-NPs) and bimetallic GBPE capped silver-gold-nanoparticles (Ag-Au-NPs).

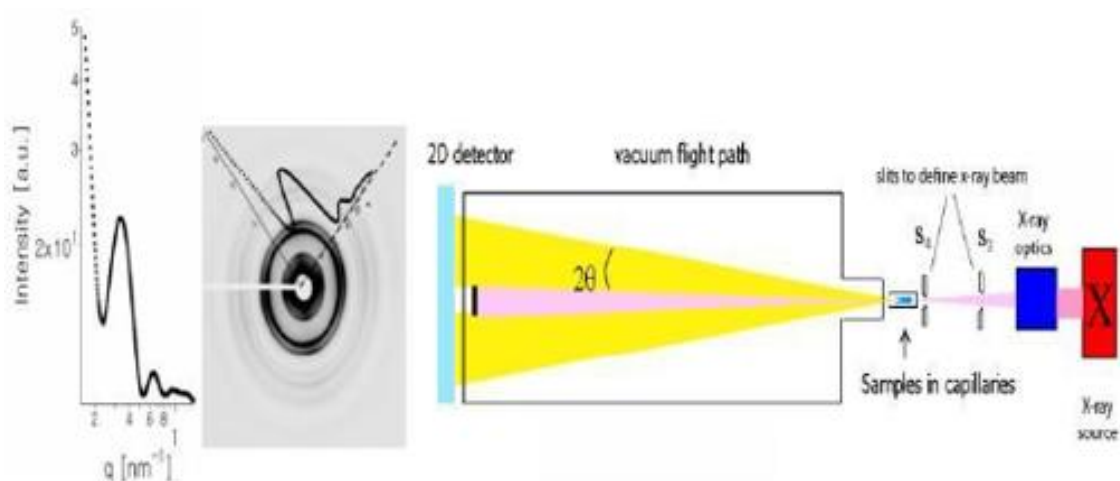


Figure 3.6: Typical representation of Small-Angle X-ray Scattering (SAXS) [20].

3.4 Electrochemical techniques:

Electrochemical techniques are the most informative and sensitive analytical methods in the field of chemistry. These techniques are generally applied in the development of sensors and are used to study physical and chemical properties. Electrochemical techniques are essential because they are cost-effective, safe, environmentally compatible, amenability to automation, energy efficiency, selective and versatile [21]. Electrochemical methods also play an essential role in determining qualities such as the number of electrons transferred, electron transfer rates, diffusion coefficients, oxidation potentials [22].

3.4.1 Cyclic Voltammetry:

Cyclic voltammetry (CV) is an electrochemical method that is used to measure current potential on an electrode surface using unstirred solutions and micro-electrodes. It is frequently used to determine electrochemical properties of analytes in aqueous media as well as redox processes. In CV the current (I) is observed when the potential (E) is applied over some time (t); thus this technique is regarded as a function of potential, current and time [23]. CV works by scanning the working electrode (WE) at a given scan rate (v) from an initial potential (E_i) to the final potential (E_f) and returned to the starting initial potential (E_i) again. The obtained information is then plotted as potential versus current, as shown in **Figure 3.7**, and the peaks show the potentials of which the reduction-oxidation (redox) processes occur. This technique can acquire the reversibility and irreversibility of electroactive species [24].

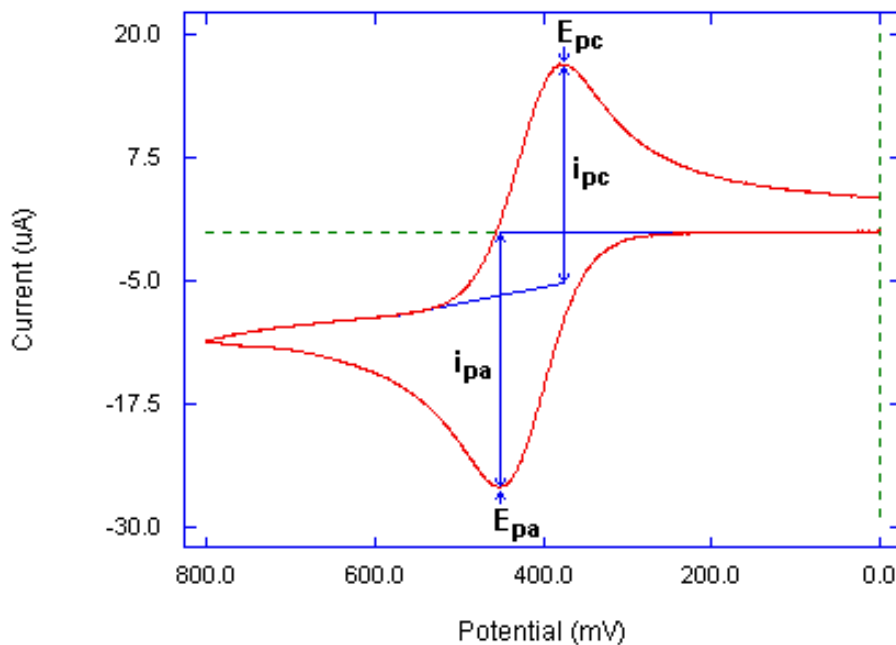


Figure 3.7: A typical cyclic voltammogram [25].

One of the advantages of CV is that it has broad accessibility of low-cost equipment and the access to extensive theory for electrochemist as well as other fields of specialists [26]. A modern electrochemical system has three basic components for voltammetric measurements, namely, electrochemical cell, potentiostat and a computer.

Each has a different function; for example, the potentiostat is for controlling the potential, for accuracy and displays the current produced. An electrochemical cell is a conventional three-electrode set up that used to carry out electrochemical measurements, as shown in **Figure 3.8**. The three electrodes are known as the counter electrode (CE), reference electrode (RE) and the working electrode (WE) as shown in **Figure 3.8**.

The counter electrode (CE) is also called an auxiliary electrode. It is a bridge for electrons so that the current can be transferred from external circuit to the cell hence the reactions that take place at the surface of this electrode are insignificant as long as the current conducts well. Usually, this electrode consists of a platinum wire or metallic foil, sometimes graphite and gold may be used.

The reference electrode (RE) is an electrode with a potential that is accurately maintained and well-known. Other electrodes use its potential as a reference for measurements. Typically the RE for aqueous solutions is silver/silver chloride (Ag/AgCl) and the saturated calomel electrode.

The working electrode (WE) is also called an indicator electrode; it is where the reaction of interest occurs. It is the main component of the electrochemical cell at which the electrochemical phenomena or the redox of the analyte that is investigated occurs. Its characteristics include reproducible surface, low resistance and wide potential range. There are different types of WE electrode, such as glassy carbon, gold and platinum electrode.

In the conventional three-electrode set-up, usually, the potential is determined between the WE and the RE and the current is determined between CE and the WE. The potentiostat ensures that the current is not transferred to the RE at any given time during the reaction.

In this present study, CV was performed using the instrument described in chapter 3 to measure the electrochemical properties of GBPE capped Au-NPs), GBPE capped Ag-NPs) and bimetallic GBPE capped (Ag-Au-NPs).

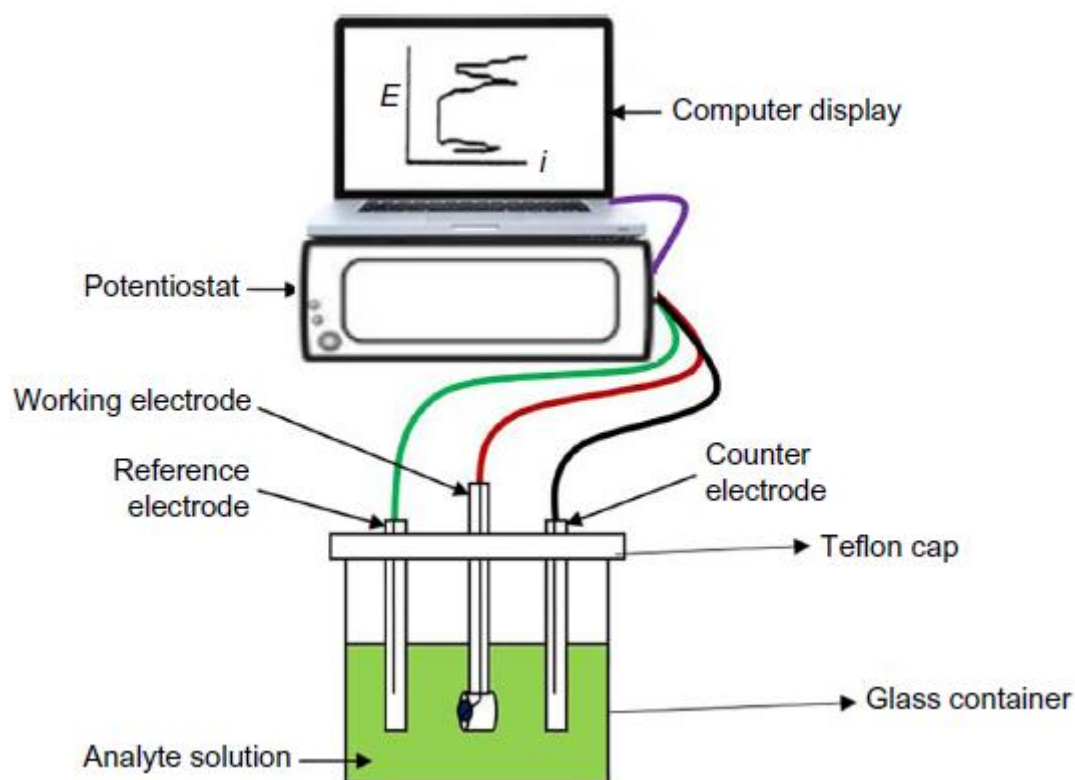


Figure 3.8: A typical representation of a connected cell-set up [27].

3.5 Material and Methods:

3.5.1 Chemicals and Reagents:

Chemicals including hydrogen tetrachloroaurate (III) hydrate ($\text{HAuCl}_4 \cdot 3\text{H}_2\text{O}$, 99.9 %); silver nitrate (AgNO_3 , 99.9 %), sodium phosphate monobasic dehydrate ($\text{H}_2\text{NaO}_4\text{P} \cdot 2\text{H}_2\text{O}$, 99.9 %) and Sodium phosphate dibasic dehydrate ($\text{HNa}_2\text{O}_4\text{P} \cdot 2\text{H}_2\text{O}$, 99.5 %) were procured from Sigma Aldrich, South Africa. Dark red grapes and fresh bananas were bought from Spar Supermarket, in Belhar Cape Town, South Africa. Distilled water was used throughout the experiment to wash and rinse the fruits. The electrolyte solution of 0.2 M of pH 7.4 phosphate buffer was prepared using sodium phosphate monobasic dehydrate ($\text{H}_2\text{NaO}_4\text{P} \cdot 2\text{H}_2\text{O}$, 99.0 %), sodium phosphate dibasic dihydrate ($\text{HNa}_2\text{O}_4\text{P} \cdot 2\text{H}_2\text{O}$, 99.5 %) both dissolved in deionised water obtained from Milli-Q water purification system. Nitrogen gas (N_2) (Afrox, South Africa) was used for degassing all the electrochemistry experiments. Polishing pads and alumina-micro polish were obtained from Buehler, IL, USA and were used for cleaning the working glassy carbon electrodes. All glassware used was cleaned thoroughly with distilled water and dried at 80 °C.

3.5.2 Preparation of Aqueous Grape and Banana peel extracts (GBPE):

Peels were separated from banana and repeatedly washed along with grapes using distilled water to remove any dust and organic impurities. After that, the grapes and cut banana peels were separated into different beakers containing 300 mL distilled water where each mixture was heated at 60 °C for 15 min. The extracts were then placed at room temperature for cooling followed by centrifugation at 1000 rpm for 30 min. The obtained product was filtered twice to remove any insoluble fractions and macromolecules. The final solutions of the

extracts were stored in the refrigerator at 4 °C for further use. The two extracts were combined at a ratio of 1 (banana): 3 (grape) and used as a bio-reducing agent for the synthesis of the synthesised nanoparticles to for a grape and banana-peel extract (GBPE).

3.5.3 Synthesis of GBPE-Au-NPs:

As indicated above, the natural reducing agents present in grapes and banana peels were used to produce gold nanoparticles. A stock solution of 2.05×10^{-5} M HAuCl_4 was prepared by dissolving 0.007 g of $\text{HAuCl}_4 \cdot 3\text{H}_2\text{O}$ in 40 mL water. Subsequently; 20 mL of HAuCl_4 stock solution was transferred into a beaker containing 20 mL of the GBPE obtained at 60 °C. The mixture was boiled in a double neck round bottom flask at a reaction time of 1 h at 60 °C, as shown in **Figure 3.9**. No further treatments were carried out.

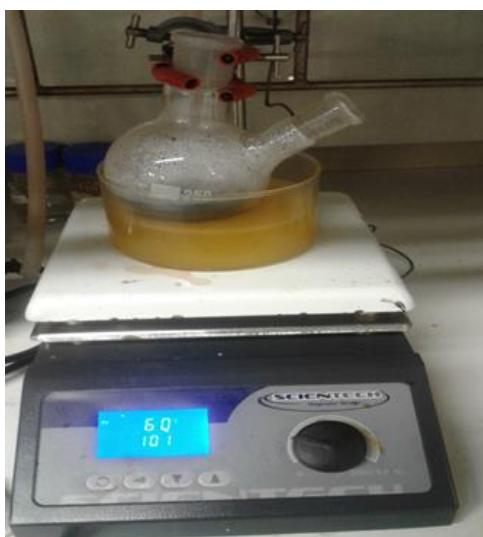


Figure 3.9: Reaction condition of GBPE-Au-NPs.

3.5.4 Synthesis of GBPE-AgNPs:

Silver nanoparticles (Ag-NPs) were synthesised through the reduction of silver nitrate (AgNO_3) using GBPE as the reducing agent. A stock solution of 10×10^{-3} M AgNO_3 was prepared by dissolving 0.0105g of AgNO_3 in 25 mL water. Then 25 mL of silver nitrate solution was mixed with 14 mL of GBPE. The mixture was boiled in a double neck round bottom flask (as shown previously in figure 3.9), at a reaction time of 1h at 75°C in the absence of light. During the process, the solution was mixed vigorously by the use of a magnetic stirrer. No further treatments were carried out. **Figure 3.10** shows the synthetic method of each gold and silver nanoparticles and their applications.

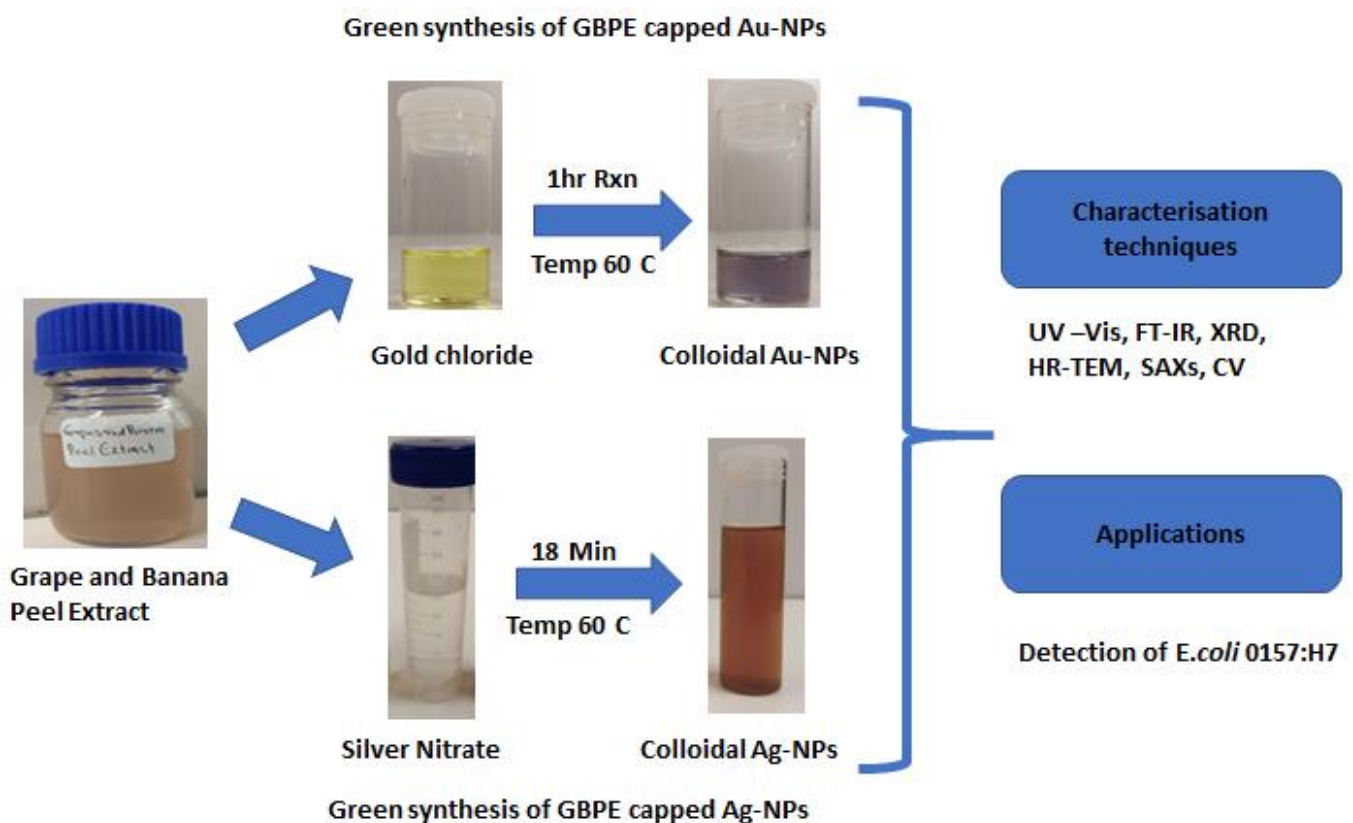


Figure 3.10: Presentation of GBPE capped nanoparticles and their application.

3.5.5 Synthesis of GBPE capped Ag-Au-NPs

Silver-gold nanoparticles (Ag-Au-NPs) were synthesised through simultaneous reduction of silver nitrate (AgNO_3) and gold chloride ($\text{HAuCl}_4 \cdot 3\text{H}_2\text{O}$) using GBPE as the reducing agent. A stock solution of 25 mL of AgNO_3 and $\text{HAuCl}_4 \cdot 3\text{H}_2\text{O}$ in a ratio of (Ag 2: Au 1) was mixed with 14 mL of GBPE in a double neck round bottom flask and heated in a water bath set at 90 °C for 1 hour. During the process, the solution was mixed vigorously by the use of a magnetic stirrer. No further treatments were carried out.

3.6 Characterisation of the functionalised nanoparticles:

3.6.1 Ultraviolet-visible (UV-Vis) analysis:

Visual observations of the changes in the reaction mixture were also recorded. UV-Vis spectrometer Nicolet Evolution 100 (Thermo Electron Cooperation, United Kingdom) was used to obtain the absorption spectra of the green synthesised nanoparticles (Ag-Au-NPs, Au-NPs and Ag-NPs) produced in the present study. Portions of the diluted nanoparticles samples were placed in quartz cuvettes and scanned from 200 – 800 nm wavelength region. Distilled water was used to run the baseline before the experiment.

3.6.2 Fourier Transformation Infrared (FT-IR) analysis:

FT-IR scans of the nanoparticles (Ag-Au-NPs, Au-NPs and Ag-NPs) and GBPE extract were taken in order to determine GBPE functional groups that may have taken part in the synthesis of the microstructures. FT-IR measurements were performed using FT-IR spectrometer Spectrum Two (PerkinElmer, USA) in a spectral range of 500–4000 cm^{-1} . A portion of (1000

μL) was poured into a glass vile and dried overnight at room temperature. Then the dried sample was mixed with potassium bromide (KBr) to make a pellet suitable for FT-IR measurements using hand press manual KBr tool. **Figure 3.11** shows an example of a mixture of the sample (GBPE capped Au-NPs) and KBr. The FTIR background correction was made using a reference blank potassium bromide pellet.

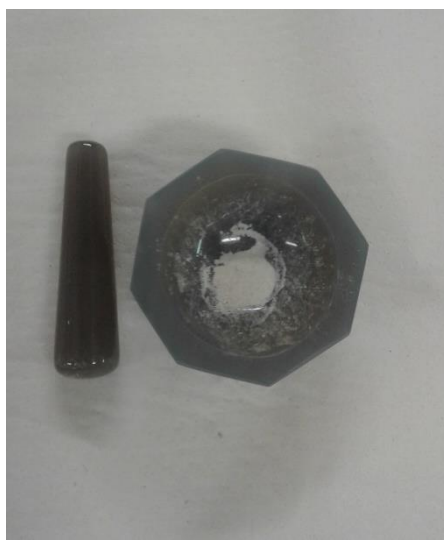


Figure 3.11: A sample mixture of KBr and GBPE capped Au-NPs.

3.6.3 X-Ray Diffraction (XRD) analysis:

The crystallinity of the GBPE-nanoparticles (Ag-Au-NPs, Au-NPs and Ag-NPs) was analysed by XRD analysis. The diffraction patterns were obtained using Bruker AXS (United States) D8 High-Resolution Diffractometer, voltage 40 KV; current 40 mA). The XRD spectra were recorded in the range 10-90° using an X-ray source of Cu $K\alpha$ ($\lambda=0.154$ nm) monochromatic radiation. The nanoparticles used for XRD analyses were prepared as in this chapter section and centrifuged and dried to a powder at room temperature after were submitted for XRD to determine their crystalline size and structure. The size of the NPs was

calculated using the Debye-Scherrer equation (**equation 3.4**) by making use of the FWHM of the most intense peak (the 111-index peak) at $2\theta = 38^\circ$ for both the Au and Ag-NPs samples and $2\theta = 37^\circ$ for Ag-Au-NPs. XRD experiment and analysis was performed at iThemba LABS, Somerset West, South Africa.

3.6.4 High-Resolution Transmission Electron Microscopy (HR-TEM) analysis:

HR-TEM equipped with energy-dispersed spectroscopy (EDS) detector together with selected area electron diffraction (SAED) was used to study the size and morphology of samples using an FEI Tecnai G2 20 field-emission gun (FEG), Oregon, United States, operated in bright field mode at an accelerating voltage of 200 kV. Energy dispersive x-ray spectra were collected using an EDAX liquid nitrogen cooled Lithium doped silicon detector. Samples were prepared by drop-coating one drop of specimen solution onto a carbon-coated copper grid. This was then dried under a xenon lamp for about 10 minutes, after which the sample coated grids were analysed under an HR-TEM microscope. The selected area electron diffraction (SAED) pattern was obtained by directing the electron beam perpendicular to one of the spheres. Images were further analysed using Image J software.

3.6.5 Small-Angle X-ray Scattering (SAX) analysis:

Scattering was carried out using Small-angle X-ray (Anton Paar, GmbH, Australia). Approximately 40 μL of the aqueous solution of nanoparticles (Ag-Au-NPs, Au-NPs and Ag-NPs) non-diluted was injected into a sample holder, and the scattering curves were collected using a SAX-drive software. Zero-point calibration was performed on the scattering curve using SAX-treat software, and background scattering removed using SAX-quant software.

GIFT software was used for SAXS calculations in order to obtain the scattering curves of pair distance distribution function (PDDF) and size by number distribution curve.

3.7 Electrochemical analysis:

3.7.1 Cyclic Voltammetry analysis:

The first to any successful electrochemical analysis is the cleaning of electrodes. The used glassy carbon electrodes were polished with 1.0, 0.3 and 0.5 μm alumina slurries using polishing pads by making a figure-eight polishing motion, as shown in **Figure 3.12**, and rinsing thoroughly with distilled water. This was followed by sonication in ethanol and water for at least 15 min, respectively. All these were done in order to remove the residual polishing material. 4 μL sample solutions of nanoparticles were drop-coated onto the surface of a thoroughly polished GCE and left to dry at room temperature.

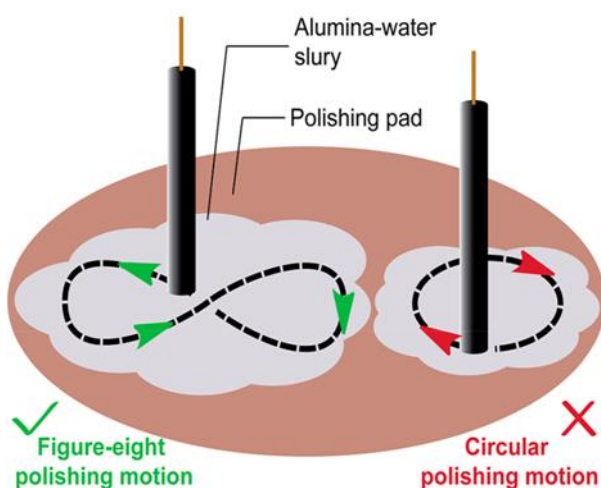


Figure 3.12: A typical example of a simple way of polishing an electrode on a cloth polishing pad [28,29].

Palm-Sensor PT trace 4.4 was used to perform cyclic voltammetry experiments connected to a computer monitor to study the electrochemical processes taking place on the working electrodes. A cell set-up consisting of platinum wire as a counter electrode (CE) / Auxiliary electrode, AgCl as a reference electrode (RE) and glassy carbon (GE) was used as working electrode (WE) as shown in **Figure 3.13**. N₂ gas was used to degas before all the experiments started. The applied potential range was set between -1.5 and 1.5 V at the scan rate was set at 50 mV/s. The experiment was carried out at a room temperature of 25 °C.

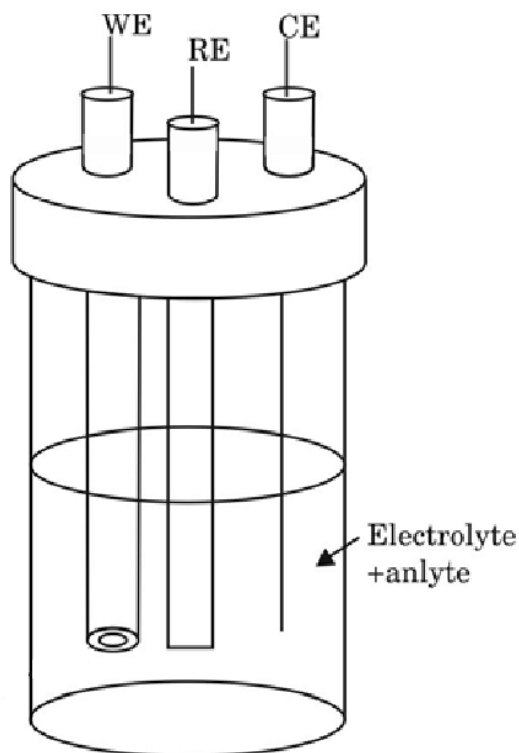


Figure 3.13: A typical representation of a three-electrode set-up in an electrochemical cell

3.8 References:

- [1] G.S. Bumbrah, R.M. Sharma, Raman spectroscopy – Basic principle , instrumentation and selected applications for the characterization of drugs of abuse, Egypt. J. Forensic Sci. 6 (2016) 209–215. <https://doi.org/10.1016/j.ejfs.2015.06.001>.
- [2] F.S. Rojas, C.B. Ojeda, Analytica Chimica Acta Recent development in derivative ultraviolet / visible absorption spectrophotometry : 2004 – 2008 A review, 635 (2009) 22–44. <https://doi.org/10.1016/j.aca.2008.12.039>.
- [3] D. Stone, UV/Vis Spectrophotometry, CHM217 Introd. to Anal. Chem. (2010).
- [4] A. Siekkinen, Y. Xia, Maneuvering the Surface Plasmon Resonance of Silver Nanostructures through, (2006) 15666–15675. <https://doi.org/10.1021/jp0608628>.
- [5] M.A. Ganzoury, N.K. Allam, T. Nicolet, C. All, Introduction to Fourier Transform Infrared Spectrometry, Renew. Sustain. Energy Rev. 50 (2015) 1–8. <https://doi.org/10.1016/j.rser.2015.05.073>.
- [6] PerkinElmer, Principles of FTIR, (2009) 17. <https://www.slideshare.net/muttaqinpapasafira/principles-of-ftir>.
- [7] A.A. Ismail, F.R. van de Voort, J. Sedman, Chapter 4 Fourier transform infrared spectroscopy: Principles and applications, Tech. Instrum. Anal. Chem. 18 (1997) 93–139. [https://doi.org/10.1016/S0167-9244\(97\)80013-3](https://doi.org/10.1016/S0167-9244(97)80013-3).
- [8] Y. Higashi, T.J. Smith, J.M. Jez, T.M. Kutchan, Crystallization and preliminary X-ray diffraction analysis of salutaridine reductase from the opium poppy *Papaver somniferum*, Acta Crystallogr. Sect. F Struct. Biol. Cryst. Commun. 66 (2010) 163–166. <https://doi.org/10.1107/S174430910904932X>.
- [9] S. V. Banne, M.S. Patil, R.M. Kulkarni, S.J. Patil, Synthesis and Characterization of Silver Nano Particles for EDM Applications, Mater. Today Proc. 4 (2017) 12054–12060. <https://doi.org/10.1016/j.matpr.2017.09.130>.
- [10] V. Accordingly, I. Boxes, Principles of X-ray Diffraction, 2006.
- [11] W. Pabst, E. Gregorova, Characterization of particles and particle systems, ICT Prague. (2007) 1–122. http://vscht.cz/sil/keramika/Characterization_of_particles/CPPS_English_version_.pdf.
- [12] K. Kato, H. Tanaka, Visualizing charge densities and electrostatic potentials in materials by synchrotron X-ray powder diffraction, Adv. Phys. X. 1 (2016) 55–80. <https://doi.org/10.1080/23746149.2016.1142830>.
- [13] T. Assemblies, Transmission Electron Microscopy of Shape-Controlled Nanocrystals and Their Assemblies, (2000) 1153–1175. <https://doi.org/10.1021/jp993593c>.
- [14] P. Yu, K. Man, AP 5301 / 8301 Instrumental Methods of Analysis and Laboratory Microscopy (III): Transmission Electron Microscopy (TEM), (n.d.).

- [15] B.R. Pauw, Corrigendum : Everything SAXS : small-angle scattering pattern collection, (2013). <https://doi.org/10.1088/0953-8984/26/23/239501>.
- [16] S.E. Flores-villaseñor, R.D. Peralta-, J.C. Ramirez-contreras, 12 - Biocompatible microemulsions for the nanoencapsulation of essential oils and nutraceuticals, Elsevier Inc., 2016. <https://doi.org/10.1016/B978-0-12-804307-3/00012-0>.
- [17] S. Hardainyan, Insights in Aquaculture and Biotechnology A Review on Nanoemulsions in Food Applications, 2 (2018).
- [18] S. Edition, Elements of Modern X-ray Physics, (n.d.).
- [19] J. Lipfert, S. Doniach, Small-Angle X-Ray Scattering from RNA , Proteins , and Protein Complexes, (2007). <https://doi.org/10.1146/annurev.biophys.36.040306.132655>.
- [20] J.A. Pople, Everything You Ever Wanted to Know About, (n.d.).
- [21] R. Fanelwa, Nanoparticulate of silver-modified poly (8-anilino-1-naphthalene sulphonic acid) nanobiosensor systems for the determination of Tuberculosis treatment drugs, (2011).
- [22] R.S. Nicholson, Theory and Application of Cyclic Voltammetry for Measurement of Electrode Reaction Kinetics, 37 (1965) 1351–1355. <https://doi.org/10.1021/ac60230a016>.
- [23] P. Paunović, Environmental electrochemistry - Importance and fields of application, Maced. J. Chem. Chem. Eng. 30 (2011) 67–74. <https://doi.org/10.20450/mjce.2011.71>.
- [24] K.J. Rountree, B.D. McCarthy, E.S. Rountree, T.T. Eisenhart, J.L. Dempsey, A Practical Beginner ' s Guide to Cyclic Voltammetry, (2017). <https://doi.org/10.1021/acs.jchemed.7b00361>.
- [25] D.J. Mazur, K. Uosakp, N.L. Weinberg, 3 (1992-1995), (1995).
- [26] J.C. Helfrick, L.A. Bottomley, Cyclic Square Wave Voltammetry of Single and Consecutive Reversible Electron Transfer Reactions, 81 (2009) 9041–9047. <https://doi.org/10.1021/ac9016874>.
- [27] P.S. Nnamchi, C.S. Obayi, Electrochemical characterization of nanomaterials, Elsevier Ltd., 2018. <https://doi.org/10.1016/B978-0-08-101973-3.00004-3>.
- [28] E.L.H. Thomas, G.W. Nelson, S. Mandal, J.S. Foord, O.A. Williams, Chemical mechanical polishing of thin film diamond, Carbon N. Y. 68 (2014) 473–479. <https://doi.org/10.1016/j.carbon.2013.11.023>.
- [29] N. Elgrishi, K.J. Rountree, B.D. McCarthy, E.S. Rountree, T.T. Eisenhart, J.L. Dempsey, A Practical Beginner's Guide to Cyclic Voltammetry, J. Chem. Educ. 95 (2018) 197–206. <https://doi.org/10.1021/acs.jchemed.7b00361>.

- [30] A. Senthil Kumar, R. Desikan, M. Gandhi, S. Huang, G. Verma, M. Deepa Rajagopalan, B. Purushotham, 3 *Electrochemistry of Phytochemicals and Natural Products*, (n.d.) 243–264.

CHAPTER FOUR

Results and Discussion: Part 1

This chapter provides the overall findings of the green synthesis of gold nanoparticles achieved through the reduction of Au⁺ ions using a combination of grape and banana peel extracts (under the conditions described in chapter 3.). The combined extract was used as a reducing and also as stabilising agent, without the addition of any form of external chemical stabilising or reducing agents. The adapted methodology is clean, environment-friendly, non-toxic and hazard-free.

4 . Gold Nanoparticles (Au-NPs):

4.1 Ultraviolet-Visible Spectroscopy (UV-vis) of (Au-NPs):

Figure 4.1 shows the photograph of grape-banana peel extract (GBPE) and gold chloride aqueous solution used in the synthesis of Au-NPs before the reaction as well as the obtained gold nanoparticles after a reaction time of 1 hour. The appearance of the purple colour after 1 hour seen from the reaction mixture of aqueous H₂AuCl₄ and the extract (under the conditions described in chapter 3), indeed revealed the presence of gold nanoparticles. According to Vijayakumar, the colour change is resultant from the unique surface plasmon vibrations of aqueous gold nanoparticles [1].

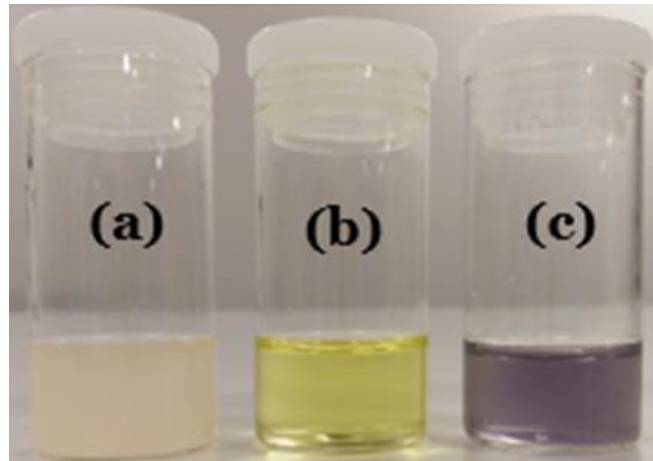


Figure 4.1: Photograph showing colour of solutions, (a) GBPE extract, (b) gold chloride, (c) GBPE Au-NPs.

Figure 4.2 shows the colour change of the reaction solution in the process of Au-NPs synthesis at different time intervals leading up to 1 hour. As the reaction time increased the colour of the solution became intense, that is, the purple colour became darker.

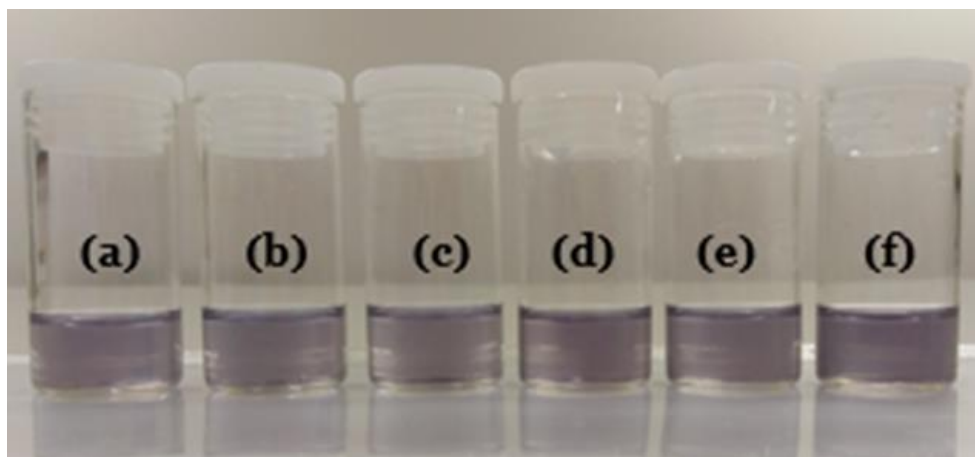


Figure 4.2: Visual inspection of the colour change after the synthesis of Au-NPs achieved at different time interval; (a) 10 min, (b) 20 min, (c) 30 min, (d) 40 min, (e) 50 min and (f) 60 min.

The resultant colloidal solutions were analysed by Ultraviolet-Visible spectroscopy (UV-vis), and the absorption spectra of the nanoparticles showed the plasmon resonance (SPR) peak at

a narrow wavelength of 535 nm as shown in **Figure 4.3**. Similar results on the visual observations of Au-NPs have been reported for tea extract synthesised gold nanoparticles where the appearance of a purple colour was observed within 5 min of the reaction, and the surface plasmon resonance peak was observed (SPR) in the 530 - 563 nm range [2]. Additionally, Sengani and co-workers also confirmed the maximum wavelength (λ max) of gold nanoparticles to be approximately 530 nm [3] while in another study by Elia and co-workers it was obtained at 530 nm [4].

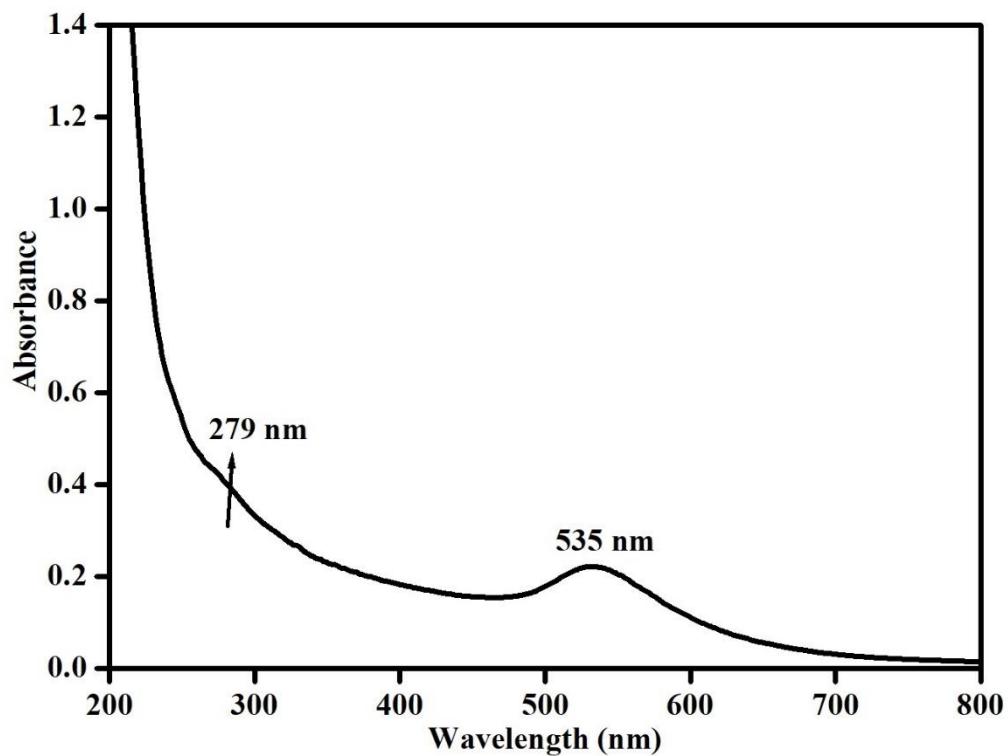


Figure 4.3: UV-Vis spectra of GBPE-Au-NPs.

Figure 4.4 shows the effect of time on the formation of the gold nanoparticles. The spectra show the reduction of Au^{3+} to Au^0 specifying the formation of Au-NPs starting from the completion time of 10 min [5]. Due to the interactions of charge transfer between chloro

ligands of H₂AuCl₄ and the metal Au a shoulder at 279 nm was observed and as the reaction time increases from 10 min to 60 min, the shoulder at 279 nm disappeared due to binding of amine groups to nanoparticles [6]. The observed maximum peak after each time interval, coupled with the gradual increase of λ_{max} indicated a redshift. The results indicate that the time needed for the formation of Au-NPs using grape-banana extract is very short and the optimal time in this study was 60 min, which is relatively less than in other reports, for instance, Yasmin and co-workers reported 1 hour 30 min for Au-NPs synthesised by Hibiscus rosa Sinensis herbal plant [7]. Additionally, this study is also in good agreement with the work of Ismail and co-workers who achieved the formation of gold nanoparticles using the extract of grape leaves and seeds [5]. Earlier studies have reported 24 – 120 hour time periods for complete reduction of gold by fungi or bacteria [8]. Recently Divakarana and co-workers also reported the formation of gold nanoparticles within 2 hours using dragon fruit extract [9].

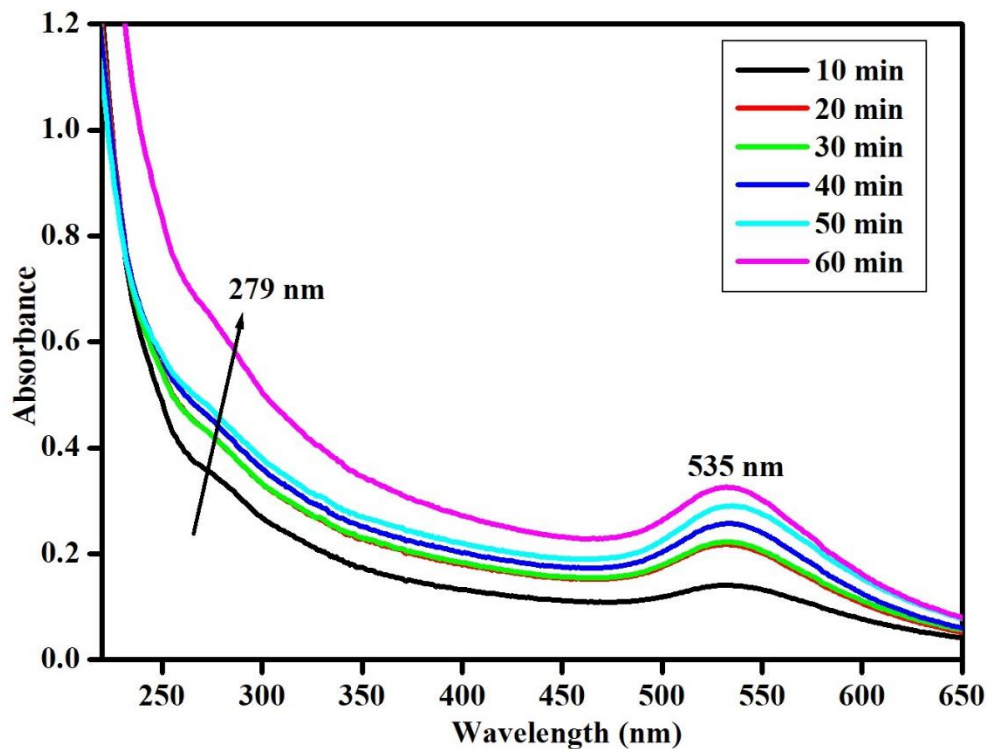


Figure 4.4: UV-Vis spectra of GBPE-Au-NPs at different time intervals.

Table 4.1 shows the comparison of the SPR bands and reaction times for the complete reduction of gold ions from previously reported studies compared to the current study. These studies were all achieved using natural products as reducing agents, as it can be seen from the table the SPR band was in a similar position in all the studies and this study showed a complete reduction in 60 min which is less compared to the other studies.

Table 4.1: Comparison of studies from literature and the present work, for the time taken for complete reduction of gold chloride using natural products as reducing agents.

| Type of Nanoparticles | Natural product used | Wavelength (nm) | Reaction time (min) | Reference |
|-----------------------|--------------------------|-----------------|---------------------|------------|
| Au-NPs | Natural Honey | 545 nm | 180 min | [10] |
| Au-NPs | <i>Salix alba</i> Leaves | 540 nm | 150 min | [11] |
| Au-NPs | Grape and Banana Peel | 535 nm | 60 min | This Study |

4.2 Fourier Transform Infrared Spectroscopy (FT-IR) of GBPE-Au-NPs:

Spectra of the colloidal GBPE-Au-NPs solution and the pure extracts were obtained using Fourier Transform Infrared (FT-IR) Spectroscopy. FT-IR was employed to validate the major functional groups in the extract and their involvement in the synthesis and stabilisation of the synthesised gold nanoparticles (Au-NPs). **Figure 4.5** represents the spectra of grape-banana peel extracts (GBPE) (black curve) and the synthesised Au-NPs (red curve) where they were compared in order to investigate the changes before and after the reaction with peak assignment. In this study, FT-IR was used to identify the type of functional groups that were responsible for the reduction of Au⁺ ions and also to identify the type of functional groups that are coated or capped onto the Au-NPs.

Similar spectra between the extract and colloidal solution were obtained, as shown in **Figure 4.5**, indicating that the same compounds existed before and after the reaction. Although the similarities were observed, some of the absorption peaks are seen to be shifted in their position after the addition of H₂AuCl₄. From the FT-IR spectra, the presence of the sharp O-H peak at 3323 cm⁻¹ was due to O-H stretch from alcohols and phenols present in the GBPE. The sharp peak at 2927 cm⁻¹ in GBPE represents the O-H stretching vibration bands characteristic of carboxylic acids and C-H stretches from alkanes. Hence, the synthesised Au-NPs are stabilised and coated by functional groups that are present in the GBPE [12]. The functional groups that are present within GBPE include polysaccharides such as cellulose, phytochemical carotenoid [13,14] as well as proteins through the binding or interaction of free NH₂ groups. After the bio-reduction of gold nanoparticles, the reduction of the peak intensities in the Au-NPs spectrum revealed that these groups are involved in the process of forming nanoparticles [15]

The FT-IR spectrum of Au-NPs showed a band at 3270 cm⁻¹ due to O-H, hydrogen-bonded stretch with phenols and alcohol groups from sugars present in flavonoids and phenolic compounds found in grape and banana peel such as myricetin and quercetin [16]. The weak peak at 2093 cm⁻¹ is due to thiols S-H stretch [17] indicating the presence of banana in the GBPE extract. The peak observed at 1725 cm⁻¹ was assigned as the stretching vibration of C=O from carboxylic acids showing the presence of hemicellulose band from banana peel [18], as well as myricetin compounds present in both grape and banana peel. The peak at 1633 cm⁻¹ is characteristic of C=C stretch in alkene and aromatic rings from phenolic compounds, and organic acids such as ellagic acid from grapes and galacturonic acid, pectic from banana peel and a slight reduction was observed in the spectrum of Au-NPs compare to the GBPE spectrum which shows the involvement of the functional groups in the synthesis. The bands at 1407 and 1253 cm⁻¹ are due to the presence of aromatic rings and nitro

compounds in flavonoids of grapes while the C=C, N-O and C-N stretch are due to amine groups from hemicellulose, lignin and pectin present in grapes and banana peel [19,20]. These peaks were reduced in intensity as compared to the Au-NPs spectrum revealing the involvement of nitrile groups from the extracts as one of the capping agents for the nanoparticles. The weak peak at 636 cm^{-1} corresponds to asymmetric stretching of C-H groups from anthocyanins present in flavonoids from grapes as shown in the spectrum and seen to disappear in the spectrum of Au-NPs due to its participation in the synthesis process. The Au-NPs spectrum also indicates another peak at 585 cm^{-1} caused by the vibrations of the nanoparticles, thus confirming the formation of the nanoparticles [21].

Finally, amine, hydroxyl and carboxyl groups were responsible for the formation of the novel gold nanoparticles [22] while the phenolic compounds that were present in the extract were the driving force in the formation of the nanoparticles [23]. The obtained results are similar to those previously reported in other studies [24,25].

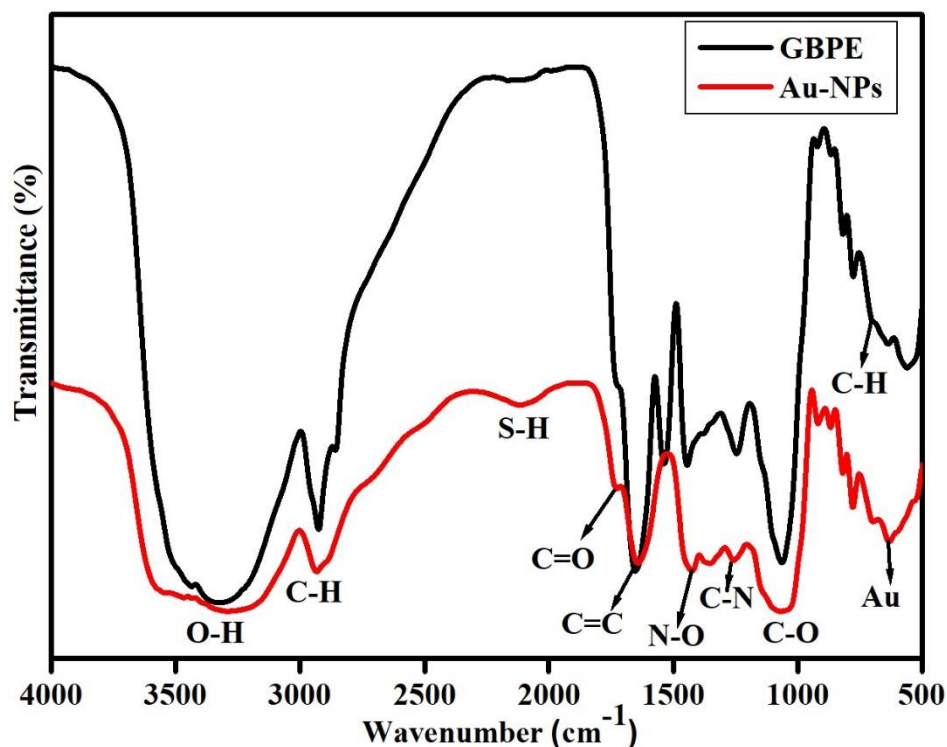


Figure 4.5: FT-IR spectra of the green synthesised Au-NPs and GBPE.

4.3 X-ray diffraction analysis (XRD) of Au-NPs:

The crystalline nature of the gold nanoparticles was confirmed using X-ray diffraction (XRD) analysis. This technique is used to characterise the crystallographic structure, the orientation and the grain size of nanoparticles. The XRD analysis shown in **Figure 4.6**, indicates that the synthesised Au-NPs have well defined firm characteristic peaks of gold an indication of the crystalline nature of the synthesised Au-NPs. Indicated herein are intense Bragg Reflection peaks at 38.185, 44.393, 64.578, 77.549 and 81.724 resultant from the following crystal planes (111), (200), (220), (311) and (222) planes, respectively [26]. According to a study by Nadagouda and co-workers and (JCPDS No. 04-0784) [27,28], these are the Bragg's reflections of the FCC (face centred cubic) structure of crystalline metallic gold nanoparticles

[29]. These peaks have a perfect match with the standard diffraction corresponding to the reflections of crystal planes and revealed that the synthesised Au-NPs are pure and crystalline. The peak corresponding to (111) plane is more intense than the other planes suggesting that the (111) plane is the predominant orientation of the nanoparticles.

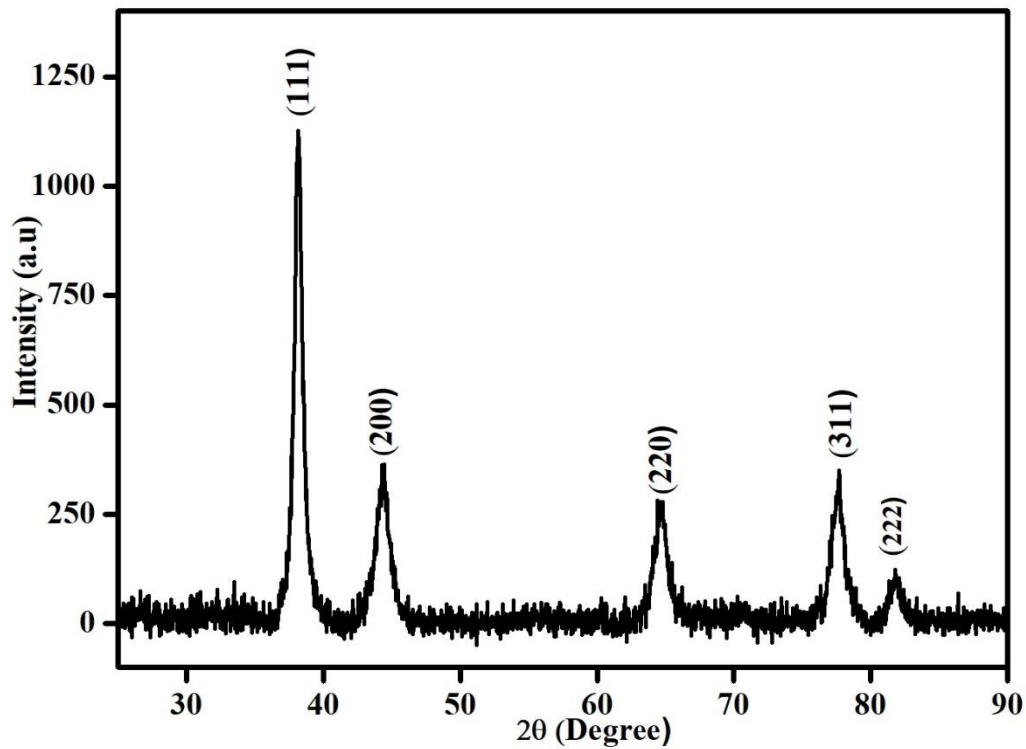


Figure 4.6: X-ray diffraction pattern of green synthesised Au-NPs.

The size of 12.3 nm of the crystallised nanoparticles was estimated from the breadths of the diffraction peak using the Scherer's equation (**equation 3.4**, chapter 3) [30].

Therefore, from the Scherer's Equation

$$d = \frac{K\lambda}{\beta \cos \theta} \quad (3.4)$$

Where: d = particle/crystal size, K is a constant and can be defined as the dimensionless shape factor and is equal to $0.94 K$ usually range from $0.5 - 1$, and λ is the X-ray wavelength (0.154 nm), β is the full-width half-maximum (FWHM in radians), θ is the angle of reflection.

These results agree with the XRD results obtained in other studies such as Biao and core-workers using Pomegranates peel extract [31]. The findings are also similar to the joint committee for powder diffraction Set (JCPDS) card number 00-407-84 of metallic gold [32,33]. **Table 4.2** shows the comparison of Bragg's diffraction peaks at 2θ value and the average crystal size of the green synthesised nanoparticles calculated using Debye-Scherrer formula (from literature) and the present work. As seen from the table, this study developed the smallest nanoparticles. The difference in the size of the synthesised nanoparticles was due to the presence of more than one reducing agent on a natural product used and different selection of suitable reaction condition for synthesis [34].

Table 4.2: Comparison of Bragg's diffraction peaks at 2θ value and the size of crystalline green synthesised nanoparticles (from literature) and the present work.

| Nanoparticles | 2 θ (Degrees) corresponding | | | | | Crystalline size (nm) | Reference |
|------------------------------------|------------------------------------|------|------|-------|------|-----------------------|-----------|
| | 111 | 200 | 220 | 311 | 222 | | |
| Psidium Guajava Leaf capped Au-NPs | 37.5 | 44.1 | 63.9 | 77.47 | 81.6 | 61 | [35] |

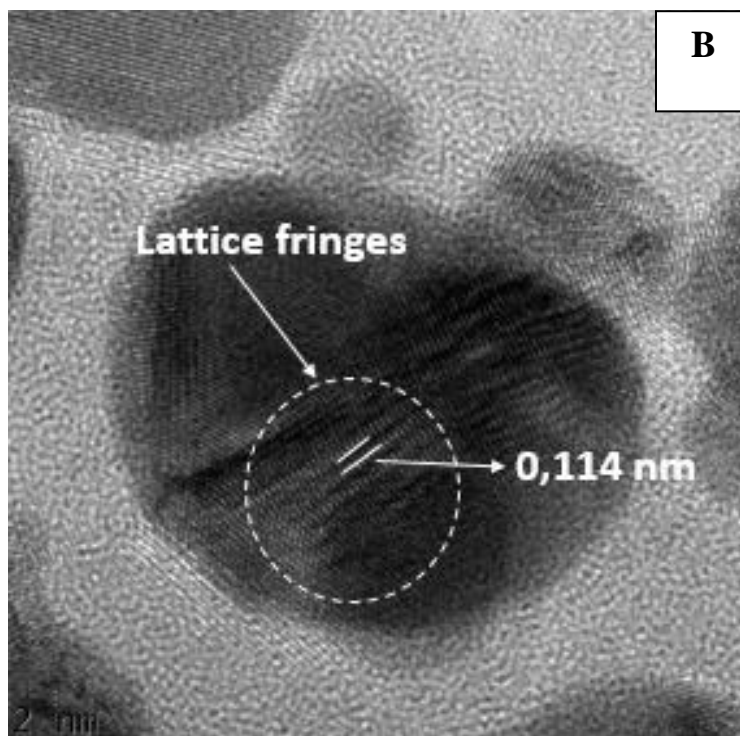
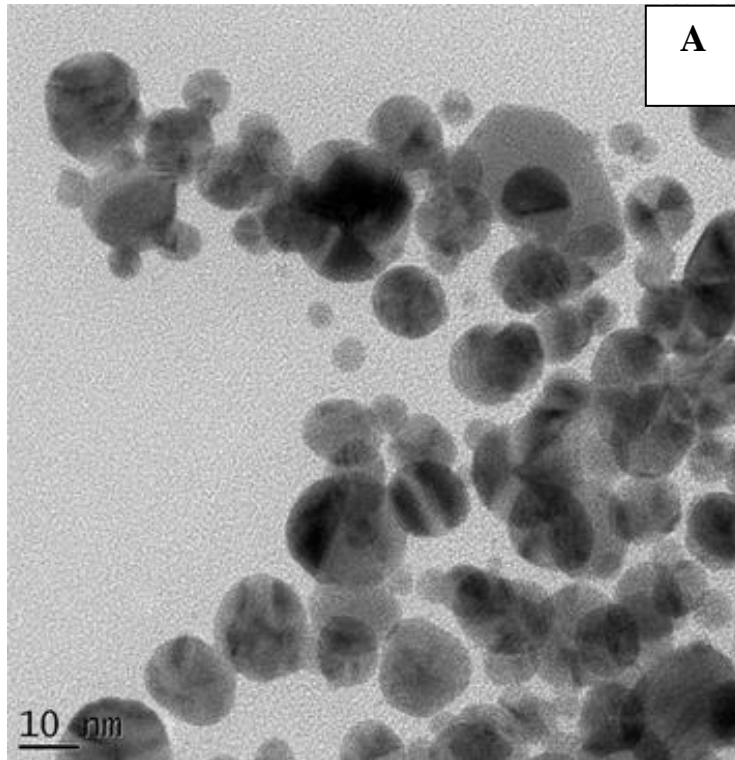
| | | | | | | | |
|-----------------------------|--------|--------|--------|--------|--------|---------|------------|
| Citrus Maxima capped Au-NPs | 38.56 | 44.67 | 64.50 | 77.58 | 81.67 | 25.7 | [36] |
| GBPE capped Ag-Au-NPs | 38.185 | 44.393 | 64.578 | 77.549 | 81.725 | 12.3 nm | This Study |

4.4 High-Resolution Transmission Electron Microscopy (HR-TEM) of GBPE Au-NPS:

The size and shape of the bio-synthesised Au-NPs were revealed with the help of High-Resolution Transmission Electron Microscopy (HR-TEM) analysis where the images confirmed the synthesis of Au-NPs [37]. **Figure 4.7 (a)** shows the HR-TEM image of the grape-banana peel capped gold nanoparticles to be predominantly spherical with sizes ranging from 10 to 17 nm, which agrees with the obtained XRD results. Similar results of spherical Au-NPs shape were obtained using different fruit extracts such as Satsuma mandarin extract [38] and Watermelon rind extract [39]. It was found that the synthesised Au-NPs had different sizes while having the same shape and were thus described as being polydisperse. An HR-TEM image of one spherical GBPE-Au-NPs is shown in **Figure 4.7 (b)**. It shows lattice fringes of the nanoparticles which reveals the polycrystalline nature of GBPE Au-NPs, the lattice fringe spacing indicated in the image is 0.114 nm which related to the (111) facet of crystal plane of the gold cubic phase. This spacing is known as inter-planar spacing (d-spacing) which is in between the vertical lattice fringes, indicating the space between the XRD Bragg's reflection [40]. **Figure 4.7 (c)** shows the selected area electron diffraction (SAED) and the following four Bragg's reflection rings (111), (200), (220), and (311). SAED is obtained by directing the electron beam perpendicular to one of the spheres of GBPE-Au-NPs, and the presence of spotlight is an indication of a single crystal. The

SAED pattern confirmed the XRD findings in terms of the identified rings and the fact that they are crystalline face centred cubic in nature [41]. Similar SAED patterns were reported for green synthesised Au-NPs as shown by a study by [10].

The particle size distribution histogram of the synthesised Au-NPs shown in **Figure 5.7(d)** was found to be in good agreement with the values obtained from HR-TEM and XRD measurements. The histogram was created by considering 100 nanoparticles obtained from the HR-TEM image analysis using Image J software suggests that the average size distribution ranged from 10 to 17 nm [42]. **Table 4.3** shows the comparative values of sizes determined using HR-TEM measurements for green synthesised Au-NPs obtained from previously reported studies versus this study. As seen from the table this study shows the smallest range in terms of size for Au-NPs. Small sized nanoparticles are considered to be better since they have large surface area to volume ratios and have improves properties in terms of applications.



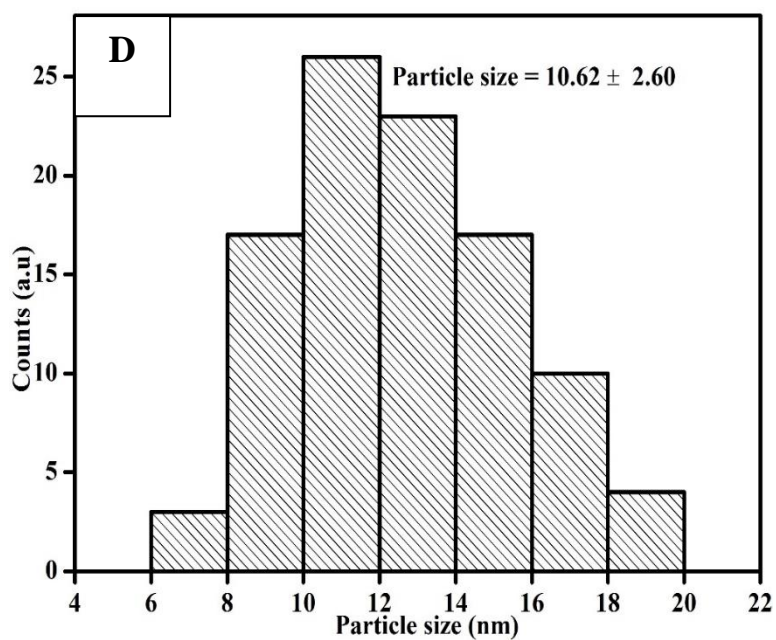
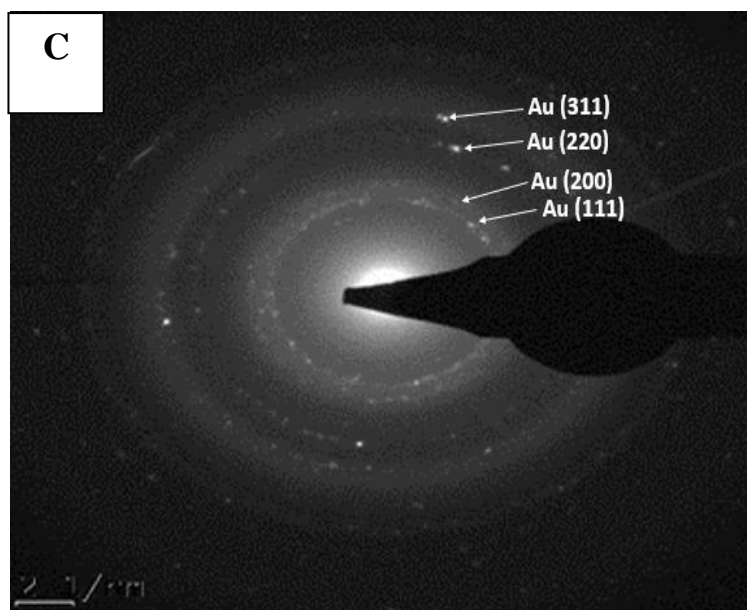


Figure 4.7: (a) HR-TEM images; (b) Lattice fringes; (c) SAED pattern; (d) Particle size distribution of the GBPE-Au-NPs.

Table 4.3: Comparison of size (calculated based on HR-TEM measurements) of green synthesised nanoparticles.

| Type of Nanoparticles | Natural Product | Reducing agent | Size (nm) | Reference |
|-----------------------|---|------------------|-----------|------------|
| Au-NPs | <i>Volvariella volvacea</i> Mushroom | Mushroom Extract | 20-150 nm | [43] |
| Au-NPs | <i>Plumeria alba</i> Flower | Flower Extract | 15-28 nm | [44] |
| Au-NPs | Grapes and Banana peel | Fruit Extract | 10-17 nm | This Study |

The presence of the elemental gold is evident in **Figure 4.8**, as indicated by energy dispersive spectroscopy analysis (EDS). EDS analysis showed the presence of a robust elemental gold signal at 2.140 keV, which matches the elemental Au in green synthesised Au-NPs in a study by Gopinath and co-workers [45]. Weak peaks of carbon and oxygen were also found and are as a result of the polyphenol groups in the GBPE extract used during the synthesis [46]. Copper signals were due to the copper grid which the sample was placed onto before analysis [47,48]. The obtained results are similar to a previously reported study by Girish and co-worker's where banana fruit waste was used to synthesise gold nanoparticles. In this study, <20 nm spherical nanoparticles were observed with 0.243 lattice fringes, as shown in HR-TEM analysis while their EDS revealed Au elemental peak at 2.120 keV values in line with our study [49].

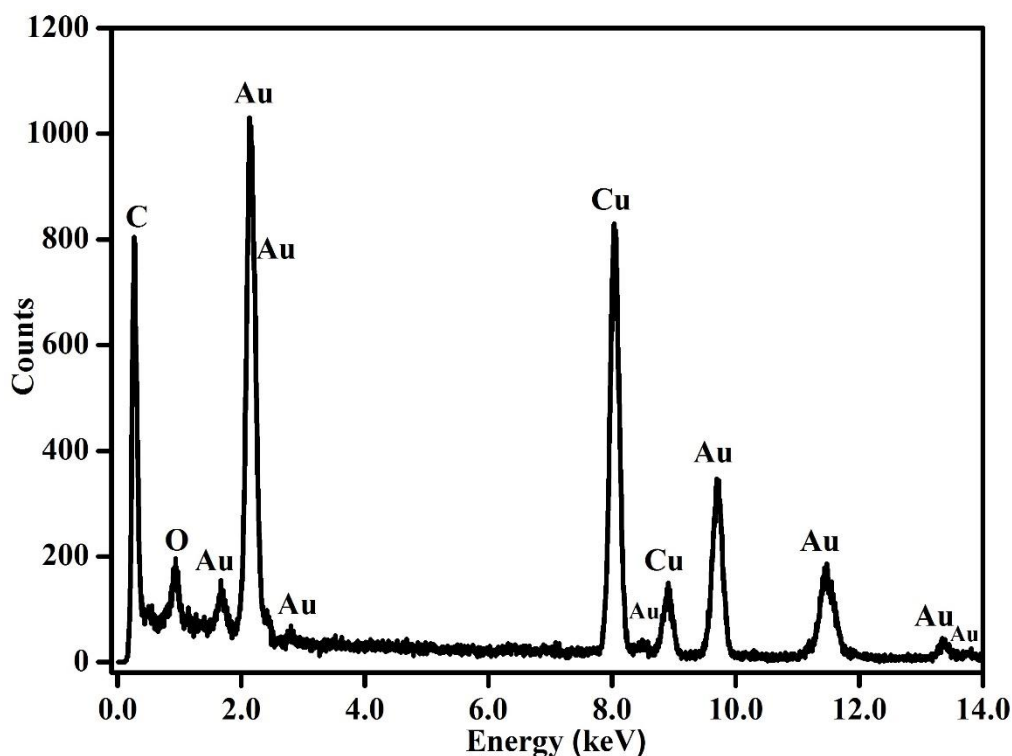


Figure 4.8: Energy Dispersive Spectroscopy patterns of GBPE capped Au-NPs.

4.5 Small-angle x-ray Scattering:

Nanometer-sized particles play a remarkable and fascinating role in material science. Interestingly, the mean size and size distribution of nanometer-sized particles are important in many applications. Hence in this study, small-angle X-ray scattering analysis, well known as (SAXS) was mainly aimed to determine the precise size distribution, shape, and internal structure of the synthesised nanoparticles. As seen in **Figure 4.9**, the free model pair-distance distribution function (PDDF) of the GBPE capped Au-NPs obtained a characteristic profile, typically observed for core-shell particles with different sizes (maximum diameter size of 157 nm) [50], extracted from PDDF data where $P(r) = 0$. Literature reveals that when $P(r) = 0$, the largest particle size can be obtained [51].

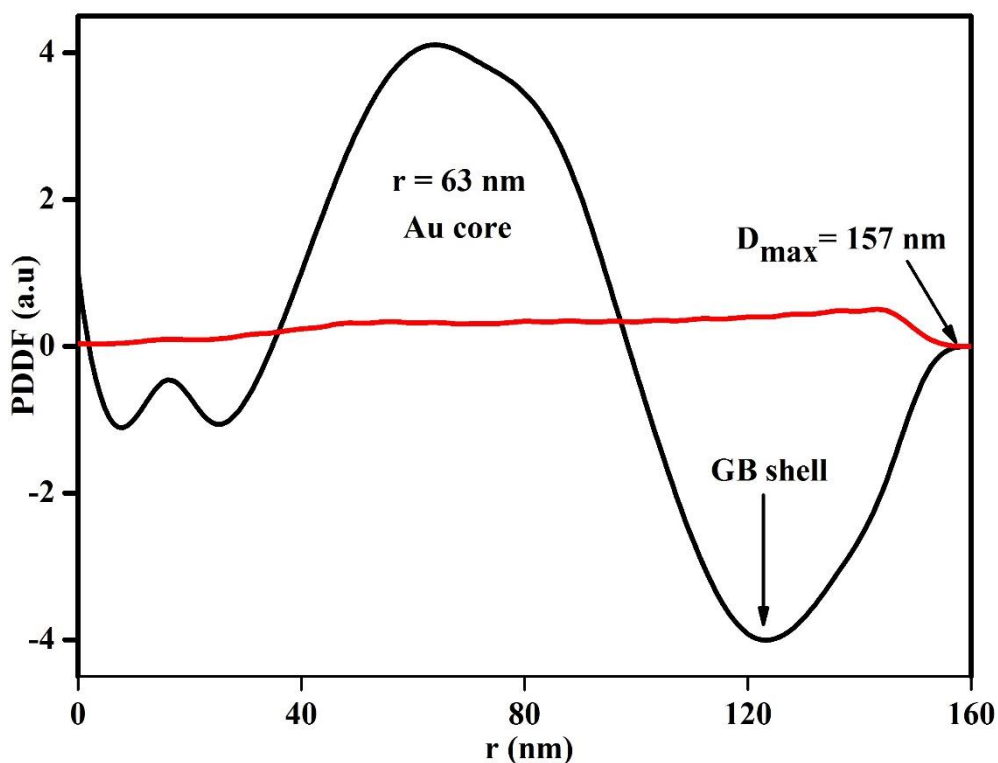


Figure 4.9: SAXS pair-distance distribution function (PDDF) of GBPE-Au-NPs.

In addition to this, the size distribution functions (**Figure 4.10**) weighted by number (black line) and intensity (red line) were calculated with program GIFT (i.e. a model fit of spheres with a log-normal size distribution) [52], where the GBPE capped Au-NPs revealed highly poly-dispersed particles with average radiuses of (16 nm, 72 nm and 127 nm), respectively [53]. Consequently, the observed poly-dispersed particles indicated that most of the particles appeared at 72 nm for both size distribution functions weighted by number and intensity. It should be noted that the size of 16 nm is consistent with the determined values as reported by HR-TEM (**Figure 4.7 (d)**). However, the appearance of an enhanced peak at 127 nm was ascribed to distribution by intensity. According to literature, colloidal suspensions consist of polydispersed particles, and the measured scattering intensity represents the sum of the scattering intensities from particles of various sizes [54]. This is given by (**Equation 5.1**):

$$\mathbf{I}(\mathbf{q}) = NV (\mathbf{p} - \mathbf{p}_0)^2 \int_0^\infty \left(\frac{\pi d^3}{6}\right)^2 f(d)P(\mathbf{q}, d) \mathbf{d}d \quad (5.1)$$

where $f(d)$ is the particle size distribution by number.

SAXS analysis reveals that Au is cored by the material of the capping agent, thus forming core-shell nanoparticles. Khatami and co-workers reported that core-shell nanoparticles are characteristic of two different materials where one nanomaterial (core) is surrounded by the other (shell). Usually, in green synthesised core-shell nanoparticles, the metal is the core then the biomolecules become the shell, thus forming heterogeneous nanoparticles [53]. EDS also confirm or support these observations as shown in **Figure 4.8**, which reveal the presence of gold, carbon and oxygen in the Au-NPs sample. Carbon and oxygen come from the antioxidant GBPE and are the main components of the material which remain even after synthesis to stabilise the Au-NPs [55]. The polydispersity nature of the synthesised Au-NPs is due to agglomeration. Agglomeration is well known as a secondary particle growth, and the secondary particle growth occurs when the powder is not monodisperse but polydispersed [56].

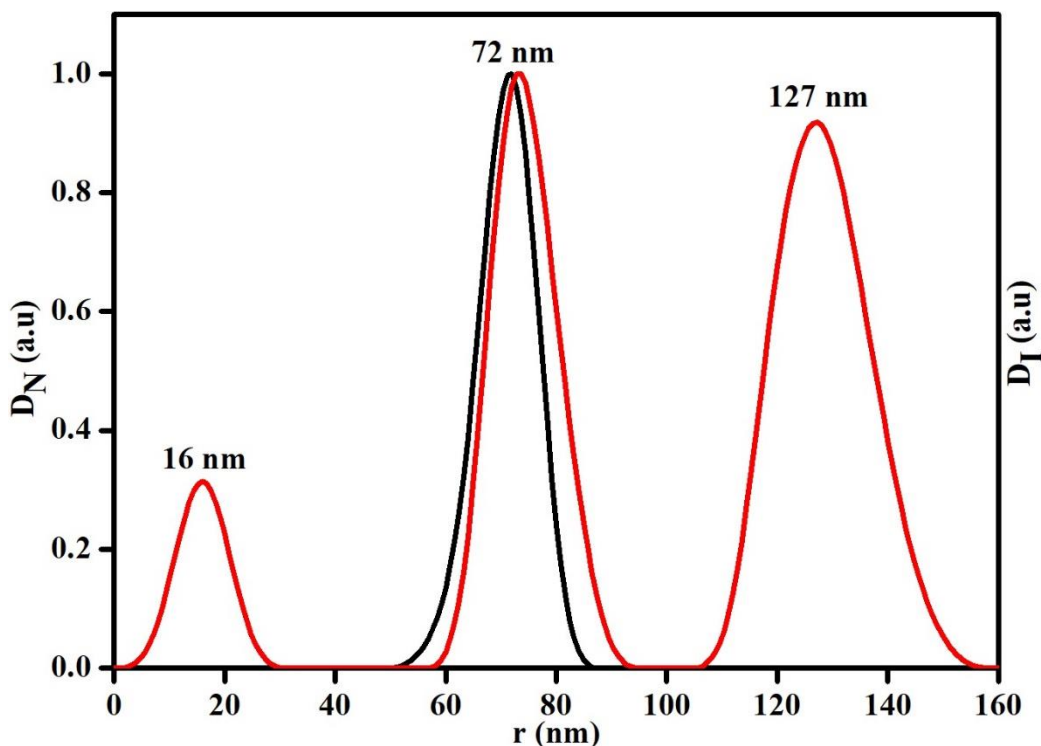


Figure 4.10: Size distribution functions weighted by number (black line) and intensity (red line).

4.6 Electrochemical characterisation of GBPE capped Au-NPs (CV) of Au-NPs:

In this study, electrochemical analyses were performed in order to establish whether or not these novel Au-NPs had any electrochemical properties. Before starting the experiment, the reaction media phosphate buffer (0.2 M, pH 7.4) was degassed while the electrodes were immersed in the solution. **Figure 4.11** shows the CV of drop casted Au-NPs compared to a bare glassy carbon electrode in a 0.2 M phosphate buffer solution (PBS) where a substantial current difference was observed for the modified electrode denoted as Au-NPs|GCE as opposed to the bare electrode. The voltammograms in **Figure 4.12** reveal how the current response changed with increased scan rates ($10 - 100 \text{ mV/s}^{-1}$) while studying the electrochemical properties of Au-NPs. For the Au-NPs|GCE electrode, a redox peak was observed with an E_{pc} value of 0.10 V and E_{pa} value of -0.06 V revealing the reduction

reaction of Au^{3+} to Au^0 while an oxygen peak was also observed at -0.65 V [46]. Both the anodic and cathodic peak currents increased with increasing scan rate [48] an indication that the nanoparticles are indeed electrochemical, a requirement in electrochemical sensor fabrication. Zhao and co-workers also observe the redox peak at similar regions on their study using electrodeposited gold nanoparticles on GCE [57].

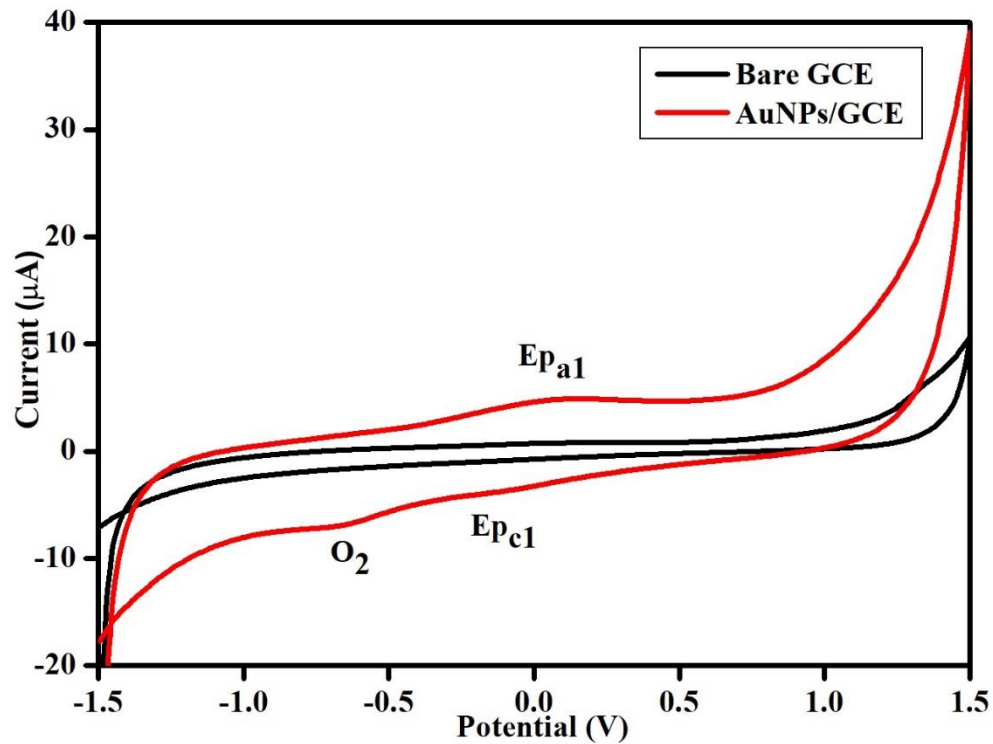


Figure 4.11: Cyclic voltammogram of bare GCE (Black line), Au-NPs|GCE (Red line) in 0.2 M PBS, pH 7.4 at 50 mV/s.

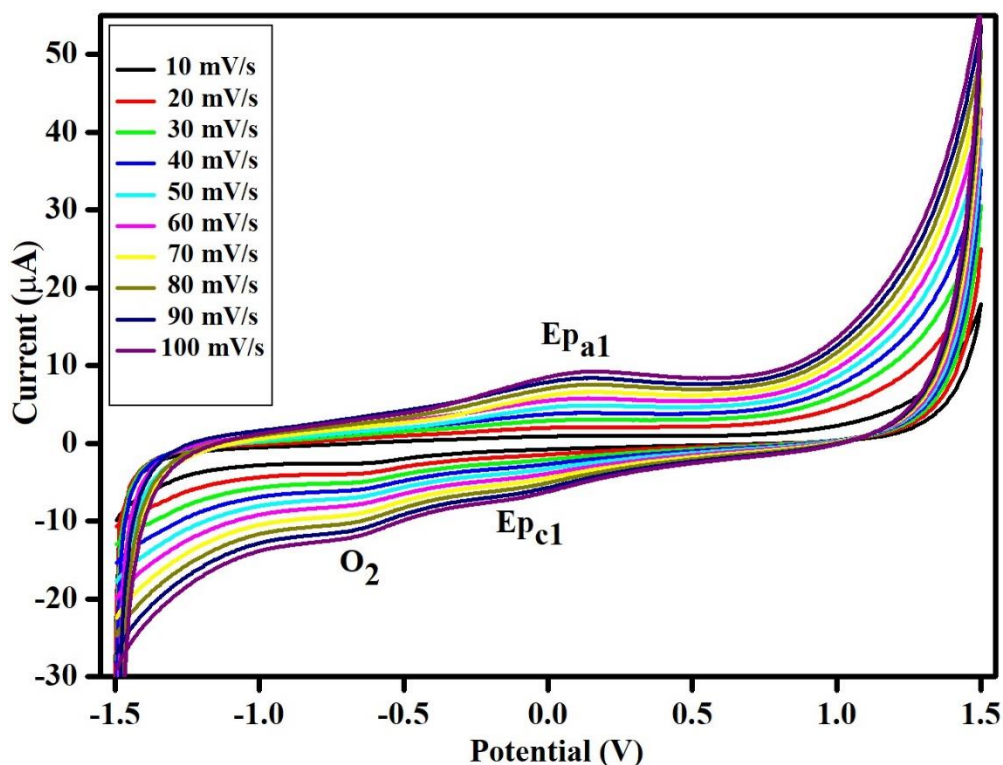


Figure 4.12: Represent Multi-scan voltammograms of Au-NPs in 0.2M PBS, pH 7.4 at (10-100 mV/s).

Cyclic voltammograms of different scan-rates can be used to construct several linear plots that could help to get information about the redox properties of the functionalised nanoparticles. Usually, the slope of log scan rate versus log current plot can be used to obtain information about whether the system is diffusion-controlled or adsorption controlled. Such that, a slope of 0.5 indicate diffusion-controlled, and a slope of 1 indicates adsorption controlled system. The intermediate values of the slope indicate "mixed" diffusion-adsorption controlled system. From the cyclic voltammograms of the modified glassy carbon electrode surfaces with GBPE capped Au-NPs at various scan rates **Figure 4.12**, the relationships of the anodic and cathodic peak potentials with the scan rate were analysed to calculate the electrochemical parameters. A plot of log anodic current peak versus the log scan rate was plotted for the GBPE-Au-NPs where nearly a straight line with a linear regression $I_{pa} (\mu A) =$

0.8326x - 0.2049 and a correlation coefficient $r^2 = 0.9983$ was determined as shown in **Figure 4.13**. The plot indicates the dependence of anodic peak current on the scan rate, and the slope indicates a mixed diffusion-adsorption system or process [58]. The ratio of the anodic and cathodic peak (I_{pa} / I_{pc}) of the system was not $\neq 1$ using current values obtained in **Figure 4.12**, and the system was determined to be quasi-reversible. The peak to peak separation $\Delta E_p = E_{pa} - E_{pc}$ (**Equation 5.2**) was determined to be $> 0.059/n$ V and the peak current was seen to increase with increasing scan-rate, thus confirming a quasi-reversible system [59]. The formal potential $E = (E_{pa} + E_{pc}) / 2$ of the system is the mid-way between E_{pa} and E_{pc} was determined to be 0.335 V. Lin and co-workers reported similar data on a study conducted using glassy carbon electrodes modified with Au-NPs [60].

Additionally, since at low scan rates, quasi-reversible processes appears to be fully reversible [61]. The reversible Randles-Sevcik equation (**Equation 5.3**) which can be written in a more concise form (**Equation 5.4**) at room temperature (25 °C) was used to calculate the diffusion coefficient (D_e) of the Au-NPs|GCE electrode [62]. From the equation, (**Equation 5.4**) I_p is the peak current (in A), n is the number of electrons, A the electrode area (in cm^2), C the concentration (in mol/cm^3), D_e the diffusion coefficient (in cm^2/s), and v the scan rate (in V/s). D_e can be defined as the amount of a substance (analyte) that diffuses across a unit area in 1 s under the influence of a gradient of one unit. A value of $5.199 \times 10^{-5} \text{ cm}^2 \cdot \text{s}^{-1}$ was determined to be the diffusion coefficient of the Au-NPs|GCE electrode. The obtained D_e was larger compared to the previously reported in literature. Larger values of D_e indicates a faster motion of analyte through the solution whereas small values of D_e indicates slower motion. Recently Zhang and co-workers reported D_e of $8.2 \times 10^{-6} \text{ cm}^2 \text{ s}^{-1}$ using AuNP/rGO HMS/GCE which was lower compared to this study [63].

$$I_p = 0.4463nFAC\left(\frac{nFvD_{eAu-NPs}}{RT}\right)^{1/2} \quad (5.3)$$

At 25 °C, equation 5.3 takes the form of equation 5.4 below

$$i_p = (2.69 \times 10^5)n^{3/2}ACD^{1/2}v^{1/2} \quad (5.4)$$

Using the Brown-Anson method (**Equation 5.5**) [64,65] the surface concentration Γ^* (mol cm⁻²) of the GBPE capped Au-NPs modified electrode was estimated to be 2.285 x 10⁻⁴ mol cm⁻². From the equation, n is the number of electrons transferred, F is the faraday constant (96485 C mol⁻¹), Γ^* represent the surface concentration of the Au-NPs (mol cm⁻²), A is the surface area of (GCE) (0.0201 cm²), v is the scan rate (V s⁻¹), R is the gas constant (8.314 J mol⁻¹ K⁻¹), T is the absolute operating temperature of the system (25 °C T in 298 K).

$$I_p = \frac{n^2F^2\Gamma^*_{Au-NPs}AV}{4RT} \quad (5.5)$$

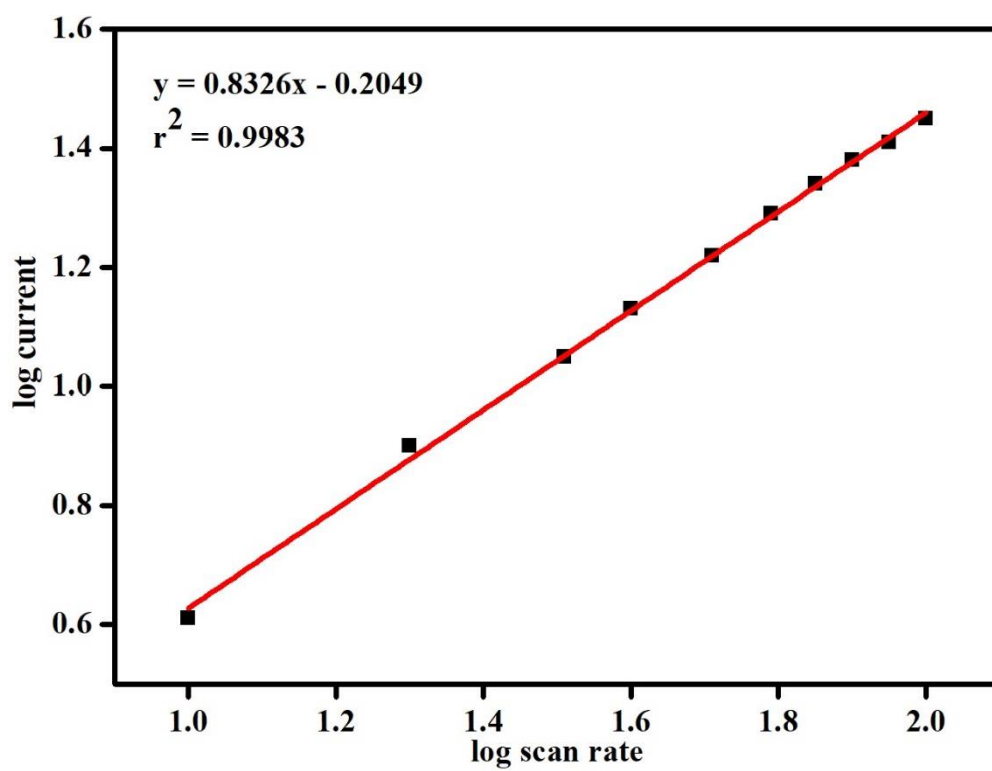


Figure 4.13: Plots of log current versus log scan rate of GBPE capped AuNPs.

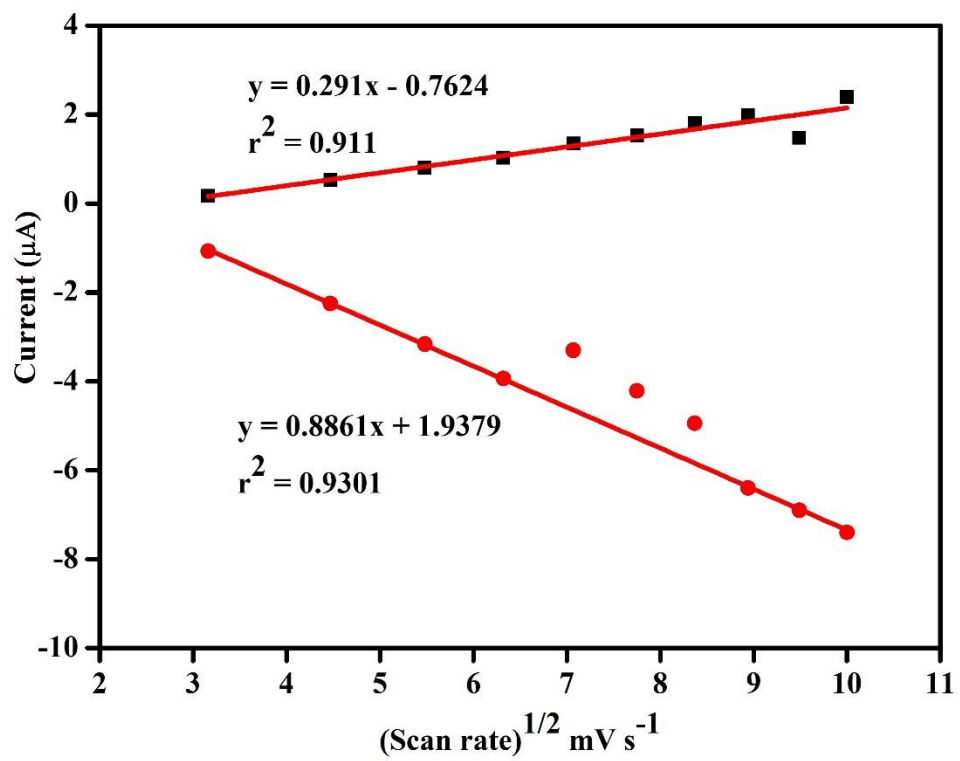


Figure 4.14: Randles-Sevcik Plot for GBPE capped Au-NPs.

4.7 References:

- [1] R. Vijayakumar, V. Devi, K. Adavallan, D. Saranya, Green synthesis and characterization of gold nanoparticles using extract of anti-tumor potent *Crocus sativus*, *Phys. E Low-Dimensional Syst. Nanostructures*. 44 (2011) 665–671. <https://doi.org/10.1016/j.physe.2011.11.002>.
- [2] R.K. Sharma, S. Gulati, S. Mehta, Preparation of gold nanoparticles using tea: A green chemistry experiment, *J. Chem. Educ.* 89 (2012) 1316–1318. <https://doi.org/10.1021/ed2002175>.
- [3] M. Sengani, A.M. Grumezescu, V.D. Rajeswari, Recent trends and methodologies in gold nanoparticle synthesis – A prospective review on drug delivery aspect, *OpenNano*. 2 (2017) 37–46. <https://doi.org/10.1016/j.onano.2017.07.001>.
- [4] P. Elia, R. Zach, S. Hazan, Green synthesis of gold nanoparticles using plant extracts as reducing agents, (2014) 4007–4021.
- [5] E.H. Ismail, M.M.H. Khalil, F.A. Al Seif, F. El-Maghdoub, Biosynthesis of gold nanoparticles using extract of grape (*Vitis vinifera*) leaves and seeds, *Prog. Nanotechnol. Nanomater.* 3 (2014) 1–12.
- [6] S.S. Dash, B.G. Bag, Synthesis of gold nanoparticles using renewable *Punica granatum* juice and study of its catalytic activity, *Appl. Nanosci.* 4 (2014) 55–59. <https://doi.org/10.1007/s13204-012-0179-4>.
- [7] A. Yasmin, K. Ramesh, S. Rajeshkumar, Optimization and stabilization of gold nanoparticles by using herbal plant extract with microwave heating, *Nano Converg.* 1 (2014) 1–7. <https://doi.org/10.1186/s40580-014-0012-8>.
- [8] S. He, Z. Guo, Y. Zhang, S. Zhang, J. Wang, N. Gu, Biosynthesis of gold nanoparticles using the bacteria *Rhodopseudomonas capsulata*, *Mater. Lett.* 61 (2007) 3984–3987. <https://doi.org/10.1016/j.matlet.2007.01.018>.
- [9] D. Divakaran, J.R. Lakkakula, M. Thakur, M.K. Kumawat, R. Srivastava, Dragon fruit extract capped gold nanoparticles : Synthesis and their differential cytotoxicity effect on breast cancer cells, *Mater. Lett.* (2018). <https://doi.org/10.1016/j.matlet.2018.10.156>.
- [10] D. Philip, C. Unni, S.A. Aromal, V.K. Vidhu, *Spectrochimica Acta Part A : Molecular and Biomolecular Spectroscopy Murraya Koenigii* leaf-assisted rapid green synthesis of silver and gold nanoparticles, *Spectrochim. Acta Part A Mol. Biomol. Spectrosc.* 78 (2011) 899–904. <https://doi.org/10.1016/j.saa.2010.12.060>.
- [11] N. Ul, K. Jalil, M. Shahid, A. Rauf, N. Muhammad, A. Khan, M. Raza, M. Atif, Green synthesis and biological activities of gold nanoparticles functionalized with *Salix alba*, *Arab. J. Chem.* 12 (2019) 2914–2925. <https://doi.org/10.1016/j.arabjc.2015.06.025>.
- [12] N.K.R. Bogireddy, U. Pal, L.M. Gomez, V. Agarwal, Size controlled green synthesis of gold nanoparticles using *Coffea arabica* seed extract and their catalytic performance

- in 4-nitrophenol reduction, *RSC Adv.* 8 (2018) 24819–24826.
<https://doi.org/10.1039/c8ra04332a>.
- [13] S.P. Akhlaghi, B. Peng, Z. Yao, K.C. Tam, Sustainable nanomaterials derived from polysaccharides and amphiphilic compounds, *Soft Matter.* 9 (2013) 7905–7918.
<https://doi.org/10.1039/c3sm50358e>.
- [14] H. Duan, D. Wang, Y. Li, Green chemistry for nanoparticle synthesis, *Chem. Soc. Rev.* 44 (2015) 5778–5792. <https://doi.org/10.1039/c4cs00363b>.
- [15] K.B. Narayanan, N. Sakthivel, Phytosynthesis of gold nanoparticles using leaf extract of *Coleus amboinicus* Lour, *Mater. Charact.* 61 (2010) 1232–1238.
<https://doi.org/10.1016/j.matchar.2010.08.003>.
- [16] M. Ibrahim, M. Alaam, H. El-Haes, A.F. Jalbout, A. De Leon, Analysis of the structure and vibrational spectra of glucose and fructose, *Eclet. Quim.* 31 (2006) 15–21. <https://doi.org/10.1590/S0100-46702006000300002>.
- [17] U. El-Nafaty, I. Muhammad, S. Abdulsalam, Biosorption and Kinetic Studies on Oil Removal from Produced Water Using Banana Peel, *Civ. Environ.* 3 (2013) 125–136. <http://iiste.org/Journals/index.php/CER/article/view/6125>.
- [18] G. Alaa El-Din, A.A. Amer, G. Malsh, M. Hussein, Study on the use of banana peels for oil spill removal, *Alexandria Eng. J.* 57 (2018) 2061–2068.
<https://doi.org/10.1016/j.aej.2017.05.020>.
- [19] M. Tammer, G. Sokrates: Infrared and Raman characteristic group frequencies: tables and charts, *Colloid Polym. Sci.* 283 (2004) 235–235. <https://doi.org/10.1007/s00396-004-1164-6>.
- [20] X. Li, Y. Tang, Z. Xuan, Y. Liu, F. Luo, Study on the preparation of orange peel cellulose adsorbents and biosorption of Cd²⁺ from aqueous solution, 55 (2007) 69–75. <https://doi.org/10.1016/j.seppur.2006.10.025>.
- [21] A. Bankar, B. Joshi, A.R. Kumar, S. Zinjarde, Banana peel extract mediated novel route for the synthesis of silver nanoparticles, *Colloids Surfaces A Physicochem. Eng. Asp.* 368 (2010) 58–63. <https://doi.org/10.1016/j.colsurfa.2010.07.024>.
- [22] A. Bankar, B. Joshi, A.R. Kumar, S. Zinjarde, Banana peel extract mediated novel route for the synthesis of silver nanoparticles, *Colloids Surfaces A Physicochem. Eng. Asp.* 368 (2010) 58–63. <https://doi.org/10.1016/j.colsurfa.2010.07.024>.
- [23] S. Khan, J. Bakht, F. Syed, Green synthesis of gold nanoparticles using *Acer pentapomicum* leaves extract its characterization, antibacterial, antifungal and antioxidant bioassay, *Dig. J. Nanomater. Biostructures.* 13 (2018) 579–589.
- [24] J. Golubtsova, Study of fruit raw material by fourier transform infrared spectroscopy, *J. Pharm. Sci. Res.* 9 (2017) 1081–1090.
- [25] V. Gude, K. Upadhyaya, M.N. V Prasad, N.V.S. Rao, Green Synthesis of Gold and

- Silver Nanoparticles Using, 5 (2013) 223–228.
<https://doi.org/10.1166/ asem.2013.1242>.
- [26] M. Irfan, T. Ahmad, M. Moniruzzaman, S. Bhattacharjee, B. Abdullah, Size and stability modulation of ionic liquid functionalized gold nanoparticles synthesized using *Elaeis guineensis* (oil palm) kernel extract, *Arab. J. Chem.* (2016).
<https://doi.org/10.1016/j.arabjc.2017.02.001>.
- [27] N.K.R. Bogireddy, L. Martinez Gomez, I. Osorio-Roman, V. Agarwal, Synthesis of gold nanoparticles using *Coffea Arabica* fruit extract, *Adv. Nano Res.* 5 (2017).
<https://doi.org/10.1007/s00217-008-0973-0>.
- [28] M.N. Nadagouda, N. Iyanna, J. Lalley, C. Han, D.D. Dionysiou, R.S. Varma, Synthesis of silver and gold nanoparticles using antioxidants from blackberry, blueberry, pomegranate, and turmeric extracts, *ACS Sustain. Chem. Eng.* 2 (2014) 1717–1723. <https://doi.org/10.1021/sc500237k>.
- [29] E.H. Ismail, A.M.A. Saqer, E. Assirey, A. Naqvi, R.M. Okasha, Successful Green Synthesis of Gold Nanoparticles using a *Corchorus olitorius* Extract and Their Antiproliferative Effect in Cancer Cells, (2018) 1–14.
<https://doi.org/10.3390/ijms19092612>.
- [30] M. Mahdavi, F. Namvar, M. Bin Ahmad, R. Mohamad, Green biosynthesis and characterization of magnetic iron oxide (Fe₃O₄) nanoparticles using seaweed (*Sargassum muticum*) aqueous extract, *Molecules.* 18 (2013) 5954–5964.
<https://doi.org/10.3390/molecules18055954>.
- [31] L. Biao, S. Tan, Q. Meng, J. Gao, X. Zhang, Z. Liu, Y. Fu, Green synthesis, characterization and application of proanthocyanidins-functionalized gold nanoparticles, *Nanomaterials.* 8 (2018). <https://doi.org/10.3390/nano8010053>.
- [32] F. Hou, Y. Zhu, Q. Zou, C. Zhang, H. Wang, Y. Liao, Q. Wang, X. Yang, Y. Yang, One-step preparation of multifunctional alginate microspheres loaded with: In situ-formed gold nanostars as a photothermal agent, *Mater. Chem. Front.* 3 (2019) 2018–2024. <https://doi.org/10.1039/c9qm00276f>.
- [33] Z. Liu, Y. Zu, Y. Fu, R. Meng, S. Guo, Z. Xing, S. Tan, Hydrothermal synthesis of histidine-functionalized single-crystalline gold nanoparticles and their pH-dependent UV absorption characteristic, *Colloids Surfaces B Biointerfaces.* 76 (2010) 311–316.
<https://doi.org/10.1016/j.colsurfb.2009.11.010>.
- [34] R. Sattari, G. Reza, R. Hoshyar, Biosynthesis of Silver – Silver Chloride Nanoparticles Using Fruit Extract of *Levisticum Officinale* : Characterization and Anticancer Activity Against MDA-MB-468 Cell Lines, *J. Clust. Sci.* 3 (2020) 3–9.
<https://doi.org/10.1007/s10876-020-01818-3>.
- [35] A. Taha, M. Shamsuddin, Biosynthesis of gold nanoparticles using *psidium guajava* leaf extract, *Malaysian J. Fundam. Appl. Sci.* 9 (2014) 119–122.
<https://doi.org/10.11113/mjfas.v9n3.95>.

- [36] J. Yu, D. Xu, H. Nan, C. Wang, L. Kun, D.F. Chi, Facile one-step green synthesis of gold nanoparticles using *Citrus maxima* aqueous extracts and its catalytic activity, 166 (2016) 110–112. <https://doi.org/10.1016/j.matlet.2015.12.031>.
- [37] B.A. Korgel, S. Fullam, S. Connolly, D. Fitzmaurice, Assembly and Self-Organization of Silver Nanocrystal Superlattices: Ordered “Soft Spheres,” *J. Phys. Chem. B.* 102 (2002) 8379–8388. <https://doi.org/10.1021/jp981598o>.
- [38] N. Basavegowda, Y. Rok Lee, Synthesis of silver nanoparticles using Satsuma mandarin (*Citrus unshiu*) peel extract: A novel approach towards waste utilization, *Mater. Lett.* 109 (2013) 31–33. <https://doi.org/10.1016/j.matlet.2013.07.039>.
- [39] R. Lakshmipathy, B. Palakshi Reddy, N.C. Sarada, K. Chidambaram, S. Khadeer Pasha, Watermelon rind-mediated green synthesis of noble palladium nanoparticles: catalytic application, *Appl. Nanosci.* 5 (2015) 223–228. <https://doi.org/10.1007/s13204-014-0309-2>.
- [40] M. Buljan, U. V Desnica, R. Kalish, Transmission electron microscopy study of carbon nanophases produced by ion beam implantation, 26 (2006) 1202–1206. <https://doi.org/10.1016/j.msec.2005.09.015>.
- [41] J. Reid, D. Crane, J. Blanton, C. Crowder, S. Kabekkodu, T. Fawcett, Tools for Electron Diffraction Pattern Simulation for the Powder Diffraction File, (2011). <https://doi.org/10.1017/S1551929510001240>.
- [42] R. Veerasamy, T.Z. Xin, S. Gunasagaran, T.F.W. Xiang, E.F.C. Yang, N. Jeyakumar, S.A. Dhanaraj, Biosynthesis of silver nanoparticles using mangosteen leaf extract and evaluation of their antimicrobial activities, *J. Saudi Chem. Soc.* 15 (2011) 113–120. <https://doi.org/10.1016/j.jscs.2010.06.004>.
- [43] D. Philip, Biosynthesis of Au, Ag and Au-Ag nanoparticles using edible mushroom extract, *Spectrochim. Acta - Part A Mol. Biomol. Spectrosc.* 73 (2009) 374–381. <https://doi.org/10.1016/j.saa.2009.02.037>.
- [44] R. Mata, A. Bhaskaran, S.R. Sadras, Green-synthesized gold nanoparticles from *Plumeria alba* flower extract to augment catalytic degradation of organic dyes and inhibit bacterial growth, *Particuology.* 24 (2016) 78–86. <https://doi.org/10.1016/j.partic.2014.12.014>.
- [45] K. Gopinath, S. Gowri, V. Karthika, A. Arumugam, Green synthesis of gold nanoparticles from fruit extract of *Terminalia arjuna*, for the enhanced seed germination activity of *Gloriosa superba*, *J. Nanostructure Chem.* 4 (2014). <https://doi.org/10.1007/s40097-014-0115-0>.
- [46] S. Vijayakumar, Eco-friendly synthesis of gold nanoparticles using fruit extracts and in vitro anticancer studies, *J. Saudi Chem. Soc.* (2019). <https://doi.org/10.1016/j.jscs.2018.12.002>.
- [47] N. Suganthi, V. Sri Ramkumar, A. Pugazhendhi, G. Benelli, G. Archunan, Biogenic

- synthesis of gold nanoparticles from *Terminalia arjuna* bark extract: assessment of safety aspects and neuroprotective potential via antioxidant, anticholinesterase, and anti-amyloidogenic effects, *Environ. Sci. Pollut. Res.* 25 (2018) 10418–10433. <https://doi.org/10.1007/s11356-017-9789-4>.
- [48] J. Zha, C. Dong, X. Wang, X. Zhang, X. Xiao, X. Yang, Green synthesis and characterization of monodisperse gold nanoparticles using *Ginkgo Biloba* leaf extract, *Optik (Stuttg)*. 144 (2017) 511–521. <https://doi.org/10.1016/j.ijleo.2017.06.088>.
- [49] G.K. Deokar, A.G. Ingale, Green synthesis of gold nanoparticles (Elixir of Life) from banana fruit waste extract-an efficient multifunctional agent, *RSC Adv.* 6 (2016) 74620–74629. <https://doi.org/10.1039/c6ra14567a>.
- [50] U. Feleni, U. Sidwaba, H. Makelane, E. Iwuoha, Core–Shell Palladium Telluride Quantum Dot-Hemethiolate Cytochrome Based Biosensor for Detecting Indinavir Drug, *J. Nanosci. Nanotechnol.* 19 (2019) 7974–7981. <https://doi.org/10.1166/jnn.2019.16866>.
- [51] H. Schnablegger, Y. Singh, The SAXS Guide, Ant. Paar GmbH. (2013) 1–122. <https://doi.org/10.1002/andp.19714810108>.
- [52] S. Goberna-Ferrón, J. Soriano-López, J.R. Galán-Mascarós, M. Nyman, Solution speciation and stability of cobalt-polyoxometalate water oxidation catalysts by X-ray scattering, *Eur. J. Inorg. Chem.* 2015 (2015) 2833–2840. <https://doi.org/10.1002/ejic.201500404>.
- [53] M. Khatami, H. Alijani, M. Nejad, R. Varma, Core@shell Nanoparticles: Greener Synthesis Using Natural Plant Products, *Appl. Sci.* 8 (2018) 411. <https://doi.org/10.3390/app8030411>.
- [54] Y. Mori, M. Furukawa, T. Hayashi, K. Nakamura, Size distribution of gold nanoparticles used by small angle X-ray scattering, *Part. Sci. Technol.* 24 (2006) 97–103. <https://doi.org/10.1080/02726350500403215>.
- [55] T. Shahwan, S. Abu Sirriah, M. Nairat, E. Boyaci, A.E. Eroğlu, T.B. Scott, K.R. Hallam, Green synthesis of iron nanoparticles and their application as a Fenton-like catalyst for the degradation of aqueous cationic and anionic dyes, *Chem. Eng. J.* 172 (2011) 258–266. <https://doi.org/10.1016/j.cej.2011.05.103>.
- [56] H. Jensen, J.H. Pedersen, J.E. Jørgensen, J.S. Pedersen, K.D. Joensen, S.B. Iversen, E.G. Søgaaard, Determination of size distributions in nanosized powders by TEM, XRD, and SAXS, *J. Exp. Nanosci.* 1 (2006) 355–373. <https://doi.org/10.1080/17458080600752482>.
- [57] G. Zhao, G. Liu, Electrochemical Deposition of Gold Nanoparticles on Reduced Graphene Oxide by Fast Scan Cyclic Voltammetry for the Sensitive Determination of As (III), (2018). <https://doi.org/10.3390/nano9010041>.
- [58] T. Peik-see, A. Pandikumar, H. Nay-ming, L. Hong-ngee, Y. Sulaiman, Simultaneous

- Electrochemical Detection of Dopamine and Ascorbic Acid Using an Iron Oxide/Reduced Graphene Oxide Modified Glassy Carbon Electrode, (2014) 15227–15243. <https://doi.org/10.3390/s140815227>.
- [59] X. Liu, Y. Zhu, K. Yan, J. Zhang, Reversibility-Dependent Photovoltammetric Behavior of Electroactive Compounds on a CdS–Graphene Hybrid Film Electrode, *Chem. - A Eur. J.* 23 (2017) 13294–1329. <https://doi.org/10.1002/chem.201703027>.
- [60] X. Lin, Y. Ni, S. Kokot, *Analytica Chimica Acta* Glassy carbon electrodes modified with gold nanoparticles for the simultaneous determination of three food antioxidants, *Anal. Chim. Acta.* 765 (2013) 54–62. <https://doi.org/10.1016/j.aca.2012.12.036>.
- [61] Y.G. Boroda, A. Calhoun, G.A. Voth, A theory for electron transfer across the electrode/electrolyte interface involving more than one redox ion, *J. Chem. Phys.* 107 (1997) 8940–8954. <https://doi.org/10.1063/1.475186>.
- [62] Z. Raheem, *Fundamentals of Electrochemistry - BAGOTSKY (2006) (1)*, 2019.
- [63] F. Zhang, Y. Yuan, Y. Zheng, H. Wang, T. Liu, S. Hou, A glassy carbon electrode modified with gold nanoparticle-encapsulated graphene oxide hollow microspheres for voltammetric sensing of nitrite, *Microchim. Acta.* 184 (2017) 1565–1572. <https://doi.org/10.1007/s00604-017-2264-6>.
- [64] R.O. Akinyeye, I. Michira, M. Sekota, A. Al Ahmed, D. Tito, P.G.L. Baker, C.M.A. Brett, M. Kalaji, E. Iwuoha, Electrochemical synthesis and characterization of 1,2-naphthaquinone-4- sulfonic acid doped polypyrrole, *Electroanalysis.* 19 (2007) 303–309. <https://doi.org/10.1002/elan.200603732>.
- [65] R.D. Nenkova, Y.L. Ivanov, T.I. Godjevargova, Influence of different nanoparticles on electrochemical behavior of glucose biosensor, *AIP Conf. Proc.* 1809 (2017). <https://doi.org/10.1063/1.4975452>.

CHAPTER FIVE

Results and Discussion: Part 2

This chapter provides the overall findings of the green method synthesis of silver nanoparticles achieved through the reduction of Ag⁺ ions using the combination of grape and banana peel extracts (under the conditions described in chapter 3). The combined extract was used as a reducing and stabilising agent, without the addition of any form of external chemical stabilising or reducing agents. The adapted methodology is clean, environment-friendly, non-toxic and hazard-free.

5 Silver Nanoparticles (Ag-NPs):

5.1 Ultra-visible Spectroscopy (UV-vis) of Ag-NPs:

The reduction of silver ions in the presence of GBPE was confirmed by the use of UV-vis. The visual observation of the reaction media changed, forming a dark brown colour, as shown in **Figure 5.1** illustrating the formation of Ag-NPs [1–4]. The colour of the reaction mixture started to change from pale brown to light brown and within 9 min formed a dark brown solution after 12 min, as shown in **Figure 5.2**. As the reaction mixture became darker, the more Ag-NPs were formed [5]. The brown colour arises due to excitation of surface plasmon resonance (SPR) vibrations in the silver nanoparticles [1-6]. This is because silver nanoparticles have free electrons which give rise to SPR absorbance bands [7].

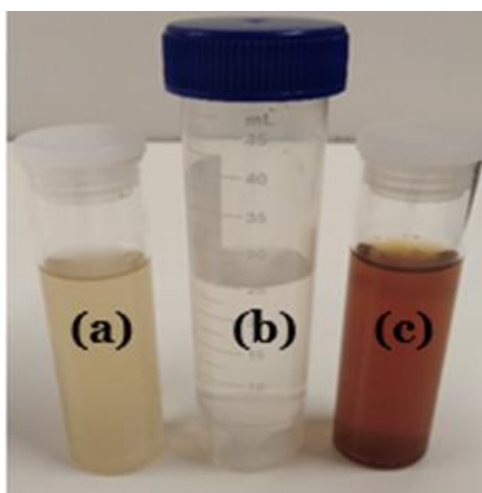


Figure 5.1: Photograph showing colour of solutions, (a) GBPE extract, (b) AgNO₃, (c) Ag-NPs.

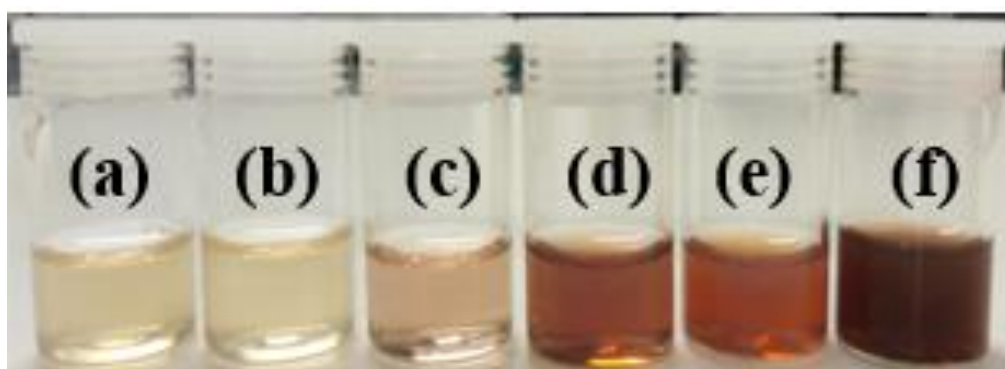


Figure 5.2: Visual inspection of the colour change of reaction solution in the process of Ag-NPs synthesis at different time intervals, (a) 3 min, (b) 6 min, (c) 9 min, (d) 12 min, (e) 15 min, (f) 18 min.

The SPR of the GBPE-Ag-NPs was observed at 440 nm as shown in **Figure 5.3**. This was confirmed by literature reports which have indicated that the nanoparticles absorb radiation in the visible regions of 400 – 500 nm [8]. Similar results on the visual observations of Ag-NPs have been reported on studies of apple extract and *Arthrobacter* sp.B4 respectively where the appearance of brown colour was observed within 5 min of the reaction in both studies, and the SPR was observed in the range of 450 nm and 433 nm respectively [9,10]. Additionally,

recently Masum and co-workers also confirmed the maximum wavelength (λ_{max}) of silver nanoparticles to be approximately 436 nm [11] while in another study by Kumar and co-workers it was obtained at 440 nm [12].

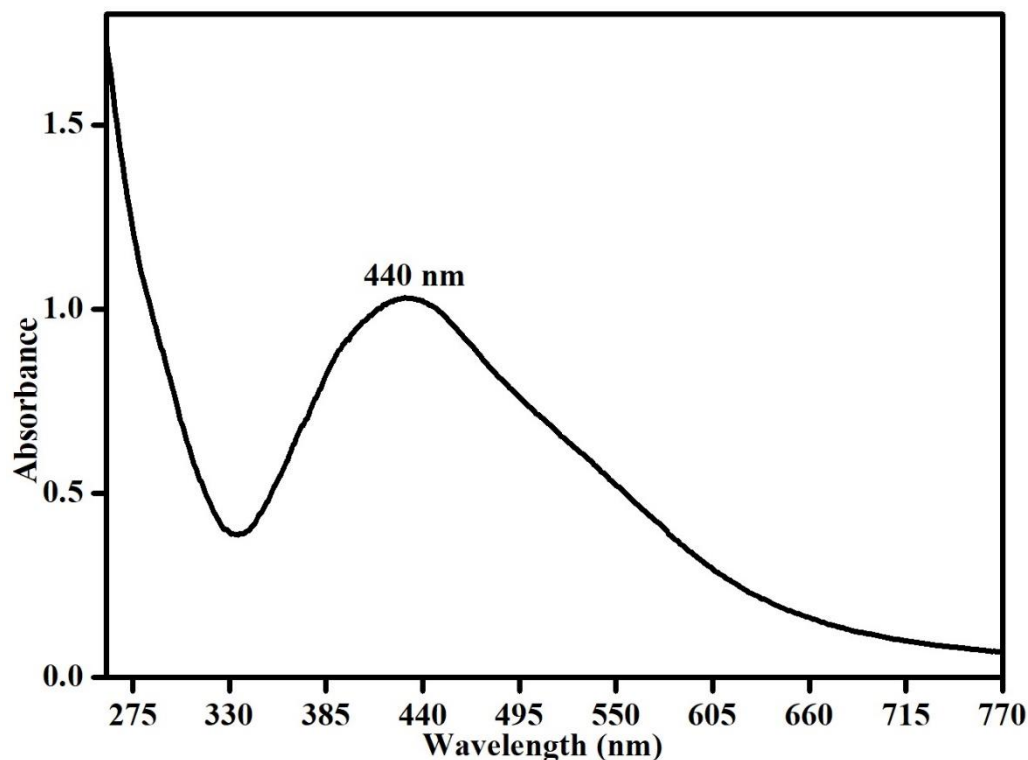


Figure 5.3: UV-Vis spectra of GBPE capped Ag-NPs.

Figure 5.4 shows the UV-vis absorbance spectra of silver nanoparticles at different time intervals. The intensity of SPR peaks increased from 3 min until 18 min. At 18 min, the maximum SPR peak was observed due to the depletion of silver ions (Ag^+) in the GBPE. The SPR peak of silver nanoparticles shifts to the higher wavelength as the reaction time increases [13–16] indicating a redshift [17]. Redshift shows that there is a gradual increment in the mean diameter of GBPE-Ag-NPs [5]. The spectra show the reduction of Ag^+ to Ag^0 specifying the formation of Ag-NPs with a completed time of 18 min. The optimal time in this study was 18 min, which is relatively less than in other reports. For instance, Kumar and

co-workers reported 60 min for Ag-NPs synthesised using Hydnocarpus Pentandra leaves [18].

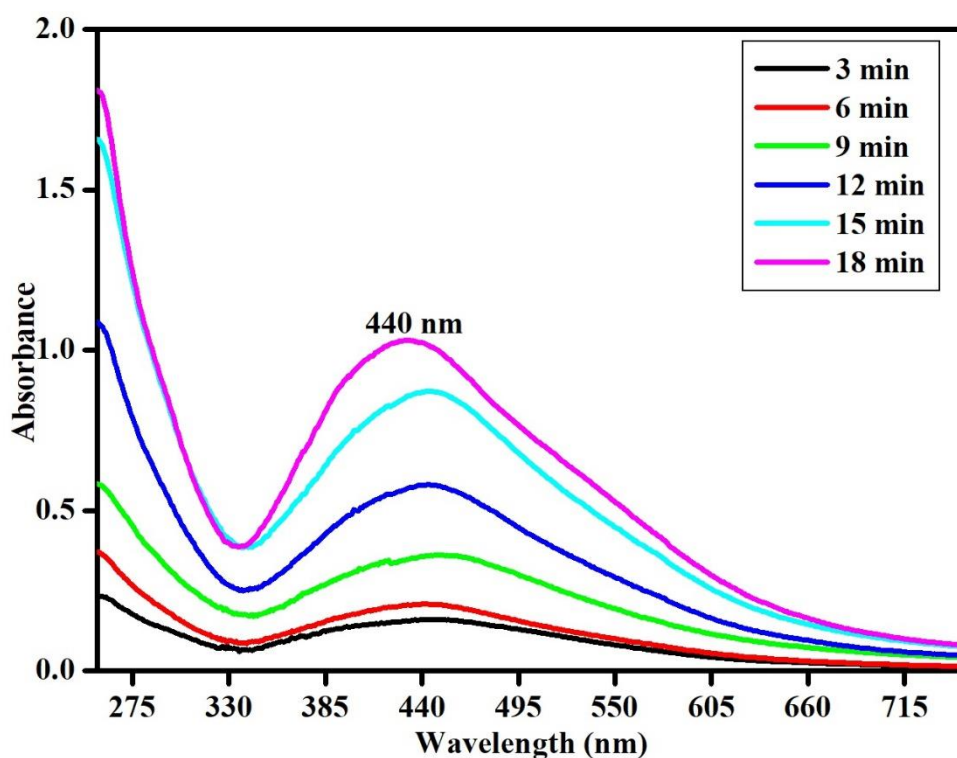


Figure 5.4: UV-Vis spectra of GBPE capped Ag-NPs at different time intervals.

Table 5.1 shows the comparison of SPR bands and reaction time for the complete reduction of silver ions from previously reported studies versus this study using natural products as reducing agents. As seen from the table, the SPR band was in a similar position in all the studies, and our study showed a complete reduction producing nanoparticles in 18 min, which is less compared to the other studies.

Table 5.1: Comparison of studies from literature and the present work, for the time taken for complete reduction of silver nitrate using natural products as reducing agents.

| Type of Nanoparticles | Natural product used | Wavelength (nm) | Reaction Time (min) | Reference |
|-----------------------|-------------------------------|-----------------|---------------------|------------|
| Ag-NPs | Pomegranate Fruit Seeds | 430 nm | 240 min | [19] |
| Ag-NPs | <i>Lippia citriodora</i> leaf | 445 nm | 1440 min | [20] |
| Ag-NPs | Gapes and Banana Peel | 440 nm | 18 Min | This study |

5.2 Fourier Transformation Infrared (FT-IR) for GBPE-Ag-NPs:

Fourier Transformation Infrared (FT-IR) Spectroscopy measurements were carried out to identify the major functional groups of the GBPE and their possible involvement in the synthesis and stabilisation of the synthesised Ag-NPs. **Figure 5.5** represents the spectra of GBPE (black curve) and the synthesised Ag-NPs (red curve). The FT-IR spectra of GBPE capped Ag-NPs shows a broadband at 3366 cm^{-1} due to the stretching vibrations of hydroxyl groups (-OH) of alcohol and phenols [21] while the weak band at 2922 cm^{-1} is due to the aliphatic C-H stretching vibrations due to low content of lignin present in both grape and banana peels. The peak at 1622 cm^{-1} is characteristic of C=O stretch of carbonyl groups and amide-I bonds due to the presence of hemicellulose bands from banana peels as well as myricetin compounds present in both grape and banana, used as both stabilising and a capping agent for the synthesis of Ag-NPs [22]. The weak peak at 2093 cm^{-1} is due to thiols S-H stretch.

Moreover, the band at 1542 cm^{-1} is attributed to C=C stretching vibrations of aromatic rings and alkenes from phenolic compounds, and organic acids from pectic, galacturonic acid in banana peel and ellagic acid from grapes present in GBPE [23,24], and a slight reduction was observed in the spectrum of Ag-NPs for this peak due to the involvement of the organic

compounds in the synthesis. The intense peaks at 1459 and 1066 cm^{-1} were assigned due to the presence of nitro compounds from flavonoids found in grapes while the N-O and C-N stretches are due to amine groups attributed to the presence of hemicellulose, lignin and pectin present in grapes and banana peel [25]. These peaks were reduced in intensity as compared to the Ag-NPs spectrum revealing the involvement of nitrile groups from the extracts as the capping agents for the nanoparticles. The appearance of a weak peak at 550 cm^{-1} was due to C-H vibration from anthocyanins present in flavonoids from grapes. It vanished in the Ag-NPs spectrum due to its involvement in the synthesis of nanoparticles. The Ag-NPs spectrum also indicates another peak at 693 cm^{-1} caused by the vibrations of the nanoparticles which was not observed at the GBPE spectrum thus confirming the formation of the nanoparticles indicating that the amine, hydroxyl and carboxyl groups in GBPE were responsible for the formation of the novel silver nanoparticles [26]. The obtained results are similar to a recent report by Singh and co-workers who reported the synthesis of Au-NPs using *Rhodiola Rosea* rhizome extract [27]. Hence from the above analysis, we concluded that amine, hydroxyl and carboxyl groups present in the extract played a significant role in the reduction of Ag^+ ion into Ag-NPs.

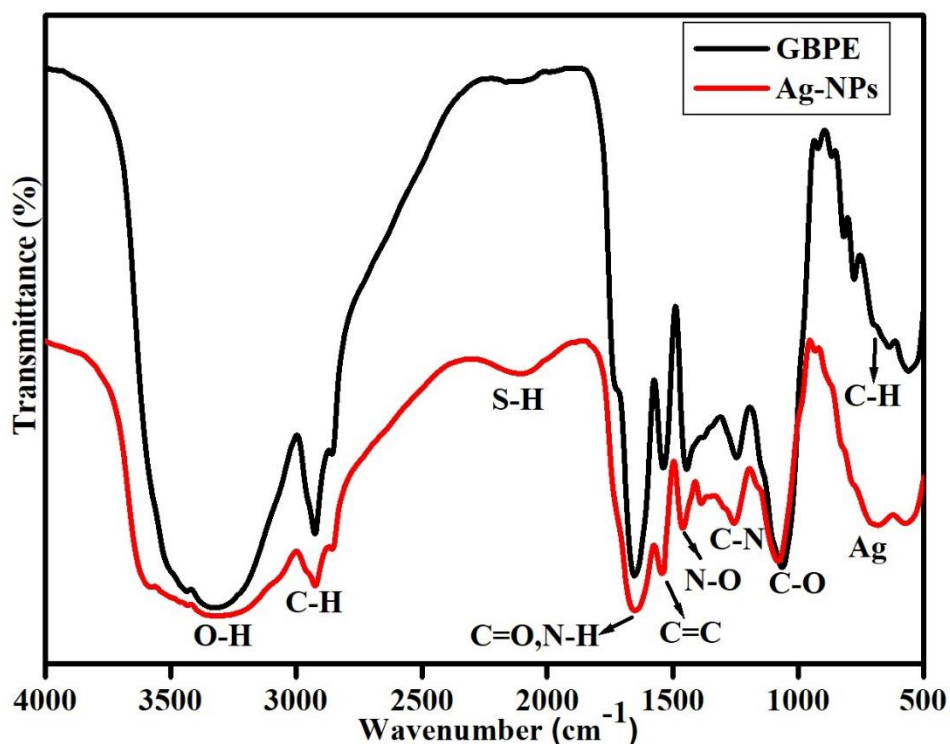


Figure 5.5: FT-IR spectra of the green synthesised Ag-NPs and GBPE.

5.3 X-ray Diffraction pattern (XRD) of Ag-NPs:

The XRD pattern of the synthesised GBPE capped Ag-NPs shown in **Figure 5.6** confirms the crystalline nature of the nanoparticles with Bragg reflection peaks at 38.17, 44.43, 64.58 and 77.64 corresponding to the silver crystal planes (111), (200), (220), (311) and (222) an indication of face centred cubic (fcc) crystalline structured metallic silver [28]. The average particle size of the nanoparticles was determined to be 30 nm based on the full-width half maximum (FWHM) data using Scherer's equation (**equation 3.4**, chapter 3). Similar reflections were also observed in the XRD spectrum of the green synthesised silver nanoparticles using Vitex Negundo [29], sufron waste [30], and Azadirachta indica leaf [31]. The five intense peaks obtained in the spectrum of nanoparticles correspond to the standard

metallic silver JCPDF NO. 04-0873[32]. Aruna and Jarayaman reported similar results for green synthesised silver nanoparticles using Gum tragacanth [33] while Dong and co-workers also reported similar results using wolfberry fruit [34]. **Table 5.2** shows the comparison of Bragg's diffraction peaks at 2θ values and the average crystal size of the green synthesised nanoparticles in previous studies calculated using Debye-Scherrer formula against the present work. As seen from the table, this study developed the smallest nanoparticles among those listed there. The difference in the size of the synthesised nanoparticles is due to the presence of more than one reducing agent on a natural product used and different selection of suitable reaction condition for synthesis [35].

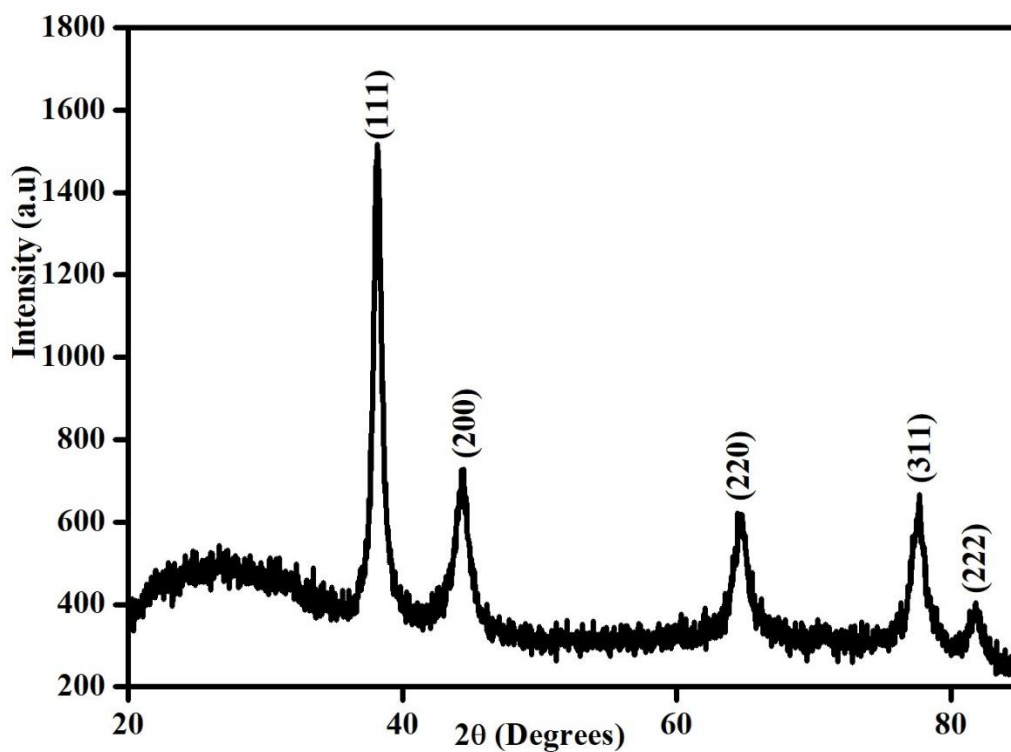


Figure 5.6: X-ray diffraction pattern of GBPE capped Ag-NPs.

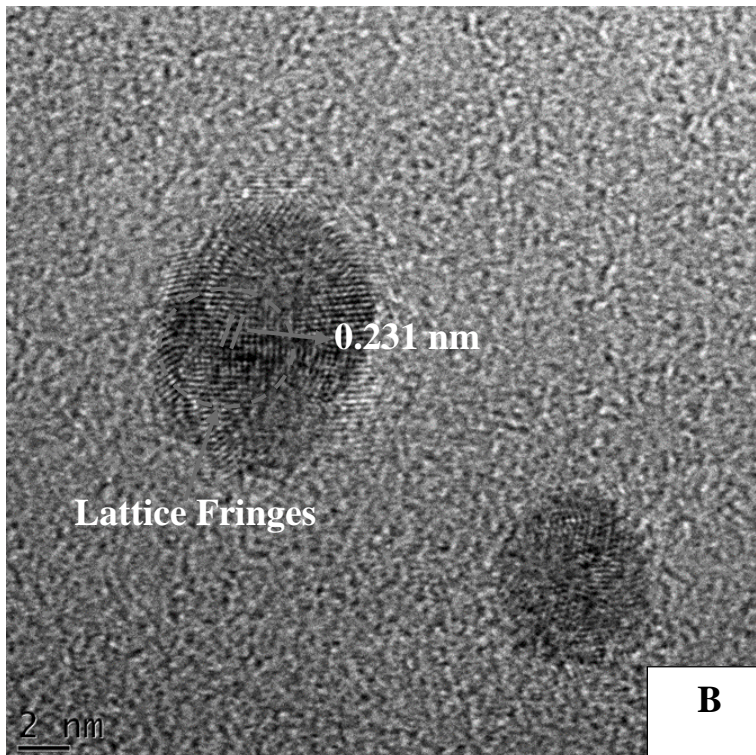
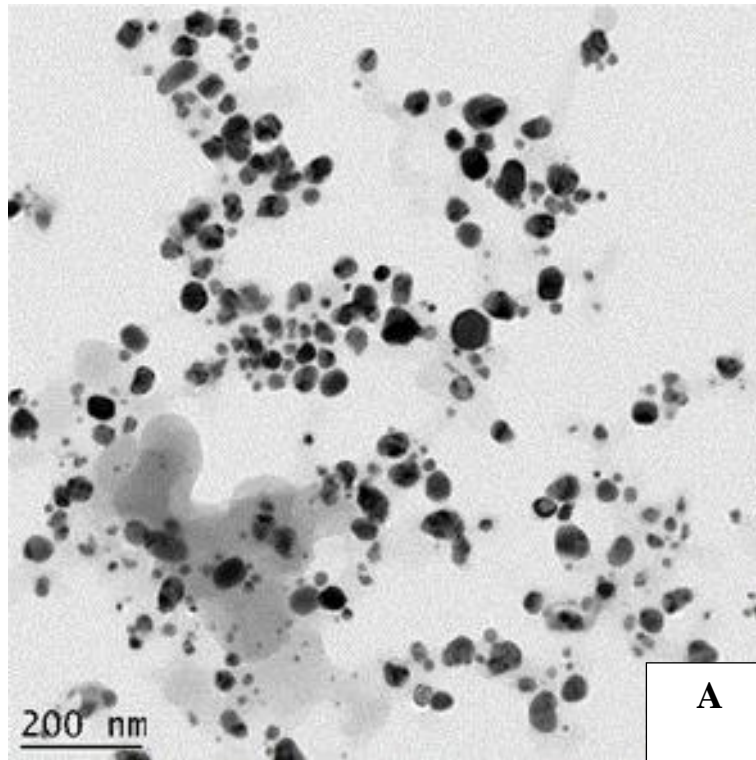
Table 5.2: Comparison of Bragg's diffraction peaks at 2θ value and the size of crystalline green synthesised nanoparticles (from literature) and the present work.

| Nanoparticles | 2 θ (Degrees) corresponding | | | | | Crystalline size (nm) | Reference |
|--|------------------------------------|------|------|------|------|-----------------------|------------|
| | 111 | 200 | 220 | 311 | 222 | | |
| Ag-NPs capped with Garcinia mangostana Fruit Peels | 37.5 | 44.1 | 63.9 | 76.5 | 81.6 | 61 nm | [36] |
| Ag-NPs capped with Myrtus communis Leaves | 38.2 | 44.4 | 64.3 | 77.8 | 81.2 | 35 nm | [37] |
| Ag-NPs capped with GBPE | 38.2 | 44.4 | 64.6 | 77.6 | 81.3 | 30 nm | This Study |

5.4 High-Resolution Electron Microscopy (HR-TEM) of Ag-NPs:

The particle size, morphology and further assessment of the crystallinity of the GBPE-Ag-NPs were evaluated using HR-TEM. Results are shown in **Figure 5.7(a)** to **Figure 5.7(d)**. From the data illustrated in **Figure 5.7(a)** it is possible to see that the synthesised silver nanoparticles were spherical, which is in agreement with the shape of the SPR band in the UV-vis spectrum [34]. The particle size distribution of Ag-NPs was calculated by Image J software. It was determined to be in the range from 25 - 39 nm. Furthermore, the lattice fringes visible in **Figure 5.7(b)** indicates good crystallinity and the lattice spacing was determined to be 0.231 nm. This spacing is known as inter-planar spacing (d-spacing) which is in between the vertical lattice fringes, indicating the space between the XRD Bragg's reflection. According to Liang and co-workers, an interlayer spacing of 0.231 nm corresponds to the lattice spacing of the silver (111) planes [38,39]. Gomati and co-workers also reported lattice spacing of 0.23 nm for Ag-NPs synthesised using Datura stramonium leaves [40].

The selected area electron diffraction (SAED) pattern shown in **Figure 5.7(c)** was obtained by directing the electron beam perpendicular to one of the spheres of GBPE-Ag-NPs [41]. The obtained SAED confirmed the crystalline nature of silver nanoparticles, and it shows bright circular rings corresponding to the (111), (220), (311) and (222) planes an indication that the nanoparticles are highly crystalline [42]. The results obtained from the XRD pattern are in good agreement with SAED bright circular rings and lattice fringes which suggests the polycrystalline nature of GBPE-Ag-NPs. Srirangam and Parameswara obtained similar SAED using the leaf extract of *Malachra capitata* [7]. The particle size from the histograms for the GBPE-Ag-NPs are indicated in **Figure 5.7(d)** illustrating that the particle sizes of the synthesized nanoparticles ranged in size from 25 to 39 nm. These values are in good agreement with the XRD data, which indicated a value of 30 nm for the nanoparticles. **Table 5.3** show comparison of size determined using HR-TEM measurements for green synthesised Ag-NPs between previously reported studies and this study. As seen from the table this study shows the smallest range in terms of size for Ag-NPs, smaller sizes of the nanoparticles are considered as better since they have large surface area to volume ratios and improved properties in terms of applications.



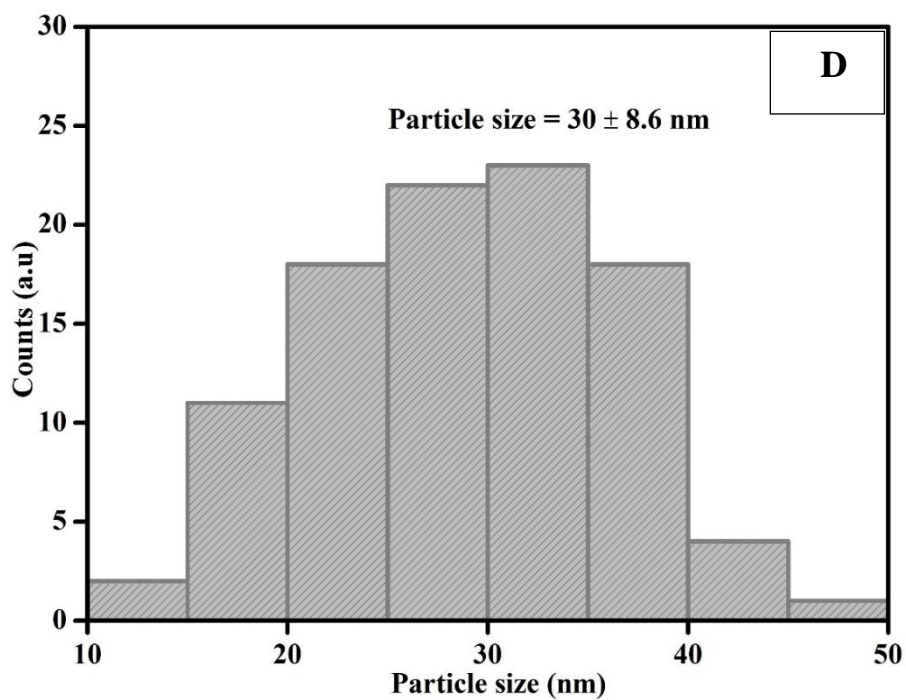
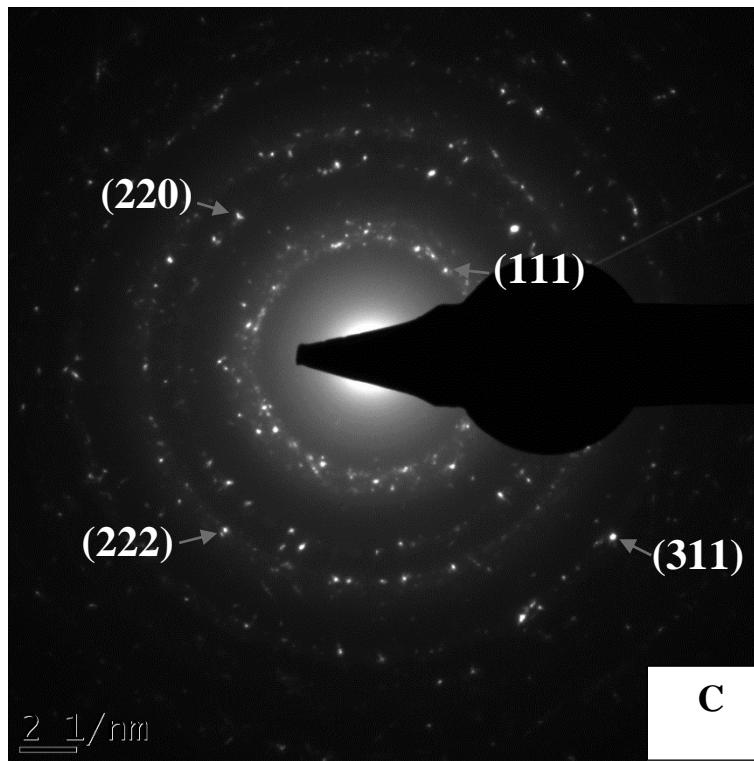


Figure 5.7: (a) HR-TEM image of Ag-NPs at 200 nm range, (b) lattice fringes, (c) Selected area electron diffraction (SAED) patterns, (d) histogram.

Table 5.3: Comparison of size (calculated based on HR-TEM measurements) of green synthesised silver nanoparticles.

| Type of Nanoparticles | Natural Product | Reducing agent | Size (nm) | Reference |
|-----------------------|----------------------------|----------------|-----------|------------|
| Ag-NPs | <i>Morus Indica L. VI</i> | Plant Extract | 54 nm | [43] |
| Ag-NPs | <i>Dioscorea bulbifera</i> | Plant Extract | 75 nm | [44] |
| Ag- NPs | Grapes and Banana peel | Fruit Extract | 25-39 nm | This Study |

The energy-dispersive x-ray spectroscopy (EDS) of the nanoparticles illustrated in **Figure 1.8** shows the presence of the silver elements at 3 KeV, which confirms the formation of silver nanoparticles [45]. The presence of carbon and oxygen in the sample was also found due to the presence of polyphenol groups originating from the extract and are bound to the surface of silver nanoparticles thus indicating the reduction of silver ions (Ag^+) to elemental silver (Ag). The analysis further shows the presence of copper contributed by the copper grid on to which the sample was coated. No other peaks were observed in the spectrum, confirming the complete reduction of silver compounds to silver nanoparticles [46]. Previously obtained reports similar to these results were also reported by [2,47].

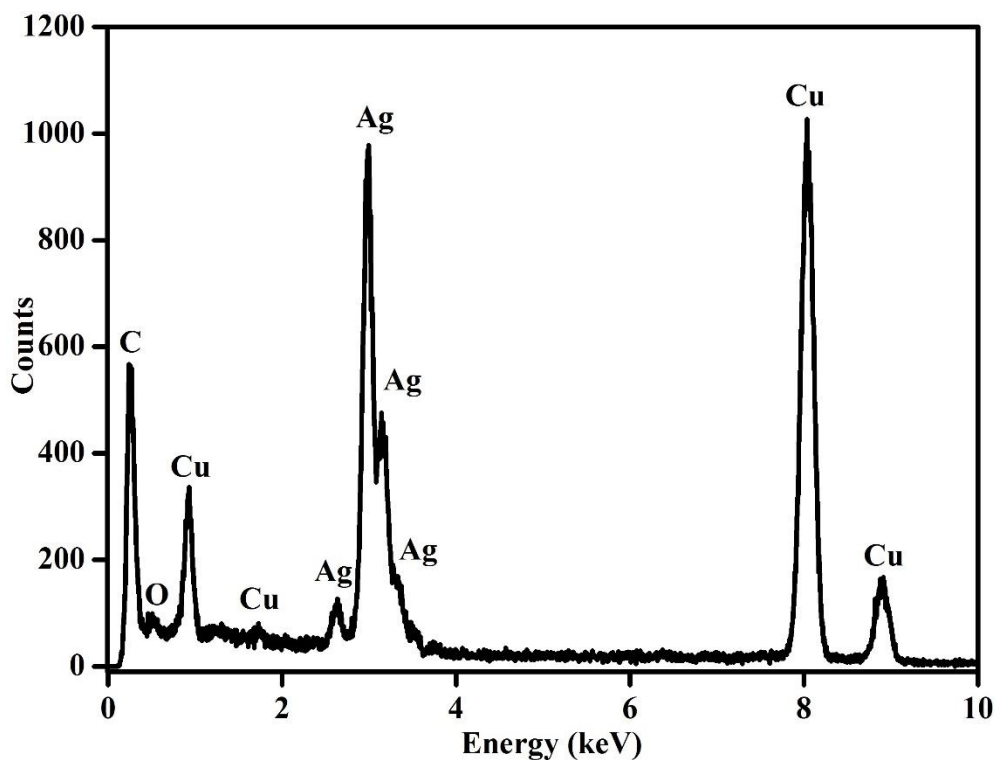


Figure 1.8: Energy Dispersive Spectroscopy patterns of GBPE capped Ag-NPs.

5.5 Small-angle x-ray Scattering (SAXS) for Ag-NPs:

Small-angle x-ray scattering (SAXS) was used to determine the particle size, stability and the size dispersion of GBPE capped Ag-NPs. The obtained data shows the free model pair-distance distribution function (PDDF) of the nanoparticles as illustrated at **Figure 1.9** and the size distributions functions as indicated in **Figure 5.10** weighted by number (black line) and intensity (red line). In **Figure 5.9**, the PDDF curve shows that the largest particles size detected to have a radius of 39 nm. In SAXS measurements it is possible to extrapolate the largest particle size where the PDDF approaches zero ($p(r) = 0$) [48,49]. From **Figure 5.10**, it is possible to see that the synthesised Ag-NPs had an average radius of 4 nm giving an average diameter of 8 nm when diluted in aqueous media. The average size of the nanoparticles obtained from SAXS is very similar to that calculated from XRD and the one

estimated from HR-TEM analysis. However, the data obtained from SAXS correspond to an average from a much larger number of particles, thus providing slightly higher averages [50].

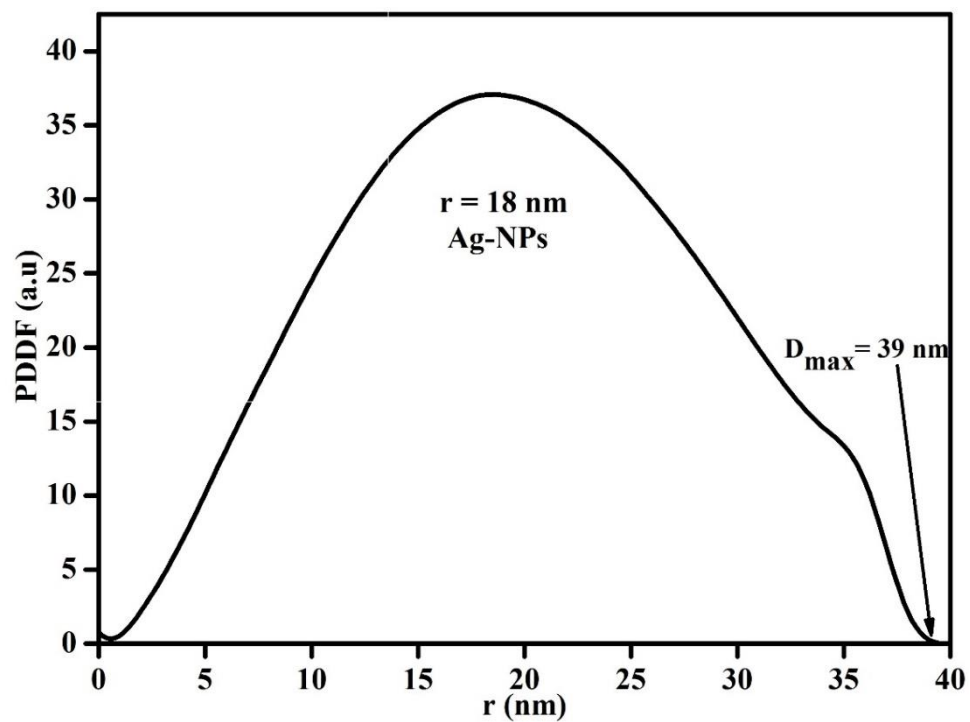


Figure 5.9: SAXS pair distance distribution function (PDDF) of GBPE-Ag-NPs.

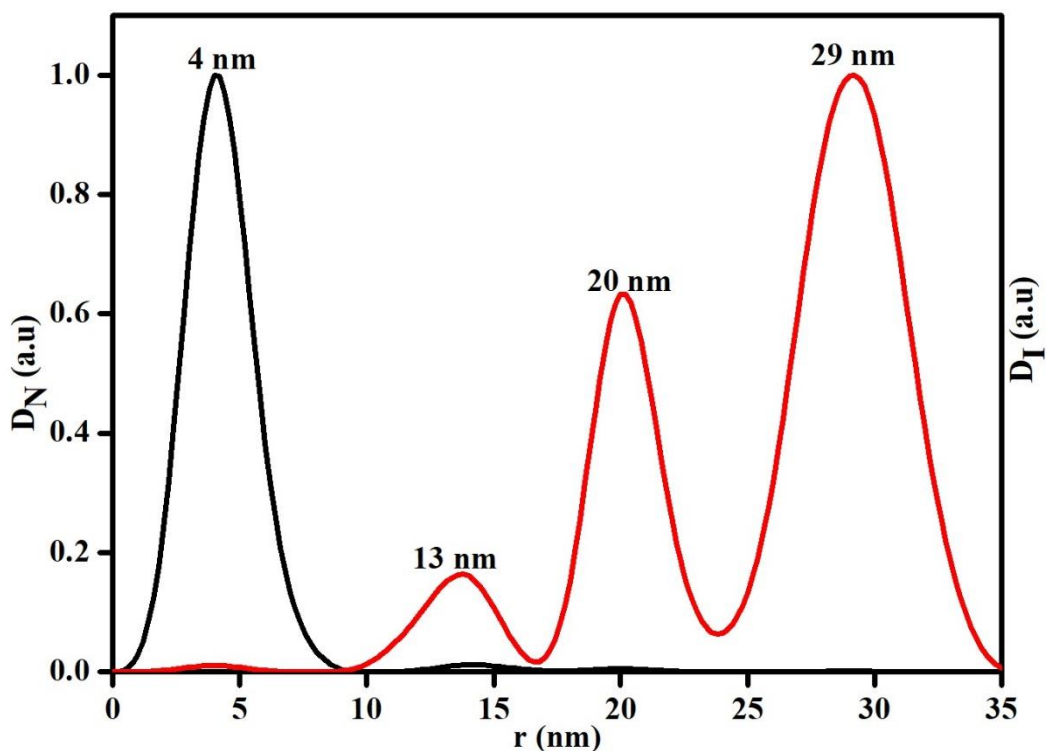


Figure 5.10: Size distribution functions weighted by number (black line) and intensity (red line).

5.6 Electrochemical behaviour of GBPE capped Ag-NPs:

In this section, we discuss the electrochemical behaviour of Ag-NPs drop-coated on the surface of GCE electrodes. Before starting the experiment, the electrodes were placed in phosphate buffer (0.2 M, pH 7.4). **Figure 5.11** shows a cyclic voltammogram of a bare GCE (black) and Ag-NPs (red) at a scan rate of $50 \text{ mV}\cdot\text{s}^{-1}$. **Figure 5.11** illustrates electrochemical responses of Ag-NPs where an oxidation peak at 0.16 V and a reduction peak at -0.75 V were observed associated with the formation of AgCl on the electrode and the reduction of this soluble salt. This was due to the oxidation of Ag to AgCl as given by (**Equation 3.7**).

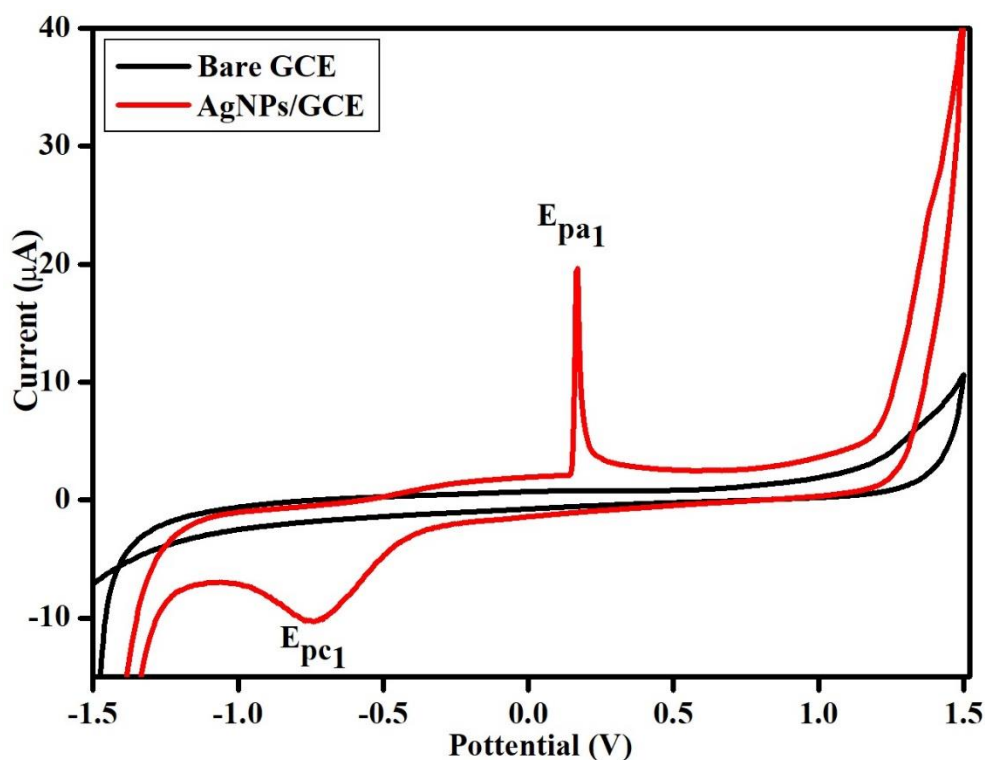


Figure 5.11: Cyclic voltammogram of bare GCE (Black line), Ag-NPs|GCE (Red line) recorded in 0.2 PBS, pH 7.4 at 50 mV/s.

Similar observations were reported by Blake and co-workers [51]. Recently Lima and co-workers also observed an oxidation peak in the same region which (0.24 V) was which was associated with the conversion of Ag^+/Ag^0 and also indicated the presence of Ag-NPs [52]. Furthermore, Shivakumar and co-workers modified GCE with green synthesised Ag-NPs produced using Eucalyptus bark extract where they observed a similar reduction peak at -0.81 V for Eucalyptus bark capped Ag-NPs [53].



From the results, it can be observed that silver nanoparticles respond differently compared to the bare GCE. **Figure 5.12** shows cyclic voltammograms of Ag-NPs at different scan rate of

10-100 mV/s. The peak current of GBPE capped Ag-NPs increased linearly with increased scan rates and shifted slightly to positive values. The oxidation peak shifts indicate the electrochemical activity of the synthesised GBPE capped Ag-NPs while the reduction peak denotes the conversion of Ag^+/Ag [54].

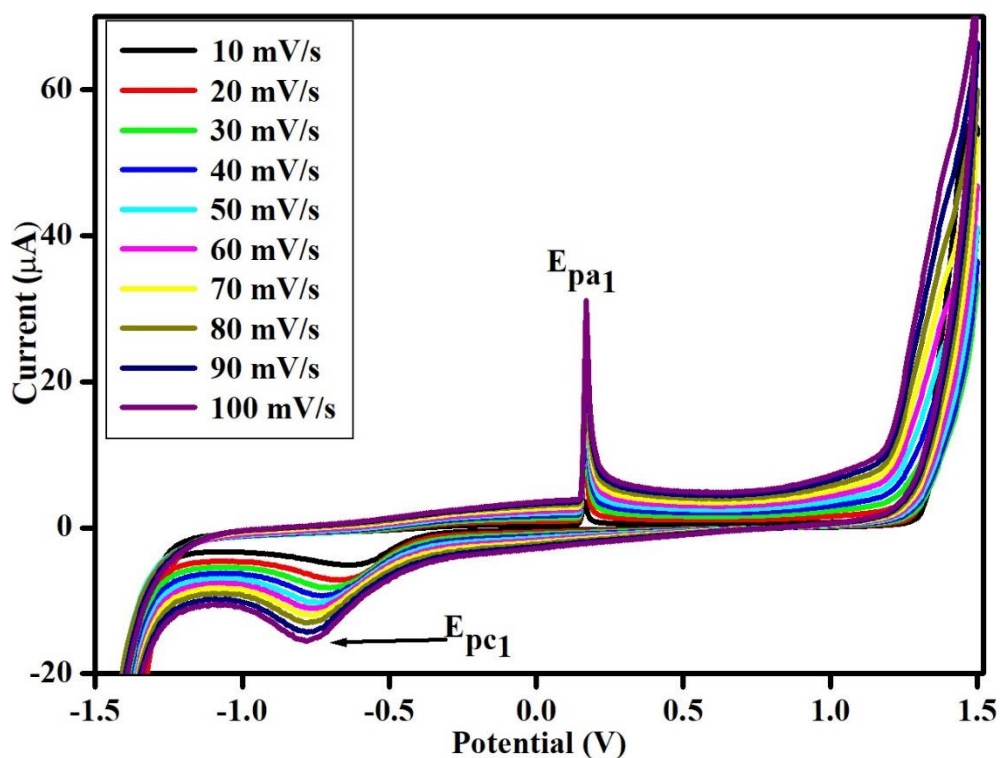


Figure 5.12: Multi-Scan Voltammograms of Ag-NPs in 0.2 PBS, pH 7.4 at (10-100 mV/s).

A plot of log anodic current peak against the log scan rate was plotted for the GBPE capped Ag-NPs where nearly a straight line with a linear regression $I_{pa} (\mu\text{A}) = 0.7095x + 0.0084$ and a correlation coefficient $r^2 = 0.9944$ was determined as shown in **Figure 5.13**.

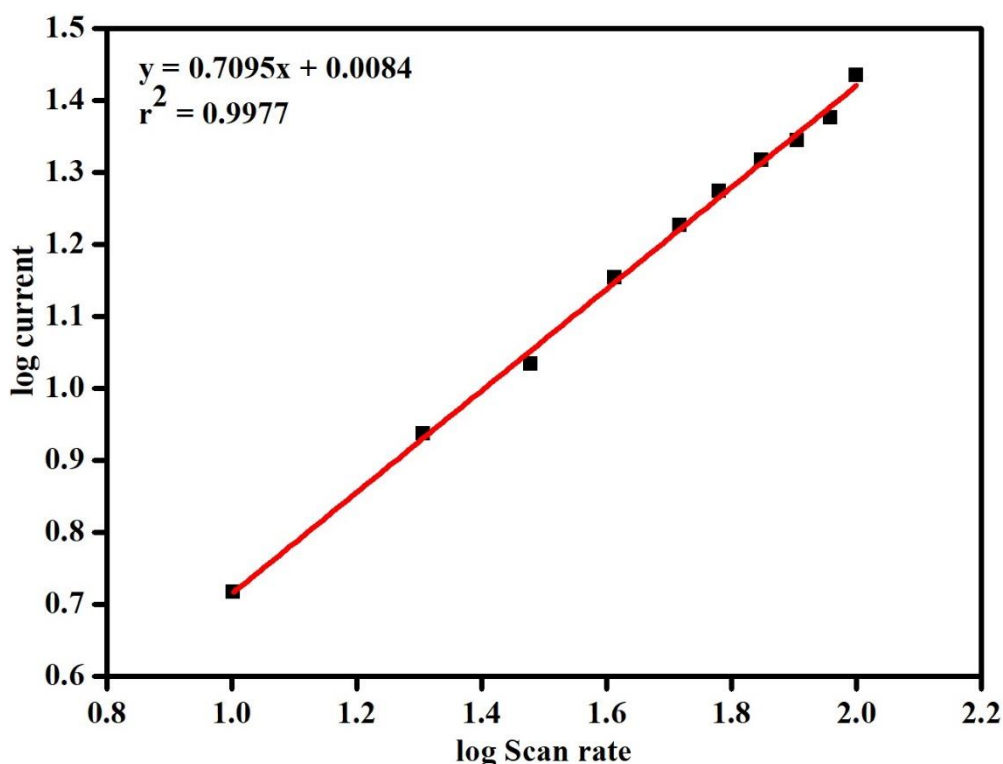


Figure 5.13: Plots of log current versus log scan rate of GBPE capped Ag-NPs.

As mentioned in the previous chapter, a linear plot between the log of scan rate versus the log of current can differentiate between diffusion-controlled system, an adsorption-controlled system or even a mixture of the two using the plots slope. A slope of 0.5 indicates a diffusion-controlled system, a slope of 1 an adsorption-controlled system and intermediate values of the slope suggest a "mixed" diffusion-adsorption controlled system [55]. In this study a slope of 0.7 $V \cdot \mu A^{-1}$ was obtained from the (log scan rate versus log current) plot in Figure 5.13 which indicates a mixed diffusion-adsorption system. The ratio of the cathodic and anodic peak (I_{pa} / I_{pc}) for the GBPE capped Ag-NPs was obtained to be 1.5, a value which was obtained using current values illustrated in **Figure 5.12**. This confirms a stable redox species adsorbed on the electrode surface that undergo a reversible process. The peak-peak separation was found to be 0.91 V meaning $\Delta E_p = E_{pa} - E_{pc} < 0.059/n$ V thus confirming

that the system is a reversible redox system and ΔE_p showed dependence on the scan rate. The formal potential $E = (E_{pa} + E_{pc}) / 2$ of the system was determined to be 0.281 V. **Figure 5.14** shows the Randel-Sevcik Plot for GBPE capped Ag-NPs, the linear plot from the graph also provides evidence for a chemically reversible redox system and the gradient of this plot was used to determine the diffusion coefficient of the analyte. Additionally, the reversible Randel-Sevcik Equation (**Equation 5.3**) was used to determine the diffusion coefficient (D_e) of GBPE capped Ag-NPs, and it was determined to be $5.221 \times 10^{-5} \text{ cm}^2 \cdot \text{s}^{-1}$. The obtained D_e was larger compared to the previously reported in literature and therefore larger values of D_e indicates a faster motion of analyte through the solution whereas small values of D_e indicates slower motion. Khan and co-workers reported D_e of $7.6 \times 10^{-6} \text{ cm}^2 \cdot \text{s}^{-1}$ using Ag-NP-MWCNT-GCE which was lower compared to this study [56]. Moreover, the Brown Anson equation (**Equation 5.5**) as described from the previous chapter, was used to determine the surface concentration denoted as (Γ) for Ag-NPs. A value of $2.413 \times 10^{-4} \text{ mol} \cdot \text{cm}^{-2}$ was determined for the surface concentration of GBPE-Ag-NPs.

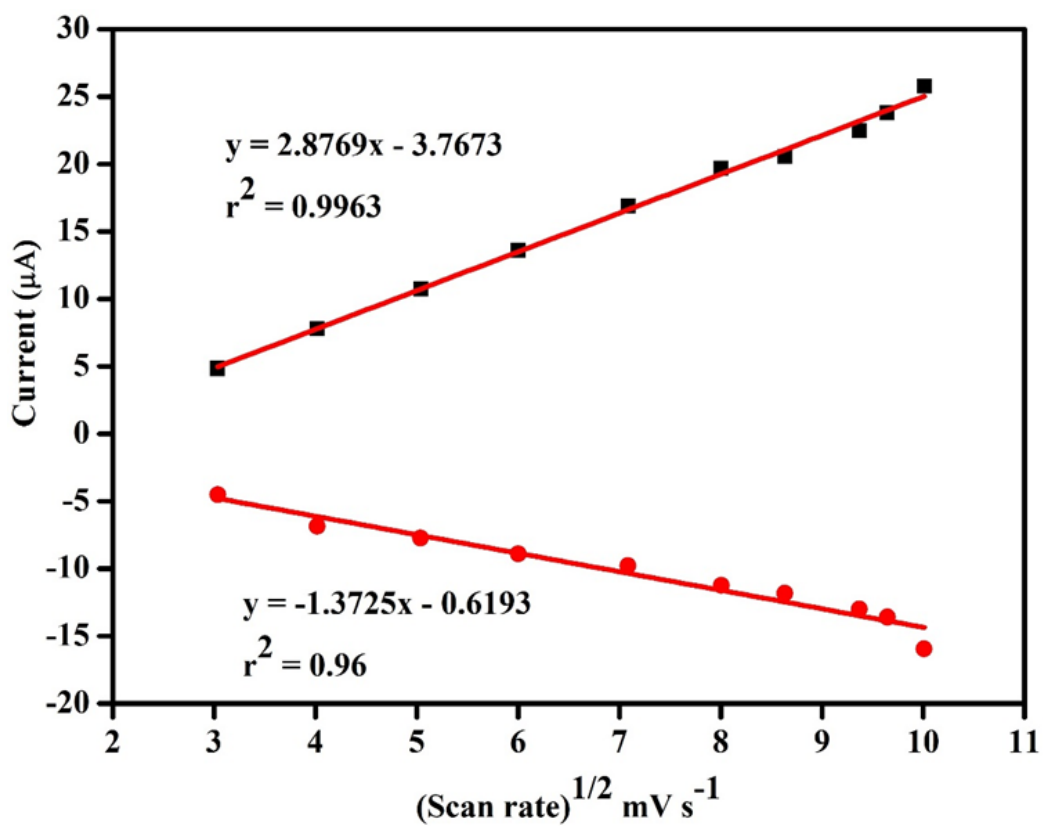


Figure 5.14: Randles-Sevcik Plot for GBPE capped Ag-NPs.

5.7 References:

- [1] S. Ahmed, M. Ahmad, B.L. Swami, ScienceDirect Green synthesis of silver nanoparticles using *Azadirachta indica* aqueous leaf extract, *J. Radiat. Res. Appl. Sci.* 9 (2015) 1–7. <https://doi.org/10.1016/j.jrras.2015.06.006>.
- [2] G. Lakshmanan, A. Sathiyaseelan, P.T. Kalaichelvan, K. Murugesan, Plant-mediated synthesis of silver nanoparticles using fruit extract of *Cleome viscosa* L.: Assessment of their antibacterial and anticancer activity, *Karbala Int. J. Mod. Sci.* 4 (2018) 61–68. <https://doi.org/10.1016/j.kijoms.2017.10.007>.
- [3] P.S. Ramesh, T. Kokila, D. Geetha, Plant mediated green synthesis and antibacterial activity of silver nanoparticles using *Emblca officinalis* fruit extract, *Spectrochim. Acta - Part A Mol. Biomol. Spectrosc.* 142 (2015) 339–343. <https://doi.org/10.1016/j.saa.2015.01.062>.
- [4] S. Farhadi, B. Ajerloo, A. Mohammadi, Low-cost and eco-friendly phyto-synthesis of Silver nanoparticles by using grapes fruit extract and study of antibacterial and catalytic effects, *Int. J. Nano Dimens.* 8 (2017) 49–60. <https://doi.org/10.22034/ijnd.2017.24376>.
- [5] J. Balavijayalakshmi, V. Ramalakshmi, *Carica papaya* peel mediated synthesis of silver nanoparticles and its antibacterial activity against human pathogens, *J. Appl. Res. Technol.* 15 (2017) 413–422. <https://doi.org/10.1016/j.jart.2017.03.010>.
- [6] R. Veerasamy, T.Z. Xin, S. Gunasagaran, T.F.W. Xiang, E.F.C. Yang, N. Jeyakumar, S.A. Dhanaraj, Biosynthesis of silver nanoparticles using mangosteen leaf extract and evaluation of their antimicrobial activities, *J. Saudi Chem. Soc.* 15 (2011) 113–120. <https://doi.org/10.1016/j.jscs.2010.06.004>.
- [7] G.M. Srirangam, K. Parameswara Rao, Synthesis and characterization of silver nanoparticles from the leaf extract of *Malachra capitata* (L.), *Rasayan J. Chem.* 10 (2017) 46–53. <https://doi.org/10.7324/RJC.2017.1011548>.
- [8] M.O. Mawaddah, A.B. Pambudi, A.R. Pratiwi, F. Kurniawan, Green synthesis of silver nanoparticles using photo-induced reduction method, *AIP Conf. Proc.* 2049 (2018). <https://doi.org/10.1063/1.5082487>.
- [9] Z.A. Ali, R. Yahya, S.D. Sekaran, R. Puteh, Green Synthesis of Silver Nanoparticles Using Apple Extract and Its Antibacterial Properties, 2016 (2016).
- [10] L. Yumei, L. Yamei, L. Qiang, B. Jie, Rapid biosynthesis of silver nanoparticles based on flocculation and reduction of an exopolysaccharide from *arthrobacter* sp. B4: Its antimicrobial activity and phytotoxicity, *J. Nanomater.* 2017 (2017). <https://doi.org/10.1155/2017/9703614>.

- [11] M.M.I. Masum, M.M. Siddiqa, K.A. Ali, Y. Zhang, Y. Abdallah, E. Ibrahim, W. Qiu, C. Yan, B. Li, Biogenic Synthesis of Silver Nanoparticles Using *Phyllanthus emblica* Fruit Extract and Its Inhibitory Action Against the Pathogen *Acidovorax oryzae* Strain RS-2 of Rice Bacterial Brown Stripe, *Front. Microbiol.* 10 (2019) 1–18. <https://doi.org/10.3389/fmicb.2019.00820>.
- [12] B. Kumar, K. Smita, L. Cumbal, A. Debut, *Ficus carica* (Fig) Fruit Mediated Green Synthesis of Silver Nanoparticles and its Antioxidant Activity: a Comparison of Thermal and Ultrasonication Approach, *Bionanoscience.* 6 (2016) 15–21. <https://doi.org/10.1007/s12668-016-0193-1>.
- [13] C. Vishwasrao, B. Momin, L. Ananthanarayan, Green Synthesis of Silver Nanoparticles Using Sapota Fruit Waste and Evaluation of Their Antimicrobial Activity, *Waste and Biomass Valorization.* 10 (2019) 2353–2363. <https://doi.org/10.1007/s12649-018-0230-0>.
- [14] S. Zafar, A. Zafar, Biosynthesis and Characterization of Silver Nanoparticles Using *Phoenix dactylifera* Fruits Extract and their In Vitro Antimicrobial and Cytotoxic Effects Abstract :, (2019) 37–46. <https://doi.org/10.2174/1874070701913010037>.
- [15] Y. Ren, H. Yang, T. Wang, C. Wang, Bio-synthesis of silver nanoparticles with antibacterial activity, *Mater. Chem. Phys.* 235 (2019) 121746. <https://doi.org/10.1016/j.matchemphys.2019.121746>.
- [16] M. Asimuddin, M.R. Shaik, N. Fathima, M.S. Afreen, S.F. Adil, M.R.H. Siddiqui, K. Jamil, M. Khan, Study of antibacterial properties of *ziziphus mauritiana* based green synthesized silver nanoparticles against various bacterial strains, *Sustain.* 12 (2020). <https://doi.org/10.3390/su12041484>.
- [17] I.O.P.C. Series, M. Science, Green synthesis of silver nanoparticles using wolfberry fruits extract and their photocatalytic performance Green synthesis of silver nanoparticles using wolfberry fruits extract and their photocatalytic performance, (2018) 0–7. <https://doi.org/10.1088/1757-899X/292/1/012017>.
- [18] M.-C. Line, Green Synthesis of Silver Nanoparticles Using *Hydnocarpus pentandra* Leaf Extract : In-vitro Cyto-Toxicity Studies Against, 10 (2018) 16–19. <https://doi.org/10.5530/jyp.2018.10.5>.
- [19] S. Chauhan, M.K. Upadhyay, N. Rishi, S. Rishi, *International Journal of Nanomaterials and Biostructures,* (2011) 17–21.
- [20] K. Jemal, B. V Sandeep, S. Pola, Synthesis , Characterization , and Evaluation of the Antibacterial Activity of *Allophylus serratus* Leaf and Leaf Derived Callus Extracts Mediated Silver Nanoparticles, 2017 (2017).
- [21] M. Vanaja, G. Gnanajobitha, K. Paulkumar, S. Rajeshkumar, C. Malarkodi, G.

- Annadurai, Phytosynthesis of silver nanoparticles by *Cissus quadrangularis*: influence of physicochemical factors, *J. Nanostructure Chem.* 3 (2013) 17.
<https://doi.org/10.1186/2193-8865-3-17>.
- [22] V. Nolasco-Arizmendi, R. Morales-Luckie, V. Sánchez-Mendieta, jp Hinestroza, E. Castro-Longoria, A.R. Vilchis-Nestor, Formation of silk–gold nanocomposite fabric using grapefruit aqueous extract, *Text. Res. J.* 83 (2013) 1229–1235.
<https://doi.org/10.1177/0040517512461697>.
- [23] X. Li, Y. Tang, Z. Xuan, Y. Liu, F. Luo, Study on the preparation of orange peel cellulose adsorbents and biosorption of Cd²⁺ from aqueous solution, 55 (2007) 69–75. <https://doi.org/10.1016/j.seppur.2006.10.025>.
- [24] T.S. Renuga Devi, S. Gayathri, FTIR And FT-Raman spectral analysis of Paclitaxel drugs, *Int. J. Pharm. Sci. Rev. Res.* 2 (2010) 106–110.
- [25] P. Fibers, The Removal of Methyl Red from Aqueous Solutions Using Banana Pseudostem Fibers The Removal of Methyl Red from Aqueous Solutions Using Banana, (2015). <https://doi.org/10.3844/ajassp.2009.1690.1700>.
- [26] B.S. Bisht, INTERNATIONAL JOURNAL OF CURRENT RESEARCH IN CHEMISTRY AND PHARMACEUTICAL SCIENCES Evaluation of Antianxiety activity of Zonisamide based on the Serendipitous action in Swiss albino mice, *Int. J. Curr. Res. Chem. Pharm. Sci.* 6 (2019) 27–32. <https://doi.org/10.22192/ijcrps>.
- [27] P. Singh, S. Pandit, M. Beshay, V.R.S.S. Mokkalapati, J. Garnaes, M.E. Olsson, A. Sultan, A. Mackevica, R.V. Mateiu, H. Lütken, A.E. Daugaard, A. Baun, I. Mijakovic, Anti-biofilm effects of gold and silver nanoparticles synthesized by the *Rhodiola rosea* rhizome extracts, *Artif. Cells, Nanomedicine Biotechnol.* 46 (2018) S886–S899.
<https://doi.org/10.1080/21691401.2018.1518909>.
- [28] K. Shameli, M. Mansor Bin Ahmad, Z. Mohsen, W.Z. Yunis, N.A. Ibrahim, A. Rustaiyan, Synthesis of silver nanoparticles in montmorillonite and their antibacterial behavior, *Int. J. Nanomedicine.* (2011) 581. <https://doi.org/10.2147/ijn.s17112>.
- [29] M. Zargar, A.A. Hamid, F.A. Bakar, M.N. Shamsudin, K. Shameli, F. Jahanshiri, F. Farahani, Green synthesis and antibacterial effect of silver nanoparticles using *Vitex negundo* L., *Molecules.* 16 (2011) 6667–6676.
<https://doi.org/10.3390/molecules16086667>.
- [30] G. Bagherzade, M.M. Tavakoli, M.H. Namaei, Green synthesis of silver nanoparticles using aqueous extract of saffron (*Crocus sativus* L.) wastages and its antibacterial activity against six bacteria, *Asian Pac. J. Trop. Biomed.* 7 (2017) 227–233.
<https://doi.org/10.1016/j.apjtb.2016.12.014>.
- [31] S.S. Shankar, A. Rai, A. Ahmad, M. Sastry, Rapid synthesis of Au, Ag, and bimetallic

- Au core-Ag shell nanoparticles using Neem (*Azadirachta indica*) leaf broth, *J. Colloid Interface Sci.* 275 (2004) 496–502. <https://doi.org/10.1016/j.jcis.2004.03.003>.
- [32] S. Raja, V. Ramesh, V. Thivaharan, Green biosynthesis of silver nanoparticles using *Calliandra haematocephala* leaf extract, their antibacterial activity and hydrogen peroxide sensing capability, *Arab. J. Chem.* 10 (2017) 253–261. <https://doi.org/10.1016/j.arabjc.2015.06.023>.
- [33] A.J. Kora, J. Arunachalam, Green fabrication of silver nanoparticles by gum tragacanth (*astragalus gummifer*): A dual functional reductant and stabilizer, *J. Nanomater.* 2012 (2012). <https://doi.org/10.1155/2012/869765>.
- [34] C. Dong, C. Cao, X. Zhang, Y. Zhan, X. Wang, X. Yang, K. Zhou, X. Xiao, B. Yuan, Wolfberry fruit (*Lycium barbarum*) extract mediated novel route for the green synthesis of silver nanoparticles, *Optik (Stuttg)*. 130 (2017) 162–170. <https://doi.org/10.1016/j.ijleo.2016.11.010>.
- [35] R. Seifipour, M. Nozari, L. Pishkar, Green Synthesis of Silver Nanoparticles using *Tragopogon Collinus* Leaf Extract and Study of Their Antibacterial Effects, *J. Inorg. Organomet. Polym. Mater.* 30 (2020) 2926–2936. <https://doi.org/10.1007/s10904-020-01441-9>.
- [36] K. Xin Lee, K. Shameli, M. Miyake, N. Kuwano, N.B. Bt Ahmad Khairudin, S.E. Bt Mohamad, Y.P. Yew, Green Synthesis of Gold Nanoparticles Using Aqueous Extract of *Garcinia mangostana* Fruit Peels, *J. Nanomater.* 2016 (2016). <https://doi.org/10.1155/2016/8489094>.
- [37] A.A. Abuderman, R. Syed, A.A. Alyousef, M.S. Alqahtani, M.S. Ola, A. Malik, Green synthesized silver nanoparticles of *Myrtus communis* L (AgMC) extract inhibits cancer hallmarks via targeting aldose reductase (AR) and associated signaling network, *Processes*. 7 (2019). <https://doi.org/10.3390/pr7110860>.
- [38] D. Philip, Green synthesis of gold and silver nanoparticles using *Hibiscus rosa sinensis*, *Phys. E Low-Dimensional Syst. Nanostructures*. 42 (2010) 1417–1424. <https://doi.org/10.1016/j.physe.2009.11.081>.
- [39] M. Rojas-Andrade, A.T. Cho, P. Hu, S.J. Lee, C.P. Deming, S.W. Sweeney, C. Saltikov, S. Chen, Enhanced antimicrobial activity with faceted silver nanostructures, *J. Mater. Sci.* 50 (2015) 2849–2858. <https://doi.org/10.1007/s10853-015-8847-x>.
- [40] M. Gomathi, P.V. Rajkumar, A. Prakasam, K. Ravichandran, Green synthesis of silver nanoparticles using *Datura stramonium* leaf extract and assessment of their antibacterial activity, *Resour. Technol.* 3 (2017) 280–284. <https://doi.org/10.1016/j.refit.2016.12.005>.
- [41] Y. Yang, S. Matsubara, L. Xiong, T. Hayakawa, M. Nogami, Solvothermal synthesis

- of multiple shapes of silver nanoparticles and their SERS properties, *J. Phys. Chem. C*. 111 (2007) 9095–9104. <https://doi.org/10.1021/jp068859b>.
- [42] J.Y. Song, B.S. Kim, Rapid biological synthesis of silver nanoparticles using plant leaf extracts, *Bioprocess Biosyst. Eng.* 32 (2009) 79–84. <https://doi.org/10.1007/s00449-008-0224-6>.
- [43] S. Some, O. Bulut, K. Biswas, A. Kumar, A. Roy, Effect of feed supplementation with biosynthesized silver nanoparticles using leaf extract of *Morus indica* L . V1 on *Bombyx mori* L . (*Lepidoptera* : *Bombycidae*), (2019) 1–13. <https://doi.org/10.1038/s41598-019-50906-6>.
- [44] D. Press, Synthesis of silver nanoparticles using *Dioscorea bulbifera* tuber extract and evaluation of its synergistic potential in combination with antimicrobial agents, (2012). <https://doi.org/10.2147/IJN.S24793>.
- [45] S. Kaviya, J. Santhanalakshmi, B. Viswanathan, J. Muthumary, K. Srinivasan, Biosynthesis of silver nanoparticles using citrus sinensis peel extract and its antibacterial activity, *Spectrochim. Acta - Part A Mol. Biomol. Spectrosc.* 79 (2011) 594–598. <https://doi.org/10.1016/j.saa.2011.03.040>.
- [46] K. Jyoti, M. Baunthiyal, A. Singh, Characterization of silver nanoparticles synthesized using *Urtica dioica* Linn. leaves and their synergistic effects with antibiotics , *J. Radiat. Res. Appl. Sci.* 9 (2016) 217–227. <https://doi.org/10.1016/j.jrras.2015.10.002>.
- [47] C. Krishnaraj, E.G. Jagan, S. Rajasekar, P. Selvakumar, P.T. Kalaichelvan, N. Mohan, Synthesis of silver nanoparticles using *Acalypha indica* leaf extracts and its antibacterial activity against water borne pathogens, *Colloids Surfaces B Biointerfaces.* 76 (2010) 50–56. <https://doi.org/10.1016/j.colsurfb.2009.10.008>.
- [48] N. Allec, M. Choi, N. Yesupriya, B. Szychowski, M.R. White, M.G. Kann, E.D. Garcin, M.C. Daniel, A. Badano, Small-angle X-ray scattering method to characterize molecular interactions: Proof of concept, *Sci. Rep.* 5 (2015) 1–12. <https://doi.org/10.1038/srep12085>.
- [49] U. Feleni, U. Sidwaba, H. Makelane, E. Iwuoha, Core–Shell Palladium Telluride Quantum Dot-Hemethiolate Cytochrome Based Biosensor for Detecting Indinavir Drug, *J. Nanosci. Nanotechnol.* 19 (2019) 7974–7981. <https://doi.org/10.1166/jnn.2019.16866>.
- [50] P.R.A.F. Garcia, K. Loza, S. Daumann, V. Grasmik, K. Pappert, A. Rostek, J. Helmlinger, O. Prymak, M. Heggen, M. Epple, C.L.P. Oliveira, Combining Small-Angle X-ray Scattering and X-ray Powder Diffraction to Investigate Size, Shape and Crystallinity of Silver, Gold and Alloyed Silver-Gold Nanoparticles, *Brazilian J. Phys.* 49 (2019) 183–190. <https://doi.org/10.1007/s13538-019-00642-z>.

- [51] B.J. Plowman, B. Sidhureddy, S. V. Sokolov, N.P. Young, A. Chen, R.G. Compton, Electrochemical Behavior of Gold–Silver Alloy Nanoparticles, *ChemElectroChem*. 3 (2016) 1039–1043. <https://doi.org/10.1002/celec.201600212>.
- [52] M.M.S. Lima Filho, A.A. Correa, F.D.C. Silva, F.A.O. Carvalho, L.H. Mascaro, T.M.B.F. Oliveira, A glassy carbon electrode modified with silver nanoparticles and functionalized multi-walled carbon nanotubes for voltammetric determination of the illicit growth promoter dienestrol in animal urine, *Microchim. Acta*. 186 (2019) 1–10. <https://doi.org/10.1007/s00604-019-3645-9>.
- [53] M.S.M.S. Dharmaprakash, S.M.K.L. Nagashree, Green synthesis of silver nanoparticles (SNPs)- modified electrode for electrochemical detection of nitrobenzene, *J. Iran. Chem. Soc.* 17 (2020) 893–900. <https://doi.org/10.1007/s13738-019-01822-z>.
- [54] V. Sreenivasulu, N. Siva Kumar, M. Suguna, M. Asif, E.H. Al-Ghurabi, Z.X. Huang, Z. Zhen, Biosynthesis of silver nanoparticles using mimosa pudica plant root extract: Characterization, antibacterial activity and electrochemical detection of dopamine, *Int. J. Electrochem. Sci.* 11 (2016) 9959–9971. <https://doi.org/10.20964/2016.12.69>.
- [55] S.H. Merza, Effect of Scan Rate and pH on Determination Amoxilline Using Screen Printed Effect of Scan Rate and pH on Determination Amoxilline Using Screen Printed Carbon Electrode Modified with Functionalized Graphene Oxide, (2020). <https://doi.org/10.30526//31.1.1863>.
- [56] I. Khan, U.J. Pandit, S. Wankar, R. Das, S.N. Limaye, Fabrication of electrochemical nanosensor based on polyaniline film-coated AgNP-MWCNT-modified GCE and its application for trace analysis of fenitrothion, *Ionics (Kiel)*. 23 (2017) 1293–1308. <https://doi.org/10.1007/s11581-016-1939-z>.

CHAPTER SIX

Results and Discussion: Part 3

In this chapter, we report the overall findings on the research obtained for the novel green method synthesis of Silver/Gold bimetallic nanoparticles. This was achieved by the reduction of aqueous Ag^+ and AuCl_4^- ions by simultaneous reduction with the combined grape and banana peel extract (as described in chapter 3). The synthesis methods, as well as the characterisation of the resultant nanoparticles, will be discussed in this chapter.

6 Silver-Gold Bimetallic Nanoparticles:

6.1 Ultraviolet-Visible Spectroscopy (UV-vis) of (Ag-Au-NPs):

The use of UV-visible spectroscopy confirmed the successful synthesis of silver-gold (Ag-Au-NPs) bimetallic nanoparticles by simultaneous reduction of silver and gold ions in a ratio of (Ag-Au = 2:1). **Figure 6.1** illustrates the colour of the solutions before the reaction commences as well as the colour of the obtained bimetallic nanoparticles. Literature reveals that silver and gold nanoparticles exhibit brown [1] and purple [2] colours in water respectively and the achieved experiments in this study complement that. The obtained bimetallic nanoparticles were obtained as black arising from the excitation of surface plasmon vibrations in the metal nanoparticles [3,4]. **Figure 6.2** shows the UV-vis absorption spectra of Au-NPs, Ag-NPs and Ag-Au-NPs. The SPR band for gold nanoparticles was

observed at 535 nm, silver nanoparticles at 440 nm and for silver-gold nanoparticles at 457 nm [5,6]. The appearance of the single peak at 457 nm also confirms the contribution by both metals in the formation of the bimetallic nanoparticles. Risting and co-workers reported an SPR at 470 nm for Ag/Au alloy for (2:1 nominal atomic position) [7]. Furthermore, the position of the observed SPR absorbance band for silver-gold nanoparticles is in excellent agreement with the linear relationship that is expected between the SPR band position and the composition of the bimetallic nanoparticles [8]. The obtained findings are in agreement with the work of David and Yaghubi [9,10]. **Table 7.1** shows the comparison of SPR bands and reaction time for complete reduction of silver/gold ions from previously reported studies. These were compared with the current study where natural products were used as reducing agents. It can be seen from the table that the SPR band was in a similar position in all the studies and this study showed a complete reduction in 90 min, which is less compared to the other studies. This is caused by phenols, amines, flavonoids and phenolic compounds found in grapes and banana peels that reduce silver nitrate as well as gold chloride faster thus making the reaction time shorter [11,12].

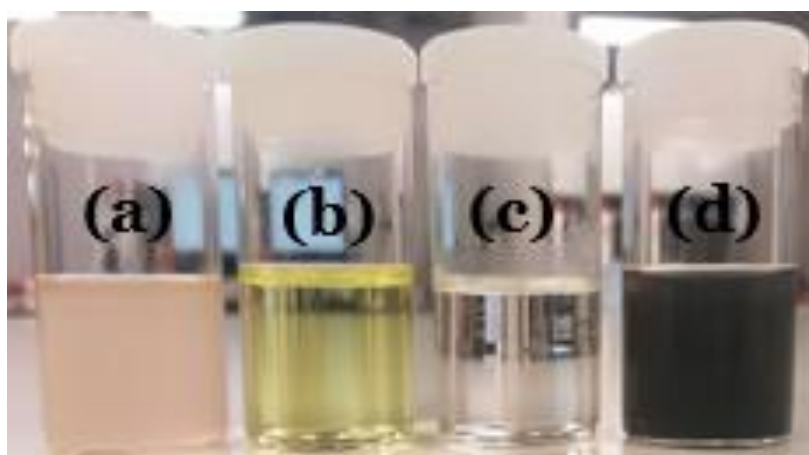


Figure 6.1: Photograph showing colour of solutions, (a) GBPE extract, (b) HAuCl_4 , (c) AgNO_3 , and Ag-Au-NPs.

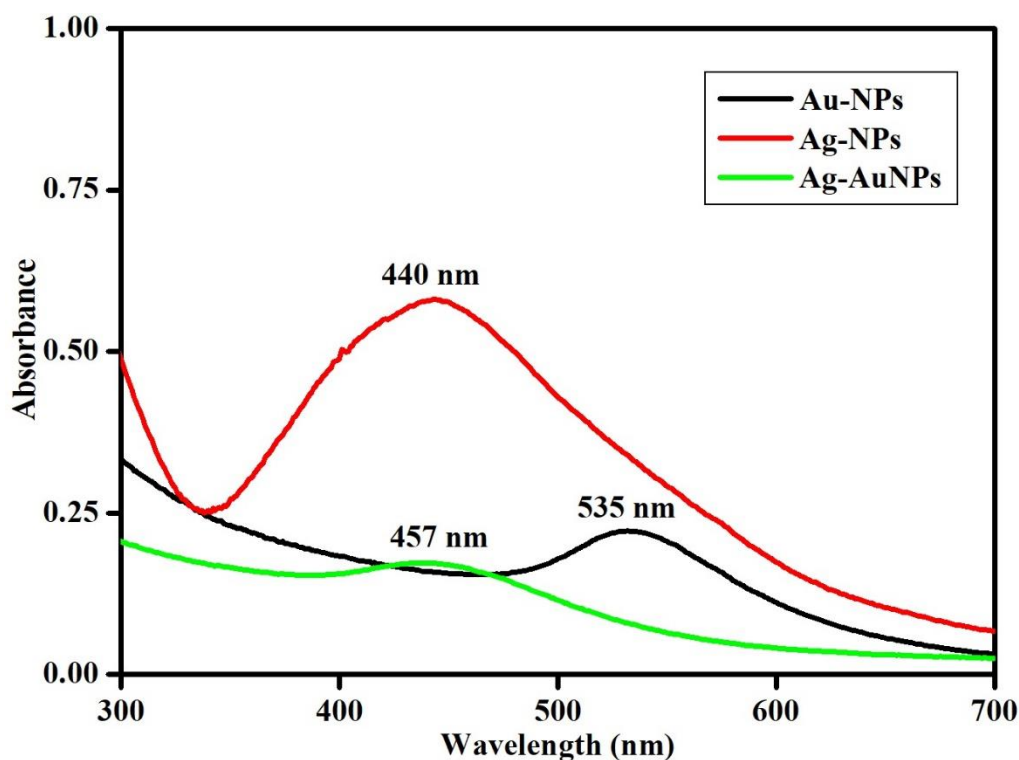


Figure 6.2: UV -visible absorption spectra of Au-NPs (Black), Ag-NPs (Red), and Ag-Au-NPs (Green).

Table 6.1: Comparison of SPR band and Reaction times for silver-gold nanoparticles synthesis via green methods from literature and this study.

| Type of nanoparticles | Natural product used | Wavelength (nm) | Reaction time (min) | Reference |
|-----------------------|------------------------|-----------------|---------------------|------------|
| Ag-Au-NPs | Pueraria plant | 428 nm | 150 min | [13] |
| Ag-Au-NPs | Potato Starch | 470 nm | 120 min | [14] |
| Ag-Au-NPs | Grapes and Banana peel | 457 nm | 90 min | This study |

6.2 Fourier Transform Infrared Spectroscopy (FT-IR) of Ag-Au-NPs:

The FTIR spectrum of bimetallic silver-gold nanoparticles derived from GBPE after a simultaneous reaction with AgNO_3 and HAuCl_4 is shown in **Figure 6.3**. The spectra of GBPE capped Ag-Au-NPs shows a broadband at 3359 cm^{-1} due to the stretching vibrations of hydroxyl groups (-OH) of alcohol and phenols from sugars present in flavonoids and

phenolic compounds found in grape and banana peel such as myricetin and quercetin [15]. The weak band at 2935 cm^{-1} is due to the aliphatic C-H stretching vibrations which shows the aliphatic nature of grape and banana peel due to low content of lignin present in grapes and banana peel. The new peak at 2428 cm^{-1} was assigned to -CH stretching vibrations of $-\text{CH}_3$ and $-\text{CH}_2$ functional groups [16]. The weak peak at 2093 cm^{-1} is due to thiols S-H stretch indicating the presence of banana in the grapes-banana peel extract. The peak at 1657 cm^{-1} is characteristic of C=O stretch of carbonyl group showing the presence of hemicellulose band from banana peel and represent the involvement of amide-I band ($-\text{C}=\text{O}$) of amines from catechin that is present in grapes and which acted as both stabilising and a capping agents of Ag-Au-NPs [17].

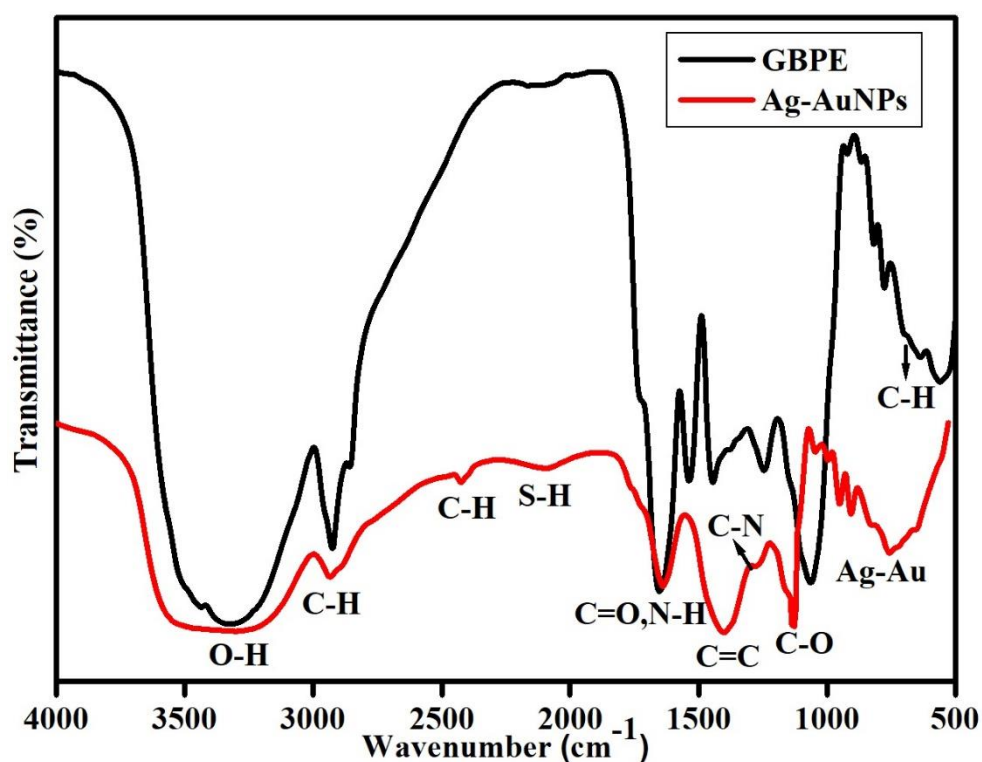


Figure 6.3: FT-IR Spectra of the Green Synthesised Ag-Au-NPs (Red curve) and GBPE (Black curve).

Moreover, the band at 1396 cm^{-1} is attributed to C=C stretching vibrations of aromatic ring and alkenes from phenolic compounds and organic acids found in tannins, flavonoids and cellulosic materials of grapes. The bands at 1276 and 1124 cm^{-1} are due C-N and C-O stretch from amine groups due to the presence of hemicellulose, lignin and pectin present in grapes and banana peel [18]. The peak at 744 cm^{-1} is contributed by vibrations of the nanoparticles, which were not observed in the GBPE spectrum, thus confirming the formation of the nanoparticles [19].

Figure 6.4 indicates the obtained FTIR spectra for the GBPE capped Au-NPs, Ag-NPs and the Ag-Au-NPs to highlight their differences. As can be seen from **Figure 6.4**, the differences in the peaks and minute shifts in the peak positions show evidence that the capping species bound differently to Au as opposed to Ag confirming that the nature of co-ordination with the metal surface is quite different in both cases.

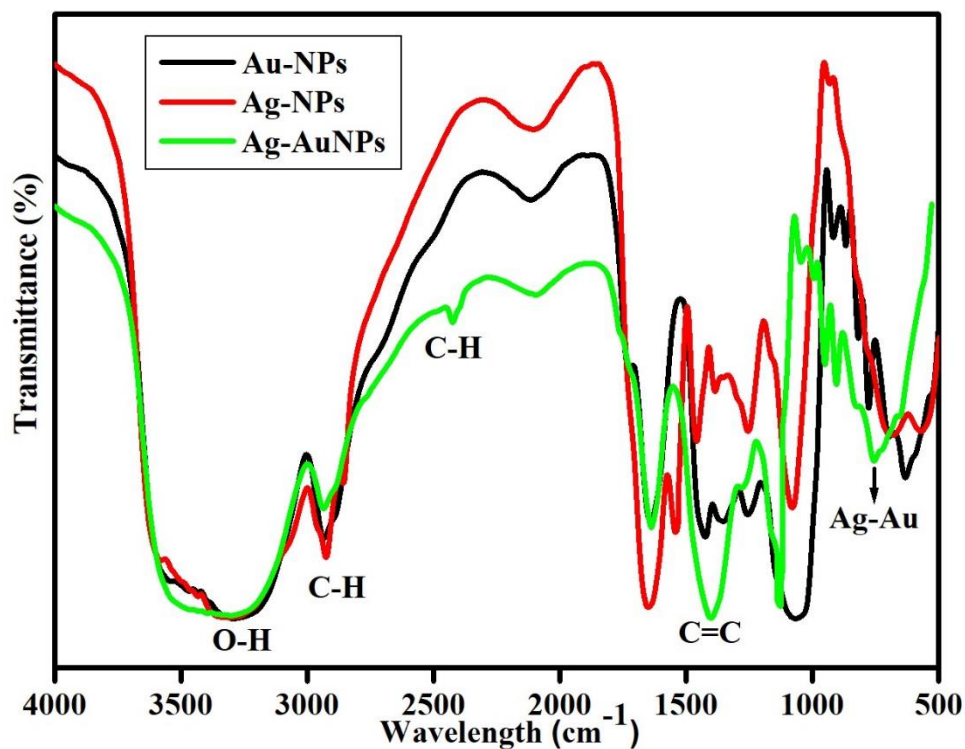


Figure 6.4: FT-IR Spectra of Au-NPs (Black), Ag-NPs (Red) and Ag-Au-NPs (Green).

6.3 X-ray Diffraction for GBPE capped Ag-Au-NPs nanoparticles:

To verify that the Ag-Au-NPs consisted of crystalline silver and gold; X-ray diffraction (XRD) analysis was performed as a confirmation tool. **Figure 6.5** shows the XRD pattern obtained for the GBPE capped Ag-Au-NPs nanoparticles showing five intense peaks. The obtained diffraction peaks at $2\theta = 36.8^\circ$, 43.7° , 57.9° , 70.9° and 75.7° , correspond to the Bragg reflection planes (111), (200), (220), (311) and (222) respectively. Earlier reports by Bonigala and co-workers are in agreement with these findings [20]. The average particle size of the GBPE Ag-Au-NPs was determined to be 13 nm based on the full-width half maximum (FWHM) data using Scherer's equation (**Equation 3.4**, chapter 3).

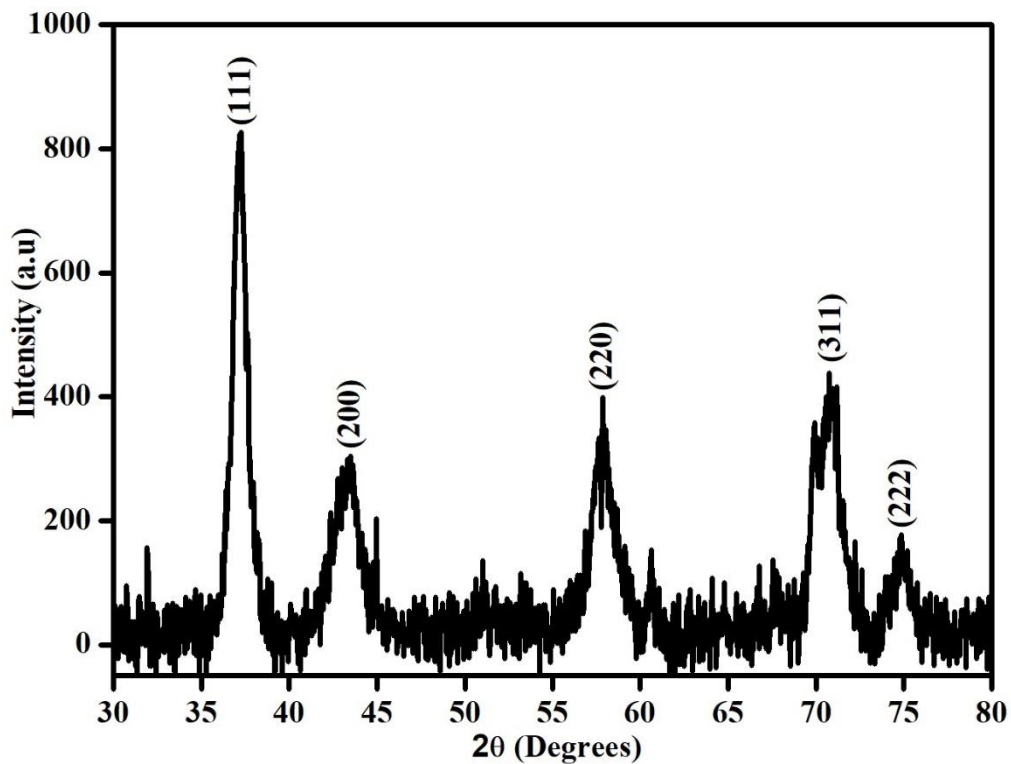


Figure 6.5: XRD pattern of the synthesised GBPE Ag-Au-NPs.

The XRD pattern of GBPE capped bimetallic Ag–Au-NPs was compared concerning the individually capped GBPE Ag and Au-NPs, as shown in **Figure 6.6**. The comparison exercise revealed that, the individual or monometallic GBPE capped Ag-NPs and Au-NPs XRD patterns had similar peaks. Literature confirms these findings, and it suggests that the patterns were similar because silver and gold have similar lattice constants JCPDS 4-0783 and 4-0784, respectively [21]. JCPDS is a database of standard XRD reference pattern, for material which is used for referencing crystal structures [22]. In case of Ag-Au-NPs, the same peaks at 35° to 82° were observed with a slight shift and with lower intensity due to lower deactivation of atoms in the structure of the face centred cubic (fcc) silver-gold nanoparticles. [23]. For the individual or monometallic nanoparticles, the peaks are weak and broad, but for the bimetallic Ag-Au-NPs, the peaks are significantly enhanced thus confirming the development of homogenous bimetallic structures. Therefore, the obtained XRD pattern clearly shows that the silver-gold bimetallic nanoparticles were formed by the reduction of Ag^+ ions and AuCl_4^- in the presence of GBPE are indeed crystalline [24].

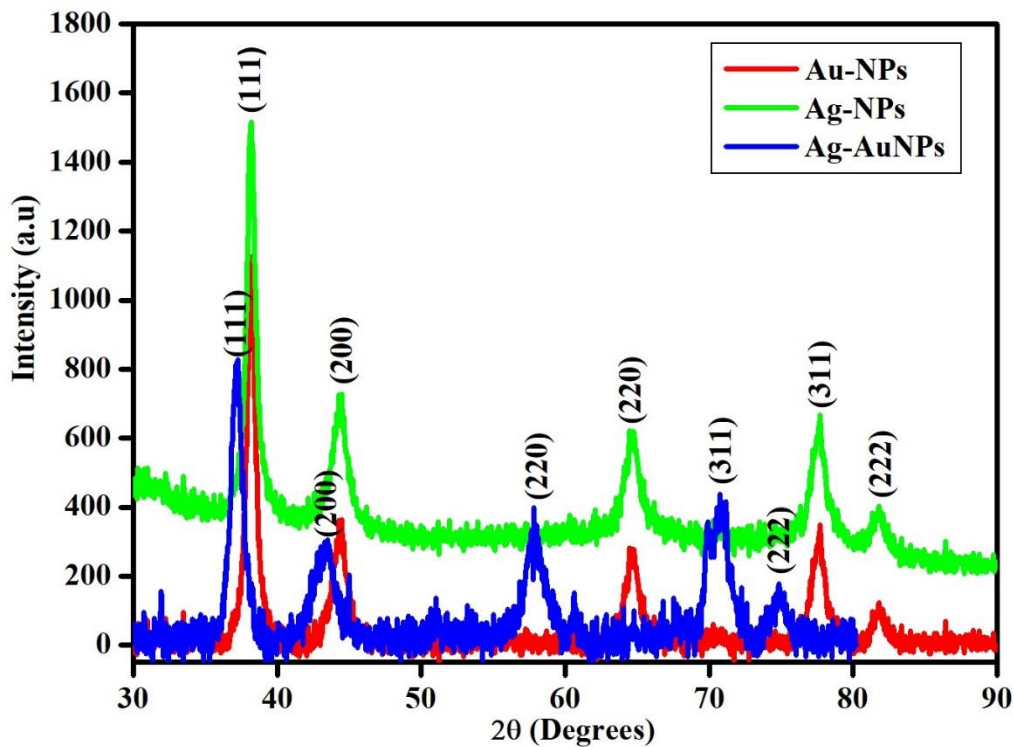


Figure 6.6: XRD pattern of GBPE capped Au, Ag and Ag-Au-NPs.

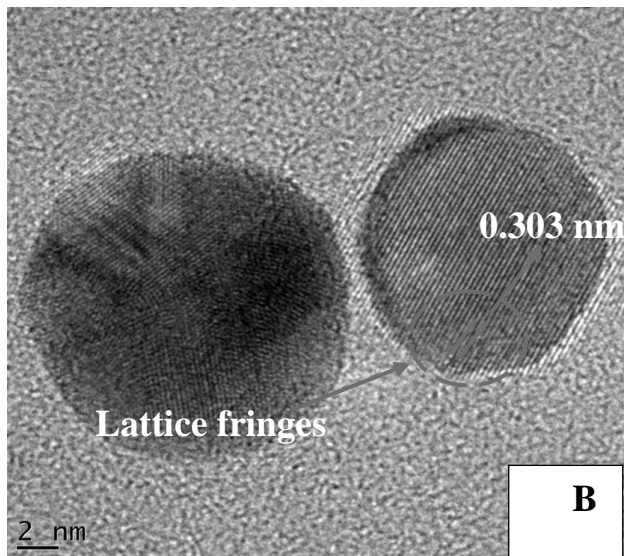
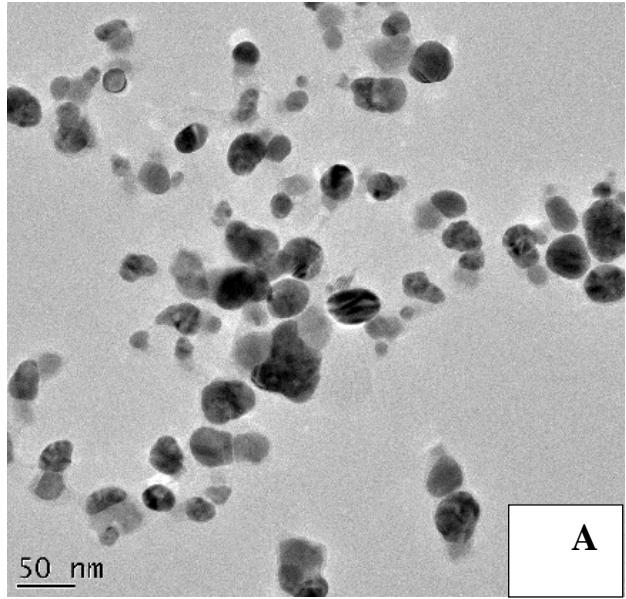
Table 6.2 shows the comparison of Bragg's diffraction peaks at 2θ value and the average crystal size of the green synthesised nanoparticles calculated using Debye-Scherrer formula (from literature) and the present work. As seen from the table, this study developed the smallest nanoparticles. The difference in the size of the synthesised nanoparticles was due to the presence of more than one reducing agent on the natural products used and different selection of suitable reaction conditions for synthesis [25].

Table 6.2: Comparison of Braggs diffraction peaks at 2Θ value and the size of crystalline green synthesised nanoparticles (from literature) and the present work.

| Nanoparticles | 2 Θ (Degrees) corresponding | | | | | Crystalline size (nm) | Reference |
|---|------------------------------------|------|------|------|------|-----------------------|------------|
| | 111 | 200 | 220 | 311 | 222 | | |
| D. radiodurans protein capped Ag-Au-NPs | 38.3 | 46.3 | 66.1 | 77.7 | 85.6 | 49 nm | [26] |
| Enzyme capped Ag-Au-NPs | 38 | 44 | 64 | 77 | 81 | 36 nm | [27] |
| GBPE capped Ag-Au-NPs | 36.8 | 43.7 | 57.9 | 70.9 | 75.7 | 13 nm | This study |

6.4 High-Resolution Transmission Electron Microscopy (HR-TEM) of Ag-Au-NPs:

HR-TEM determined the morphology and size of the synthesised Ag-Au bimetallic nanoparticles, and the images are illustrated in **Figure 6.7(a)** to **Figure 6.7(d)**. From **Figure 6.7(a)** it can be observed that the HR-TEM images of Ag-Au-NPs are spherical with particle size diameter in the range of 12–14 nm as confirmed in **Figure 6.7 (d)**. The lattice fringes are visible in **Figure 6.7(b)** and indicate good crystallinity with an interlayer spacing of 0.303 nm, which corresponds to the lattice spacing of the silver-gold (111) planes. From the image, it was possible to see that the nanoparticles have the correct atomic ordering within each particle since there was no mismatching as expected from a highly similar lattice JCPDS constants of silver and gold.



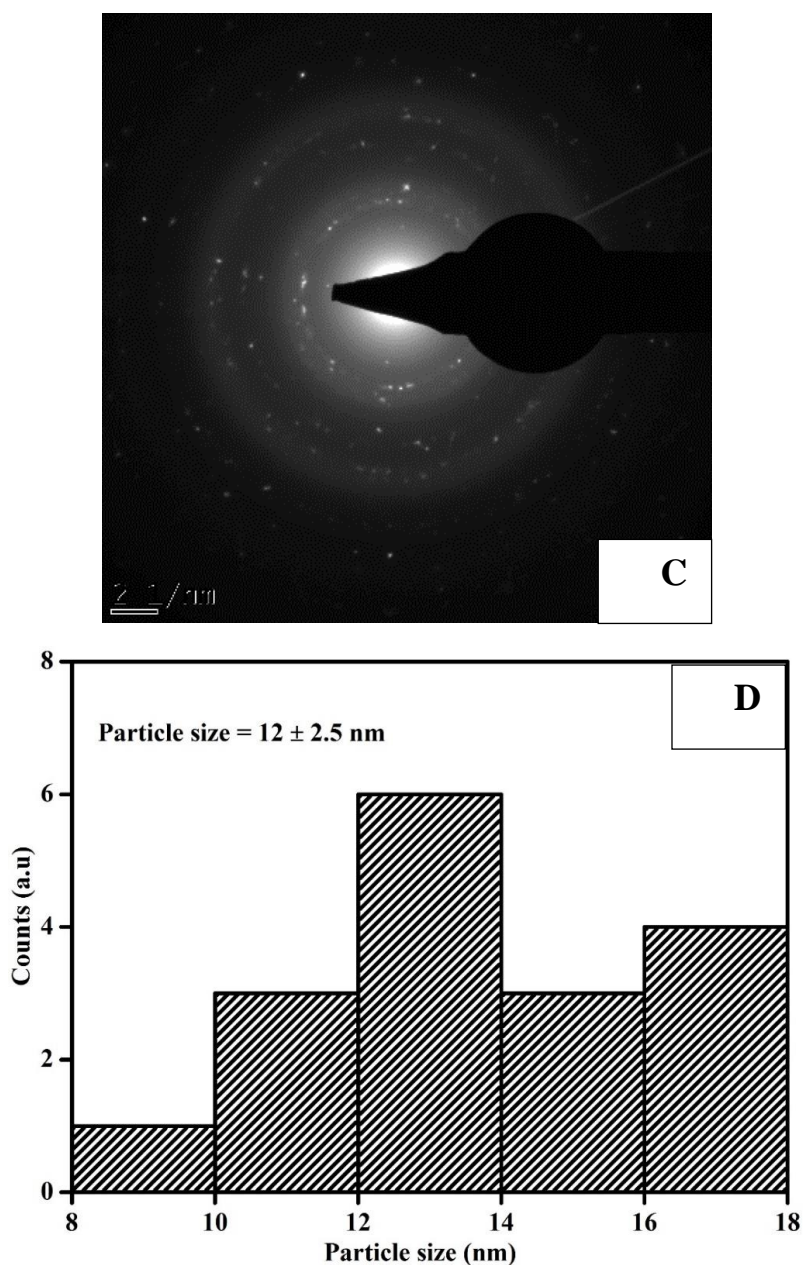
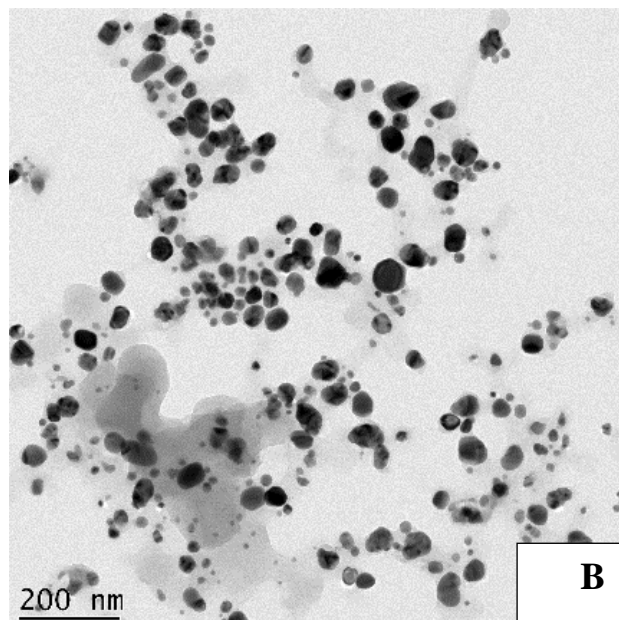
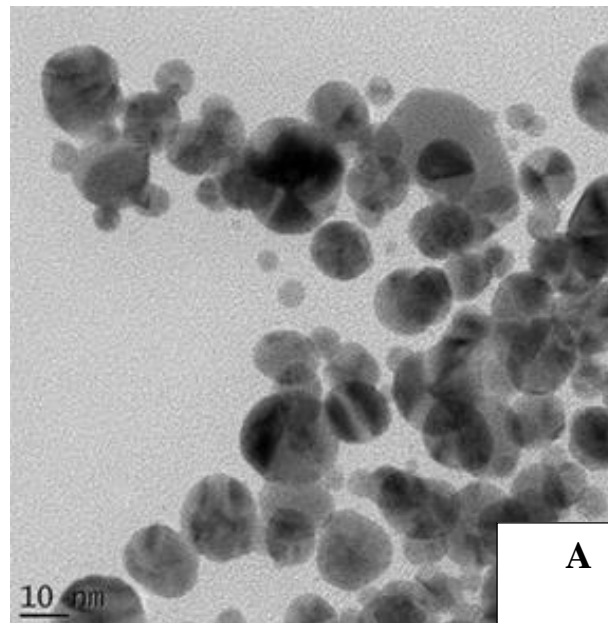


Figure 6.7: HR-TEM image of Ag-Au-NPs at 50 nm range (a); lattice fringes (b); selected area electron diffraction (SAED) patterns (c); histogram (d).

In this study, we also observed that nanoparticles of different sizes with the same shapes were successfully synthesised using grape-banana peel extract (under the conditions described in chapter 3). **Figure 6.8** shows HR-TEM images of GBPE capped Au-NPs, Ag-NPs and (2:1, Ag: Au) Ag-Au bimetallic nanoparticles with particle sizes in the range of 10-17 nm, 25-39 nm and 12-14 nm, respectively. **Table 6.3** shows comparison of sizes determined using HR-

TEM measurements for green synthesised Ag-Au-NPs between previously reported studies and this study. As seen in the table. this study shows the smallest range in terms of size for Ag-Au-NPs, the smaller size of the nanoparticles is considered as better since they have a large surface area to volume ratios and improve properties in terms of applications [28]



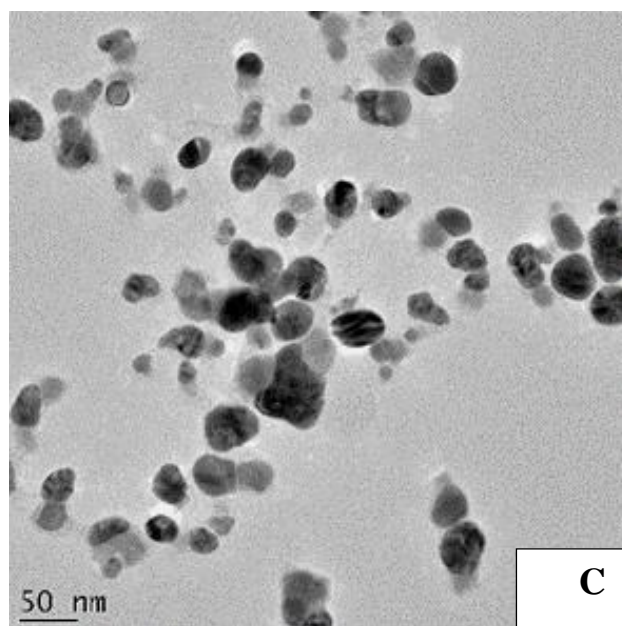


Figure 6.8: HR-TEM images of GBPE capped (a) Au-NPs (b) Ag-NPs (c) Ag-Au-NPs (2:1) bimetallic alloy nanoparticles.

Table 6.3: Comparison of size (calculated based on HR-TEM measurements) of green synthesised silver-gold bimetallic alloy nanoparticles.

| Type of Nanoparticles | Natural product | Reducing agent | Size (nm) | Reference |
|-----------------------|-------------------------|----------------|-----------|------------|
| Ag-Au-NPs | Avocado peel | Fruit extract | 44-55 nm | [29] |
| Ag-Au-NPs | Gloriosa superba leaves | Plant extract | 14-26 nm | [30] |
| Ag-Au-NPs | Grapes and Banana peel | Fruit extract | 12-14 nm | This study |

The Electron Diffraction X-ray Spectrum (EDS) profile **Figure 6.9** of Ag-Au-NPs showed intense peak signals of gold (Au) metal at 2.2 KeV and silver (Ag) metal at 3.1 KeV [31]. Other signals observed also include those of carbon (C), oxygen (O) and copper (Cu). The presence of carbon and oxygen are attributed to polyphenol groups originated from the extract and are bounded to the surface of the nanoparticles. Copper is attributed to the supporting copper grid [32] used during the analysis. Similar EDS profile was reported by

Ganaie and co-workers who reported the preparation of bimetallic nanoparticles using leptopus plant via a green synthesis method were they observed elemental Ag at 3.0 KeV and Au at 2.2 KeV [33]. Sun and co-workers also obtain similar results using chines wolfberry extract to synthesise silver-gold alloy nanoparticles [34], and Liang and co-workers also reported similar results for gold-silver nanoparticles obtained using *Lysimachia christinae* polysaccharide [35].

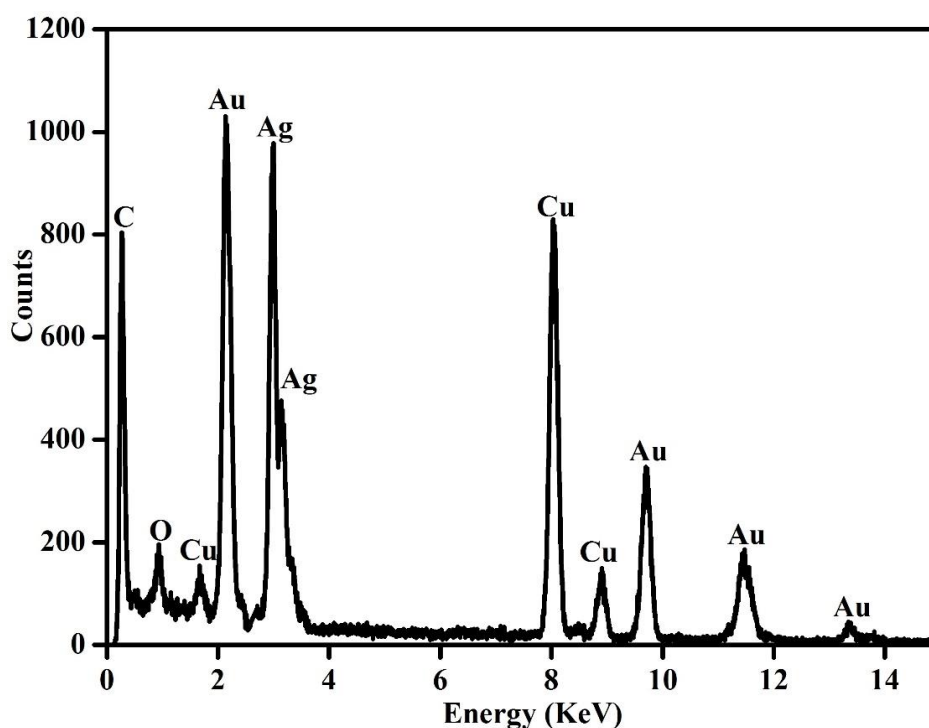


Figure 6.9: Energy Dispersive Spectroscopy patterns of GBPE Ag-Au-NPs.

6.5 Small Angle X-ray Scattering for GBPE Ag-Au-NPs:

Small Angle X-ray Scattering (SAXS) measurements were used to investigate the particle size and the size distribution of the synthesised silver-gold bimetallic nanoparticles through

pair distance distribution function (PDDF), size distribution by number function and the intensity function. In **Figure 6.10**, the PDDF curve indicates that the most massive particles size detected have a maximum diameter of 30 nm. Furthermore, the regular shape of the curve (PDDF) confirms that Ag-Au-NPs has less possibility to aggregates or they do not aggregate at all. The size distributions functions of Ag-Au-NPs in **Figure 6.11** weighed by number (Black curve) and intensity (Red curve) revealed mono-dispersed particles with average radiuses of 16 nm. The curves overlap one another (size distribution by number = size distribution by intensity), giving an illusion that only one curve is present. **Table 6.4** shows a summary of the average particle size of GBPE capped nanoparticles determined by XRD, HR-TEM and SAX in this study.

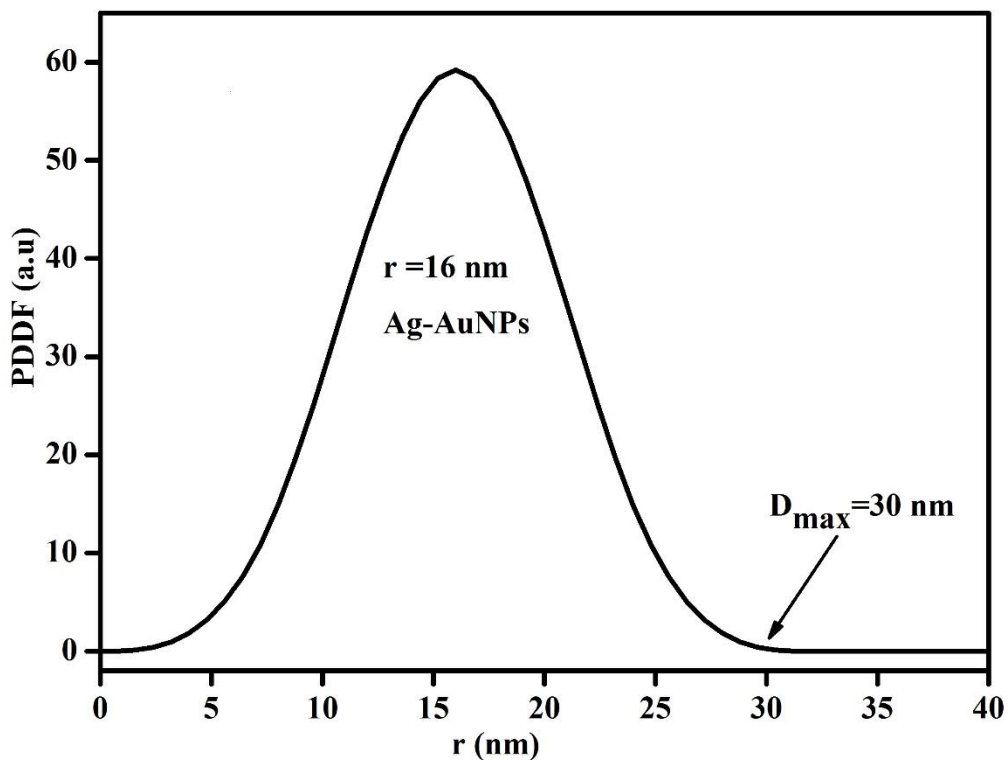


Figure 6.10: SAXS pair-distance distribution function (PDDF) of GBPE capped Ag-Au-NPs.

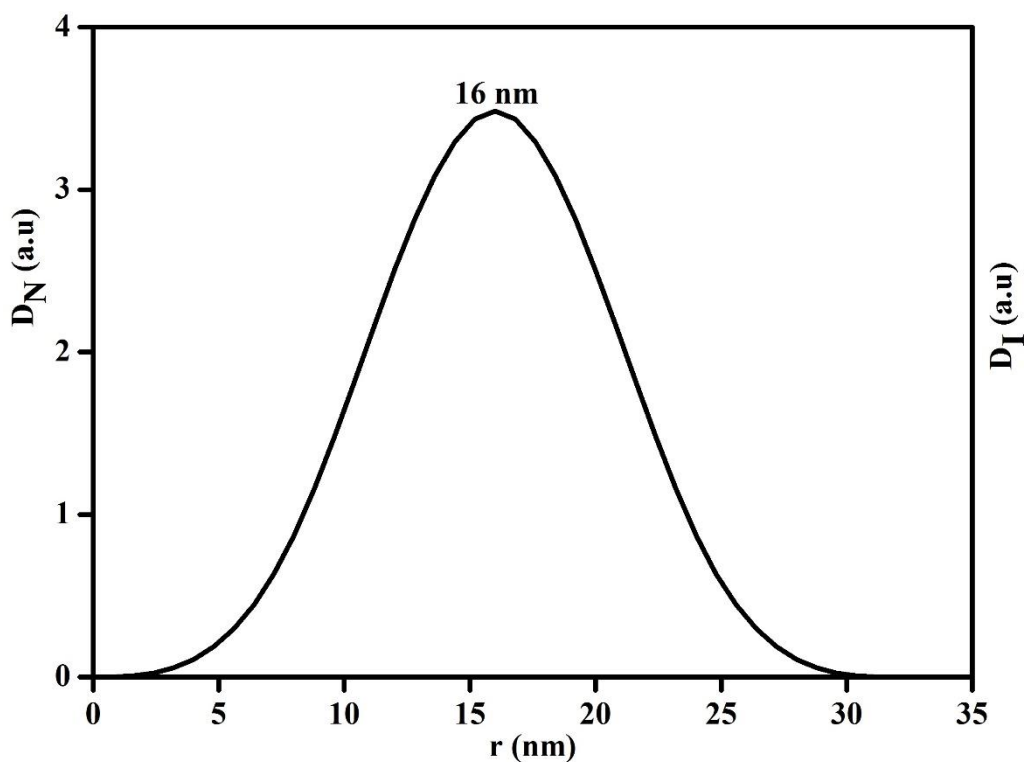


Figure 6.11: Size distribution functions weighted by number and intensity.

Table 6.4: Summary of the average particle size of GBPE capped nanoparticles determined by XRD, HR-TEM and SAX in this study.

| Nanoparticles | XRD size (nm) | HR-TEM size (nm) | SAX size (nm) |
|----------------|---------------|------------------|---------------|
| GBPE-Au-NPs | 12.3 nm | 10-17 nm | 16 nm |
| GBPE-Ag-NPs | 30 nm | 25-39 nm | 39 nm |
| GBPE-Ag-Au-NPs | 13 nm | 12-14 nm | 16 nm |

6.6 Electrochemical characterisation of GBPE capped Ag-AuNPs:

The use of cyclic voltammetry technique (CV) also characterised the synthesised Ag-Au (2:1) bimetallic alloy nanoparticles. Cyclic voltammograms at a scan rate of 50 mV/s in degassed

phosphate buffer (0.2 M, pH 7.4) for the blank GCE and the GCE modified with monometallic Ag and Au-NPs were previously recorded in previous chapters. **Figure 6.12** shows the cyclic voltammogram of GBPE capped Ag-Au-NPs modified GCE (Red curve) and of bare GCE electrode (Black curve). The electrochemical response of the Ag-AuNPs was observed at 0.43 V and 1.03 V indicating the oxidation peaks 1 & 2 ($E_{p_{c1}}$ and $E_{p_{c2}}$) respectively and reduction peak ($E_{p_{a1}}$) at -0.99 V. In **Figure 6.12** the modified GCE electrode showed higher electrochemical properties compared to the unmodified GCE electrodes and similar observation were reported in the literature [36].

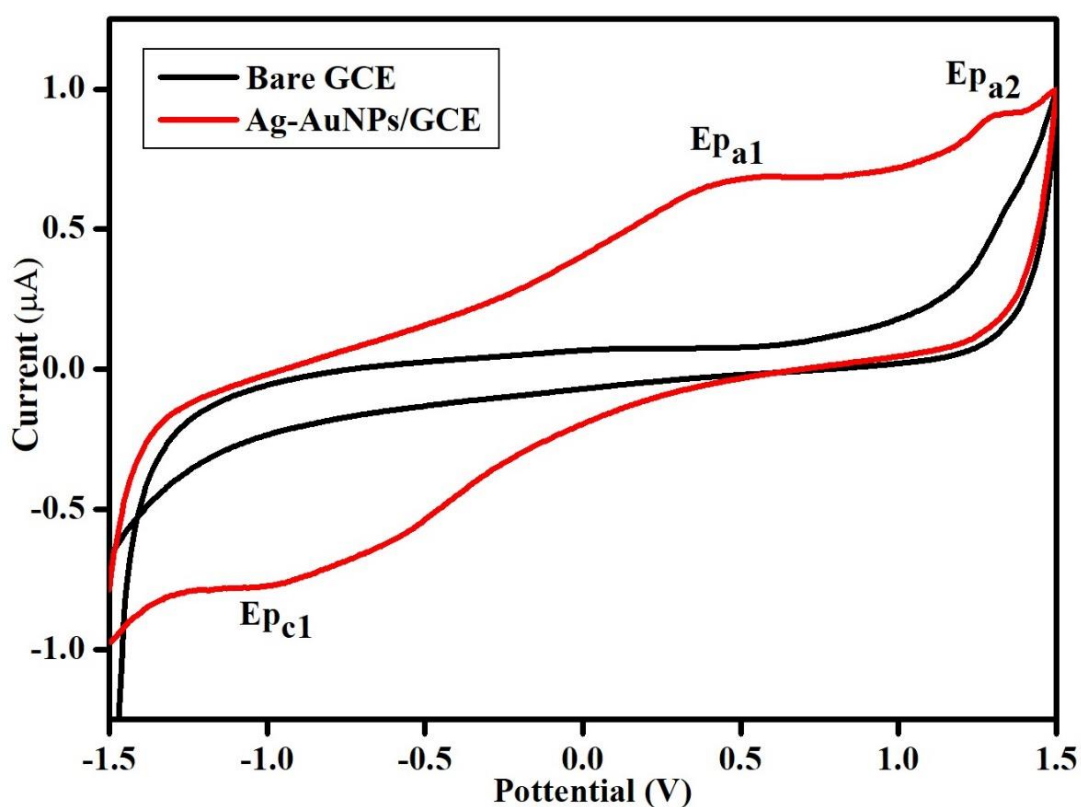


Figure 6.12: Cyclic voltammogram of a Bare GCE (Black Curve) and Ag-Au-NPs|GCE (Red Curve) in 0.2 M PBS (pH 7.4) Scan rate 50 mV/s.

Figure 6.13 shows cyclic voltammograms of GBPE capped Ag-Au-NPs|GCE at different scan rates (10 - 100 mVs⁻¹) where it was observed that the oxidation peak current (I_{pa}) against the scan rate (v) was linear over the range of 10 - 100 mV/s. The data presented in **Figure 6.13** indicate that the anodic peak current was linear with the scan rate, and as the scan rate increased, a shift in the potential to more positive values was observed. This indicates that the GBPE capped Ag-Au-NPs nanoparticles are conductive while transferring electrons with the electrode surface [37]. Similar results were reported by Lanh and co-workers using 0.1 M PBS pH 7 and 0.1 M LiClO₄ instead of 0.2 M PBS pH 7.4 [38] thus, confirming that the synthesised GBPE capped Ag-AuNPs were relatively homogeneous and formed alloy bimetallic nanoparticles. The voltammograms correspond to a reversible system with $I_{pa} / I_{pc} = 0.99$ which is approximately = ~ 1.0 and the peak to peak separation (ΔE_p) was determined to be = 1.111V, which means that $(E_p) = E_{pa} - E_{pc} > 0.059/n$ V.

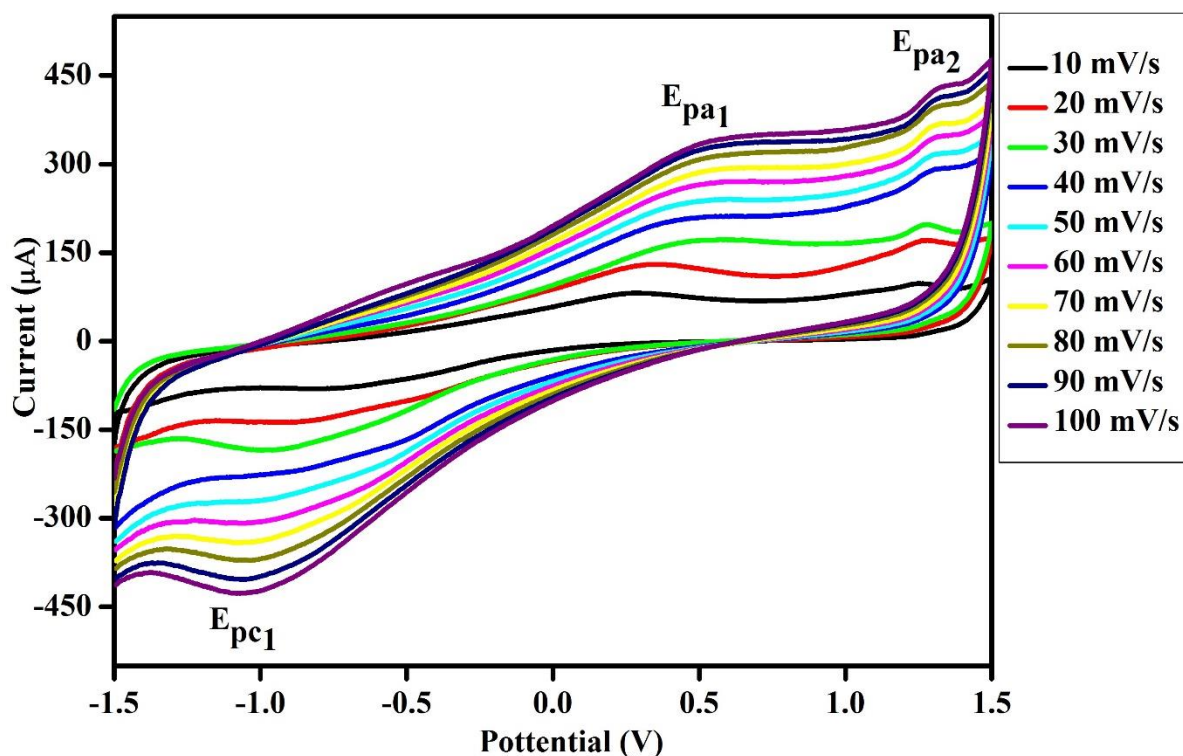


Figure 6.13: Cyclic voltammograms of Ag-Au-NPs|GCE in 0.2M PBS at different scan rates (10-100 mV/s)

A plot of log anodic peak current against the log scan rate was plotted for the GBPE capped Ag-Au-NPs where nearly a straight line with a linear regression $I_{pa} (\mu A) = 0.8282x - 0.1915$ and a correlation coefficient $r^2 = 0.9984$ was determined as shown in **Figure 6.14**. The slope value of 0.8 from the plot indicates a mixed diffusion-adsorption process. For a reversible redox system the ratio of the anodic to cathodic current should be unity and ΔE_p is meant to be a minimal value, but it also depends on the number of electrons involved; however the system shows a reversible system and log current versus log scan rate plot further proves the reversibility since it shows values of the surface-bound kinetics and reversibility. The formal potential $E = (E_{pa} + E_{pc}) / 2$ of the system was determined to be 0.1785 V. **Figure 6.15** shows the Randel-Sevcik plot for GBPE capped Ag-Au-NPs where the surface concentration of the GBPE capped Ag-Au-NPs was estimated to be $5.322 \times 10^{-5} \text{ mol cm}^{-2}$ using the Brown-Anson

method (Equation 5.5) as described from the previous chapters. Moreover, the reversible Randel-Sevcik equation (Equation 5.3) was used to determine the diffusion coefficient (D_e) of GBPE capped Ag-Au-NPs. A value of $7.925 \times 10^{-4} \text{ cm}^2 \cdot \text{s}^{-1}$ was determined for the synthesised GBPE capped Ag-Au-NPs. The obtained D_e was larger compared to the previously reported in literature. Larger values of D_e indicates a faster motion of analyte through the solution whereas small values of D_e indicates slower motion. Okomu and co-workers reported D_e of $1.87 \times 10^{-5} \text{ cm}^2 \text{ s}^{-1}$ using Ag-Pt|GCE which was lower compared to this study [39]. Table 6.5 shows a summary of electrochemical data obtained from this study. As seen from the table Ag-Au-NPs show better electrochemical properties.

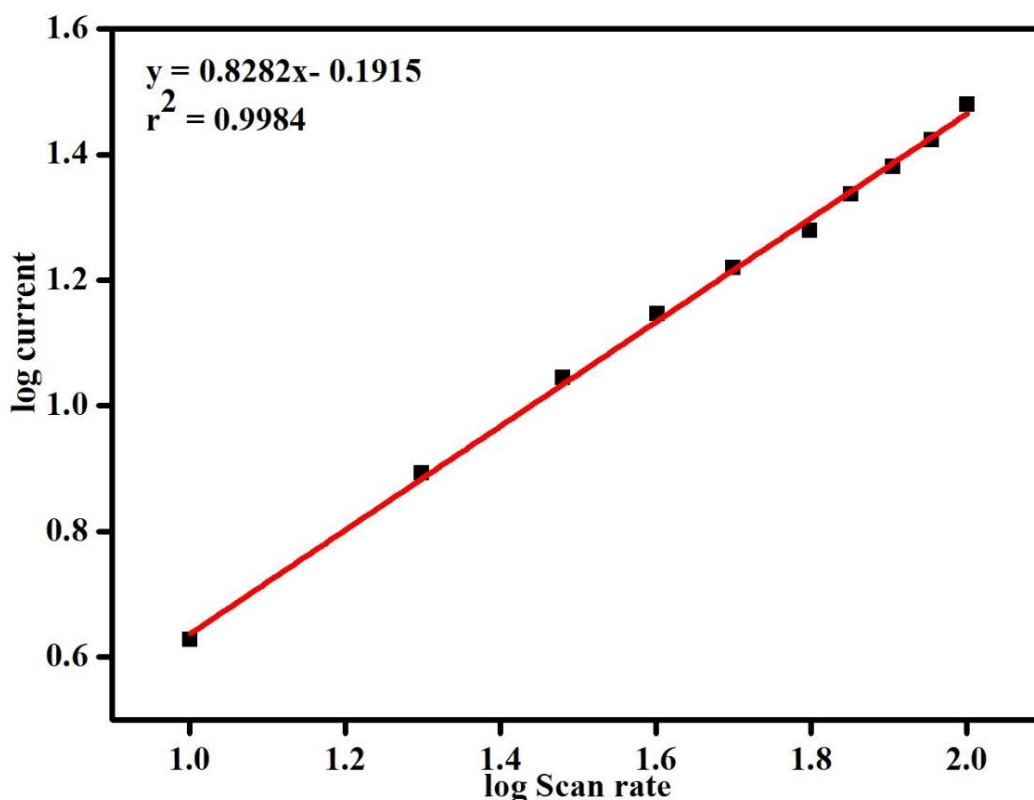


Figure 6.14: Plots of log current versus log scan rate of GBPE capped Ag-Au-NPs.

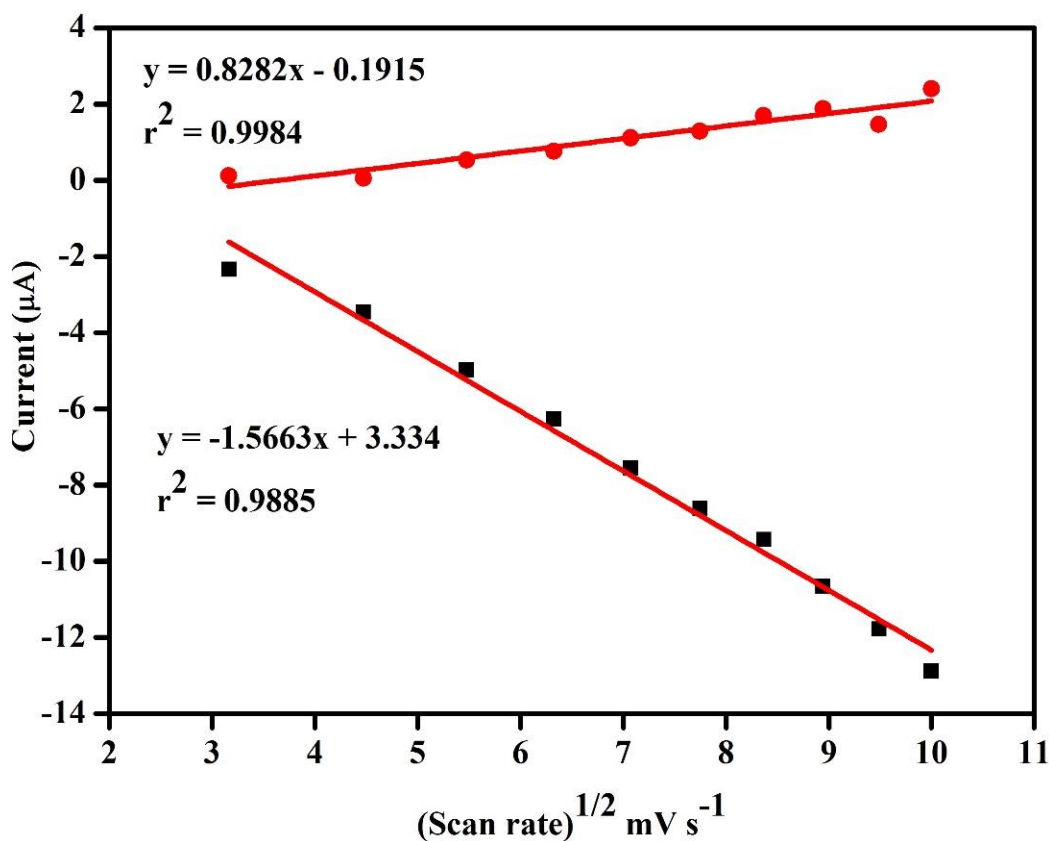


Figure 6.15: Randel-Sevcik plot for GBPE capped Ag-Au-NPs.

Table 6.5: Summary of electrochemical data obtained in this study.

| Electrode | I_{pa} / I_{pc} | Formal Potential | Peak-to-peak separation | Surface concentration (mol. cm ⁻²) | Diffusion Coefficient (cm ² .s ⁻¹) |
|---------------------------|-------------------|------------------|-------------------------|--|---|
| GBPE capped Au-NPs GCE | 0.68 | 0.336 | 0.91 | 2.285×10^{-4} | 5.199×10^{-5} |
| GBPE capped Ag-NPs GCE | 1.5 | 0.28 | 0.055 | 2.413×10^{-4} | 5.22×10^{-5} |
| GBPE capped Ag-Au-NPs GCE | 0.99 | 0.178 | 0.038 | 5.3×10^{-4} | 7.295×10^{-4} |

The electrochemical properties of the synthesised nanoparticles namely GBPE capped Au-NPs, GBPE capped Ag-NPs, GBPE capped Ag-Au-NPs were also investigated. All the cyclic voltammograms of the GBPE capped nanoparticles showed pronounced redox peaks and

more enhancements in the magnitude of the current compared to bare glassy carbon electrode. This can be attributed to the electroactive properties of the nanoparticles, as shown in previous chapters. The results of GBPE capped Ag-Au-NPs shown in **Figure 6.13** suggest that the bimetallic alloy nanoparticles improve the relative electron transfer since it showed enhanced peak current than the monometallic Au-NPs and Ag-NPs which indicated that the modified GBPE capped Ag-Au-NPs electrodes could also be used in the development of electrochemical sensors. Filho and co-workers also observed similar results for Ag-NPs, f-MWCNT and Ag-NPs/f-MWCNT on GCE, where their composite showed enhanced peaks and enhanced electrochemical properties compared to monometallic. The diffusion coefficient of bimetallic GBPE capped Ag-Au-NPs is higher compared to monometallic capped Au-NPs and Ag-NPs, meaning that GBPE capped Ag-Au-NPs allows efficient GBPE transfer of electrons hence it was chosen for the fabrication of the nanosensors of interest in this study [40].

6.7 References:

- [1] P. Velmurugan, K. Anbalagan, M. Manosathyadevan, K.J. Lee, M. Cho, S.M. Lee, J.H. Park, S.G. Oh, K.S. Bang, B.T. Oh, Green synthesis of silver and gold nanoparticles using *Zingiber officinale* root extract and antibacterial activity of silver nanoparticles against food pathogens, *Bioprocess Biosyst. Eng.* 37 (2014) 1935–1943. <https://doi.org/10.1007/s00449-014-1169-6>.
- [2] I. Kumar, M. Mondal, V. Meyappan, N. Sakthivel, Green one-pot synthesis of gold nanoparticles using *Sansevieria roxburghiana* leaf extract for the catalytic degradation of toxic organic pollutants, *Mater. Res. Bull.* 117 (2019) 18–27. <https://doi.org/10.1016/j.materresbull.2019.04.029>.
- [3] S.S. Shankar, A. Rai, A. Ahmad, M. Sastry, Rapid synthesis of Au, Ag, and bimetallic Au core-Ag shell nanoparticles using Neem (*Azadirachta indica*) leaf broth, *J. Colloid Interface Sci.* 275 (2004) 496–502. <https://doi.org/10.1016/j.jcis.2004.03.003>.
- [4] P. Mulvaney, Surface plasmon spectroscopy of nanosized metal particles, *Langmuir.* 12 (1996) 788–800. <https://doi.org/10.1021/la9502711>.
- [5] A. Pal, S. Shah, V. Kulkarni, R.S.R. Murthy, S. Devi, Template free synthesis of silver-gold alloy nanoparticles and cellular uptake of gold nanoparticles in Chinese Hamster Ovary cell, *Mater. Chem. Phys.* 113 (2009) 276–282. <https://doi.org/10.1016/j.matchemphys.2008.07.072>.
- [6] T.Y. Suman, S.R. Radhika Rajasree, A. Kanchana, S.B. Elizabeth, Biosynthesis, characterization and cytotoxic effect of plant mediated silver nanoparticles using *Morinda citrifolia* root extract, *Colloids Surfaces B Biointerfaces.* 106 (2013) 74–78. <https://doi.org/10.1016/j.colsurfb.2013.01.037>.
- [7] S. Ristig, O. Prymak, K. Loza, M. Gocyla, W. Meyer-Zaika, M. Heggen, D. Raabe, M. Epple, Nanostructure of wet-chemically prepared, polymer-stabilized silver-gold nanoalloys (6 nm) over the entire composition range, *J. Mater. Chem. B.* 3 (2015) 4654–4662. <https://doi.org/10.1039/c5tb00644a>.
- [8] S. Link, Z.L. Wang, M.A. El-Sayed, Alloy formation of gold-silver nanoparticles and the dependence of the plasmon absorption on their composition, *J. Phys. Chem. B.* 103 (1999) 3529–3533.
- [9] A.K. Aimukhanov, N.K. Ibrayev, A.A. Ishchenko, A. V. Kulinich, Effect of Silver and Gold Nanoparticles on the Spectral and Luminescent Properties of a Merocyanine Dye, *Theor. Exp. Chem.* 54 (2019) 369–374. <https://doi.org/10.1007/s11237-019-09583-9>.
- [10] B.J. Plowman, B. Sidhureddy, S. V. Sokolov, N.P. Young, A. Chen, R.G. Compton, Electrochemical Behavior of Gold–Silver Alloy Nanoparticles, *ChemElectroChem.* 3 (2016) 1039–1043. <https://doi.org/10.1002/celec.201600212>.
- [11] I.M. El-Sherbiny, E. Salih, F.M. Reicha, Green synthesis of densely dispersed and stable silver nanoparticles using myrrh extract and evaluation of their antibacterial

- activity, *J. Nanostructure Chem.* 3 (2013) 1–7. <https://doi.org/10.1186/2193-8865-3-8>.
- [12] T. Ahmad, M. Irfan, M.A. Bustam, S. Bhattacharjee, Effect of Reaction Time on Green Synthesis of Gold Nanoparticles by Using Aqueous Extract of *Elaise Guineensis* (Oil Palm Leaves), *Procedia Eng.* 148 (2016) 467–472. <https://doi.org/10.1016/j.proeng.2016.06.465>.
- [13] L. Castillo-Henríquez, K. Alfaro-Aguilar, J. Ugalde-álvarez, L. Vega-Fernández, G.M. de Oca-Vásquez, J.R. Vega-Baudrit, Green synthesis of gold and silver nanoparticles from plant extracts and their possible applications as antimicrobial agents in the agricultural area, *Nanomaterials.* 10 (2020) 1–24. <https://doi.org/10.3390/nano10091763>.
- [14] D. Lomelí-marroquín, D.M. Cruz, A. Nieto-argüello, A.V. Crua, J. Chen, A. Torrescastro, T.J. Webster, J.L. Cholula-díaz, Starch-mediated synthesis of mono- and bimetallic silver / gold nanoparticles as antimicrobial and anticancer agents, (2019) 2171–2190.
- [15] M. Ibrahim, M. Alaam, H. El-Haes, A.F. Jalbout, A. De Leon, Analysis of the structure and vibrational spectra of glucose and fructose, *Eclat. Quim.* 31 (2006) 15–21. <https://doi.org/10.1590/S0100-46702006000300002>.
- [16] S. Kamsonlian, S. Suresh, C.B. Majumder, S. Chand, Characterization of Banana and Orange Peels : Biosorption Mechanism, *Int. J. Sci. Technol. Manag.* 2 (2011) 1–7.
- [17] Y.L. Lai, M. Thirumavalavan, J.F. Lee, Effective adsorption of heavy metal ions (Cu^{2+} , Pb^{2+} , Zn^{2+}) from aqueous solution by immobilization of adsorbents on Calcium alginate beads, *Toxicol. Environ. Chem.* 92 (2010) 697–705. <https://doi.org/10.1080/02772240903057382>.
- [18] H. Zheng, L. Wang, Banana Peel Carbon Containing Functional Groups Applied to the Selective Adsorption of Au (III) from Waste Printed Circuit Boards, (2016). <https://doi.org/10.4236/snls.2013.32006>.
- [19] D.K. Ban, S.K. Pratihar, S. Paul, Controlled modification of starch in the synthesis of gold nanoparticles with tunable optical properties and their application in heavy metal sensing, *RSC Adv.* 5 (2015) 81554–81564. <https://doi.org/10.1039/c5ra16473g>.
- [20] B. Bonigala, B. Kasukurthi, V.V. Konduri, U.K. Mangamuri, R. Gorrepati, S. Poda, Green synthesis of silver and gold nanoparticles using *Stemona tuberosa* Lour and screening for their catalytic activity in the degradation of toxic chemicals, *Environ. Sci. Pollut. Res.* 25 (2018) 32540–32548. <https://doi.org/10.1007/s11356-018-3105-9>.
- [21] Y. Shin, I.T. Bae, B.W. Arey, G.J. Exarhos, Facile stabilization of gold-silver alloy nanoparticles on cellulose nanocrystal, *J. Phys. Chem. C.* 112 (2008) 4844–4848. <https://doi.org/10.1021/jp710767w>.
- [22] C.R. Hubbard, A.D. Mighell, JCPDS-ICDD Research Associateship (Cooperative Program with NBS/NIST), 106 (2001) 1013–1028.

- [23] Y. Liu, X. Liu, X. Wang, Biomimetic synthesis of gelatin polypeptide-assisted noble-metal nanoparticles and their interaction study, *Nanoscale Res. Lett.* 7 (2012) 1–11. <https://doi.org/10.1186/1556-276X-7-22>.
- [24] N.A. Alarfaj, M.F. El-Tohamy, Eco-friendly synthesis of gelatin-capped bimetallic Au-Ag nanoparticles for chemiluminescence detection of anticancer raloxifene hydrochloride, *Luminescence*. 31 (2016) 1194–1200. <https://doi.org/10.1002/bio.3089>.
- [25] R. Seifipour, M. Nozari, L. Pishkar, Green Synthesis of Silver Nanoparticles using *Tragopogon Collinus* Leaf Extract and Study of Their Antibacterial Effects, *J. Inorg. Organomet. Polym. Mater.* 30 (2020) 2926–2936. <https://doi.org/10.1007/s10904-020-01441-9>.
- [26] X. Ding, H. Xu, Functionalized Gold and Silver Bimetallic Nanoparticles Using *Deinococcus radiodurans* Protein Extract Mediate Degradation of Toxic Dye Malachite, (2020).
- [27] R. Thapa, C. Bhagat, P. Shrestha, S. Awal, P. Dudhagara, Enzyme - mediated formulation of stable elliptical silver nanoparticles tested against clinical pathogens and MDR bacteria and development of antimicrobial surgical thread, *Ann. Clin. Microbiol. Antimicrob.* (2017) 1–10. <https://doi.org/10.1186/s12941-017-0216-y>.
- [28] H. Han, The effect of nanoparticle size on in vivo pharmacokinetics and cellular interaction, 11 (2016) 673–692.
- [29] A.E. Adebayo, A.M. Oke, A. Lateef, A.A. Oyatokun, O.D. Abisoye, I.P. Adiji, D.O. Fagbenro, T. V Amusan, J.A. Badmus, T.B. Asafa, L.S. Beukes, S.H. Abbas, Biosynthesis of silver , gold and silver – gold alloy nanoparticles using *Persea americana* fruit peel aqueous extract for their biomedical properties, *Nanotechnol. Environ. Eng.* (2019). <https://doi.org/10.1007/s41204-019-0060-8>.
- [30] K. Gopinath, S. Kumaraguru, K. Bhakayaraj, S. Mohan, K.S. Venkatesh, M. Esakkirajan, P.R. Kaleeswaran, S.A. Naiyf, S. Kadaikunnan, M. Govindarajan, G. Benelli, A. Arumugam, Graphical abstract SC, *Microb. Pathog.* (2016). <https://doi.org/10.1016/j.micpath.2016.10.011>.
- [31] K.S. Shin, J.H. Kim, I.H. Kim, K. Kim, Poly(ethylenimine)-stabilized hollow gold-silver bimetallic nanoparticles: Fabrication and catalytic application, *Bull. Korean Chem. Soc.* 33 (2012) 906–910. <https://doi.org/10.5012/bkcs.2012.33.3.906>.
- [32] C. Van der Horst, B. Silwana, E. Iwuoha, V. Somerset, Synthesis and Characterization of Bismuth-Silver Nanoparticles for Electrochemical Sensor Applications, *Anal. Lett.* 48 (2015) 1311–1332. <https://doi.org/10.1080/00032719.2014.979357>.
- [33] S.U. Ganaie, T. Abbasi, S.A. Abbasi, Rapid and green synthesis of bimetallic Au – Ag nanoparticles using an otherwise worthless weed *Antigonon leptopus*, 8080 (2016). <https://doi.org/10.1080/17458080.2015.1070311>.

- [34] L. Sun, Y. Yin, P. Lv, W. Su, L. Zhang, Green controllable synthesis of Au – Ag alloy nanoparticles using Chinese wolfberry fruit extract and their tunable photocatalytic activity †, *RSC Adv.* 8 (2018) 3964–3973. <https://doi.org/10.1039/C7RA13650A>.
- [35] M. Liang, G. Zhang, Y. He, P. Hou, M. Li, B. Lv, *Lysimachia christinae* polysaccharide mediated facile synthesis of gold- silver alloy nanoparticles for catalytic reduction of 4-nitrophenol *Lysimachia christinae* polysaccharide mediated facile synthesis of gold-silver alloy nanoparticles for catalytic red, (2019). <https://doi.org/10.1088/1755-1315/330/4/042053>.
- [36] M. Tominaga, T. Shimazoe, M. Nagashima, I. Taniguchi, Composition – activity relationships of carbon electrode-supported bimetallic gold – silver nanoparticles in electrocatalytic oxidation of glucose, 615 (2008) 51–61. <https://doi.org/10.1016/j.jelechem.2007.11.030>.
- [37] M. Tominaga, A.T. Shimazoe, M. Nagashima, I.T. A, Electrochemical Oxidation of Glucose at Carbon Electrodes Modified with Gold and Gold – Platinum Alloy Nanoparticles in an Alkaline Solution, 34 (2005) 202–203. <https://doi.org/10.1246/cl.2005.202>.
- [38] T.L. Le, Q.K. Dinh, T.H. Tran, H.P. Nguyen, T. Le, H. Hoang, Q.H. Nguyen, Synthesis of water soluble chitosan stabilized gold nanoparticles and determination of uric acid, (2014). <https://doi.org/10.1088/2043-6262/5/2/025014>.
- [39] F. Okumu, M. Matoetoe, Electrochemical characterization of silver-platinum various ratio bimetallic nanoparticles modified electrodes, *J. Nano Res.* 44 (2016) 114–125. <https://doi.org/10.4028/www.scientific.net/JNanoR.44.114>.
- [40] M.M.S. Lima Filho, A.A. Correa, F.D.C. Silva, F.A.O. Carvalho, L.H. Mascaro, T.M.B.F. Oliveira, A glassy carbon electrode modified with silver nanoparticles and functionalized multi-walled carbon nanotubes for voltammetric determination of the illicit growth promoter dienestrol in animal urine, *Microchim. Acta.* 186 (2019) 1–10. <https://doi.org/10.1007/s00604-019-3645-9>.

CHAPTER SEVEN

Detection and Discussion: Part 1

This chapter presents data about the development of a sensitive and straightforward strategy for detection of E.coli 0157:H7 in real water samples using GBPE functionalised Au-NPs, Ag-NPs, and Ag-Au-NPs. UV-Vis Spectrophotometer was used to record all the data with regards to the detection of E.coli 0157:H7.

7 Detection of Escherichia coli 0157:H7:

7.1 Culture preparation and media plating methods:

For the preparation of the test culture, 5 grams of Luria Broth (LB) powder was transferred into 200 mL distilled water and dissolved to make the media. The media was then autoclaved at 121°C for 25 min and allowed to cool at room temperature.

7.2 Bacterial preparation:

E.coli 0157:H7 was taken as the target organism. The Bacterial strains of *E.coli* 0157:H7 were prepared at the University of the Western Cape's Biotechnology Department. Suspensions were prepared by transferring 20 mL LB in a tube and a single colony of glycerol stock *E.coli* 0157:H7 strain. This was then placed in the shaking oven at 37 °C to grow bacteria for 24 hours

After that, the bacteria were serially diluted between 10^{-1} – 10^{-6} CFU/mL with LB media in test tubes. From each diluent 100 mL was poured on different agar plates, and the plates were incubated at 37 °C overnight, and after 24 hours microbial clouds of growths were observed. The number of colonies was counted on plates to determine the colony-forming units per millilitre (**equation 7.1**) [1,2]. **Figure 7.1** shows a schematic flow diagram of the sample preparation steps.

$$E.coli / 100 \text{ mL} = \frac{\text{Number of E.coli colonies}}{\text{Volume of sample (mL)}} \times 100 \quad (7.1)$$

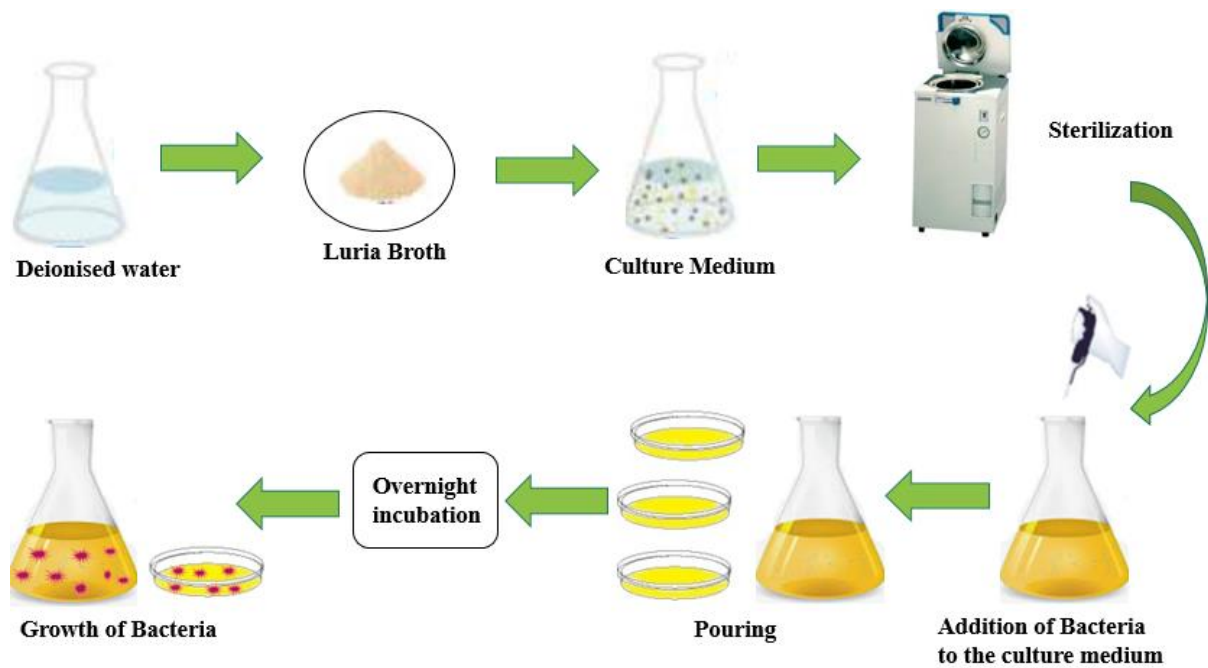


Figure 7.1: Schematic diagram of preparing *E. coli* 0157:H7.

7.3 UV-Vis detection of *E. coli* 0157:H7:

To confirm the effect of the nanoparticles, a comparative study of the GBPE capped Au-NPs, Ag-NPs, and Ag-Au-NPs before and after the interaction with *E. coli* 0157:H7 was performed

using UV-vis spectrophotometer. **Figure 7.2** shows the UV-Vis spectra of gold nanoparticles before and after their interaction with *E.coli* 0157:H7 at different concentrations. As seen from **Figure 7.2**, gold nanoparticles in the absence of *E.coli* 0157:H7 show an SPR band at 535 nm in water (black spectrum). In the presence of *E.coli* 0157:H7 in water, we observed a reduction in the peak intensity with a redshift taking place at the same time. The decrease in peak intensity is the evidence of the interaction between Au-NPs and bacteria. The redshift was observed by the change in SPR to more extended wavelength regions from 535 nm to 541 nm [3] which is due to many factors such as capping agent replacement, surface plasmon coupling or aggregation or agglomeration between closely spaced nanoparticles [4]. These results were similar to the work reported by Pang and co-workers who detected *E.coli* in seawater using Au-NPs and phage M13 as a binder to nanoparticles [5].

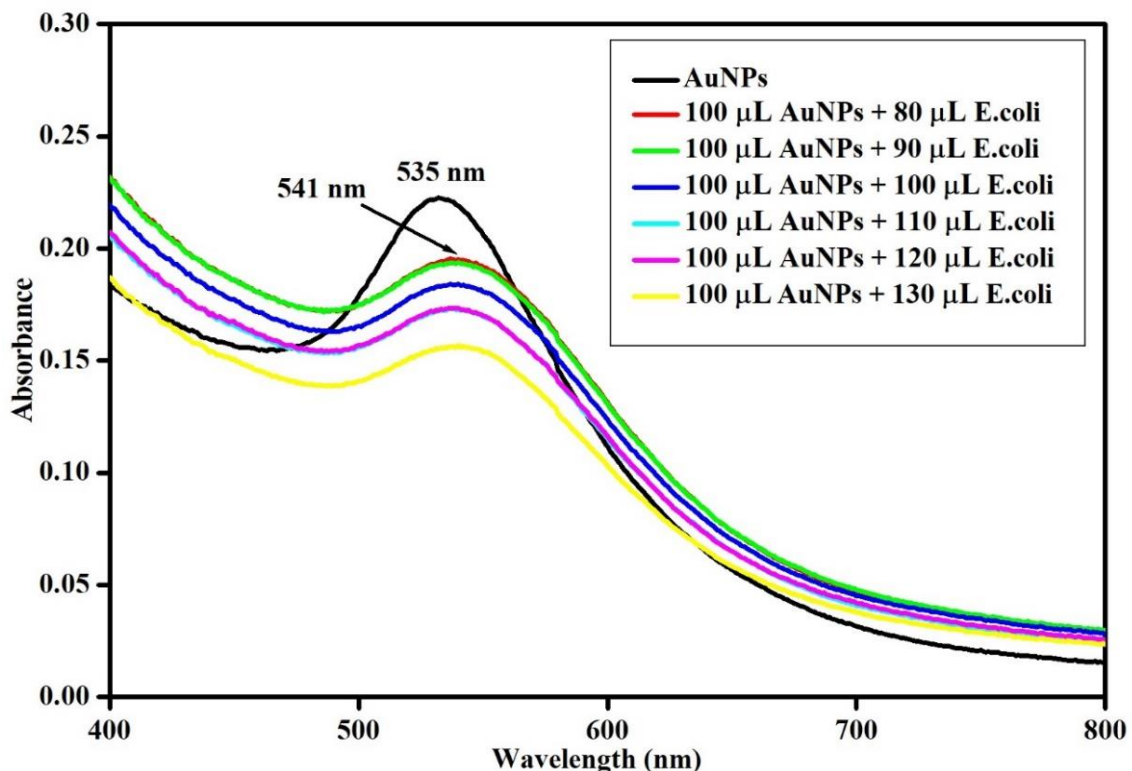


Figure 7.2: Detection of *E.coli* 0157:H7 in water, Au-NPs before the interaction (Black line) with the interaction of *E.coli* at different concentration $10^1 - 10^6$ (red, green, navy, blue, purple, yellow).

In the case of GBPE capped Ag-NPs and Au-NPs, similar results were observed. The SPR band changed from 440 nm to 450 nm for the GBPE capped AgNPs, as seen in **Figure 7.3**. Similar results were reported by Boken and co-workers who also observed changes in SPR bands from 395 nm before the interaction to 408 nm after the interaction with *E.coli* O157:H7 when using robust silver nanoparticle [6]. For both the synthesised Au-NPs and Ag-NPs it was found that as the concentration of the *E.coli* O157:H7 increased, the SPR intensity decreased, this is caused by nanoparticle destabilisation which is the depletion of stable nanoparticles [7]. In this research study, the limit of detection was determined using **(equation 7.2)**. The limit of detection (LOD) is the lowest concentration that can be measured or detected, and it was found to be 10^2 CFU/mL for both Au-NPs and Ag-NPs [8,9]. A study by Yaghubi and co-workers reported similar results using Au-NPs conjugated with antibodies [10]. Our results were much lower or better compared to the reported literature, for example, Haicao and co-workers reported LOD of 2×10^8 CFU/mL using mercaptoethylamine modified Au-NPs for *E.coli* O157:H7 [11]. Bhat and co-workers also observed that silver nanoparticles alone could enhance antibacterial activity [12].

$$\text{LOD} = 3.3 \frac{S}{M} \quad (7.2)$$

From the equation, 3.3 is the coefficient, S represents the value of the standard deviation of the blank samples, and M is the slope of the standard curve within the concentration range.

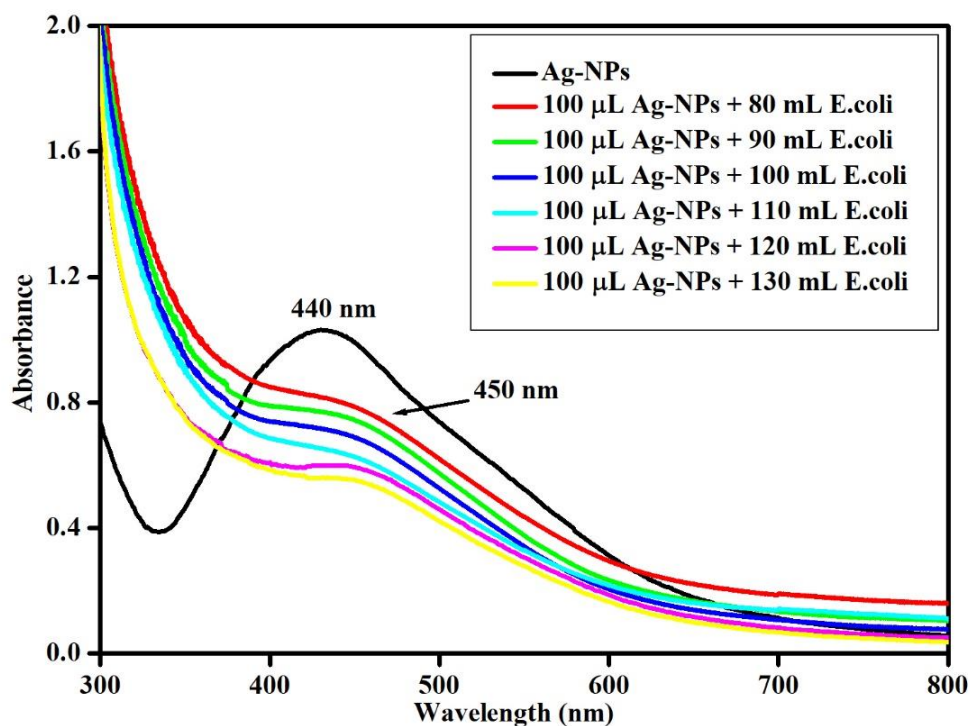


Figure 7.3: Detection of *E.coli* 0157:H7 in seawater, Ag-NPs before the interaction (Black line) with the interaction of *E.coli* at different concentration (other).

Researchers have reported the use of aptamers or antibodies for targeting *E.coli* 0157:H7. Our main aim was to create a sensor without using aptamers or antibody to decorate nanoparticles for bacterial targeting because these strategies are based on charge interactions and are easily interfered by surroundings such as metal ions, pH values, or proteins [7]. **Figure 7.4** shows a schematic flow of the detection process. This study proposed a new method involving the use of UV-Vis as a source of response when GBPE capped Ag-Au-NPs were subjected to the presence of *E.coli* 0157:H7 in water. As seen, the proposed sensor was able to detect *E.coli* 0157:H7 bacteria in water using Ag-Au-NPs without the antibody.

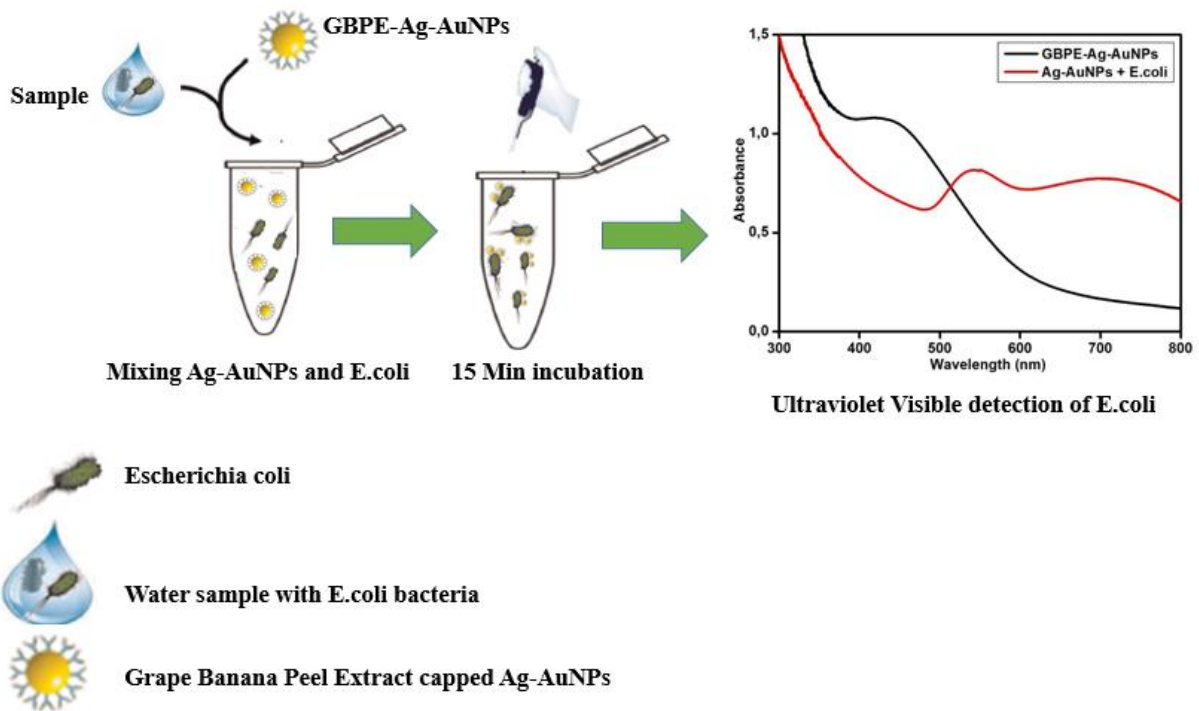


Figure 7.4: Schematic procedure for attaching GBPE Ag-Au-NPs to *E.coli* 0157:H7 and its assay detection concept.

Figure 7.5 shows the detection of *E.coli* 0157:H7 in water using GBPE capped Ag-Au-NPs bimetallic nanoparticles. The SPR band shifted from 457 nm to 527 nm, indicating a redshift. The absorption spectra of GBPE capped Ag-Au-NPs show a redshift after the addition of bacteria an indication that the nanoparticles aggregate when they bind to *E.coli* 0157:H7. When the GBPE capped Ag-Au-NPs interacted with *E.coli* 0157:H7 the antioxidants, flavonoids, polyphenols and amines that surrounds the nanoparticles and bind to the cell wall of the bacteria through amine, sulfhydryl (-SH) and thiol groups [13–15] which are part of peptidoglycan which is the main component of the bacterial cell wall that surrounds bacteria [16]. However, literature reports amino acids as a major source of binding or crosslinker in the peptidoglycan since both the nanoparticles and the microorganism have it [17]. After binding the bacteria consumes the GBPE capped Ag-Au-NPs then the capping molecules unbinds from the surface of silver-gold nanoparticles, and the silver-gold nanoparticles

become unstable and aggregates because the surface is no longer coated. The nanoparticles release the Ag^+ and Au^+ ions inside the bacteria, and they damage the microorganism DNA and cause oxidative stress which leads to cell death [18]. Similar results were reported by other researchers such as Yang and co-workers using Au-NPs modified with D-alanyl-D-alanine for Bacterial detection [19] while Din reported similar binding process between copper nanoparticles and gram-negative bacteria's [20]. The test was conducted using concentrations of 1×10^1 CFU/mL to 1×10^7 CFU/mL of *E.coli* 0157:H7 while the volume of the Ag-Au-NPs was kept constant at 100 μL and the time taken for each detection was 1 min 45 seconds. The detection limit was determined to be 1×10^1 CFU/mL for Ag-Au-NPs, which was better than the detection of the mono-metallic nanoparticles capped using GBPE. Song and co-worker reported a detection limit of 1×10 CFU/ mL using AuNRs-SiO₂ for the detection of *E.coli* 0157:H7 [21]. This data showed that our approach is appropriate in detecting *E.coli* 0157:H7 in real water samples.

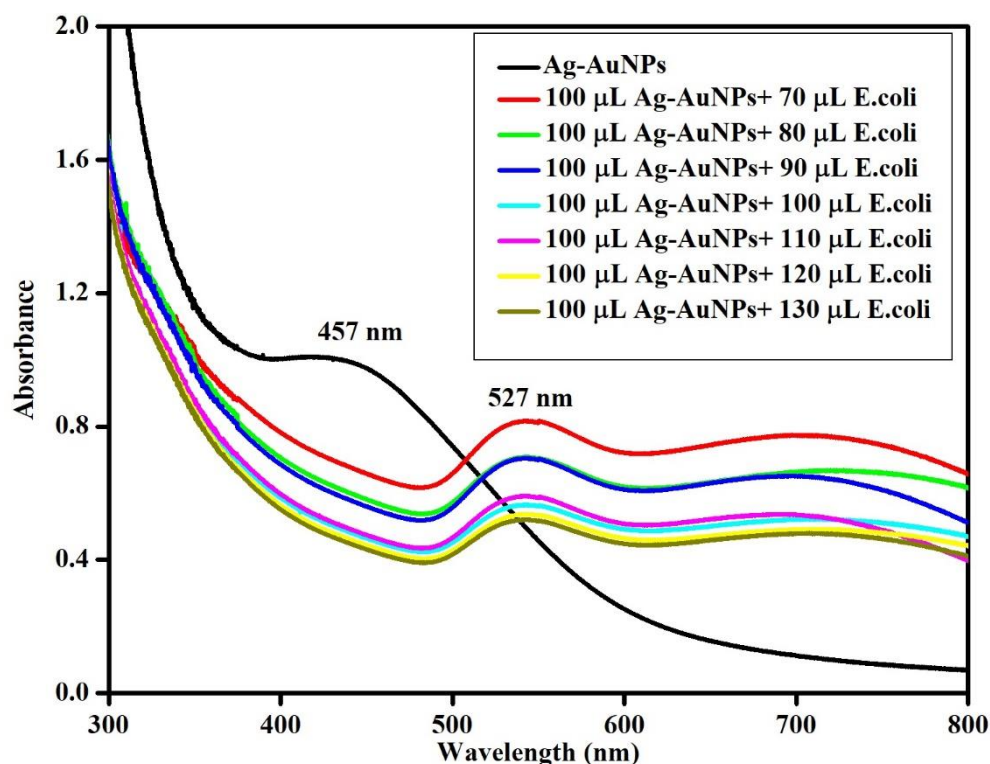


Figure 7.5: Detection of *E.coli* 0157:H7 in water, Au-NPs before the interaction (Black line) with the interaction of *E.coli* (other) at different concentration.

From **Figure 7.5**, the absorbance at 457 nm decreased, and the absorbance at 527 nm increased. The observed trend was caused by aggregation, the rate or the degree of aggregation was calculated using the absorbance ratio (A_{527} / A_{457}) as shown in **Figure 7.6**, in which the A_{527} and A_{457} represent the relative quantity of aggregated and dispersed Ag-Au-NPs, respectively. Literature reports that a high ratio shows the aggregation of Ag-Au-NPs while a low ratio shows that the Ag-Au-NPs disperse well. Data presented in **Figure 7.6** shows a high value of the ratio ($A_{527} \text{ nm} / A_{457} \text{ nm}$) when the concentration of *E.coli* 0157:H7 is high, showing that the Ag-Au-NPs become more sensitive with the increase of bacteria's concentration. Therefore the results confirm that Ag-Au-NPs indeed can detect *E.coli* 0157:H7 in water.

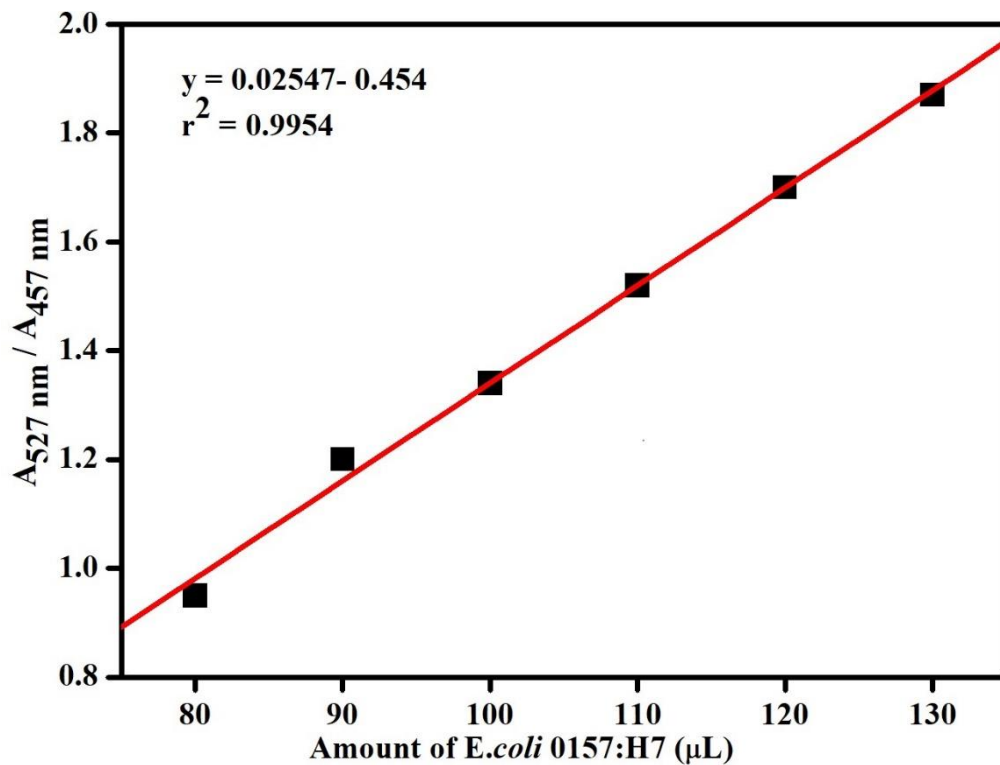


Figure 7.6: The linear relationship between the $A_{527\text{ nm}} / A_{457\text{ nm}}$ values and the volume of *E.coli* 0157:H7.

In conclusion, we report an adaptable and stable platform based on GBPE capped Ag-Au-NPs and its use towards the UV-Vis detection of *E.coli* 0157:H7 in water samples. This is the first study that combines grapes and banana peels and nanoparticles to detect bacteria using UV-vis. The sensing potential of both GBPE-Au-NPs and GBPE-Ag-NPs showed similar LOD which was 1×10^2 CFU/mL for both, and this might be because Au and Ag have very similar lattice constants and similar interparticle plasmon coupling [22]. The results were better when using GBPE Ag-Au-NPs bimetallic nanoparticles, where a LOD value of 1×10^1 CFU/mL for GBPE Ag-Au-NPs was determined. The determined value was found to be similar to the previously reported study by Wang and co-workers using gold nanoparticles labelled with an antibody for the detection of *E.coli* 0157:H7; however, their detection time was 45 min which was longer compared to this study [23]. Bouguelia and co-workers

obtained LOD of 10^6 CFU/mL when detecting *E.coli* 0157:H7 in mineral water using surface plasmon resonance technique [24]. **Table 7.1** show detection limits obtained in studies where *E.coli* 0157:H7 bacteria were detected using Surface Plasmon Resonance (SPR) sensors. From the table, it is evident that this study illustrated data far better in comparison to the previously reported studies from the literature. Therefore, the developed sensor can detect *E.coli* 0157:H7 in water using green synthesised nanoparticles without the support of antibodies. The developed sensors can achieve detection within 3 min, during which the bacterium has sufficient time to bind and for analysis to be achieved. The obtained detection limit in this study falls within the range 1×10^{-3} to 1×10^7 CFU/ mL of the currently accepted methods reported in the literature [25,26].

Table 7.1: Comparison of SPR sensor for detection *E.coli* 0157:H7 using different material.

| Material Used | Technique Used | LOD | Reference |
|---------------------------|-----------------------|--------------------------|------------------|
| Au-NPs modified with 3MPA | SPR | 1.8×10^3 CFU/mL | [27] |
| AuNR nanoprobos | SPR | 1×10^2 CFU/mL | [28] |
| Magnetic NPs | SPR | 1×10^5 CFU/mL | [29] |
| AgNPs-rGO bimetallic | SPR | 5×10^2 CFU/mL | [30] |
| GBPE Au-NPs | SPR | 1×10^2 CFU/ mL | This Work |
| GBPE Ag-NPs | SPR | 1×10^2 CFU/ mL | This Work |
| GBPE Ag-Au-NPs | SPR | 1×10^1 CFU / mL | This Work |

References:

- [1] USEPA, in *Water by Membrane Filtration Using membrane-Thermotolerant Escherichia coli Agar (mTEC)*, Stand. Methods. (2006).
- [2] U. Dharmasiri, M.A. Witek, A.A. Adams, J.K. Osiri, M.L. Hupert, T.S. Bianchi, D.L. Roelke, S.A. Soper, Enrichment and detection of escherichia coli O157:H7 from water samples using an antibody modified microfluidic chip, *Anal. Chem.* 82 (2010) 2844–2849. <https://doi.org/10.1021/ac100323k>.
- [3] V. Raj, A.N. Vijayan, K. Joseph, Cysteine capped gold nanoparticles for naked eye detection of E. coli bacteria in UTI patients, *Sens. Bio-Sensing Res.* 5 (2015) 33–36. <https://doi.org/10.1016/j.sbsr.2015.05.004>.
- [4] L. Sepunaru, K. Tschulik, C. Batchelor-McAuley, R. Gavish, R.G. Compton, Electrochemical detection of single E. coli bacteria labeled with silver nanoparticles, *Biomater. Sci.* 3 (2015) 816–820. <https://doi.org/10.1039/c5bm00114e>.
- [5] H. Peng, I.A. Chen, Rapid Colorimetric Detection of Bacterial Species through the Capture of Gold Nanoparticles by Chimeric Phages, *ACS Nano.* 13 (2019) 1244–1252. <https://doi.org/10.1021/acsnano.8b06395>.
- [6] B. J, Detection of Pathogenic Escherichia coli (E. coli) Using Robust Silver and Gold Nanoparticles, *J. Chem. Eng. Process Technol.* 04 (2013) 4–9. <https://doi.org/10.4172/2157-7048.1000175>.
- [7] X. Xu, Y. Yuan, G. Hu, X. Wang, P. Qi, Z. Wang, Q. Wang, X. Wang, Y. Fu, Y. Li, H. Yang, Exploiting pH-Regulated Dimer-Tetramer Transformation of Concanavalin A to Develop Colorimetric Biosensing of Bacteria, *Sci. Rep.* 7 (2017) 1–8. <https://doi.org/10.1038/s41598-017-01371-6>.
- [8] R. Article, Methods for the determination of limit of detection and limit of quantitation of the analytical methods, 2 (2011) 21–25. <https://doi.org/10.4103/2229-5186.79345>.
- [9] D.A. Armbruster, M.D. Tillman, L.M. Hubbs, Limit of detection (LOD)/limit of quantitation (LOQ): Comparison of the empirical and the statistical methods exemplified with GC-MS assays of abused drugs, *Clin. Chem.* 40 (1994) 1233–1238. <https://doi.org/10.1093/clinchem/40.7.1233>.
- [10] F. Yaghubi, M. Zeinoddini, Design of Localized Surface Plasmon Resonance (LSPR) Biosensor for Immunodiagnostic of E . coli O157 : H7 Using Gold Nanoparticles Conjugated to the Chicken Antibody, (2020).
- [11] H. Su, Q. Ma, K. Shang, T. Liu, H. Yin, S. Ai, Gold nanoparticles as colorimetric sensor: A case study on E. coli O157:H7 as a model for Gram-negative bacteria, *Sensors Actuators, B Chem.* 161 (2012) 298–303. <https://doi.org/10.1016/j.snb.2011.10.035>.
- [12] M.A. Bhat, B.K. Nayak, A. Nanda, Evaluation of Bactericidal Activity of Biologically Synthesised Silver Nanoparticles from *Candida albicans* in Combination with

- Ciprofloxacin, *Mater. Today Proc.* 2 (2015) 4395–4401.
<https://doi.org/10.1016/j.matpr.2015.10.036>.
- [13] R. Das, S. Gang, S.S. Nath, R. Bhattacharjee, Linoleic acid capped copper nanoparticles for antibacterial activity, *J. Bionanoscience*. 4 (2010) 82–86.
<https://doi.org/10.1166/jbns.2010.1035>.
- [14] J.H. Kim, H. Cho, S.E. Ryu, M.U. Choi, Effects of metal ions on the activity of protein tyrosine phosphatase VHR: Highly potent and reversible oxidative inactivation by Cu²⁺ ion, *Arch. Biochem. Biophys.* 382 (2000) 72–80.
<https://doi.org/10.1006/abbi.2000.1996>.
- [15] F. Fatima, S.R. Verma, N. Pathak, P. Bajpai, Extracellular mycosynthesis of silver nanoparticles and their microbicidal activity, *J. Glob. Antimicrob. Resist.* 7 (2016) 88–92. <https://doi.org/10.1016/j.jgar.2016.07.013>.
- [16] A. Typas, M. Banzhaf, C.A. Gross, W. Vollmer, From the regulation of peptidoglycan synthesis to bacterial growth and morphology, *Nat. Rev. Microbiol.* 10 (2012) 123–136. <https://doi.org/10.1038/nrmicro2677>.
- [17] G.W. Liechti, E. Kuru, E. Hall, A. Kalinda, Y. V. Brun, M. Vannieuwenhze, A.T. Maurelli, A new metabolic cell-wall labelling method reveals peptidoglycan in *Chlamydia trachomatis*, *Nature*. 506 (2014) 507–510.
<https://doi.org/10.1038/nature12892>.
- [18] B. Reidy, A. Haase, A. Luch, K.A. Dawson, I. Lynch, Mechanisms of silver nanoparticle release, transformation and toxicity: A critical review of current knowledge and recommendations for future studies and applications, *Materials (Basel)*. 6 (2013) 2295–2350. <https://doi.org/10.3390/ma6062295>.
- [19] X. Yang, Y. Dang, J. Lou, H. Shao, X. Jiang, D-alanyl-D-alanine-modified gold nanoparticles form a broad-spectrum sensor for bacteria, *Theranostics*. 8 (2018) 1449–1457. <https://doi.org/10.7150/thno.22540>.
- [20] M.I. Din, F. Arshad, Z. Hussain, M. Mukhtar, Green Adeptness in the Synthesis and Stabilization of Copper Nanoparticles: Catalytic, Antibacterial, Cytotoxicity, and Antioxidant Activities, *Nanoscale Res. Lett.* 12 (2017).
<https://doi.org/10.1186/s11671-017-2399-8>.
- [21] L. Song, L. Zhang, Y. Huang, L. Chen, G. Zhang, Z. Shen, J. Zhang, Z. Xiao, T. Chen, Amplifying the signal of localized surface plasmon resonance sensing for the sensitive detection of *Escherichia*, *Sci. Rep.* 7 (2017) 1–8. <https://doi.org/10.1038/s41598-017-03495-1>.
- [22] S. Link, Z.L. Wang, Alloy Formation of Gold - Silver Nanoparticles and the Dependence of the Plasmon Absorption on Their Composition, (1999) 3529–3533.
<https://doi.org/10.1021/jp990387w>.
- [23] Y. Wang, E.C. Alcocilja, Gold nanoparticle-labeled biosensor for rapid and sensitive

- detection of bacterial pathogens, *J. Biol. Eng.* (2015) 1–7.
<https://doi.org/10.1186/s13036-015-0014-z>.
- [24] V.A. Online, S. Bouguelia, Y. Roupioz, S. Slimani, L. Mondani, G. Casabona, C. Durmort, T. Vernet, R. Calemczuk, T. Livache, Lab on a Chip very low levels of bacteria 3, (2013). <https://doi.org/10.1039/c3lc50473e>.
- [25] C.A. Meeusen, B. Engineer, E. Science, B. Vista, E.C. Alocilja, E. Lansing, W. Osburn, E. Lansing, Detection of, 0300 (2001) 1–12.
- [26] J.L. Elkind, D.I. Stimpson, A.A. Strong, D.U. Bartholomew, J.L. Melendez, Integrated analytical sensors : the use of the TISPR-1 as a biosensor, 54 (1999) 182–190.
- [27] S. Wang, J. Xie, M. Jiang, K. Chang, R. Chen, L. Ma, J. Zhu, Q. Guo, H. Sun, J. Hu, The Development of a Portable SPR Bioanalyzer for Sensitive Detection of Escherichia coli O157 : H7, (2016) 1–9. <https://doi.org/10.3390/s16111856>.
- [28] Gold Nanorod Probes for the Detection of Multiple Pathogens**, (2008) 2204–2208. <https://doi.org/10.1002/sml.200800309>.
- [29] M. Cui, H. Chang, Y. Zhong, M. Wang, T. Wu, X. Hu, Z.J. Xu, C. Xu, Detection of Bacteria in Water with β -Galactosidase-Coated Magnetic Nanoparticles, (2018). <https://doi.org/10.1177/2472630318773407>.
- [30] C. Zhou, H. Zou, M. Li, C. Sun, D. Ren, Y. Li, Biosensors and Bioelectronics Fiber optic surface plasmon resonance sensor for detection of E . coli O157 : H7 based on antimicrobial peptides and AgNPs-rGO, *Biosens. Bioelectron.* 117 (2018) 347–353. <https://doi.org/10.1016/j.bios.2018.06.005>.

CHAPTER EIGHT

Detection and Discussion: Part 2

*This chapter presents data about the development of a sensitive and straightforward strategy for detection of *E.coli* 0157:H7 in real water samples using GBPE functionalised Au-NPs, Ag-NPs, and Ag-Au-NPs. Cyclic Voltammogram was used to record all the data with regards to the detection of *E.coli* 0157:H7.*

8. Detection of Escherichia coli 0157:H7:

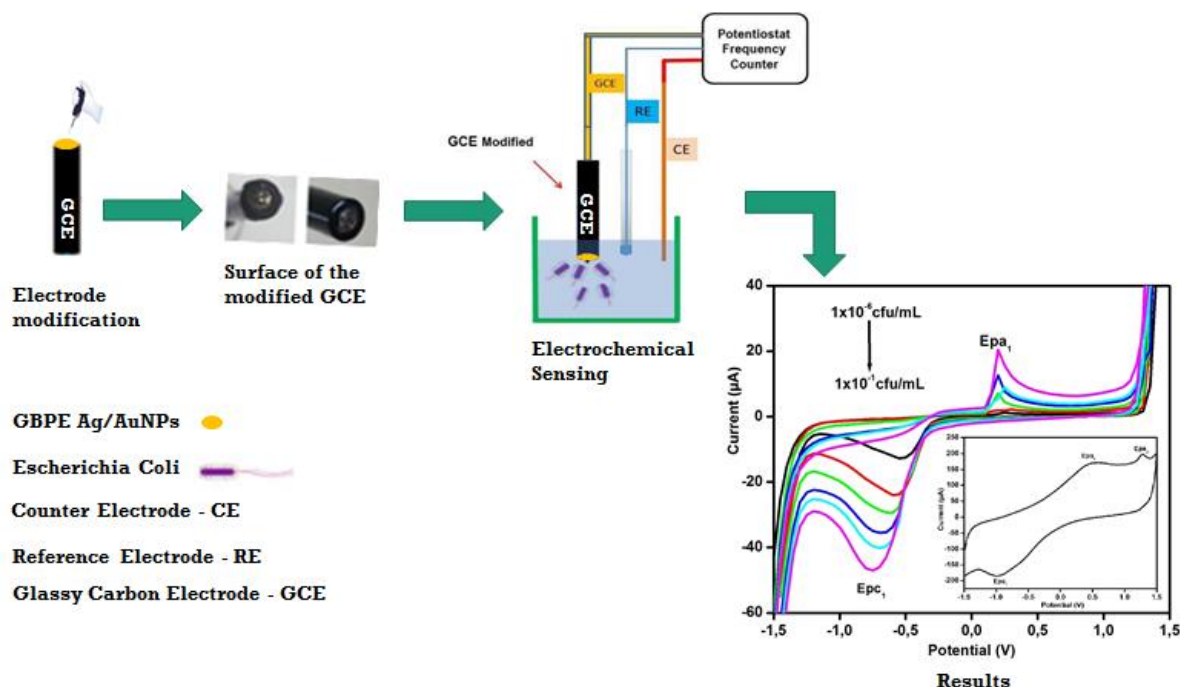


Figure 7.7: Schematic procedure for detection *E.coli* 0157:H7 using GBPE Ag-Au-NPs|GCE to *E.coli* 0157:H7.

8.1 Cyclic Voltammetric detection of *E.coli* 0157:H7:

An electrochemical sensor for Escherichia coli 0157:H7 was developed, as shown in **Figure 8.1**. In this study, six different *E.coli* concentrations from 1×10^1 to 1×10^6 CFU/mL were prepared through serial dilution method as described in the previous chapter. The electrochemical detection of *E.coli* was performed immediately after 24hr incubation period. The electrochemically active GBPE capped Au-NPs, Ag-NPs, Ag-Au-NPs were electrodeposited on GCE. The choice of this electrode was made due to the cost-effective nature of the electrode as well as its reliable and stable properties. Panhwar and co-workers studied three different electrodes namely (glassy carbon electrode, platinum electrode and screen-printed electrode) for the detection of *E.coli*, and they reported GCE as the better electrode for the detection of *E.coli* [1]. All the experiments were performed at optimum conditions at the potential window of -1.5 to 1.5 V, using a scan rate of 50 mV/s under continuous magnetic stirring as, and a sample of 100 uL was analysed from each bacterial concentration. The green synthesised nanoparticles analyses were used to detect targeted bacteria by measuring the electrochemical response of the nanoparticles before and after their interaction with the bacteria.

Figure 8.2 to 8.3 shows the current response of the developed electrochemical sensor towards different concentrations of *E.coli* 0157:H7 bacteria. **Figure 8.2** shows GBPE capped Ag-NPs|GCE with different concentrations of *E.coli* 0157:H7 in PBS solution (0.2M pH 7.4). The change in current response or electrochemical signal, anodic (I_{pa}) and cathodic (I_{pc}) peak current response before the interaction of Au-NPs|GCE with *E.coli* is compared with the current response after the interaction with *E.coli* 0157:H7. The change in the current response for the anodic peak (I_{pa1}) = 18.777 μ A and cathodic peak currents (I_{pc1}) = 0.738 μ A peaks before the interaction of Ag-NPs|GCE with *E.coli* 0157:H7 compared with the current

response after the interaction with anodic (I_{pa1}) = 6.851 μ A and cathodic (I_{pc1}) = -8.235 μ A indicate the presence of *E.coli*. Similar results were reported by Klabunde and co-workers when using highly reactive metal oxide nanoparticles to treat *E.coli* [2]. **Figure 8.3** shows GBPE Ag-Au-NPs|GCE detecting different concentrations of *E.coli* 0157:H7 in PBS solution (0.2M pH 7.4) and the insert represents GBPE capped Ag-Au-NPs before interaction with *E.coli* 0157:H7. The change in the anodic peak currents (I_{pa1}) = 170.68 μ A, (I_{pa2}) = 196.46 μ A and cathodic peak currents (I_{pc1}) = -184.34 μ A before the interaction of Ag-Au-NPs|GCE with *E.coli* compared to the change in current response with anodic (I_{pa1}) = 18.02 μ A and cathodic (I_{pc1}) = -48.26 μ A indicate the presence of *E.coli* 0157:H7. Similar results were obtained by Kaur and co-workers using boron carbon nanorods coated with nickel nanoparticles for the detection of *E.coli* 0157:H7 in faecal samples [3]. The functionalised nanoparticles show enhanced current responses before their interaction with *E.coli*. Following the interaction, the movement of electrons on GCE is reduced due to the presence of other materials, indicating that the bacteria detection has occurred. Shin ho and co-workers reported similar behaviour, in the detection of *E.coli* in river water using Prussian blue coated with titanium dioxide particles [4]. From the plots, a change of electrochemical signal was observed due to the interaction of nanoparticles with *E.coli*. As the concentration of *E.coli* increased the current response also increased due to the interaction between *E.coli* and nanoparticles. Thus, the concentration of the *E.coli* has a linear relationship with the current.

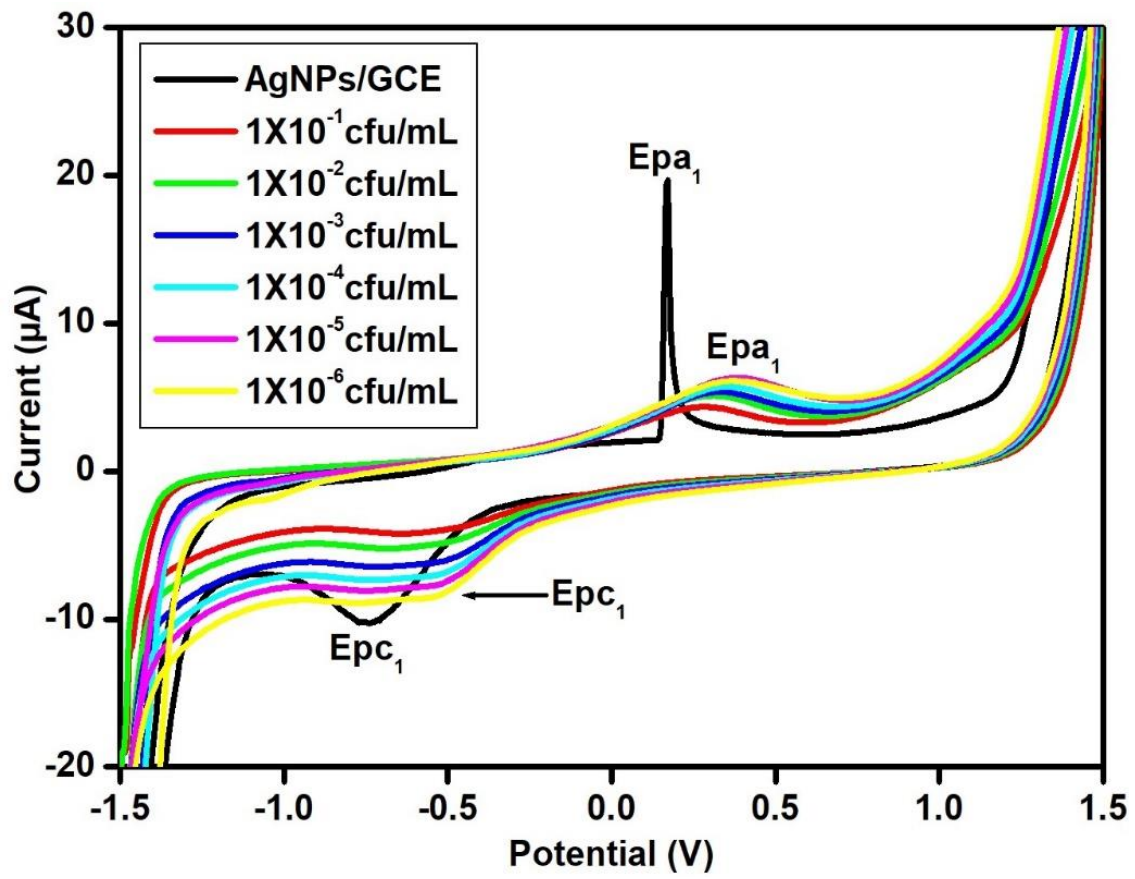


Figure 7.8: GBPE Ag-NPs/ GCE modified electrode with different concentration of *E.coli* 0157:H7 in PBS solution (0.2M pH 7.4).

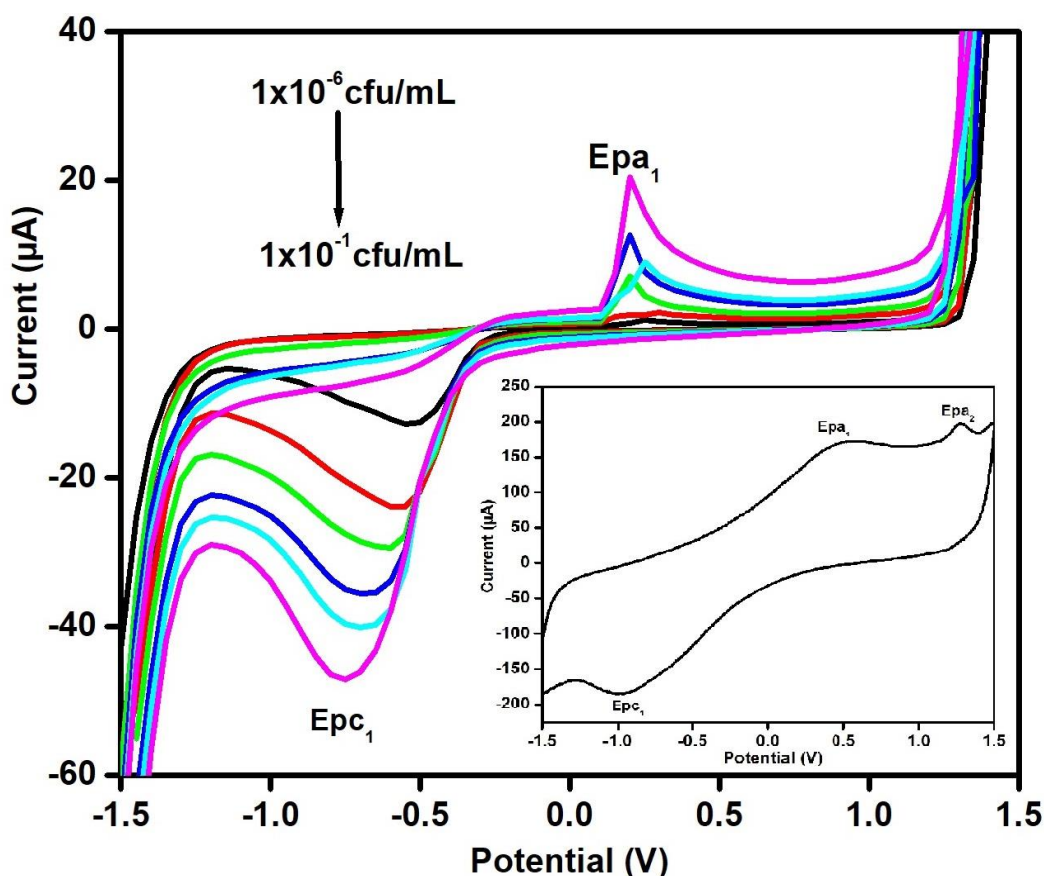


Figure 7.9: GBPE Ag-Au-NPs|GCE modified electrode with different concentration of *E.coli* 0157:H7 in PBS solution (0.2M pH 7.4) and the insert represent GBPE Ag-Au-NPs before interaction with *E.coli* 0157:H7.

In this study, the limit of detection was determined using (equation 7.2, chapter 7). the sensing potential of GBPE|Au-NPs|GCE and GBPE|Ag-NPs|GCE separately and our experimental results showed LOD of 4.0×10^1 CFU/ mL and 3.5×10^1 CFU/ mL respectively. This may be because silver ions are more toxic to microorganisms than gold ions making silver to have more antimicrobial activity than gold or other elements. Literature report that the antimicrobial effect of silver is due to its complexation to cellular components such as nucleic acids, enzymes and membranes. Ag^+ complex strongly to electron donor groups that contain sulphur, oxygen and nitrogen, these groups are present in bacterial cells as thiols, phosphate, hydroxyl and amines. Ag is also known to react fast with sulphur-containing compounds [5]. Slawson and co-workers also reported similar results between silver and

germanium for the detection of *E.coli* [6]. The results were better when using GBPE Ag-Au-NPs bimetallic nanoparticles, and we obtain LOD of 3.0×10^1 CFU/mL for GBPE Ag-Au-NPs. The calculated limit of detection was better or much lower compared to the previously reported sensors from literature. In a report by Zhang and co-workers, they obtained a limit of detection of 4.5×10^1 for the detection of *E.coli* in wastewater using copper-gold as a sensing platform using an electrochemical immunoassay sensor [7]. Another study reported by Li and co-workers fabricated an impedimetric biosensor with a LOD of 10^6 for *E.coli* detection [8]. Most of the reported studies in literature used modified electrodes for *E.coli* detection; for example, a study by Tang and co-workers developed a self-assembled monolayer-biosensor based on an enzyme for the detection of *E.coli*. In contrast, Rabeah and co-workers used a polypyrrole-amine modified GCE to fabricate a highly sensitive amperometric biosensor for the detection of *E.coli* [9,10]. The modification and cleaning process require much time, our electrochemical sensor used GBPE Ag-Au-NPs without modification on the GCE surface; thus, it took less time than the previously reported sensors.

Table 8.1 shows the Limit of Detection of more relevant electrochemical studies reported in the literature for the detection of *E.coli* 0157:H7 compared to this study. From the table, it is evident that the results obtained in this study were better compared to previous reports. Therefore, the developed sensor can detect *E.coli* 0157:H7 in water using green synthesised nanoparticles without any further modifications. The electrochemical detection process takes 45 min, which is less than 1 hr for the bacterium to bind and for analysis to commence. The obtained detection limit in this study falls within the range 1×10^{-3} to 1×10^7 CFU/ mL of the currently accepted methods reported in the literature. **Figure 8.4** is the calibration curve (N = 3) of the GBPE|Ag-AuNPs|GCE. **Figure 8.4** shows a good linear relationship between the current response and the logarithms of different concentrations of *E.coli* 0157:H7. The linearity that was accomplished from the graph was used to calculate linear regression

equation which was ($r^2 = 0.9997$) and the slope was used to calculate the LOD which was already mentioned above. The slope of the calibration also gives information about the sensitivity of the sensor, the higher the slope of the calibration curve the higher the sensitivity of the sensor for that specific component [11]. Therefore, the slope was determined to be $0.61071 \mu\text{A}/\text{CFU}/\text{mL}$. The sensitivity of GBPE|Ag-AuNPs|GCE was more improved compared to the reported sensors in literature, for example our sensitivity was higher than the recently reported study by Cimafonte and co-workers using a Impedimetric Immunosensor based on a screen printed electrode for detection of *E.coli* [12].

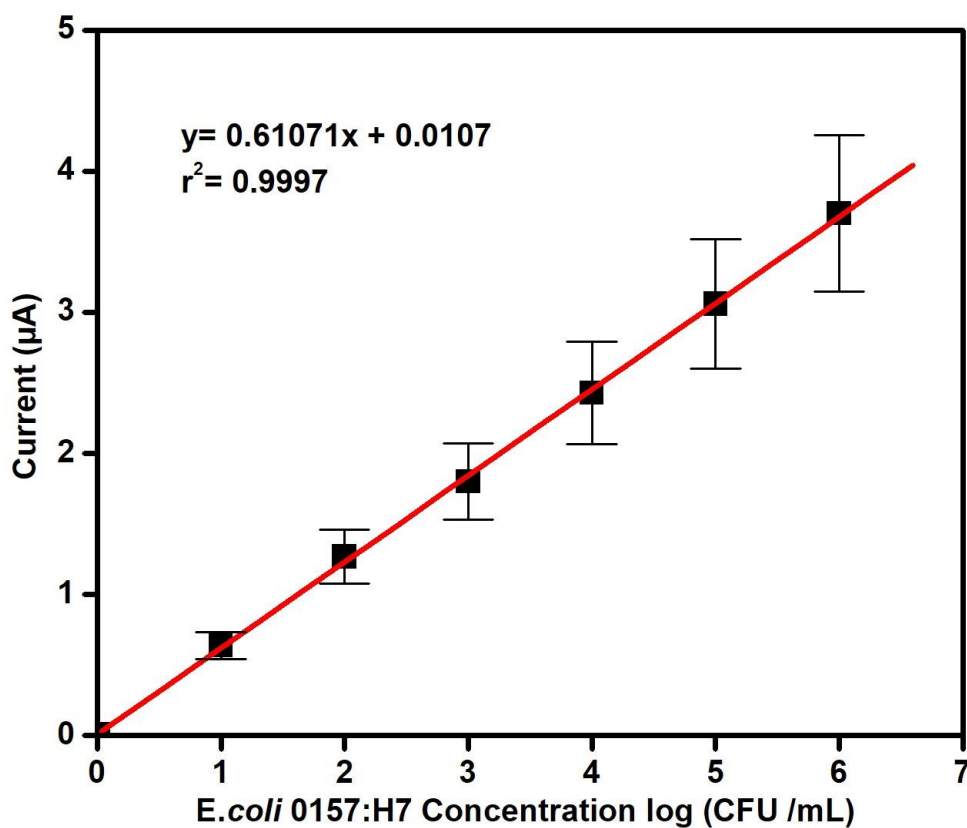


Figure 7.10: Calibration curve for electrochemical response corresponding to different concentration of *E.coli* 0157:H7 bacteria in a range of 10^1 to 10^6 CFU/ mL.

Table 7.2: Limit of Detection of more relevant studies reported in the literature for detection of *E.coli* 0157:H7 compared to this study.

| Material used | Electrode used | LOD | Reference |
|---------------------------------|--|---------------------------|------------------|
| Multi-walled carbon nanotubes | GCE | 6.2×10^5 CFU/ mL | [13] |
| Au-NPs modified with antibodies | Screen-printed carbon electrodes (SPCEs) | 3.09×10^2 CFU/mL | [14] |
| GBPE Au-NPs | GCE | 4.0×10^1 CFU/ mL | This work |
| GBPE Ag-NPs | GCE | 3.5×10^1 CFU/ mL | This work |
| GBPE Ag-Au-NPs | GCE | 3.0×10^1 CFU /mL | This work |

8.2 References:

- [1] S. Panhwar, S.S. Hassan, R.B. Mahar, K. Carlson, M. ul H. Rajput, M.Y. Talpur, Highly Sensitive and Selective Electrochemical Sensor for Detection of Escherichia coli by Using L-Cysteine Functionalized Iron Nanoparticles , *J. Electrochem. Soc.* 166 (2019) B227–B235. <https://doi.org/10.1149/2.0691904jes>.
- [2] P.K. Stoimenov, R.L. Klinger, G.L. Marchin, K.J. Klabunde, Metal oxide nanoparticles as bactericidal agents, *Langmuir.* 18 (2002) 6679–6686. <https://doi.org/10.1021/la0202374>.
- [3] H. Kaur, M. Shorie, P. Sabherwal, Electrochemical aptasensor using boron-carbon nanorods decorated by nickel nanoparticles for detection of E. coli O157:H7, *Microchim. Acta.* 187 (2020). <https://doi.org/10.1007/s00604-020-04444-y>.
- [4] J.S. Ho, C.-S. Toh, A Rapid Low Power Ultra-Violet Light-Assisted Bacterial Sensor for Coliform Determination, *Am. J. Anal. Chem.* 04 (2013) 1–8. <https://doi.org/10.4236/ajac.2013.410a1001>.
- [5] N. Silvestry-rodriguez, E.E. Sicairos-ruelas, C.P. Gerba, K.R. Bright, Silver as Disinfectant Silver as a Disinfectant, (2016). <https://doi.org/10.1007/978-1-4614-1533-6>.
- [6] R.M. Slawson, M.I.V.A.N. Dyke, H. Lee, J.T. Trevors, Germanium and Silver Resistance , Accumulation , and Toxicity in Microorganisms, 79 (1992) 72–79.
- [7] L.U. Wen-jie, Z. Xin-ai, L.I. Chang-feng, S. Jian-zhong, J. Yu-xiang, Electrochemical Immunosensor for Detection of E . coli in Urban Sludge Based on Dendrimer - encapsulated Au and Enhanced Gold Nanoparticle Labels, 44 (2016). [https://doi.org/10.1016/S1872-2040\(16\)60942-8](https://doi.org/10.1016/S1872-2040(16)60942-8).
- [8] L. Yang, Y. Li, G.F. Erf, Interdigitated Array Microelectrode-Based Electrochemical Impedance Immunosensor for Detection of Escherichia coli O157 : H7, 76 (2004) 1107–1113. <https://doi.org/10.1021/ac0352575>.
- [9] K. Abu-rabeah, A. Ashkenazi, D. Atias, L. Amir, R.S. Marks, Biosensors and Bioelectronics Highly sensitive amperometric immunosensor for the detection of Escherichia coli, 24 (2009) 3461–3466. <https://doi.org/10.1016/j.bios.2009.04.042>.
- [10] P. Geng, X. Zhang, W. Meng, Q. Wang, W. Zhang, L. Jin, Z. Feng, Z. Wu, Self-assembled monolayers-based immunosensor for detection of Escherichia coli using electrochemical impedance spectroscopy, 53 (2008) 4663–4668. <https://doi.org/10.1016/j.electacta.2008.01.037>.
- [11] D.A. Armbruster, T. Pry, Limit of blank, limit of detection and limit of quantitation., *Clin. Biochem. Rev.* 29 Suppl 1 (2008) S49-52. <http://www.ncbi.nlm.nih.gov/pubmed/18852857> <http://www.pubmedcentral.nih.gov/articlerender.fcgi?artid=PMC2556583>.
- [12] M. Cimafonte, A. Fulgione, R. Gaglione, M. Papaianni, R. Capparelli, A. Arciello,

- S.B. Censi, G. Borriello, R. Velotta, B. Della Ventura, Screen printed based impedimetric immunosensor for rapid detection of *Escherichia coli* in drinking water, *Sensors (Switzerland)*. 20 (2020) 1–17. <https://doi.org/10.3390/s20010274>.
- [13] L.V. Tarditto, F.J. Arévalo, M.A. Zon, H.G. Ovando, N.R. Vettorazzi, H. Fernández, Electrochemical sensor for the determination of enterotoxigenic *Escherichia coli* in swine feces using glassy carbon electrodes modified with multi-walled carbon nanotubes, *Microchem. J.* 127 (2016) 220–225. <https://doi.org/10.1016/j.microc.2016.03.011>.
- [14] A.R.H.A.A. Hassan, A. de la Escosura-Muñiz, A. Merkoçi, Highly sensitive and rapid determination of *Escherichia coli* O157: H7 in minced beef and water using electrocatalytic gold nanoparticle tags, *Biosens. Bioelectron.* 67 (2015) 511–515. <https://doi.org/10.1016/j.bios.2014.09.019>.

CHAPTER NINE

This chapter presents conclusion of the study and future recommendations.

9.1 Conclusion:

This work presents a novel optical and electrochemical sensor based on green synthesised Au-NPs, Ag-NPs and Ag-Au-NPs as a sensing platform. As far as we know, the described procedure for the synthesis of Au-NPs, Ag-NPs and Ag-Au-NPs using grape-banana peel extract has been demonstrated for the first time. This study revealed that the combination of grape extract and banana peel extract could play a significant role in stabilising as well as in the reduction of nanoparticles. The synthesised nanoparticles are spherical with different sizes of 10-17 nm, 25-39 nm and 12-14 nm for GBPE Au-NPs, Ag-NPs and Ag-Au-NPs respectively calculated using image J software. The monometallic structure of GBPE capped Au-NPs and Ag-NPs as well as the bimetallic structure of GBPE Ag-Au-NPs, and their chemical composition was confirmed by UV-vis, HR-TEM, EDS and Sax-space.

In this study clean water was contaminated with *E.coli* 0157:H7 bacterium to simulate real contamination. Following that, six different *E.coli* concentrations from 1×10^1 to 1×10^6 CFU /mL were prepared through serial dilution. Nanoparticles were used as a sensing part during the detection of *E.coli* 0157:H7 and the nanoparticles interacted with *E.coli* bacteria through sulphhydryl (-SH) and amino (-NH₂) groups via non-covalent interactions. The fabricated optical sensor showed LOD values of 1×10^2 CFU/ mL, 1×10^2 CFU/ mL, 1×10^1 CFU/ mL for GBPE capped Au-NPs, Ag-NPs and Ag-Au-NPs whereas the electrochemical

sensor showed LOD values of 4.0×10^1 CFU/ mL, 3.5×10^1 CFU/ mL, 3.0×10^1 CFU/ mL respectively. Between the two novel, fabricated sensors, the optical sensor showed better LOD values with regards to the bimetallic GBPE capped Ag-Au-NPs when compared to the electrochemical sensor. In all these experiments, the values are reported for three independent experiments with different sensors. Therefore, the fabricated sensors hold promise for fast detection of several pathogens in clinical analysis and environmental analysis.

Since the slope of the calibration curve gives information about the sensitivity of the sensor, we observe that our sensor is highly sensitive to high bacterium concentrations; the sensitivity is higher than the previously reported methods using antibody or aptamers. The current conventional sensors are based on antibodies which are based on charge interactions and are easily interfered by surroundings such as pH values, metal ion or proteins, thus making the developed sensor better. We believe that GBPE capped Ag-Au-NPs is promising in sensor development for simple detection of bacterial contaminants.

This study aimed to develop a sensor with enhanced sensitivity of optical and electrical based on green synthesised nanoparticles detection of *E.coli* O157:H7. The developed sensor can detect the targeted bacteria without secondary antibody or any labelling, which make it quicker, low cost and stable with excellent potential for detection of *E.coli* O157:H7 in water.

9.2 Future aims:

- Application of the fabricated sensors to multiple systems
- Application of the fabricated sensor to gram-positive bacteria
- Detection of *E.coli* O157:H7 from food
- Validation, test and specificity for the performance of the fabricated sensor under non-laboratory environmental conditions.

- These sensors can be used to monitor emergency samples for microbial detection in biosecurity and biodefense.
- To test nanoparticles as a drug to kill *E.coli* instead of using them as sensors.